Catalytic Reactions and Energy Conservation in the Cytochrome bc 1 and b 6 f Complexes of Energy-Transducing Membranes

Marcin Sarewicz, Sebastian Pintscher, Rafal Pietras, Arkadiusz Borek, Łukasz Bujnowicz, Guy Hanke, William Cramer, Giovanni Finazzi, Artur Osyczka

Catalytic reactions and energy conservation in the cytochrome bc_1 and b_6f complexes of energy-transducing membranes

Marcin Sarewicz[1] (ORCID: 0000-0001-6813-5997), Sebastian Pintscher[1] (ORCID: 0000-0001-6356-2607), Rafał Pietras[1] (ORCID: 0000-0001-8424-6590), Arkadiusz Borek[1] (ORCID: 0000-0003-3195-3579), Łukasz Bujnowicz[1] (ORCID: 0000-0002-7446-7063), Guy Hanke[2] (ORCID:0000-0002-6167-926X), William A. Cramer[3] (ORCID: 0000-0002-1762-5133), Giovanni Finazzi[4] (ORCID: 0000-0003-0597-7075), Artur Osyczka[1] (ORCID: 0000-0002-1637-2365)

[1] Department of Molecular Biophysics, Faculty of Biochemistry, Biophysics and Biotechnology, Jagiellonian University in Kraków, Poland

[2] School of Biological and Chemical Sciences, Queen Mary University of London, UK

[3] Department of Biological Sciences, Purdue University, West Lafayette, IN 47907 U. S. A.

[4] Laboratoire de Physiologie Cellulaire et Végétale. Université. Grenoble Alpes, Centre National Recherche Scientifique, Commissariat Energie Atomique et Energies Alternatives, Institut National Recherche l'agriculture, l'alimentation et l'environnement, 38054 Grenoble Cedex 9, France

Table of Contents

List of abbreviations

$\Delta\tilde{\mu}_H^+$	The transmembrane electrochemical potential gradient
2Fe2S	Rieske 2Fe-2S cluster
ADP	Adenosine diphosphate
ATP	Adenosine triphosphate
b_H	The high-potential heme *b* of Cytbc_1
b_H/b_n	The high-potential heme *b* of Cytbc_1 or heme *b* at *n*-side of Cytb_6f
b_L	The low-potential heme *b* of Cytbc_1
b_L/b_p	The low-potential heme *b* of Cytbc_1 or heme *b* at *p*-side of Cytb_6f
b_n	Heme *b* at *n*-side of Cytb_6f
b_p	Heme *b* at *p*-side of Cytb_6f
C*c*O	Cytochrome c oxidase
CET	Cyclic Electron Transfer
CW	Continuous wave
Cyt-*bc*	Enzyme belonging to cytochrome bc_1 or cytochrome b_6f
Cyt*b*	Cytochrome *b*
Cytb_6	Cytochrome b_6
Cytb_6f	Cytochrome b_6f complex
Cytbc_1	Cytochrome bc_1 complex
Cyt*c*, Cytc_2, Cytc_6	Cytochrome c, c_2, c_6
Cytc_1	Cytochrome c_1
Cyt*f*	Cytochrome*f*
DBMIB	Dibromothymoquinone
DMPO	5,5-Dimethyl-1-pyrroline N-oxide (spin trap)
ECS	Electro Chromic Band Shift
E_m	Redox midpoint potential
$E_{m,x}$	Redox midpoint potential at pH=x
EPR	Electron paramagnetic resonance
ES	Enzyme – substrate complex
ET	Electron transfer
ETC	Electron transport chain
Fd	Ferredoxin
heme c_1	Type c heme in cytochrome c_1
IMS	Intermembrane space
ISP	Iron-sulfur protein
ISP-HD	Mobile head domain of the iron-sulfur protein
K_d	Dissociation constant
MD	Molecular dynamics
MK	Menaquinone

NMR	Nuclear magnetic resonance
p, n side	Electochemically positive, negative sides of membrane
PC	Plastocyanin
P_f	An inhibitor which fixes ISP-HD at b-position
P_i	Phosphate
P_m	An inhibitor which does not fix ISP-HD
pmf	Transmembrane electrochemical potential gradient, Δp_H^+
PQ	Plastoquinone
$PQ(H_2)$	Plastoquinone or plastoquinol
PQH_2	Plastoquinol
PSI	Photosystem I
PSII	Photosystem II
PSQ	Plastosemiquinone
PT	Proton transfer
Q	Quinone (in general)
$Q(H_2)$	Quinone or quinol
QH_2	Quinol
Q_i	Quinone reduction site of cytochrome bc_1 complex
Q_i/Q_n	The quinone reduction site of Cytbc_1 or Cytb_6f
Q_n	Plastoquinone reduction site of cytochrome b_6f complex
Q_o	quinol oxidation site of cytochrome bc_1 complex
Q_o/Q_p	The quinol oxidation site of Cytbc_1 or Cytb_6f
Q_{os}	The strong-binding niche of Q_o site
Q_{ow}	The weak-binding niche of Q_o site
Q_p	Plastoquinol oxidation site of cytochrome b_6f complex
RC	reaction center
$^{Rh}Axxx$, $^{Bt}Axxx$, $^{Sc}Axxx$, $^{Ml}Axxx$	A residue of code "*A*" at position number *xxx* from *Rhodobacter capsulatus/sphaeroides, Bos taurus, Saccharomyces cerevisiae, Mastigocladus laminosus (*Cytb_6f*),* respectively
ROS	reactive oxygen species
SMP	Submitochondrial particles
SMP	Sub-mitochondrial particles
SQ	General semiquinone
SQ^-	Semiquinone anion
SQ-2Fe2S	The semiquinone at the Q_o/Q_p site spin-coupled to the reduced 2Fe2S cluster
SQH	Protonated semiquinone
SQ_i	Semiquinone at the Q_i site of Cytbc_1
SQ_o	Semiquinone at the Q_o site of Cytbc_1
TMH	Transmembrane helix
UQ	Ubiquinone
$UQ(H_2)$	Ubiquinone or ubiquinol
UQH_2	Ubiquinol

UQH_2^{Qos}	Ubiquinol bound at the strong-binding niche
UQH_2^{Qow}	Ubiquinol bound at the weak binding niche
UQ^{Qos}	Ubiquinone bound at the strong-binding niche
UQ^{Qow}	Ubiquinone bound at the weak binding niche
USQ	Ubisemiquinone

Abstract

This review focuses on key components of respiratory and photosynthetic energy-transduction systems: the cytochrome bc_1 and b_6f (Cytbc_1/b_6f), membranous multi-subunit homodimeric complexes. These remarkable molecular machines catalyze electron transfer from membranous quinones to water-soluble electron carriers (such as cytochromes *c* or plastocyanin), coupling electron flow to proton translocation across the energy-transducing membrane and contributing to the generation of a transmembrane electrochemical potential gradient which powers cellular metabolism in the majority of living organisms. Cytsbc_1/b_6f share many similarities but also have significant differences. While decades of research have provided extensive knowledge on these enzymes, several important aspects of their molecular mechanisms remain to be elucidated. We summarize a broad range of structural, mechanistic and physiological aspects required for function of Cytbc_1/b_6f, combining textbook fundamentals with new intriguing concepts that have emerged from more recent studies. The discussion covers, but is not limited to: i) mechanisms of energy-conserving bifurcation and energy-wasting superoxide generation at the quinol oxidation site, ii) the mechanism by which semiquinone is stabilized at the quinone reduction site, iii) interactions with substrates and specific inhibitors, iv) inter-monomer electron transfer and the role of a dimeric complex, and v) higher levels of organization and regulation that involve Cytsbc_1/b_6f. In addressing these topics we point out existing uncertainties and controversies which, it is suggested, will drive further research in this field.

1 Introduction

Cytochromes *bc* (Cyt*bc*) constitute one of the broadest groups of energy-transducing enzymes, present in almost every living cell. They are key components of both respiratory and photosynthetic electron transport chains and their function is often indispensable for the operation of these chains.

In this review we focus on two important enzymes from that group: cytochrome bc_1 (Cytbc_1) – involved in respiration and bacterial photosynthesis and cytochrome b_6f (Cytb_6f) – studied in plant, algal and cyanobacterial photosynthesis. We summarize a broad range of structural, mechanistic and physiological aspects required for function of these enzymes, presenting both the textbook fundamentals based on the well-established ideas and the new intriguing concepts and attractive hypotheses emerging from more recent studies.

It is remarkable that the extensive knowledge gathered so far on Cyt*bc* has left many key issues not satisfactorily understood and opened new intriguing issues for consideration. Among subjects still intensely debated are: the molecular mechanism of the catalytic electron bifurcation and the basis of high energetic efficiency of the enzyme, the mechanism of proton transfer to and from the catalytic sites, the role of dimer and the inter-monomer electron transfer, and the role of Cyt*bc* in regulation of electron flow and in redox (ROS) signaling.

It should be noted that in some cases there are questions about mechanisms of Cyt*bc* structure-function have been regarded as beyond doubt. Despite the fact that the catalytic Q cycle, the conceptual framework in which Peter Mitchell described principles of his chemiosmotic theory, is widely accepted for Cytsbc_1, its applicability to details of the function of Cytsb_6f remain subject to some questions. Although that the scheme showing cyclic electron transfer (CET) appears in every textbook of photosynthesis, the actual pathway through which electrons recycle back to the main electron transport chain remains controversial. It is clear that all these and many other questions related to this important group of enzymes await resolution in future studies.

Even though our intention was to comprehensively cover the knowledge on Cyt*bc*, the breadth of the subject makes it impossible to include all issues which relate to it. The reader is referred to several excellent reviews on this subject that have appeared in the literature.[1–26]

2 Energy Conserving and Regulatory role of Intracellular Cytochromes-*bc*

Conversion of solar or chemical energy into a biologically useful form is one of the most fundamental processes of living organisms. As described by chemiosmotic theory [27,28], this process

involves generation of a transmembrane electrochemical potential gradient, $\Delta\tilde{\mu}_H^+$ (or proton motive force, pmf) by enzymes which use external sources of energy to couple electron transfer to proton translocation between cellular compartments separated by a membrane (termed energy-transducing membrane)[29]. PMF forces the ATP-synthase to convert ADP and P_i into ATP, and the energy is stored by maintaining the concentrations of ATP, ADP, and P_i far from their equilibrium values, thus providing the universal source of energy that powers cellular metabolism.[29]

The enzymes that generate pmf are typically organized in chains, such as the mitochondrial and photosynthetic electron transfer chains, where the individual membrane-embedded electron transport protein complexes are linked functionally by components having diffusional freedom to move between complexes: hydrophobic low-molecular weight electron carriers and water-soluble protein electron carriers, respectively, inside and outside the membrane[30,31]. These carriers shuttle electrons between complexes which, overall, catalyze electron flow from a primary electron donor to a final electron acceptor, while the energy released during this process is used to transfer protons across the membrane.

There are two general mechanisms in electron transport chains by which protons are transferred across the energy-transducing membrane. In one mechanism, reduction of a quinone (coupled to proton uptake) occurs at one side of the membrane while quinol oxidation (coupled to proton release) takes place at the opposite side of the membrane (Mitchell's redox loop[27,32,33]). In the other mechanism, a series of protonation/deprotonation reactions taking place within the specific proton channels of an electron transfer complex (e.g. complex I and IV of mitochondrial electron transport chain) involving successive pK changes of amino acids in the trans-membrane pathway, allow the pumping of protons between the two sides of the membrane without involvement of quinone molecules.

Cytochromes *bc* complexes (Cyt-*bc*) comprise a set of the ubiquitous complexes contributing to generation of pmf, through a mechanism involving quinone/quinol oxidation-reduction reactions. This superfamily of complexes includes cytochrome bc_1 (Cytbc_1) (ubiquinol: cytochrome *c* oxidoreductase, EC 7.1.1.8) and cytochrome b_6f (Cytb_6f) (plastohydroquinone:plastocyanin oxidoreductase, EC 7.1.1.6). Cytbc_1 provides an electronic connection between quinone molecules and water-soluble electron carriers (such as cytochrome *c*, c_2 or c_6) catalyzing a net reaction of oxidation of quinol (ubiquinol in mitochondria and several prokaryotic cells or menaquinol some bacteria, see section 4.1) and reduction of water-soluble electron carrier (section 4.2.1). Cytb_6f catalyzes an analogous reaction between membrane embedded plastoquinol molecules and the water-soluble plastocyanin (PC) of chloroplasts or Cytc_6 (in cyanobacteria and some microalgae) (section 4.2.2). In all cases, the energy released in these electron transfer reactions powers the oxidation of

quinol and reduction of quinone, taking place at the distinct catalytic sites located on the opposite sides of the membrane, according to the first mechanism of H^+ translocation described above.

Cytbc_1 participates in respiration in oxygen-utilizing cells and also electron transfer in numerous bacteria which utilize alternative terminal electron acceptors in addition to oxygen (Fig. 1). In mitochondria, Cytbc_1 (also referred to as mitochondrial complex III or respiratory complex III) is a confluence point for reducing equivalents from the various dehydrogenases (mitochondrial complexes I, II) (Fig 1 A). In animal mitochondria, with the sole exception of some parasites, it is essential for mitochondrial respiration, as there is no alternative route to oxidation of ubiquinol by molecular oxygen. This enzyme is not essential in bacteria, where alternative mechanisms to oxidize ubiquinol usually exist in parallel to Cytbc_1. On the other hand, Cytbc_1 is an essential enzyme, in some photosynthetic bacteria such as *Rhodobacter sphaeroides* or *R. capsulatus* for cyclic, non oxygenic, photosynthetic electron transfer in the absence of a terminal electron acceptor but it is not essential when these organisms are grown heterotrophically (Figure 1 B) [34].

Cytb_6f participates in oxygenic photosynthesis in cyanobacteria, and plant and algal chloroplasts. It is a crucial component of the linear electron transfer ('Z scheme' or LET) linking photosystem I (PSI) with photosystem II (PSII) (Figure 1 C). In addition it also participates in cyclic electron transfer (CET) (Fig. 1 C) (see sections 3.6.5 and 10.1).

Apart from the involvement in generating pmf, Cyt*bc* are believed to be potential points of regulation of electron flow. This stems from the fact that their two quinone binding sites are directly connected with the two main redox pools (intra-membrane ubiquinone/plastoquinone and soluble cytochrome *c*/plastocyanin) of respiration/photosynthesis. Hence, by virtue of catalyzing opposite chemical reactions, these sites may influence one another (the product of one catalytic site becomes a substrate for the second site and *vice versa*). Another regulatory function of Cytb_6f is to trigger changes in the chloroplasts' light harvesting capacity in response to changes in the ambient light intensity by sensing variations in the redox state of the plastoquinone pool. These changes modulate the interaction of Cytb_6f with a kinase able to reversibly phosphorylate the light harvesting complexes, leading to their preferential association with one of the two photo centers (PSII and PSI) in a process called 'state transitions' (section 10.3) [35].

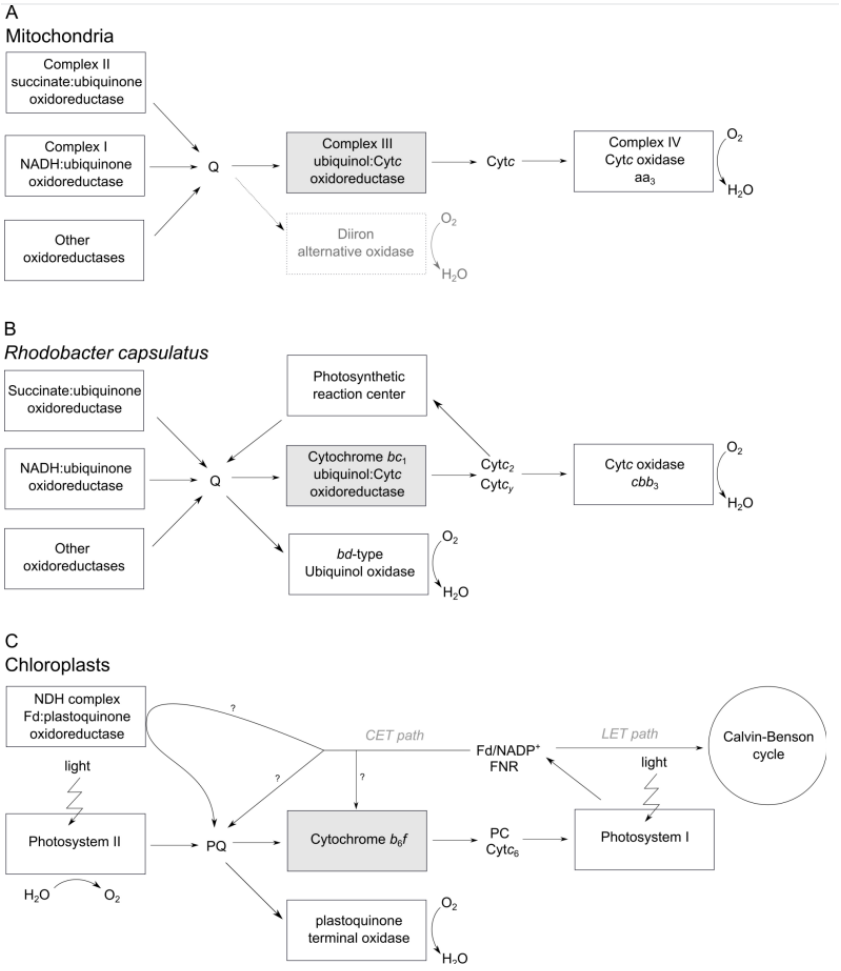

Figure 1. Overview of electron transfer paths involving Cyt-*bc* complexes: Cytbc_1 in mitochondrial respiratory chain (A) and in anoxygenic photosynthesis or respiration of purple bacteria (B); Cytb_6f in oxygenic photosynthesis in chloroplasts (C). Q and PQ denote ubiquinone and plastoquinone pool, respectively. PC, Fd and FNR denote plastocyanin, ferredoxin and ferredoxin/$NADP^+$ oxidoreductase. LET depicts linear electron transfer in photosynthesis while CET shows cyclic electron transfer path which recycles the electrons from Fd pool back to the PQ(H_2) pool. Scheme in A considers mitochondria of both plants and animals (the diiron alternative oxidase is not present in animal mitochondria except for rare cases, such as in *Trypanosoma*).

Moreover, although the activities of Cytbc_1 and Cytb_6f complexes are different, because of the above reactions, they are also inferred to be involved in mitochondrial and chloroplast redox signaling.[36]

Finally under specific conditions, Cyt*bc* can generate a limited amount of superoxide, as a side reaction of the catalytic cycle (section 7.5).[37]

$$O_2 + e^- \rightarrow O_2^{\cdot-};\ E_m = -140\ mV$$

It is noted that the specific rate of superoxide (O_2^-) production in purified active crystallizable Cytb_6f, normalized to the rate of electron transport, is more than an order of magnitude greater than that of the yeast respiratory Cytbc_1 [38]

3 Overview of Structure and Function of Cytochromes *bc*

Cytbc_1 and Cytb_6f share several structural and mechanistic features. Both are homodimers with each monomer containing a set of similarly arranged spatially separated quinone binding sites and redox active cofactors required for completion of the catalytic cycle (fig. 2). The general features common to both complexes, are summarized in sections 3.1-3.4. Despite these similarities, several important differences exist between them. Therefore the two following sections of this chapter 3.5 and 3.6 discuss separately Cytbc_1- and Cytb_6f-specific properties.

3.1 Catalytic Sites, Redox cofactors, and Cofactor Chains

In each monomer of the Cyt-*bc* dimeric complex, the hemes and the iron-sulfur 2Fe-2S Rieske-type cluster (2Fe2S) assemble into two chains of cofactors designed to link the two catalytic quinone binding sites with diffusible pools of substrates (quinone and Cyt*c*/PC). The two quinone binding sites catalyze opposing reactions (quinol oxidation / quinone reduction) as integral parts of the catalytic cycle (see section 3.2).

In Cytbc_1, the quinol oxidation site (the Q_o site) is linked with Cyt*c* by the *c*-chain composed of 2Fe2S and heme c_1. The *b*-chain, composed of heme b_L/b_p and heme b_H/b_n, connects the Q_o/Q_p site with the quinone reduction site (the Q_i/Q_n site) located at the opposite side of the membrane. Considering the relative values of the redox midpoint potentials of cofactors, the *c*-chain and the *b*-chain are commonly named the high- and low-potential chain, respectively. A characteristic feature of this arrangement is that the Q_o site is located between the *c*- and *b*-chains, which has crucial consequences for the catalytic Q cycle mechanism (Figure 2).

In Cytb_6f, the high- and low-potential chains and the quinone catalytic sites (the Q_p and Q_n for quinol oxidation and quinone reduction, respectively, see section 11 for explanation on the usage of the names of the catalytic sites in this review and on other nomenclatural issues) are arranged in the similar manner, but some variation in the redox cofactor exist: heme *f* (E_m = +370 mV) is present in the high-potential chain in place of heme c_1 and the low-potential chain contains an additional and atypical heme c_n (not present in Cytbc_1).

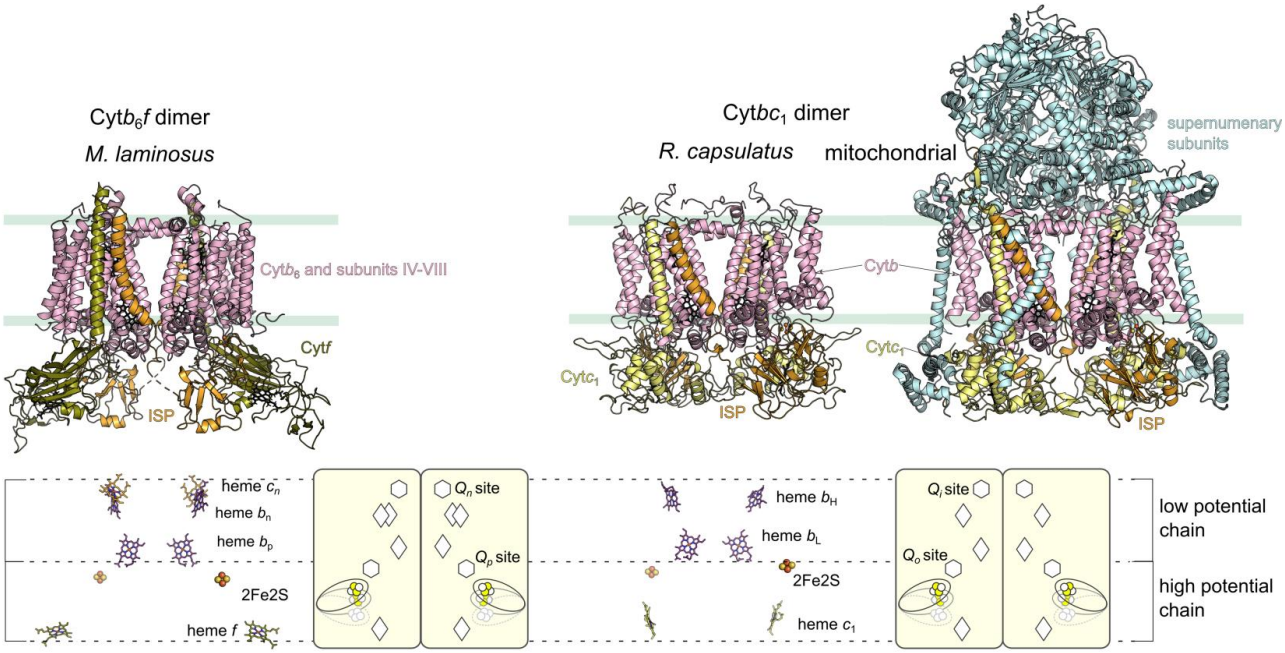

Figure 2. Overview of structures and cofactor chains in dimeric Cyt-*bc* complexes. Top: Crystal structure representations of *M. laminosus* Cytb_6f (left, PDB ID: 4H13), *R. capsulatus* Cytbc_1 (middle, PDB ID: 1ZRT) and mitochondrial Cytbc_1 (right, PDB ID: 1KYO). Bottom: Spatial arrangement of cofactors extracted from the structures above. The layout of cofactors in *R. capsulatus* and mitochondrial Cytbc_1 is the same. The simplified cartoon models depict symbols for cofactors that are used throughout the figures.

3.2 Brief Overview of Catalytic Cycle

The mechanism by which Cytbc_1 links electron transfer and proton translocation reactions is the proton motive Q cycle.[33,39] In engages the high- and low-potential -chains (*c*- and *b*-chains, respectively) and the Q_o, and the Q_i sites. Protons are taken up at the Q_i site, carried across the membrane by the quinol (QH_2), and released at the Q_o site. The Q_i site and the Q_o site are located toward the electronegative and electropositive sides of the membrane (*n* and *p* sides, respectively). For that reason, the Q_i site and Q_o of Cytbc_1 site are alternatively named Q_n and Q_p, respectively (see section 11).

The Q_o site, being positioned between the *c*- and *b*-chains, oxidizes QH_2 and passes its two electrons in a highly specific manner: one electron is delivered to the *c*-chain while the other electron is delivered to the *b*-chain. This process occurs in a so-called bifurcation reaction in which QH_2 is oxidized by 2Fe2S of the *c*-chain and by the heme b_L of the *b* chain. The reduced 2Fe2S passes 1 electron to heme c_1, which subsequently reduces diffusible Cyt*c*. The reduced heme b_L passes 1 electron to heme b_H. The electron is then used for quinone (Q) reduction at the Q_i site. This way the Q_o-site-mediated oxidation of QH_2 delivers one electron to the Q_i site at the time, meaning that two cycles of the Q_o site are needed to fully reduce a Q to QH_2 at the Q_i site. Overall, the net oxidation of one QH_2 molecule and transfer of two electrons to two molecules of Cyt*c* leads to the uptake of two

protons from the *n* side (mitochondrial matrix or bacterial cytoplasm) and the release of four protons on the *p* side (intermembrane space of mitochondria or bacterial periplasm). A step-wise scheme of the reaction taking place during the Q cycle in Cytbc_1 is shown in figure 3.

In the case of Cytb_6f, although details of the Q cycle have been studied less completely and flash-induced reduction of heme b_n separate from that of heme b_p not defined experimentally[40], the general principles of the Q cycle and proton translocation mechanism are believed by most researchers in the field to be essentially the same as for Cytbc_1 (see perspective on this issue in section 3.6.4). This includes the bifurcation reaction taking place at the PQ oxidation site (Q_p site) with electrons delivered into the high- and low-potential chains. One of the main differences is the presence of an additional cofactor within the low-potential chain. This is an atypical high-spin and relatively high-potential, heme c_n covalently attached to the protein through a single thioether bond [41,42]. The planes of hemes b_n and c_n are oriented perpendicularly and share electrons[43] with each other with the latter being close to the PQ binding niche. Although a role of this heme is still unknown it was proposed that together with heme b_n it forms a pair of cofactors that can deliver two electrons to PQ in order to reduce it to PQH_2 in a virtually one-step event. This idea, however, has not been experimentally validated yet. Because the heme c_n is exposed to the stromal side of the thylakoids, this cofactor could provide an additional entray point for electrons at the level of the Q_n site, possibly triggering a different Q cycle mechanism, or providing an oxidant for stromal electrons in cyclic electron flow (see below and discussion in section 3.6.5). Another difference between Cytbc_1 and Cytb_6f, due to the variation in the composition of the high-potential chain, is the fact that electrons from the 2Fe2S are transferred to heme *f* which further reduces diffusible PC or Cytc_6 (instead of Cyt*c* interacting with Cytc_1).

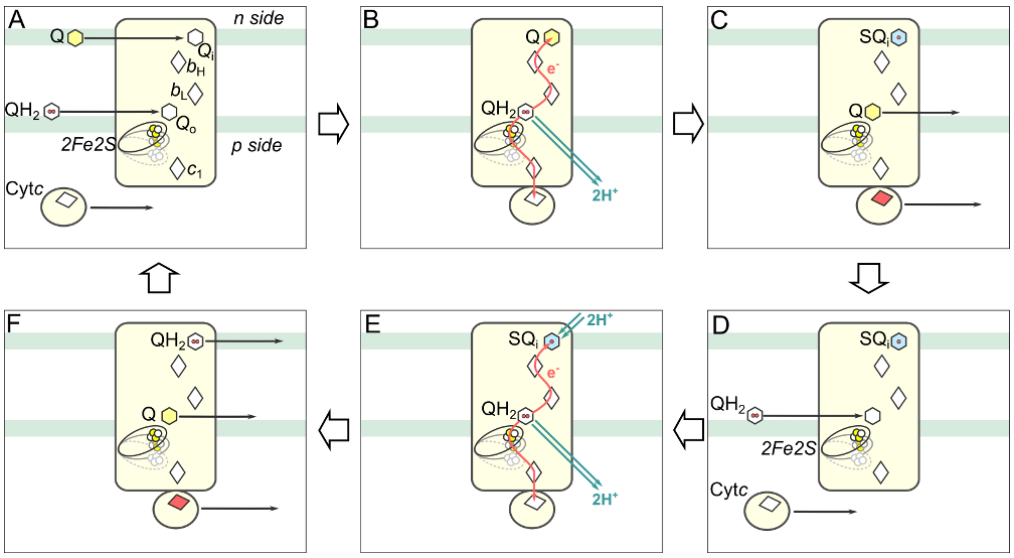

Figure 3. A simplified, static scheme, showing step-wise reactions taking place during the catalytic cycle of Cytbc_1. (A) Quinone (Q) and Quinol (QH_2) (*yellow hexagon and white hexagon with 2 dots*) bind to the Q_i and Q_o sites, respectively, while oxidized Cyt*c* (*oval with white rhombus*) binds to the Cytc_1 domain. (B) After binding, QH_2 is oxidized, 2 protons are released (*turquoise arrows*) to the *p* side, one electron is transferred (*red arrow*) to Cyt*c* through the high-potential chain, while the second electron goes (*red arrow*), through the low-potential chain, to Q bound at the Q_i site. (C) Reduced Cyt*c* (*oval with red rhombus*) and Q diffuse out of the respective sites (*black arrows*) while SQ_i (*blue hexagon with dot*) stays stably bound at the Q_i site. (D) Second molecule of QH_2 and oxidized Cyt*c* bind to the Q_o site and Cytc_1, respectively. (E) Oxidation of QH_2 takes place as in case B, but the electron from the low potential chain reduces SQ_i to QH_2, which is associated with uptake of two protons from the *n* side. (F) Q, QH_2 and reduced Cyt*c* diffuse out of the Q_o, Q_i and Cytc_1, respectively, and the cycle starts again. Hemes are shown as rhombuses, the 2Fe2S is shown as yellow-white circles. Lipid bilayer is marked as green lines. For simplicity, only one monomer is shown and the motion of the head domain of iron-sulfur protein (ISP-HD) was not included. The scheme in general is believed to hold true also for Cytb_6f with some modifications at the Q_n site associated with the presence of additional heme c_n and possible modifications to the electron transfer sequence associated with the involvement of this enzyme in CET (see Fig.4).

The Q cycle originally proposed by Mitchell[32] considered a mechanistic link between electron bifurcation at the Q_o site and electron confurcation at the Q_i site. As mentioned above, the bifurcation at the Q_o site results in one electron delivered to the Q_i site, implying that a completion of confurcation at the Q_i site requires the functional link with another redox-active enzyme/cofactor cooperating with Cytbc_1 and serving as an additional source of electrons for that site. The second electron to complete reduction of SQ at the Q_i site was initially proposed to originate from the activity of another dehydrogenase. Further studies revealed that Cytbc_1 does not need to be associated with any source of electrons but QH_2 to complete the cycle. Instead, Cytbc_1 must oxidize two QH_2 molecules at the Q_o site to sequentially deliver two electrons to the Q_i site [39]. On the other hand the idea that the complex interacts with another dehydrogenase could be relevant to account for the possible role of Cytb_6f in CET. Indeed, it has been proposed that electrons donated by PSI to the $NADPH^+$ / ferredoxin pool could be reinjected into the PQ(H_2) pool by electron transfer to PQ or putative plastosemiquinone (PSQ) at the Q_n site. In such a case, the catalytic cycle of Cytb_6f under conditions favoring CET, could operate according to the original Mitchell Q cycle (Fig. 4).

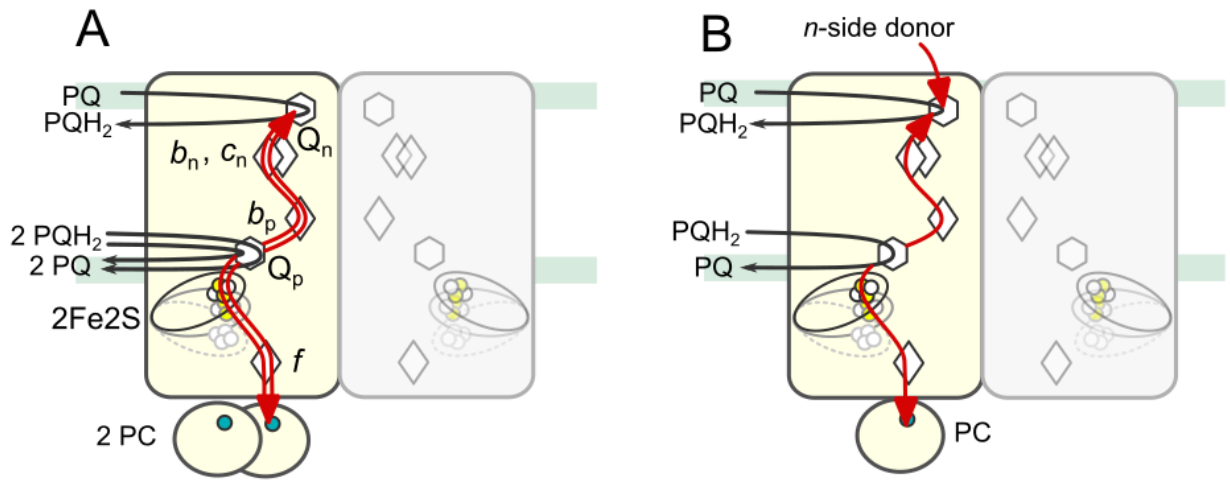

Figure 4: Two possible mechanisms of Q cycle in Cytb_6f. (A) The "modified Q cycle" [39] which is similar to Cytbc_1 - two electrons are delivered to the Q_n site from Q_p site, which requires oxidation of 2 PQH_2 and reduction of 2 PC, per 1 reduced PQ at the Q_n site. (B) Original Mitchell Q cycle [32] in which one electron delivered to the Q_n site comes from the PQH_2 oxidation at the Q_p site and the second electron comes from electron donors at the *n* side (Fd/FNR). According to the original Mitchell mechanism 1P PQH_2, 1 PC, 1 PQ and 1 *n* side donor are needed to complete the cycle. Color code and symbols as in Fig 3. Copper in PC is marked as blue dot. For simplicity proton paths are omitted and reactions in one monomer are shown while the second monomer is grayed out.

The bifurcation reaction taking place at the Q_o/Q_p site is essential for the energetic efficiency of the catalytic cycle, and has long been considered a unique feature of Cyt*bc*. However, more recent findings indicate that bifurcation reaction may exist in other systems, such as those utilizing flavins [44].

3.3 The H-shaped electron transfer system in the dimer

Cytbc_1 complexes from mitochondria and bacterial cells have been crystallized and their structures solved to atomic resolution. The mitochondrial Cytbc_1 is a symmetrical, oligomeric homodimer, in which each monomer encompasses the three catalytic subunits (Cyt*b*, Cytc_1 and ISP) surrounded by a periphery of non-redox, supernumerary subunits. The bacterial enzyme is also dimeric and the overall structure of the catalytic subunits as well as the position of the redox cofactors are highly similar to the mitochondrial enzyme (Fig 5). The major difference is a general lack of the supernumerary subunits in the bacterial enzyme.

One unusual aspect of the dimeric structure is that ISP spans the dimer. This ISP subunit is anchored in one monomer by a single transmembrane helix, while the peripheral, hydrophilic domain that contains 2Fe2S (ISP-HD) is located in the other monomer, where it forms part of the quinol

oxidation Q_o site [20,21,45]. A comparison of the structures of enzymes crystallized in the absence or presence of the Q_o site inhibitors indicated that the ISP-HD occupies different positions with respect to the other parts of the complex. This suggested that movement of ISP-HD between positions proximal to Cyt*b* and Cytc_1 is necessary to transfer an electron between the Q_o site and heme c_1 in the c-chain. This hypothesis was confirmed by site-directed mutagenesis studies which demonstrated that such movement was essential for enzyme activity. However, the mechanistic rationale behind the movement is not clear (see section 3.4).

In view of the topographic arrangement of ISP, the functional module at the level of the Cytbc_1 monomer consists of the Cyt*b* and Cytc_1 and ISP linked to them through its ISP-HD, while also interacting with Cyt*b* and Cytc_1 of the other monomer through its hydrophobic anchor. The same structure feature applies to Cytb_6f (see below). [46] The crystal structures of Cytbc_1 revealed that large distances separate the cofactors from different monomers, except for the two hemes b_L that are positioned close enough to allow electron transfer between the monomers (Fig 5). The capacity of this electron transfer bridge to connect the monomers on a catalytically-relevant timescale was further proven in studies that exploited cross-inactivated forms of the enzyme [47]. The existence of the heme b_L-b_L electron transfer bridge implicates that cofactor chains in the dimer assemble into an H-shaped electron transfer system that connects the two Q_o sites with the two Q_i sites. Given that the functional module of each of the monomers provides all necessary elements to support the catalytic Q cycle (the *c*- and *b*-chains, the Q_o and Q_i sites), the mechanistic and physiological meaning of the H-shaped electron transfer system remains unclear but intriguing (see section 9 for details).

Cytb_6f is also a homodimer. The topographic arrangement of ISP that are intertwined with the dimer and the movement of ISP-HD are conserved, as is the distance between the two hemes b_p. In view of the general similarity of cofactor architecture between Cytbc_1 and Cytb_6f it is reasonable to assume that the characteristic H-shaped electron transfer system is a shared feature of all Cyt*bc*.

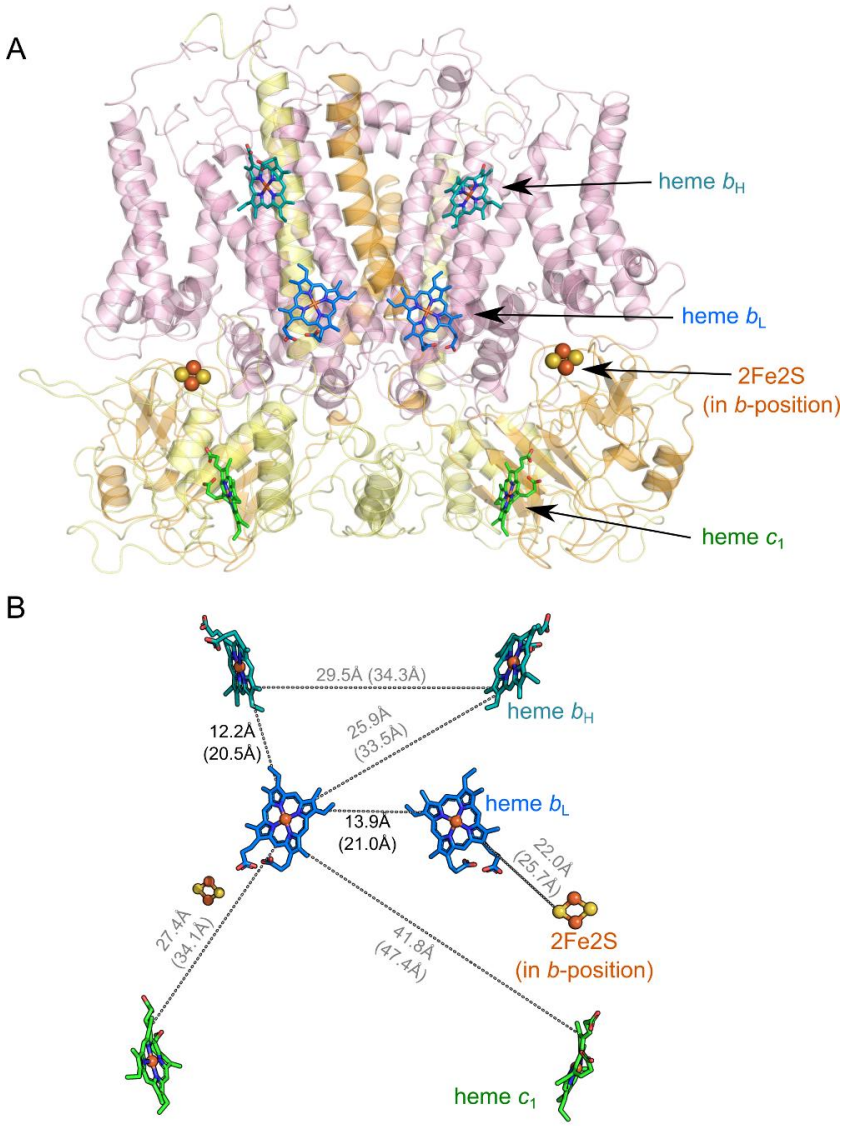

Figure 5. Crystal structure and spatial arrangement of electron-transfer cofactors in Cytbc_1 from *Rhodobacter capsulatus* (PDB ID: 1ZRT [48]). A) Ribbon structure showing all catalytic subunits in the dimer with the overlaid cofactors. B) Redox-active cofactors in the dimer with edge-to-edge (numbers) and iron-to-iron distances (numbers in brackets).

3.4 Large-scale movement of ISP-HD

The large-scale movement of the extrinsic domain of the iron-sulfur protein (ISP-HD) is an inherent part of the catalytic cycle of Cytbc_1 and Cytb_6f. The movement alternately brings the 2Fe2S either to the position close to the catalytic Q_o/Q_P site (referred to as the Q_o position or the b-position) or close to heme c_1/f, (the c-position) separating in time and space the two electron transfers within the high potential chain: 2Fe2S at the b-position exchanges electrons exclusively with quinol bound at the site, while at the c-position it exchanges electrons exclusively with heme c_1/f. This movement was proven obligatory in many studies showing that impairment of the mobility of ISP-HD entails a severe limitation or complete loss of enzymatic activity[49–55]. This is commonly explained considering

the effect of changing in distance between cofactors on electron transfer rate:[56] the ISP-HD arrested at a specific position permanently (due to the presence of some inhibitors) or for prolonged period of time (due to specific mutations) cannot efficiently shuttle electrons between the Q_o/Q_P site and heme c_1/f as specific distances between the cofactors in a frozen configuration are not optimal for rapid electron transfer along the entire cofactor chain. For example, in a configuration with the ISP-HD arrested at the Q_o site, a large distance between the 2Fe2S and heme c_1 prevents rapid electron transfer between these two cofactors and consequently enzymatic activity is lost.

First structural indications for ISP-HD movement. The possibility that conformational changes might be associated with the catalytic reactions involving 2Fe2S was considered before the first crystallographic structures of Cyt*bc* became available[57,58]. Although the movement itself was not mentioned, a mechanism evoking a "catalytic switch" of 2Fe2S was formulated on the basis of different affinities of MOA-stilbene and UHNQ inhibitors to the Q_o site that depended on the redox state of 2Fe2S. The concept of ISP-HD movement during the catalytic cycle was born soon after crystallographic structures with resolved ISP became available[59–61]. Early structures of chicken Cytbc_1 revealed two conformations of ISP-HD[61], suggesting that it might switch between different positions during the catalytic cycle. This was further substantiated by the mammalian Cytbc_1 structures containing all 11 monomer subunits[60], which clearly showed that ISP-HD can adopt different conformations for which 2Fe2S was found at the b-position, at the c-position or somewhere in between. Further crystallographic and cryo-EM structures of Cyt*bc* originating from many different organisms: bacteria [42,48,62–67], chlorophyta[41], fungi[68–72], plants[73] to avian[74–76] and mammalian proteins[77–79], including humans[80], were all consistent with the concept that ISP-HD must undergo a constrained diffusion in order to facilitate electron transfer between the Q_o/Q_p site and Cytc_1/Cyt*f*. One recognized exception comes from recent analysis of the structure of Cyt-*bc* in supercomplex with cytochrome *c* oxidase from *Mycobacterium smegmatis*, which suggests that a globular domain of a diheme Cyt*c* (equivalent of Cytc_1) might move instead of ISP-HD to support the catalytic cycle[81,82]

Effects of the Q_o/Q_p site inhibitors. It is recognized that two types of inhibitors exert opposite effects on the average position of ISP-HD seen in crystals[83]. The first group of inhibitors includes compounds, such as stigmatellin, famoxadone, *n*HDBT, atovaquone and DBMIB in Cytb_6f, which fix ISP-HD at the b-position and thus are classified as P_f inhibitors (f- for fixed). The second group includes compounds that do not arrest the ISP-HD at a single b-position, but, quite oppositely, expel ISP-HD from the Q_o/Q_p site forcing the domain to adopt positions remote from the Q_o/Q_p site, including the c-position[21,74,77,84]. As they do not prevent the motion of ISP-HD, they are classified as

P_m inhibitors (m- for mobile). Typical inhibitors of this group are myxothiazol, MOA-stilbene and strobilurin derivatives (see section 5).

Constrained diffusion or allosteric control. There are several mechanistic aspects of the movement of ISP-HD which remain the subject of discussion[20]. One of the most important and still unsolved issues concerns a fundamental question of whether the motion is simply a stochastic, thermally-activated process or whether it is rather controlled by a particular state or states of the enzyme during the catalytic cycle[21,85–90]. The simplest answer one may consider is that the motion represents a stochastic process of constrained diffusion[51,90–92], which is fast enough (~80 000 s^{-1})[93] not to limit the overall rate of catalysis[94]. The stochastic diffusion, in contrast to any mechanism that would rely on a specific element or elements of control imposed on the ISP-HD movement, has the clear advantage of not requiring energy expenditure for "information gain" needed to control the cycle. This seems important given that the primary function of the enzyme is to conserve energy.

However, the general difficulty with understanding the high energetic efficiency of bifurcation taking place at the Q_o/Q_p site and associated with its efficient suppression of side reactions (see section 7.4) prompted scientists to look for structural factors responsible for controlled docking/release of the domain from the b-position during the catalysis. This seemed additionally justified by the specific effects of the P_f and P_m inhibitors on modulation of the position of ISP-HD and on interactions of ISP-HD with Cyt*b*. None of the available structures succeeded in resolving the position of natural substrates, UQ/PQ or UQH_2/PQH_2, bound at the Q_o/Q_p site[20] which left room for interpretation of any observed structural effects in the context of possible effects of the presence of Q or QH_2 at the catalytic site on the ISP-HD motion. Some additional clues have been drawn from MD simulations[95–97].

Structural changes in brief. Prior to discussions on the mechanisms of the ISP-HD motion, it is necessary to briefly describe key structural elements of ISP. The ISP subunit can be divided into 3 domains[98]: a) ISP-HD harbouring the redox-active [2Fe-2S] Rieske cluster (2Fe2S) b) the membranous anchor, consisting of a single hydrophobic helix (residues $^{Rh}1 – 38$, $^{Bt}1 – 61$), and c) the neck or hinge region (residues $^{Rh}39 – 48$ or $^{Bt}62 – 74$) containing highly conservative amino acid sequence[99] connecting the anchor with the ISP-HD (see Fig. 6). The two ISPs interwind the dimer in such a way that each of the ISP-HD, interacting with Cytc_1 or Cyt*b* of one monomer, has its anchor associated with Cyt*b* of the second monomer (see Fig 5). The movement of ISP-HD is associated with conformational change within the flexible neck region (described below), rotation of the domain by approximately 57 to 65^o [92,100] and displacement of the domain by approximately 2 nm.

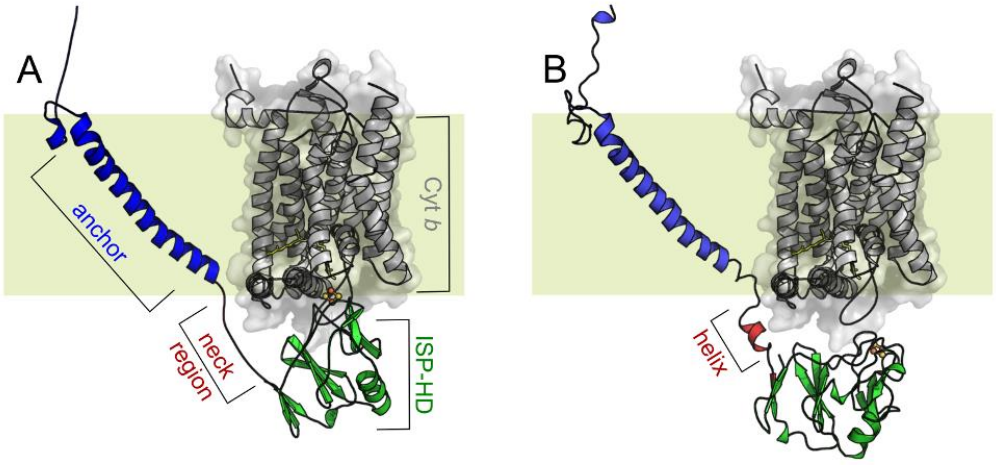

Figure 6. Structure of Cyt*b* and two conformations of ISP in one monomer. (A) Structure based on PDB:1sqx with ISP-HD at the b-position (B) Structure based on PDB:1be3 with ISP-HD being at the c-position. The hydrophobic anchor of ISP (blue helix) is embedded in the lipid membrane (pale green square). In A and B the neck region connecting ISP-HD (green) with the anchor has two different conformations. Cyt*b* is shown in gray.

Different positions of ISP-HD in crystal structures. Comparing different crystal structures Berry et al.[20] proposed that the observed populations of ISP-HD fall into 4 main groups if one considers differences in distances and angles of the position of the 2Fe2S in the structure relative to the stigmatellin bound at the Q_o site (Fig. 7). The first group encompasses a population of ISP-HD in "b-positions" or "fixed positions" with distances of up to ~0,15 nm and angles up to 7°. The second group gathers "famoxadone-positions" for which the distance is between ~0.15 and ~0.2 nm with the angle ~10°. The third group encompasses "low-affinity fixed positions" at distances ~0.4 to 0.45 nm and angles ~17 to ~20°. The last group considers ISP-HD at the "c-positions" for which angles fall between 55° – 60° and distances ~1.5 to ~2.0 nm. It is of note that the diagram by Berry et al.[20] includes a structure originally resolved by Iwata et al.[60] which was not classified to the group of c-positions and for which distance is ~2.3 nm and angle ~65°. For this structure, the distance between ^{Bt}H161 (^{Rh}H156) of ISP and heme c_1 is short enough to allow the formation of a H-bond between this histidine N_τ atom and the propionate group of heme c_1 indicating the most probable conformation predisposed to fast electron exchange between the cluster and heme c_1.

Structure-function relationships for the neck region of ISP-HD. While detailed comparisons of structures revealed several elements that might undergo specific conformational changes upon the motion of ISP-HD, the cause-effect relationships of these elements in the context of the mechanism are not fully understood. The most evident structural change concerns the neck region which, depending on the position of ISP-HD, adopts conformations differing in length[21,51]. When the ISP-

HD is at the c-position, the neck forms a small helical structure, whereas docking the domain to the Q_o site coincides with the "melting" of this small helix, thus lengthening the connection between the anchor and the ISP-HD (Fig. 6). However, helix formation was seen upon transition of ISP-HD from the "low-affinity fixed position" (group 3) to b-position (group 1)[20].

The first evidence for involvement of the neck region in ISP-HD mobility can be found in studies showing that mutations in the conserved fragment of the *Box 1* sequence of the ISP (ISP:^{Rh}L136) that destroy sensitivity of 2Fe2S to UQ at the Q_o site, were mitigated by mutations in the hinge region (ISP:^{Rh}V44 or ISP:^{Rh}A46)[101,102]. Further mutational studies systematically investigated the effects of changing the length and amino acid composition of the neck region on movement of ISP-HD. Elongating the neck by insertion of 1, 2 or 3 alanine residues (+1Ala, +2Ala, or +3Ala mutants, respectively) was found to decrease overall electron transfer through the high-potential chain and the magnitude of this decrease depended on the length of the insertion. In +1Ala, the electron transfer to heme *c* was found to occur within the millisecond timescale, while in +2Ala and +3Ala – in the second timescale, which is orders of magnitude slower than in the native enzyme (micro to milliseconds). Apparently ISP-HD movement, which in the native enzyme is fast and not rate-limiting, becomes rate-limiting in the mutants[51,93,103,104].

Interestingly, +1Ala is still functional *in vivo*, while +2Ala and +3Ala are not, indicating that some level of functional tolerance to restrictions of the ISP-HD movement exists Detailed analysis of the kinetic data lead to the proposal that these mutants progressively restrict the movement in such a way that the ISP-HD gets arrested for a prolonged period of time at the b-position (for milliseconds in +1Ala or seconds in +2Ala or +3Ala)[50,52,90,105–107]. Also, replacement of the neck-region residues with 6 prolines[50,106] all but abolished helix formation and precluded the release of the domain from the b-position. Surprisingly, shortening of the neck region by 1 to 5 amino acids did not lead to loss of catalysis and the EPR spectra obtained for deletion mutants still reflected the ability of 2Fe2S to interact with the UQ and UQH_2 bound at the Q_o site, albeit with stoichiometry of ISP to Cyt*b* progressively decreasing to 0.2 in 5-residue-deletion mutant[50].

The conclusion reached from analysis of kinetic data that the alanine insertions arrest the ISP-HD at the b-position was confirmed by EPR studies with oriented membranes[88,100,108–111] and pulse EPR with isolated Cytbc_1[90,107,112,113]. The latter studies allowed direct monitoring of changes in the average position of the ISP-HD with respect to heme b_L by measuring the distance-dependent enhancement of reduced 2Fe2S relaxation by oxidized heme b_L. The average distance between these two cofactors was found to increase in the following order +2Ala mutant, +1Ala mutant, WT[107]. These measurements also revealed that the position of ISP-HD in +2Ala is no longer influenced by

P_m inhibitors but remains sensitive to the addition of stigmatellin[90]. This suggests that conformational changes at the neck region can be overwhelmed by the energy of stigmatellin binding, with a large contribution coming from H-bond formation (typical value of energy required to break an H-bond is ~21 kJ/mol) [20.]

Structure-function relationships for the interaction of ISP-HD with Cytb. Given that the P_f and P_m inhibitors exert different effects on the position of ISP-HD the question arises as to how the P_f inhibitors fix the domain at a position close to the Q_o site. One of the most obvious structural effects of the presence of stigmatellin, *n*HDBT, atovaquone, crocacin D and ascochlorin (group-1 of P_f inhibitors) at the Q_o site is formation of the H-bond between ^{Rh}H156 (^{Bt}H161 or ^{Sc}H181) of the ISP subunit and the inhibitor. Formation of this bond is not only associated with docking of ISP-HD to the Q_o site, but also stabilizes the reduced state of 2Fe2S by significantly raising its redox potential[114–116]. This suggests stabilization of the reduced cluster under conditions when it forms the H-bond with a molecule occupying the Q_o site. Indeed, the observation that the reduced cluster is detected by EPR at the b-position in membranes indicates that interactions of the reduced 2Fe2S and the natural quinone at the Q_o site are also stabilized. On the other hand ISP-HD appears to favor the c-position when the cluster is oxidized[100]. This difference in affinity to quinones at the Q_o site between the reduced and oxidized cluster may be one of the elements contributing to the mechanism that diminishes the risk of energy-wasting short-circuits (see section 7.4.1). It should be noted however, that some inhibitors (famoxadone, fenamidione or JG-144 inhibitors, all belonging to the group 2 of P_f inhibitors) hold the domain at the b-position without creating an H-bond to ^{Rh}H156/^{Bt}H161[117]. This indicates that factors other than the H-bond between ^{Rh}H156/^{Bt}H161 of ISP and the occupant of the Q_o site can also stabilize binding of ISP-HD to Cyt*b*. While formation of this bond would be expected to significantly strengthen the interaction, it is clearly not an absolute requirement for the domain fixation to Cyt*b* or Cytb_6.

It seems reasonable to assume that some changes in conformation on the surface of Cyt*b* or Cytb_6 contribute to the process of fixing to or release of the domain from the b-position[20,21,78,85]. The potential "holding and release lever", if it exists, would be expected to localize to the part of the Cytb/b_6 which remains in close contact with the surface of ISP-HD. These regions encompass small helices that are connected to the transmembrane ones by loops: *cd1*, *cd2* and *ef* loop[18,20,55,64,118]. However, when structures containing P_f and P_m inhibitors are compared, there is no significant change in the position of helices in Cyt*b*, except for the *cd1* helix, which seems to be slightly pushed inside Cyt*b* by ISP-HD upon interaction of stigmatellin with 2Fe2S[20]. Furthermore, a comparison of the structures of intermediate positions (group 3) and the *c*-position (group 4) reveals no changes in the

cd1 and *cd2* helices, suggesting that the motion of ISP-HD between "low-affinity fixed positions" (group 3) and the c-position (group 4) is a free diffusional process constrained by the neck region of the ISP acting as a peptide tether.

It is not clear if the shift of the *cd1* helix upon docking ISP-HD at the Q_o site is an effect of the inhibitor itself, allowing the 2Fe2S cluster to "come closer" or if the H-bond between the inhibitor and ^{Rh}H156 induces "pressure" of ISP-HD on the structure forcing *cd1* to move. Such a pressure could be an element of the "spring-loaded" mechanism which proposes that H-bond formation between ISP-HD and a substrate present in the Q_o site stores some energy which is released after the reaction and facilitates the dissociation of ISP-HD from the b-position[119].

The involvement of the *cd1* helix in binding of ISP-HD to the Q_o site is also implicated by mutational studies in which ^{Rh}G167, located at the end of the *cd1* and before the *cd2* helix, was replaced by proline. This significantly perturbed the docking of ISP-HD to Cyt*b,* which was reflected in an observed shift in the equilibrium distribution of the ISP-HD toward the c-position [120,121]. As a result, the interaction of 2Fe2S with UQ or UQH_2 at the Q_o site was broken and the enzymatic activity of the ^{Rh}G167P mutant dramatically decreased, abolishing the functionality of the enzyme *in vivo*. Also superoxide generation by the Q_o site increased in this mutant (see section 7.5 for details). Despite these effects, the mutant remained sensitive to stigmatellin. Interestingly, addition of the +1Ala or +2Ala mutation to the ^{Rh}G167P mutant was found to mitigate the inhibitory effects of ^{Rh}G167P mutation to various extent. A remarkable example was the double ^{Rh}G167P/+2Ala mutant in which the equilibrium distribution of ISP-HD was similar to that of single mutant +1Ala mutant, partially restoring sensitivity of the reduced 2Fe2S to UQ at the Q_o site. This brought back some level of functionality to the enzyme *in vivo* even though both single mutations were non-functional. Clearly, the opposite effects of ^{Rh}G167P mutation ("pushing" ISP-HD away from the b-position) and the alanine insertions (arresting ISP-HD at the b-position) can partly compensate one another, establishing that dynamics of the docking/release of ISP-HD to/from cytochrome Cyt*b* can be effectively coinfluenced by the specific interactions at the ISP-HD-Cyt*b* interface and the conformational changes taking place within the neck region. A functional link between these two distinct structural domains was also documented in other mutational studies[122].

Another eye-catching structural element which may somehow influence the ISP-HD movement is the region of the *ef* loop – (Cyt*b*: ^{Rh}286-292, ^{Bt}262-268) a small peptide fragment connecting the transmembrane E helix, the conserved PEWY sequence and the transmembrane F helix[20,55,60]. It is considered to be the main "obstacle" that forms a barrier to ISP-HD on its trajectory from the b- to c-position. The role of the *ef* loop was proposed following the finding that mutations

in this region can compensate the effect of +1Ala[51,53]. Further mutational studies revealed that bulky side chains located in the middle part of the loop limit the ability of ISP-HD to move outside the Q_o site[122]. This leads to the proposal that the *ef* loop acts as a switch increasing or decreasing the rate of electron transfer between the Q_o site and heme c_1[55,103], which together with the *cd1* helix constitutes the mechanism of binding and release of ISP-HD depending on the redox state of hemes *b*[78,86,88,89]. However, as demonstrated by mutational studies, amino acid side chains such as ^{Rh}L286, ^{Rh}I292 on the *ef* loop in fact may serve to resist in transitions between *b*- and *c*-position[55]. The control mechanisms steering this loop during the catalytic cycle is a matter of discussion. The observed effect of modifications on the motion caused by mutations in the *ef* loop does not preclude a simple stochastic model for the movement of ISP-HD in which the mobile loop regions undergo random thermal fluctuations rather than specifically-controlled motion.

Not only the redox state of hemes *b*, but also specific events taking place at the Q_i site have been considered as potential factors that influence the mobility of ISP-HD. In view of topographical arrangement of ISP-HD in the dimer, this would imply a highly ordered communication between monomers which would allow transfer of information over ~ 4 nm across Cyt*b*, possibly through the membranous anchor of ISP that ends in proximity to the Q_i site. Most of the proposals on this type of allosteric influence are derived from analysis of the effects of antimycin bound at the Q_i site. However, as we discuss below, the interpretation of these effects needs to be treated with caution.

Effect of the Q_i site inhibitor, antimycin. Evaluating the influence of antimycin on the basis of crystallographic structures containing antimycin bound at the Q_i site is difficult as the majority of the antimycin-containing structures were obtained with stigmatellin bound at the Q_o site, which overrides any possible structural effects of antimycin on the Q_o site. To our knowledge, until now, there are two PDB crystallographic structures in the database, containing antimycin bound at the Q_i and no other inhibitor at the Q_o site[117,123]. As discussed by Berry and Huang (ibidem), antimycin does not seem to change the ground state of the structure but might change dynamics of the structure[117]. The dynamic change was considered to accommodate several biochemical studies suggesting that antimycin induces effects that might be associated with changes to the different mobility of the domain.

The first series of experiments was based on the susceptibility to proteolytic cleavage of the neck region (between residues ^{Rh}46 and 47) as a sensor of conformational changes taking place in this region. It was found that the cleavage was substantially limited by fixing of ISP-HD at b-position by P_f inhibitors, when compared to the enzyme with P_m or without any bound inhibitors[124]. On the other hand addition of antimycin increased proteolysis, suggesting that this inhibitor induced changes that increased accessibility of this fragment for thermolysin.

The second series of experiments focused on various EPR methods to monitor the FeS. Continuous wave (CW) EPR spectra of microscopically disordered samples containing antimycin- or HQNO-supplemented membranes did not show any significant changes in the spectra when compared to the non-inhibited samples[111]. However, analysis of the samples containing ordered layers of membranes revealed that after addition of antimycin, the angular-dependent amplitudes of g_x and g_y transitions of the 2Fe2S cluster are different from those detected in samples not containing antimycin[88,111]. Pulse EPR measurements with isolated Cytbc_1 showed that the presence of antimycin at the Q_i site caused an increase in distance between the reduced 2Fe2S and oxidized heme b_L[90] and an increase in the efficiency of spin-lattice relaxation of the 2Fe2S cluster *via* two-phonon Raman process. All recognized changes associated with the presence of antimycin at the Q_i site consistently indicate that this inhibitor induces some structural changes that modify the average position of ISP-HD. This effect was interpreted by some authors as evidence for allosteric inter- and/or intra-monomer interactions between the Q_i/Q_n and Q_o/Q_p site that lead to specific sequences of a "duty cycle" of Cytbc_1/b_6f during the catalysis[86–88,125,126].

In our view, the observed effects of antimycin on the ISP-HD are associated with a decrease in the rigidity of the Cytbc_1 structure which decreases the energetic barrier for moving from b- to c-positions. This simple concept assumes that the population of ISP-HD domains is distributed over different conformations and various inhibitors, including antimycin, just modify a barrier for this movement[90]. In fact, pulse EPR measurements revealed that the average position of ISP-HD can be effectively modified by mutations and/or inhibitors and the observed shifts in this position can be placed in the following order (starting from b-position and going further toward the c-position): +2Ala mutant > stigmatellin > Cyt*b*:^{Rh}G167P/ISP:+2Ala double mutant > +1Ala mutant > Cyt*b*:^{Rh}G167P/ISP:+1Ala double mutant > no-inhibitor WT > WT + myxothiazol ≈ Cyt*b*:^{Rh}G167P ≈ WT + antimycin > WT + antimycin + myxotiazol[47,90,120]. In all cases, addition of stigmatellin overrides any other effect, which suggest that the energy of H-bonding between the inhibitor and ISP^{Rh}H156 exceeds the energy associated with changing the structure of the neck region. Although stigmatellin is able to overcome the effects of alanine insertion into the neck region, neither P_m inhibitors (myxotiazol) nor antimycin influence the ISP-HD position in +2Ala mutations[90]. Gathering all these observations we can propose that the strength of factors that influence the ISP-HD mobility can be put in the following order: P_f inhibitors which form H-bonds > conformation of *cd1* helix (^{Rh}G160P mutation) > increase in the length of the neck region > P_m and Q_i inhibitors (myxothiazol, antimycin). The *ef* loop was not included in this list since no direct spectroscopic measurements of distance distribution of ISP-HD were done for mutants in this particular region. However, comparing

the kinetic data and the effect of the redox potential of 2Fe2S, it may be suggested that the energetic barrier of crossing the *ef* loop by ISP-HD is lower than the barrier imposed by +2Ala, comparable with the effect of +1Ala insertion and higher than the barrier imposed by P_m-type or Q_i inhibitors[53,55].

We note that most of the structural studies involving EPR spectroscopy have been performed under conditions for which 2Fe2S was reduced. Although no changes on the surface of the ISP-HD associated with the changes in the redox state of the cluster, were observed[20], the domain with a reduced 2Fe2S appear to show a greater tendency to occupy the b-position compared to the domains with the oxidized 2Fe2S. This is in line with the observation that E_m of 2Fe2S depends on the position of ISP-HD[106].

Effect of movement on redox potential of the 2Fe2S cluster. There are numerous studies showing that the E_m of 2Fe2S depends on interaction between ISP-HD with the Q_o site [50,52,53,106,109,113,114,116]. In general, the greater the tendency for ISP-HD to be at the b-position, the more positive the redox potential of 2Fe2S. For the mutants +1Ala, +2Ala and 6Pro, that were discussed above, the E_m values of 2Fe2S were found to increase by the same order. This could suggest decreased in water accessibility, which changes pK of ^{Rh}H156 (^{Bt}H161). However, the position of the ISP-HD is not alone in influencing the redox potential of 2Fe2S. Another important factor is the interaction of the domain with the occupant of the Q_o site. The most prominent effect is formation of a H-bond with stigmatellin, which increases the midpoint potential by more than 200 mV. Other inhibitors that form a H bond with ^{Rh}H156 of the ISP-HD, such as tridecylstigmatellin or UHDBT, exert a weaker effect on the rise in the redox potential[106]. Also, the presence of Q bound at the Q_o site appears to slightly contribute to a slight increase in the redox midpoint potential of 2Fe2S[109]. However, it should be noted that the effect of Q bound at the Q_o site has been recognized in +nAla mutant but not in WT[109] (see table I in ref [127]). On the other hand, P_m inhibitors such as myxotiazol or MOA-stilebene slightly decrease the E_m value of the 2Fe2S[128]. Thus, it was proposed that H-bonding is the factor which controls the redox potential and stabilizes binding of substrate and enzyme[128].

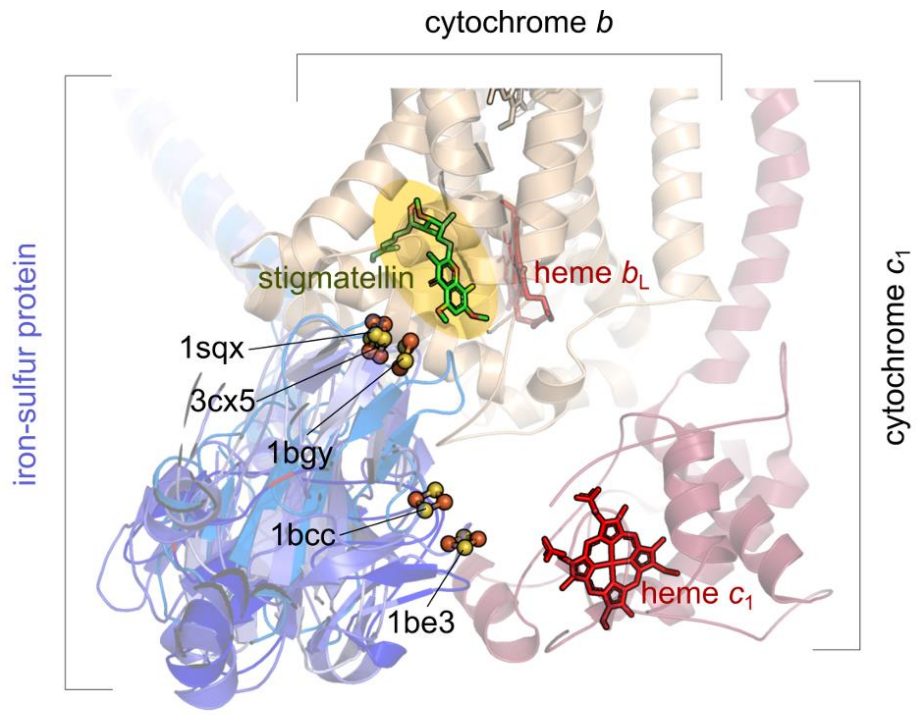

Figure 7. Several crystal structures of Cytbc_1 monomers with different conformations of ISP-HD. The figure shows positions of 2Fe2S clusters (yellow and orange spheres) from the overlaid positions from bovine (PDB IDs: 1sqx, 1bgy, and 1be3), mouse (PDB ID 3cx5) and chicken (PDB ID: 1bcc) crystallographic structures of ISP. Blue, ochre and red ribbons represent ISP, Cyt*b* and Cytc_1, respectively. Hemes are shown as red sticks. Green sticks show the stigmatellin from 1sxq structure bound at the Q_o site (yellow oval).

3.5 Cytochrome bc_1 – specific structural and functional elements

3.5.1 Subunit composition of Cytochrome bc_1

All Cyts bc_1 contain three protein subunits per monomer with redox prosthetic groups: the diheme Cyt*b*, the monoheme Cytc_1 and the ISP (Rieske iron-sulfur protein). Cyt*b* is built of 8 transmembrane helices and contains a relatively high-potential heme b_H and a lower potential heme b_L. Cytc_1 and the ISP are membrane-anchored and their water-soluble, globular domains contain prosthetic groups (high-potential heme c_1 and 2Fe2S, respectively). All these three subunits are necessary for the catalytic function of Cytbc_1. In some bacteria, such as *Paracoccus denitrificans, Rhodospirillum rubrum,* or *Rhodobacter* (*R.*) *capsulatus*, Cytbc_1 contains only these three subunits. Other bacteria, including *R. sphaeroides*, contain a fourth subunit of unknown function that lacks prosthetic groups. [129]

In addition to the catalytic subunits, Cytsbc_1 of mitochondria contain as many as seven (in some yeast) or eight (in bovine and human) supernumerary subunits. The largest supernumerary subunits associate to the catalytic subunits from the mitochondrial matrix side. The functions of the supernumerary subunits are not known, expect for the established mitochondrial processing peptidase

activity of large subunits in plants. The supernumerary subunits are believed to contribute to the increased stability of mitochondrial complexes, but are not required for the electron transfer and proton translocation activities of the enzyme; the three-subunit bacterial enzymes have the same electron transfer and proton translocation functionality as the mitochondrial enzymes.

3.5.2 Structure and spectral properties of hemes b_L, b_H, c_1 and 2Fe2S cluster.

The redox-active components of Cytbc_1 in all organisms are evolutionary conserved within the catalytic core.[1] Remarkably, as shown by the crystal structures of Cytbc_1 from various organisms, the positions of the stationary cofactors, hemes *b* and c_1, are unchanged among them.[21,48,60]

The two *b*-type hemes, (heme b_L and b_H) of Cyt*b* subunit are embedded within the four-helix-bundle, assembling in what appears to be a common (evolutionary conserved) structural motif of many bioenergetic complexes.[130–132] In the Cyt*b* subunit, helices named A-D are involved in bundle formation (Fig. 8 A), with helices B and D providing axial ligands for the heme iron of both hemes (Fig. 8 A,B).[133] Both hemes *b* are axially coordinated by the two conserved histidines (referred to as a bis-His ligation pattern), via bonds between the heme iron and Nε atom of the respective imidazole ring (Fig. 8 B).[48,132]

The heme c_1, is a c-type heme attached to the globular head of Cytc_1 (Fig. 8 C). It is covalently bound to the apoprotein via thioether linkers formed by its two vinyl side chains and two cysteine residues[48,60], belonging to a characteristic CXXCH motif.[134] The heme iron of heme c_1 is axially coordinated by Nε of the conserved histidine from this motif and Sδ of the conserved methionine (referred to as a His-Met ligation pattern).[48,135] Interestingly, in some bacterial species, the ligation of heme c_1 is secured by an additional pair of cysteines, that form a disulfide bond to stabilize the distant loop of the globular part of Cytc_1.[135] However, the freedom retained for conformational rearrangement results in a partial weakening of the methionine ligation when the cytochrome is in its oxidized form, which is reflected in an ability to bind small exogenous ligands, such as cyanide.[136] Removing the disulfide by mutations was found to significantly perturb the conformational stability and further weaken the methionine ligation. As a result, the potential of the heme dropped dramatically (more than 300 mV) and the reduced cytochrome showed a capability to bind carbon monoxide, all of which imply change in the heme ligation pattern[135]. In other Cytochromes c_1, such as mitochondrial Cytc_1, the disulfide is not present. Instead, the βXM structural motif (where β stands for the β-branched amino acid located one residue away from the methionine axial ligand) appears to restrict the conformational flexibility of the domain of the methionine axial ligand to the point that

the binding of external ligands is not observed.[136] Some bacterial Cytsc_1 have both the disufide and the βXM motif.[135,137]

Similarly to the heme c_1, 2Fe2S is attached to ISP-HD and situated between the two loops of the protein backbone, that are hooked by a disulfide bridge formed between two cysteine residues.[138] The cluster is coordinated by the thiolate side chains of the two conserved cysteine residues, acting as ligands for one Fe ion, and Nδ atoms of the two conserved histidine residues, acting as ligands for second Fe ion (Fig. 8 D) [48,138]. This type of [2Fe-2S] cluster coordination by two Cys and two His residues is almost exclusive to ISP of Cyt*bc* and aromatic ring-hydroxylating monooxygenases and dioxygenases.[139,140]

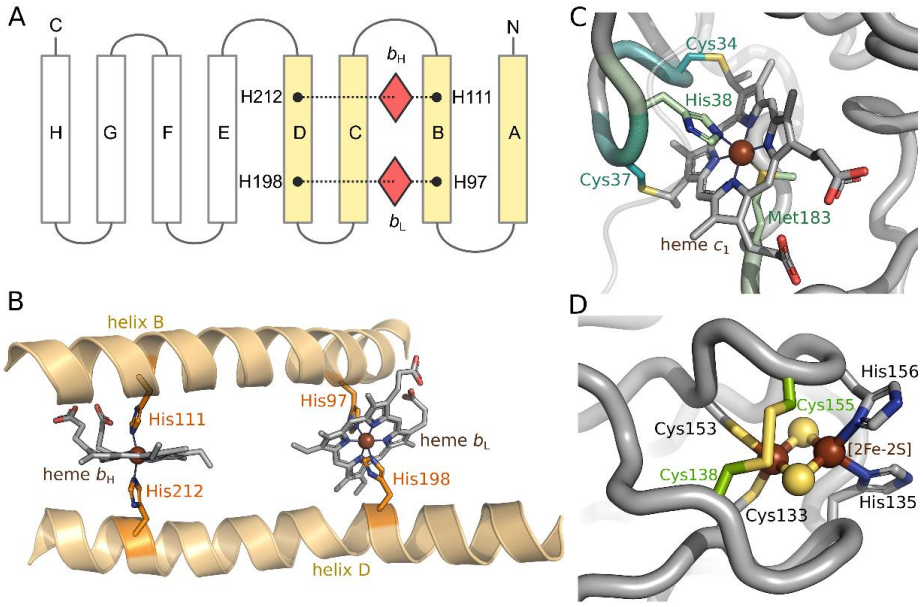

Figure 8. Structural features and binding motifs of metallic cofactors of Cyt*bc*$_1$. A) Schematic representation of the transmembrane part of Cyt*b*, showing helices involved in formation of the heme-bearing 4-helix bundle (A-D, pale orange rectangles). Hemes are shown as orange polyhedrons, positions of axial ligands of hemes are marked by black dots, *R. capsulatus* residue numbering is used. **B)** Structural model showing hemes *b* orientation within the transmembrane bundle and orientation of their axial ligands. Helices providing axial ligands are shown in pale orange cartoon, ligating histidines are colored orange. **C)** Structural model showing heme c_1 binding site in the globular domain of Cytc_1. Cysteines of the binding motif are colored light blue, axial ligands are colored pale green. **D)** Structural model showing the [2Fe-2S] cluster binding site in ISP. Coordinating residues are labeled in black, cysteines that form the disulfide bridge are colored and labeled in green. All representations are based on PDB 1ZRT entry.

Iron atoms in all the hemes of Cytbc_1 are hexa-coordinated and have strong axial ligands (with bis-His and His-Met ligation pattern for hemes *b* and heme c_1, respectively). Therefore, they all exist

in low spin states. In the reduced (ferrous) state, the hemes exhibit partially overlapping α/β absorbance bands in the visible region of the UV-VIS spectrum (Fig. 9 A), with α-band maxima at 560-562 and 552-553 nm for hemes *b* and c_1, respectively [141–144]. The spectral resolution of heme b_H and heme b_L by optical spectroscopy is difficult. In the bacterial Cytbc_1 a deconvolution of the spectra obtained upon redox titration implicates a dominant contribution from the heme b_H at 562 nm and a significantly smaller contribution from heme b_L, which has a split α-peak spectrum with maxima at 564–566 and ~558 nm.[39,145,146] On the other hand, the heme c_1, due to its much higher redox midpoint potential and α-band maximum at a lower wavelength, can be easily isolated spectrally from hemes *b* in the partially-reduced enzyme (Fig. 9 A, in orange).[141] In their oxidized (ferric) state, hemes *b* and c_1 are paramagnetic (S = ½)[147], thus detectable by electron paramagnetic resonance (EPR) spectroscopy at low temperatures (<20 K). All three hemes fall into the HALS (Highly Axial/Anisotropic Low Spin) hemes category, with only their g_z (often called g_{max}) transition being observable by EPR. [132] In general, the bis-His coordinated hemes *b* exhibit a HALS signal when the imidazole rings of the two His residues are nearly perpendicular to each other.[148] In the case of hemes b_L and b_H the angles between the two imidazole ring planes are ~84˚ and ~58˚, respectively[132], which translates into the two separate EPR transitions at $g = 3.78$ and $g = 3.44$, respectively (Fig. 9 B)[149,150]. Thus, EPR, unlike optical spectroscopy, offers a full spectral separation of the two hemes *b*. It is of note that the g_z transition of heme b_H is sensitive to Q_i site occupancy: when the site is occupied by antimycin A (a specific Q_i site inhibitor) or semiquinone radical (SQ_i), the g_z value is shifted to $g =$ 3.47 or 3.42, respectively (Fig. 9 B) [149,151]. In *R. capsulatus* Cytbc_1, the g_z transition of heme c_1 occurs at $g = 3.16$.[152] The exact *g*-values for g_z transitions of each heme may differ among organisms. Some of them were included in Table 1.

organism (reference)	g_z value (concerns Cytbc_1)		
	heme b_L	heme b_H	heme c_1
Rhodobacter capsulatus			
[153]	3.78	3.45	n.d.
[151]	3.78	3.44 (3.47 /antimycin) (3.42 /SQ_i)	n.d.
[152,150]	3.78	3.44	3.16
Rhodobacter sphaeroides			
[153]	3.78	3.49	3.36
Saccharomyces cerevisiae			
[141]	3.76	3.60	3.49
Bos taurus			
[155]	3.79	3.43	3.37

[153]	3.78	3.45	3.35
[154]	3.78	3.44 (3.47 /antimycin)	n.d.
Aquifex aeolicus			
[156]	3.70	3.45	3.55

Table 1. g_z values measured for hemes in selected Cytbc_1 variants.

It is difficult to use optical spectroscopy in studies on the 2Fe2S, as it has no prominent spectrum[157] and its transitions are dominated by the spectra of hemes. The one-electron reduced form ([2Fe-2S]$^{1+}$) is paramagnetic (due to its ground state with S = ½ resulting from the antiferromagnetic spin coupling between Fe^{3+} (S = $^5/_2$) and Fe^{2+} (S = 2) ions) and can only be detected by EPR at temperatures <50K. The fully oxidized ([2Fe-2S]$^{2+}$) cluster is in the EPR-silent (S = 0) ground state (the spins of the two Fe^{3+} ions are spin-coupled).[140,158] The EPR spectrum of the reduced cluster ([2Fe-2S]$^{1+}$) exhibits a unique rhombic symmetry (Fig. 9 C), with transitions at g_z = 2.03, g_y = 1.90 and g_x between 1.78 and 1.76, resulting in the average g value of approximately 1.9.[157] In bacterial Cytbc_1, the shape and the position of the g_x transition was found to be sensitive to the occupant of the Q_o site (whether it is occupied by substrate, or inhibitor or remains empty), the redox state of quinone (whether quinone or quinol are present) and the size of the quinone pool/potential number or quinone molecules at the Q_o site (see section 7.2). For those reasons, EPR analysis of the cluster has proven to be a convenient spectroscopic tool for monitoring the status of the Q_o site.[50,159]

Midpoint redox potentials (E_m) of hemes *b*, heme c_1 and 2Fe2S may vary in different systems, depending on the quinone derivatives employed by the organism to serve as electron/proton carriers. In organisms using menaquinones, they are usually lower than in organisms that employ ubiquinones.[160] However, a general rule can be drawn, that the hemes *b* have much lower E_m's than 2Fe2S and heme c_1. For this reason, the chain of cofactors built by hemes *b* is referred to as a low-potential chain, while that formed by the 2Fe2S and heme c_1 – high-potential chain. The large gap in potential between components of the high- and low-potential chains is crucial for electron bifurcation and efficiency of the catalytic cycle (see section 7.4). Among the hemes *b*, heme b_L has lower E_m (-290 to -50 mV) than heme b_H (-160 to 100 mV).[21,160] This difference in E_m's of the hemes *b* is evolutionary conserved. [149,160] It is generally assumed to facilitate cross-membrane electron transfer and assist in overcoming the barrier of membrane potential.[161,162] However, such a function becomes less obvious in light of recent studies demonstrating that the difference in E_m's of the hemes *b* is not required to support the *in vivo* and *in vitro* functionality of the enzyme.[149] Interestingly, E_m of heme b_H depends on the occupant (and the redox state) of the Q_i site. When the Q_i site is occupied by Q, heme b_H has a higher potential than when the site is occupied by SQ_i. This results in a biphasic titration

of the heme. [163] However, when the Q_i site is occupied by an inhibitor, the b_H titrates as a single species.[163,164] The 2Fe2S and the heme c_1 usually have close values of E_m, both falling in range of 100 to 350 mV. [21,160] Some of the known values of E_m for each of cofactors in various organisms were included in Table 2.

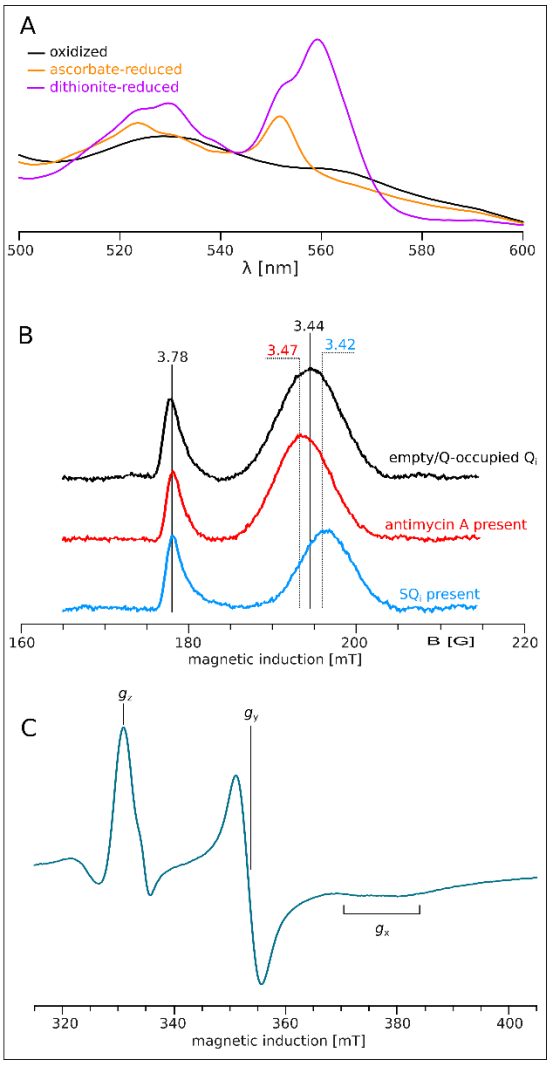

Figure 9. **Spectral features of Cyt*bc*$_1$ redox cofactors. A)** Optical spectra of α/β-band region of hemes. Spectrum of the fully oxidized enzyme is shown in black, spectrum after reduction with sodium ascorbate is shown in orange (showing prominent contribution from heme c_1) and spectrum of the fully reduced enzyme (with dithionite) is shown in magenta. **B)** EPR spectra of g_z transitions of hemes b_L and b_H in an air-oxidized sample (top), sample of the enzyme inhibited with antimycin A (middle) and a sample with generated SQ_i (bottom). Numbers indicate *g* values. **C)** EPR spectrum of a one-electron reduced [2Fe-2S] cluster in isolated Cyt*bc*$_1$.

Organism (reference), [pH]	E_m value [mV] (concerns Cyt*bc*$_1$)			
	[2Fe2S]	heme c_1	heme b_L	heme b_H*

Rhodobacter capsulatus				
[150], [7.0]		+295	-138	+43, +134
[163], [7.0]			-137	+35, +202
[104], [7.0]		+335		
[135], [7.0]		+320		
[51], [7.0]	+310			
Rhodobacter sphaeroides				
[143], [7.0]	+280/+325	+240	-100	+48
[170], [7.0]		+237	-87	+41
Rhodospirillum rubrum				
[142], [7.4]		+320	-90	-30
Paracoccus denitrificans				
[165], [n.d.]	+265	+190	-95	+30, +120
Aquifex aeolicus				
[156], [7.0]	+210	+160	-190	-60
Saccharomyces cerevisiae				
[166,167]. [7.0]	+285		-60	+82
[168] [7.4]	+286	+270	-20	+62
Bos taurus				
[21], [7.0]		+238	-83, -60	+26, +85
[169], [7.0]	+250	+230	-30	+100

Table 2. E_m values of redox cofactors in selected Cytbc_1 variants.

* Two values of E_m for heme b_H results from two-component fit to data obtained for Cytbc_1 without antimycin.

3.6 Cytochrome b_6f – specific structural and functional elements

The discussion of structure-function of Cytb_6f is based on a high resolution (2.50 Å) crystal structure (PDB ID: 4OGQ) of the complex. The complex consists of a 250 kDa hetero-oligomeric intra-membrane lipo-protein complex containing, per monomer, thirteen transmembrane α-helices and seven prosthetic groups, the latter consisting of five hemes, one chlorophyll *a* molecule and one β-carotene. In addition, each monomer contains 23 lipid binding sites, the function of which involves a new area of research into the structure-function of intra-membrane proteins, both for Cytb_6f and the entire field of membrane proteins.

Comparison of Cytochromes f and c_1. In contrast to the conserved nature of Cyt*b*, for the Cytc_1 and Cyt*f*, except for the single transmembrane helix (TMH) which binds the subunit to the membrane, the structures are different. The only conserved sequence segment is the CXXCH motif, responsible for covalent binding of the *c*-type heme. The *p* side heme binding domain has a completely different secondary structure, β sheet and α-helical, respectively in Cyt*f* and Cytc_1 [171,172]. In fact, all three of the *p* side electron transfer proteins which are part of Cytb_6f, or interact with it, the ISP, Cyt*f*, and PC,

which mediate electron transfer between the quinol hydrogen donor and the P700 PSI reaction center are predominantly in the β-conformation. Both Cyt*f* and Cytc_1 have a relatively positive potential, + 370 mV and + 260 mV, respectively, sufficient to provide an oxidant for the ISP.

3.6.1 Subunit composition of Cytochrome b_6f

Crystal structures have been obtained for the Cytb_6f from the green alga, *C. reinhardtii* [41] and cyanobacteria[42,46,65–67,173,174].

The crystal structures of the mitochondrial and bacterial Cytbc_1 contain 11 and 3 or 4 polypeptide subunits, respectively, compared to 8 in the Cytb_6f from cyanobacteria [42,174] and the green alga, *C. reinhardtii* [41]. This subunit count refers to those which remain after the purification and crystallization procedures, and does not include relatively weakly bound peptides which may be important for function but are lost during purification and crystallization. Molecular weights (MW) and pI values for the 8 core subunits of Cytb_6f are summarized in table **Erreur ! Source du renvoi introuvable.**.

Subunit	MW (kDa)*	pI
Cyt*f* [a]	30.9	4.7
Cytb_6 [a]	24.7	8.5
ISP[a]	19.3	5.3
SubIV[a]	17.5	7.8
Pet G[a]	3.9	8.1
Pet L[a]	3.2	9.9
Pet M[a]	3.5	4.3
Pet N[a]	3.3	9.5
FNR[b]	35.4	6.3
PetO[c]	15.1	9.6
PetP[d]	7.4	8.2

[a] From cyanobacterium *Nostoc* sp. PCC 7120; [b] PetH; resolved on SDS-PAGE, spinach prep; MW, *A. Thaliana*; [c] PetO, *C. reinhardtii* ; [d] PetP, *A. platens*

Table 3: Parameters of Subunits of Cytb_6f

Subunits containing redox prosthetic groups with a high degree of conservation between Cytb_6f and Cytbc_1 are: (i) Cyt*b* in the Cytbc_1, which is equivalent in many structure-function aspects to Cytb_6 and subunit IV in the Cytb_6f [175] ; and (ii) the high potential ($E_{m,7}$ = + 300 mV) 2Fe2S, often

called the "Rieske" protein because of the origin of its discovery [176]. The protein subunit containing the covalently bound *c*-type cytochrome, Cyt*f* and Cytc_1, respectively, is not conserved between Cytb_6f and Cytbc_1 complexes.

The Four Small Peripheral Subunits, Pet G, L, M, and N. A unique lattice of four short (3.3 – 4.1 kDa), single TMH "hydrophobic sticks," denoted as PetG, PetL, PetM, and PetN (Table 3), provides a hydrophobic lattice, or "picket fence," around each monomer, a structure which is unique among all known integral membrane protein structures. Of these four subunits, PetM [177], along with the ISP, are the only subunits among the thirteen in the complex that are nuclear-encoded. Specific functions of these four subunits are not defined, although PetL interacts sterically with the TMH of the ISP and may provide a constraint on the membrane-spanning orientation of the latter. The position of much of the lipid in the complex (Fig. 12) between the Pet picket fence and the conserved Cytb_6-subIV core of the complex suggests a "boundary lipid" function and that the "picket fence" may have been added to the core of the complex relatively late in the evolution of the complex.

3.6.2 Structure and spectral properties of hemes *b*, *f*, c_n and 2Fe2S cluster.

High resolution structures of a C-terminal soluble domain of the 250 residue extrinsic C-terminal domain of Cyt*f* [171,172], and of the N-terminal soluble domain of the ISP[178], were obtained prior to their determination in the intact multi-subunit complex. The crystallized complex is a symmetric (C2 symmetry) dimer that consists of eight transmembrane polypeptide subunits in plants, green algae, and cyanobacteria [42]. The analogous Cytbc_1 consists of eleven subunits in the yeast, PDB 1KYO [68] and bovine, PDB 1QCK, 1BE3 [60] complex, and three in the complex from the photosynthetic bacterium, *Rhodobacter sphaeroides* [63]. In all cases, the dimeric structure of the complex is required for a physiologically significant electron transfer activity, 250 – 400 electrons transferred (Cyt*f*/sec)$^{-1}$ [179–181]. This is possibly because of a defined inter-monomer quinol entry pathway.

A ribbon diagram of Cytb_6f (PDB 2ZT9, 4H44, 4OGQ) derived from crystal structure analysis of the cyanobacterium *Nostoc sp*. PCC 7120 [65,66,174], is shown in 2 views differing by a 180° rotation in order to display more clearly the arrangement of the 8 subunits that span the membrane with 13 TMH per monomer containing 7 prosthetic groups, including 5 with redox function consisting of 4 hemes, one 2Fe2S, one chlorophyll *a* [182] and one β-carotene [183] (fig 10 A, B and fig. 11). These features were confirmed in a lower resolution (3.6 Å) cryo-EM structure of the spinach Cytb_6f.[73]

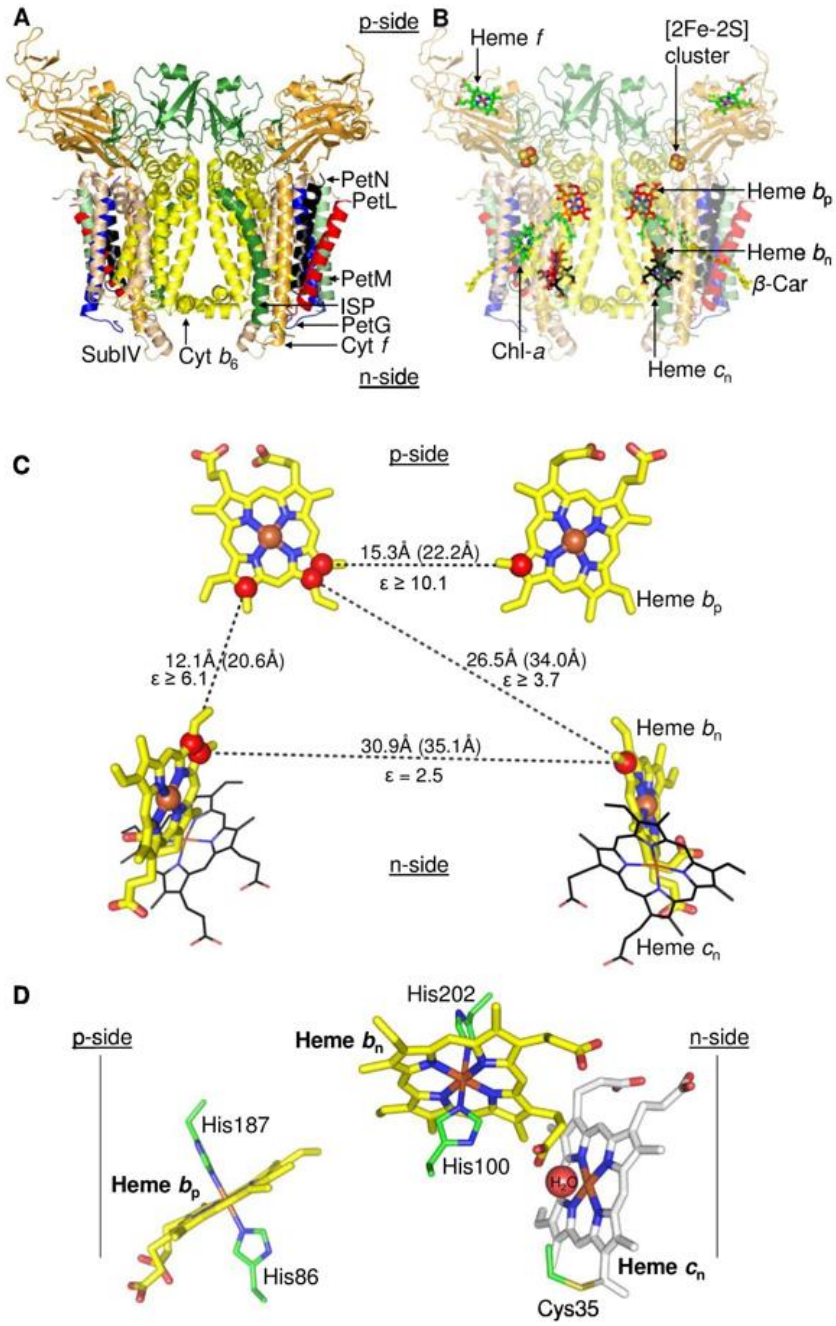

Figure 10. The Dimeric cytochrome b_6f complex. (**A**) Polypeptide subunits from the cyanobacterium *Nostoc* sp PCC 7120 (PDB ID 4OGQ) are shown in ribbon format- Cytb_6 (yellow), subIV (light brown), Cyt*f* (orange), ISP (dark green), PetL (red), PetM (light green), PetG (blue), PetN (black). (**B**) Prosthetic groups of Cytb_6f. Transmembrane hemes b_p, b_n (red/blue), and c_n (black/blue) are shown as sticks. On the *p* side, heme *f* (green/blue) is shown as sticks, the [2Fe-2S] cluster as spheres (brown/yellow), and the Chl-*a* (green/blue) and *β*-car (yellow) as sticks. (**C**) Heme-heme distances within the transmembrane domain of the complex (PDB ID 4OGQ). Distances shown as black dashes. Heme edge-edge, and center-center (Fe-Fe) distances are shown, respectively, outside and inside parentheses (selected atoms shown as spheres). The dielectric constant, εij, between each pair of hemes, $\varepsilon_{n1,p1}$, $\varepsilon_{n1,p2}$, $\varepsilon_{n2,p1}$, etc. [184] is shown. (**D**) Transmembrane heme ligation in Cytb_6f. The central Fe atom of heme b_p and b_n is axially ligated, respectively, by residues His86/His187 and His100/His202 which bridge the B and D TMH of Cyt*b*, Heme c_n is covalently attached to the protein via Cys35. Heme c_n is unique as it lacks an amino acid axial ligand, and the central Fe-atom is penta-coordinated. The sole ligand of

heme c_n, is provided by H_2O or OH^- on the heme b_n side. Fe of heme c_n separated by 4.0 Å from a propionate oxygen of heme b_n, which results in electronic coupling, a high spin g =12 EPR signal [43,185], and an oxidase-like reaction with nitric oxide [186]. Electrochemically positive, negative sides of membrane labeled p, n. (Reprinted/adapted by permission from Springer Nature,Cytochrome Complexes: Evolution,Structures, Energy Transduction, and Signaling; Structure-Function of the Cytochrome b6f Lipoprotein Complex by William A. Cramer, S. Saif Hasan, 2016).

Figure 11. High potential electron acceptor of Cyt-*bc*: Cyt*f* of Cytb_6f (**A, B**) and Cytc_1 of Cytbc_1 complex (**C, D**). Cyt*f* and Cytc_1 are attached to the respective complexes and membrane through one TMH. Cyt*f* binds *c*-type heme (heme *f*, red/blue sticks) in the *β*-sheet extrinsic domain. Cyt*f* extrinsic domain of Cytc_1, with c-type heme (heme c_1, red/blue sticks) is mostly *α*-helical. **B** and **D** rotated 90° about horizontal axis relative to **A, C**. **E,** tridecyl-stigmatellin (TDS, blue sticks), bound in an 11 Å long channel of Cytb_6 (purple) terminating proximal to the 2Fe2S cluster. The Q_p-portal in Cytb_6f is marked as the black rectangle. ISP-HD is shown as orange ribbons. A chlorophyll molecule (Chl *a*), inserted between F and G helices of subunit IV (cyan), using its phytyl tail, functions as a gate for quinol/quinone traffic in the Q_p-portal. Drawing by S. Saif Hasan

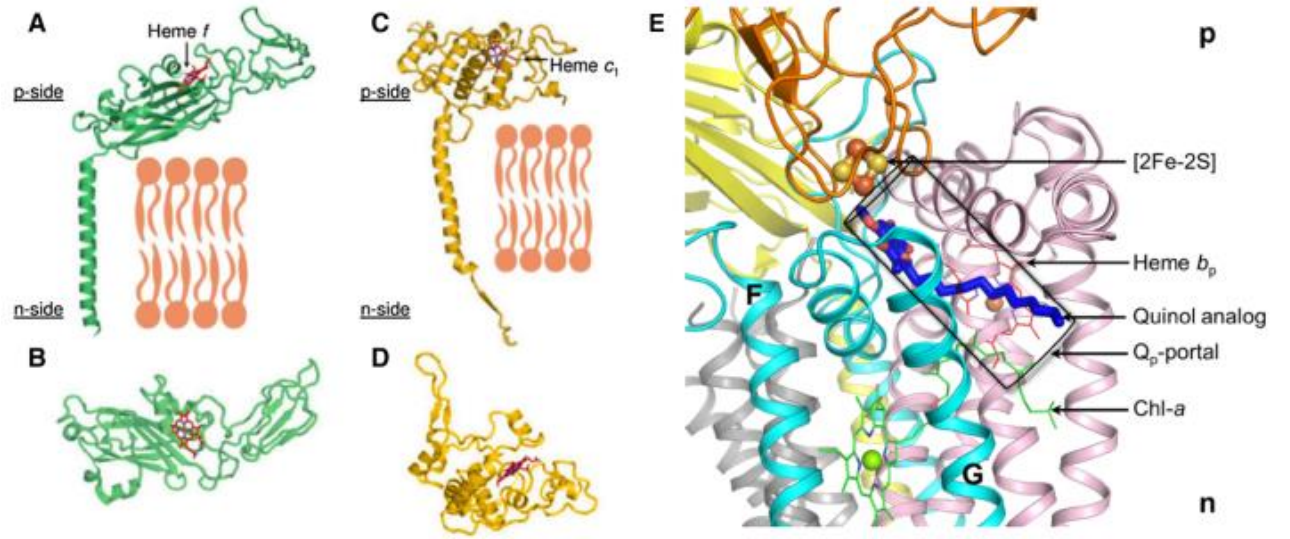

Unique Chlorophyll a and β-Carotene. The presence of a single chlorophyll *a* [182,187,188] and β-carotene [183] in each monomer of Cytb_6f is enigmatic. The β-carotene is separated by 14 Å from the chlorophyll [41,42], too large to allow β-carotene to quench a chlorophyll excited triplet state [189]. (ii) The β-carotene protrudes by approximately 11 Å from the complex between the TMH of Pet G and Pet M.

Transmembrane Hemes, b_n and b_p. The four TMH of the Cytb_6 are connected by loops at the *p* and *n* side membrane interfaces. SubIV (~17 kDa) has three TMH (E–G) that form a *p* side saddle around the four helix bundle of Cytb_6. Helix E of SubIV is located in proximity to the A- and B-helices of Cytb_6 while the F and G-TMH span the four helix bundle, close, respectively, to the C, D and B-TMH (Fig. 12). The C-terminus of the E-TMH is separated from the N-terminus of the F-TMH by a distance of ~40 Å, which is bridged by the *p* side *ef*-loop. This seven TMH assembly forms the

conserved core of Cytb_6f, which is bounded in each monomer by the four subunit hydrophobic "picket fence".

The arrangement of the two pairs of transmembrane *b*-hemes, b_p and b_n, with inter-heme edge-edge and center-center (Fe-Fe) distances (in parentheses) is shown (Fig. 10), along with the heterogeneity of the inter-heme dielectric constants [184], and the complex of heme b_n with a skeleton of the covalently bound *c*-type heme c_n [43,185,186,190,191]. The heme b_n-c_n complex, a unique feature of the Cytb_6f compared to the Cytbc_1, in which the close proximity of the two hemes results in sharing of the 3d electronic shells is displayed in a g = 12 EPR signal[43,185].

Hemes, b_n and b_p, Oxidation-Reduction Potentials. Determination of the oxidation-reduction potentials of these hemes in Cytbc_1 are consistent in showing a separation of 100-150 mV between the E_m's of the two hemes, which are thus often labeled b_H and b_L (high and low potential hemes). For the two hemes in the Cytb_6f, there is disagreement as to whether the E_m's of the two hemes are [191] or are not [40,192] separable in a redox titration of thylakoid membranes. A simulation shows that a midpoint potential difference of 50 mV or less of a one electron titration cannot be resolved. For the isolated complex, the midpoint potentials of the two hemes in the Cytb_6f are separated by approximately 90 mV.

Reducibility of b Hemes; Heterogeneity of Internal Dielectric Constants. Excitonically split circular dichroism (CD) spectra of the Cytbc_1 [193] and the Cytb_6f [184,194] arise from interactions of the reduced hemes. Determination of the time course of heme reduction and the onset of the split CD spectra for the isolated complex shows that the heme pair that is preferentially reduced is the intra-monomer pair, b_p and b_n. This result contrasts with that which is expected. If heme b_n, whatever its exact redox potential, has a more positive potential in isolated Cytb_6f than heme b_p, the two hemes b_n should be preferentially reduced under equilibrium conditions. The straight-forward explanation is that the protein medium between hemes b_p and b_n is more polarizable, i. e., has a higher dielectric constant, than the medium between the two hemes b_n [184] implying that the dielectric constant in the complex is heterogeneous and anisotropic.

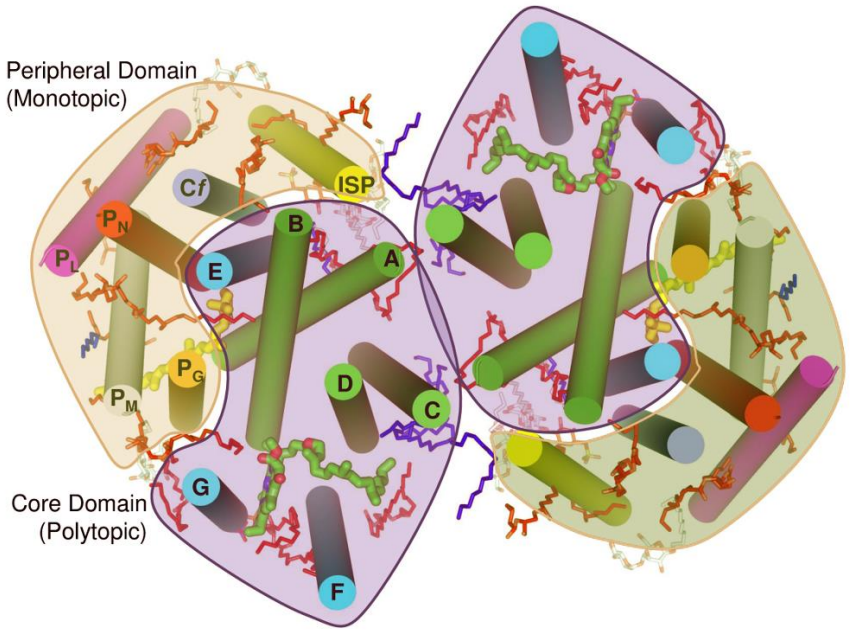

Figure 12. Transmembrane helices and distribution of lipid in Cytb_6f complex (Figure drawn by S. Saif Hasan). Reprinted/adapted by permission from Springer Nature,Cytochrome Complexes: Evolution,Structures, Energy Transduction, and Signaling; Structure-Function of the Cytochrome b_6f Lipoprotein Complex by William A. Cramer, S. Saif Hasan, 2016.

The unique heme c_n at the *n* side quinone (Q_n) binding site of Cytb_6f [173,191], located in close (4 Å) proximity to heme b_n, constitutes a major structure difference between Cytbc_1 and Cytb_6f complexes. Consequently, it would also imply a difference, compared to the mitochondrial and bacterial Cytbc_1, in the details of the involvement of heme b_n in the transmembrane electron transport pathway [*n.b.*, heme c_n is designated heme c_i in the *C. reinhardtii* crystal structure, which first emphasized its unique existence in the structure of Cytb_6f [41]].

Heme c_n has no axial ligand on the heme surface facing the intermonomer cavity. As shown by EPR studies which document its open axial ligand position [186], and co-crystallization of the Cytb_6f complex with quinone analog inhibitors [173], it has been inferred that heme c_n serves as the *n* side quinone binding site (Q_n site). The Q_n site is located closer to the membrane–water interface in Cytb_6f complex than in the respiratory Cytbc_1, as noted in the original crystal structure [41]. This surface-proximal location of the Q_n site implies that a short pathway may suffice for proton conduction to the *n* side bound quinone from the *n* side aqueous phase. The crystal structure of Cytb_6f from the filamentous cyanobacterium *Nostoc* PCC 7120, revealed a unique anhydrous Asp20→Arg207

(Cytb_6) pathway for proton conduction from the *n* side aqueous phase to the Q_n site for reduction and quinone protonation [66].

ISP Electron Transfer; a p Side Conformation/Mobility Problem. One remaining structure-function problem is that the closest approach distance of the Cyt*f* heme to 2Fe2S in Cytb_6f is 28 Å, which is much too large to support physiologically meaningful millisecond electron transfer rates [195,196]. How, then does 2Fe2S of ISP transfer electrons to Cyt*f*? A major gap in understanding of the *p* side electron transfer reactions for the Cytb_6f results from the absence of the structure data that would allow kinetically competent electron transfer from 2Fe-2S to the heme of Cyt*f*. Given the documented conformation change determined from crystal structure data for the avian mitochondrial Cytbc_1 (see section 3.4 for details), electron transfer from 2Fe2S to the Cyt*f* heme must involve a rotational-translational conformational change in the ISP [66].

3.6.3 Lipid content and other subunits

Lipids in the Cytb_6f Lipoprotein Complex. **(i)**'Boundary lipids' define a domain structure. Because the conserved Cytb_6-SubIV core of the complex is separated by a lipid layer from the "picket fence", it is implied, as noted above, that the "picket fence," was added to the core structure at a later stage in the evolution of the Cytb_6f, perhaps to facilitate interaction with the reaction center complexes. As noted above, the β-carotene, which protrudes from the surface of the picket fence, may act as a "latch" to facilitate super-complex formation with the PSI reaction center complex [197].

Lipid Content The dominant lipid species in plant Cytb_6f are monogalactosyl-diacylglycerol (MGDG), digalactosyl-diacylglycerol (DGDG), phosphatidyl-glycerol (PG) and sulfoquinovosyl diacylglycerol (SQDG). The galactolipids (MGDG, DGDG and SQDG) and phospholipids dilinolenoyl-,phosphatidyl glycerol (DLPG), 1,2-dioleoylphosphatidylglycerol (DOPG) and 1, 2 dioleoyl-sn-glycerol-3-phosphatidylcholine DOPC) stabilize the Cytb_6f to a varying extent [198].

PGRL Components. A 35.7 kDa (pK = 5.2) protein, "PGRL1," is present at unknown stoichiometry in the PSI super-complex *C. reinhardtii* [197], and at a stoichiometry comparable to, although smaller (0.5:1), that of ISP in *Arabidopsis thaliana, and* has been inferred to be the ferredoxin-quinone reductase [199]. The absence of the protein results in a partial decrease of the chlorophyll fluorescence yield that results from reduction of the quinone pool. The redox function is believed to be derived from the six cysteine residues in the protein, perhaps in conjunction with iron that is present in the preparation. PGRL1 is also inferred to be able to bind to the Cytb_6f [199], although it has not been detected in mass spectroscopic analysis of isolated Cytb_6f [200]. In addition, it is noted: (a) the fluorescence yield effects ascribed to PGRL1 are perhaps not quantitative indicators of an

obligatory function in the ETC, as they involve changes of a factor of 2-3 on a time scale of 10 seconds, approximately a factor of 1000 times slower than the rate-limiting step of electron transport in this region of the ETC; (b) the rate of P700 reduction, a standard kinetically competent assay for cyclic electron transport, in the presence and absence of the peptide has not been reported. (c) Details of the chemical nature and quantitative properties of the hexaCys-Fe redox moiety in PGRL1, proposed to serve as the redox group responsible for FQR activity, are not presently available. The significance of the PGRL1 components may need to be re-evaluated in light of the recent information on their very diminished stoichiometry relative to the known electron transport components [201]

3.6.4 Q cycle in cytochrome *b*$_6$*f*: mechanism and controversies

The observation of oxidant-induced reduction [202] in Cyt*bc*$_1$ (see details in section 7), and measurement of a greater than unity ratio of coupled protons translocated to electrons transferred, $H^+/e > 1$, was important in the formulation of the 'modified Q cycle' mechanism [39], whose general formulation and application to photosynthetic membranes [27] followed 15 years after the original inference of the chemiosmotic concept of membrane energization [28]. The demonstration of oxidant-induced reduction of Cyt*b* heme in the mitochondrial Cyt*bc*$_1$ and the requirement in this electron transfer reaction for the high potential (ca. +0.25 V) 2Fe2S was elucidated in studies by B. Trumpower [203]. An apparently anomalous reduction of the Cyt*b* component was observed in a preparation of mitochondrial membrane protein 'complex III'. Support for the Q cycle model ofr proton translocation in the mitochondrial Cyt*bc*$_1$ was provided in studies by Wikstrom and Saraste [204], and Rich [205].

Support for the application of Q cycle model to Cyt*bc*$_1$ in the purple photosynthetic bacteria has been well documented and discussed extensively in reviews [1,2,13,39,117,118,206–208]. Studies on function and, lately also the structure of the related Cyt*b*$_6$*f* functioning in chloroplasts, green algae, and cyanobacteria, have been reviewed in the last decade [17,19,22,184,209–216].

While there is a general consensus on the occurrence of the "modified Q cycle" in the case of Cyt*bc*$_1$,(see section 3.2 for details) experimental evidences exist that are not completely in agreement with this hypothesis in the case of Cyt*b*$_6$*f*. In the following, we summarize this evidence, compare contrasting results, and summarize different interpretations of the results.

Arguments which imply that the PQ/PQH$_2$ cycle in Cyt*b*$_6$*f* is different from the "modified Q cycle" proposed for regeneration of UQH$_2$ through function of Cyt*bc*$_1$ in the respiratory chain and photosynthetic bacteria are:

i) the presence of an additional heme c_n, which could act as a PQ reductase. Based on its redox

properties and location within the complex, this heme could catalyze the injection of an electron into the quinone binding side using stromal reductants as a donor (i.e. the presence of ferredoxin: $NADP^+$ reductase (FNR) bound to purified plant (spinach) Cytb_6f, see below). The electronic coupling between hemes b_n and c_n, would imply that PQ reduction need not proceed through a semiquinone intermediate but perhaps cooperatively through hemes b_n and c_n, providing protection against the formation of superoxide and other reactive oxygen species. This mechanism is not compatible with the modified Q cycle mechanism, but, as introduced in section 3.2, it is actually consistent with the original mechanism of the Q cycle as proposed by Mitchell (see Mulkidjanian [19] for a discussion) (see also Fig. 4).

The possibility of direct injection of stromal electron in the *b* hemes could also account for another observation that is not entirely compatible with the modified Q cycle in Cytb_6f:

ii) the 'slow' electrochromic phase attributed to oxidation of the PSQ in the Q_p site and transfer of its electron across part of the low dielectric membrane to reduce the intra-membrane *b* hemes is also observed when the hemes were chemically reduced and therefore not able to function as an electron acceptor [192]. In principle, injecting 1 electron into the stromal site via the heme c_n would allow oxidation of one *b* heme, generating one PQH_2 and regenerating the Q cycle (the so called 'activated' Q cycle mechanism, [19]). Note, however, that another explanation has been proposed by Joliot and Joliot, who suggest that the slow electrochromic phase observed in reducing condition could reflect the transmembrane movement of a charged SQ, (the SQ cycle hypothesis, [217], see however [218] for a different view). This mechanism may represent an adaptation to reducing conditions when no Q is available at the Q_n site. Note, however, that some inhibitors of Cytb_6f (NQNO, stigmatellin and MOA-stilbene) act on the *n* side at the side of heme c_n that faces the quinone-exchange cavity, as shown in crystal structure[173] and prevent oxidant-induced reduction in Cytb_6f, in agreement with the modified Q cycle hypothesis.

iii) the initial slope of the 'slow' electrochromic phase shows a pronounced isotopic effect, being slowed four-fold by a H_2O/D_2O substitution, in contrast to the redox-reactions of Cyt*f* and Cytb_6 that were only slightly affected [219]. These findings have led to the hypothesis that proton pumping across Cytb_6f could be triggered by the oxidation of PQH_2 [220], an idea that is not conceived in the frame of the 'modified' Q cycle, but that is supported by the analysis of Cytb_6f mutants of *Chlamydomonas* [221].

iv) one component of the 'driving force' for the Q cycle in mitochondria and the purple photosynthetic bacteria is the pronounced difference (> 100 mV) in the redox potentials of the two b-type hemes, (i.

e., b_L and b_H) which span the membrane. However, it has not been possible, in redox titrations done *in situ*, i. e., in thylakoid membranes to define, through anaerobic redox titrations a difference in midpoint redox potentials of the two *b* hemes, b_p and b_n [40,192,222]. More recently, however, Alric and colleagues used a different approach for redox titrations and found E_m differences between the two *b* hemes of isolated Cytb_6f from *Chlamydomonas* (-130 mV and -35 mV)[191], which are closer to those predicted by the 'modified' Q cycle. Thus, an E_m difference is seen for the isolated Cytb_6f complex, but this difference is not clear in titrations done *in situ*, in membrane preparations.

v) studies on the kinetics of heme *b* reduction show that an intramonomer pair (hemes b_n and b_p) is reduced first, rather than the two hemes b_n being preferentially reduced as implied by the Q cycle [184]. Moreover, reduction of the two *b* hemes is not observed with repetitive laser flashes [40].

vi) The existence of CET in oxygenic photosynthesis could help to maintain a high H^+/e^- ratio, as required for proper CO_2 assimilation, thereby making the occurrence of a Q cycle less stringent in photosynthesis than in respiration. One of the main purposes of the Q cycle is to couple electron and proton transfer generating a H^+/e^- ratio = 2 for proton translocation across the complex. Thus, the transfer through the high potential chain of the Cytb_6f of the 4 electrons arising from water splitting and oxygen evolution can result in the translocation of 8 protons into the chloroplast lumen which, together with the 4 translocated protons released into the lumen with each O_2 molecule, would provide 12 of the 14 H^+ needed to drive a full rotation of the rotatory c-ring of the chloroplast ATP synthase and therefore the synthesis of the three ATP molecules needed to fix a CO_2 molecule. In plants, the additional 2 H^+ could be generated by CET, assuming that it runs at a prescribed rate of 25 % of the linear non-cyclic pathway. Applying the same reasoning to the cyanobacterium, *Spirulina platensis*, where the ATP synthase c-ring contains 15 subunits, implies that CET would have to run at 3/8 or 37.5 % of the rate of the linear pathway to generate the additional three H^+ needed to drive a complete rotation. However, no such percentage of CET is observed in most photosynthetic organisms, at least under steady state conditions (see section 10). This suggests that CET alone, is not sufficient to provide the 'extra' H^+ for ATP synthesis. Consistent with this conclusion, Kramer and colleagues measured the H^+/e^- ratio illumination in intact tobacco leaves and found that it was constant under low to saturating illumination. Therefore, they inferred that this ratio was maintained by a continuously engaged, proton-pumping Q cycle at Cytb_6f [223]

Although, the Q cycle mechanism has a readily conceived role in contributing to the transmembrane proton flux required to provide ATP levels commensurate with the need

for CO_2 assimilation, it may be suggested that the Q cycle mechanism applied to Cyt b_6f is not obligatory (see however Cape et al, [224] for a different conclusion). An alternative mechanism is a membrane Bohr effect, a mechanism which is prominent in the description of the mechanism of proton pumping in the classical bacteriorhodopsin system [225], and which has been applied to the problem of proton translocation in the mitochondrial cytochrome *c* oxidase[226].

3.6.5 An additional electron path related with cyclic electron transfer in photosynthesis

Electrons generated at the PSI reducing side can be re-injected into its donor side via the CET pathway. Discovered by Arnon in the 50's [227], this process is now considered as a relevant mechanism to counterbalance over-reduction of the PSI acceptor side [228] and to inject 'extra' protons into the thylakoid lumen, to adjust the ATP/NADPH ratio for CO_2 assimilation. Although the ratio of ATP/NADPH generated by LET is still uncertain [229], it could be insufficient to fuel CO_2 accumulation in chloroplasts and its assimilation via the Calvin, Benson and Bassham cycle (see Allen 2002 [230] for a discussion). In *viridiplantae* (including green algae and higher plants) CET could be the main route to optimise this process, by bypassing NADPH production while permitting the formation of the pmf, and therefore ATP synthesis.

Two main pathways have been proposed for CET (see section 10 for further details). The first one involves the activity of a chloroplast NAD(P)H dehydrogenase (NDH) complex (review in Peltier et al. [231]). In plants, this enzyme has similar characteristics to the mitochondrial complex I, while mainly sharing features with bacterial complex one in algae [232]. The plant complex would mainly use Fd as an electron donor, while the algal counterpart (Nda2 complex) uses NADPH as a source of electrons in the green alga *Chlamydomonas reinhardtii* [231].

The second CET pathway would correspond to the so called Ferredoxin-Quinone Reductase complex (FQR), the existence of which was proposed by Bendall and coworkers in the 90's [233], based on the effect of antimycin – a putative inhibitor of this complex – on photosynthetic electron flow. An alternate target of antimycin in the chloroplast has been proposed by Sugimoto and colleagues as PGR5, a thylakoid protein [234] previously identified as a component of the CET pathway by a genetic screening or the *Arabidopsis thaliana* [235]. The FQR complex itself has been putatively identified as a membrane complex [199], containing PGR5 as well as PGRL1, another protein previously invoked as an essential component of the CET machinery in plants [236]. However, see the critique of these studies in section 3.6.4.

Alternatively, the FQR may correspond to Cytb_6f itself, mediating electron flow from reduced Fd to the PQ(H_2) pool through the additional *c* heme in the stromal pocket [41,42]. This pprocess could take place thanks to the interaction between the cytochrome complex and the Ferredoxin-NADP Reductase (FNR) enzyme (see section 4.3).

4 Characteristics of substrates for cytochrome bc_1 and b_6f

As a main function of Cyt*bc* is the generation of proton motive force utilizing energy associated with electron transfer from low-potential electron donors (membranous pool of quinone derivatives) to water soluble c-type cytochrome (*c*, c_2, c_6) or plastocyanin, it is worth introducing basic information on the substrates that are used by these enzymes. A brief summary on structure and redox properties of quinones is especially important as proton translocation and electronic bifurcation is largely associated with quinone chemistry.

4.1 Basic redox properties of Quinones

A role of quinones in electron transfer between membranous respiratory complexes was first proposed by Crane et al. in 1957 [237,238]. It was shown that extraction of relatively low-weight molecules – ubiquinones from the membrane completely abolished the process of electron transfer within the mitochondrial respiratory chain[239]. In biology, the most widespread quinones belong to a family of 1,4-benzoquinone derivatives. While in eukaryotic cells quinones are generally restricted to ubiquinones (in mitochondria) and plastoquinones (in chloroplasts), prokaryotic organisms can use several other quinone derivatives as membranous electron carriers. Besides ubiquinones and plastoquinones that are commonly found in bacteria or cyanobacteria, respectively, there is a relatively large group encompassing naphthoquinone derivatives – menaquinones[240]. In some bacteria there are numerous, less common quinones that are based on other chemical structures of the redox-active rings. These are not discussed in this review. Interested readers are referred to a comprehensive review on biological quinones[241].

Despite differences in chemical structure of the redox-active quinone rings, a common feature shared between of mena- ubi- and plastoquinones is a relatively long hydrocarbon chain consisting of several isoprenoid fragments. This imposes a high level of hydrophobicity on natural quinones. The number of isoprenoid fragments in the chains is usually given by a number put after the name of the respective quinone[241]. For example, UQ-10 means that the ubiquinone posses the tail built of 10 isoprene molecules. The extent of hydrophobicity of quinones is expressed by a large partition

coefficient ($log_{10}P$) for organic/water mixtures such as octanol and water[242]. Quinol forms are generally slightly more hydrophilic than the respective quinone forms. In case of ubiquinone-1 or plastoquinone-1, $log_{10}P$ exceeds 3 and further increase in the length of isoprenoid tail increases the hydrophobicity, forcing quinone molecules to be constrained to a lipid environment[242]. The natural quinones engaged in electron transfer usually have the hydrophobic tail built of 7 – 10 isoprenoid moieties, depending on the organism and very rarely exceeds 10. In plastoquinones the number of isoprenoids is usually 9, while in mammalian mitochondria ubiquinones usually have 9 or 10. For menaquinones, the length of the chain most often varies between 7 and 8[241]. Comparison of the chemical structure of menaquinone-7, ubiquinone-10 and plastoquinone-9 is presented in figure 13.

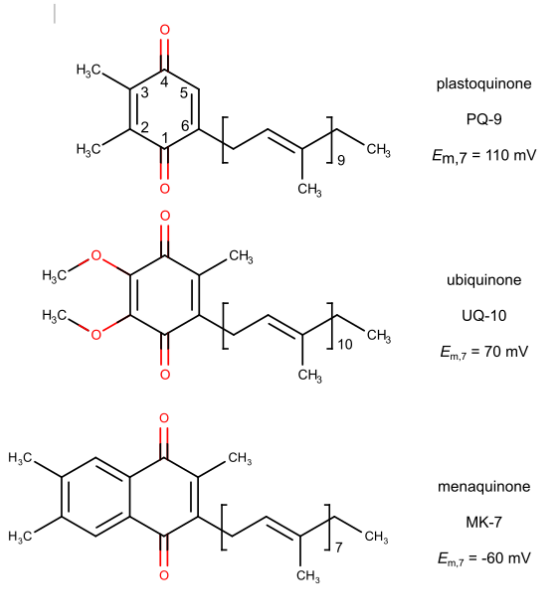

Figure 13. Chemical structures of biologically important quinones with a different number of isoprenoid molecules comprising the hydrophobic side chains. From top to bottom there are: plastoquinone-9 (PQ-9), ubiquinone-10 (UQ-10) and menaquinone-7 (MK-7). The $E_{m,7}$ values corresponds to the average redox midpoint potentials at pH 7 for the respective Q/QH_2 couples.

Another common feature that makes quinones important members of nearly all enzymatic processes of electron exchange between the membranous enzymes is their ability to undergo reversible two-electron, two-proton reactions of oxidation or reduction without damaging the chemical structure of the redox-active ring[243]. This reaction can be generally described as:

$$Q + 2H^+ + 2e^- = QH_2 \qquad \text{(eq. 1)}$$

where Q stands for quinone (fully oxidized form) and QH_2 – for quinol or hydroquinone (fully reduced form)

The complete oxidation/reduction reaction of eq. 1 can be divided into two, one-electron steps involving a semiquinone (SQ) intermediate.

$$Q + e^- = SQ^- \quad \text{(eq. 2)}$$

$$SQ^- + e^- + 2H^+ = QH_2 \text{ (eq. 3)}$$

Equations 2 and 3 assume that reduction of quinone leads to the semiquinone anion, and further reduction of SQ^- is coupled to the protonation of the reduced quinone. This particular proton/electron sequence is supported by the fact, that pK of neutral semiquinone (SQH) is significantly lower than the first pK (pK_1) of the first proton dissociation of QH_2 [244].

The average redox midpoint potential (E_m) of Q/QH_2 couple is equal to the arithmetic mean of redox midpoint potentials of the Q/SQ^- and SQ^-/QH_2 couples[245].

$$E_m\,(Q/QH_2) = 0.5(E_1 + E_2) \quad \text{(eq. 4)}$$

where: E_1 and E_2 represent E_m values of Q/SQ^- and SQ^-/QH_2 couples, respectively.

The average redox potential of Q/QH_2 couple depends on the type of the redox-active ring of a particular quinone molecule and it generally decreases upon substituting the 2,3 and 5,6 positions of the ring with a methyl group[246]. Conversely, when the ring is substituted with a group that has high electronegativity such as chlorine or bromine, the E_m of Q/QH_2 rises considerably[246–248]. For example, when one considers a simple case of 1,4-benzoquinone, its average redox midpoint potential at pH 7 ($E_{m,7}$) is approximately +300 mV and decreases to +230 and +176 mV upon attachement of one or two methyl groups to the ring at position 2 and 2,3, respectively[246]. On the other hand, substituting the ring with chlorine at position 2 and 5 increases the E_m to approximately +540 mV. Attachment of methoxy groups to the ring also increases the measured E_m in relation to 1,4-bezoquinone. For example, the E_m of 2,6-dimethoxy-1,4-benzoquinone is approx. +340 mV, which is higher by about 200 mV than the E_m of 2,6-dimethylo-1,4-bezoquinone. The redox midpoint potentials of quinones belonging to the family of menaquinones are significantly lower than those of benzoquinone derivatives, for example the $E_{m,7}$ of 2-methy-1,4-naphtoquinone (menadione) is only -5 mV, which is much lower than +230 mV of methyl-1,4-benzoquinone. Due to such a low redox midpoint potentials of menaquinones, they are considered as “ancient devices” for electron transport in living organisms recruited at early stages of evolution by some eubacteria and/or archaebacteria, at a time, when the atmosphere on Earth was anaerobic[160,241].

This general rule of changes in the E_m values of quinones containing different groups substituted to the ring holds true for natural, biologically active quinones that are used by living organisms as substrates for Cyt*bc*. It means, that the E_m of Q/QH_2 couples increases in the order:

menaquinone/menaquinol ($E_{m,7}$[MK/MKH_2] = - 60 mV), ubiquinone/ubiquinol ($E_{m,7}$[UQ/UQH_2] = 70 mV) and plastoquinone/plastoquinol ($E_{m,7}$[PQ/PQH_2] = 110 mV) (see fig. 13)

As the redox reactions of quinones involve 3 electron and 3 protonation states, the theoretical number of possible states is 9. However, from all these possible states (electrons and protons), QH^+ (protonated quinone), QH_2^{2+} (doubly-protonated quinone) and SQH_2^+ (doubly-protonated semiquinone) are not possible since their expected pK values are less than 0[244,249]. The typical pK_1 and pK_2 values for the first deprotonation of QH_2, leading to QH^-, and the second deprotonation, leading to Q^{2-} are separated by 2, thus $pK_2 = pK_1+2$. Interestingly, pK_1 and pK_2 are inversely correlated with the redox midpoint potential of Q/SQ^- couples and for mena- ubi- and plastoquinone pK_1 is in the range 9-11[246]. For semiquinone, the pK value also depends on the E_m of Q/SQ^- couple with typical values falling in the range 4 - 5[244].

4.1.1 Stability and reactivity of semiquinone radical with molecular oxygen

A potential danger associated with quinone redox reactions, not only those catalyzed by enzymes, is the possibility of reaction of SQ with molecular oxygen[248,250–254]

$$SQ^- + O_2 = Q + O_2^- \qquad \text{(eq. 5)}$$

Although this reaction is reversible, occurrence of superoxide dismutation or superoxide scavenging by, for example Cyt*c* or PC, will shift the equilibrium to the right side[246]. A superoxide release during the enzymatic catalysis by Cytbc_1 or Cytb_6f is considered deleterious and leads to a decrease in energetic efficiency of the enzyme, as generation of superoxide decouples the oxidation of QH_2 at the Q_o/Q_p site with Q reduction at the Q_i/Q_n site. Thus, this side reaction decreases the number of protons translocated across the membrane during the catalytic cycle. However, in living cells some portion of O_2^- can be scavenged by electron donation from the radical to the oxidized Cyt*c*[255] or PC[256] with a relatively large second order rate constant. Such scavenging of superoxide can be considered as a protection and partial remedy to energy-wasting side reactions, as the electrons that leak to oxygen can be subsequently used to generate pmf at the level of cytochrome *c* oxidase (C*c*O) (complex IV)[257].

The second-order reaction rate constant for the reaction of SQ^- with O_2^- depends on the E_m value of the Q/SQ^- couple and generally increases when the potential of the E_m of the Q/SQ^- couple decreases. When $E_m(Q/SQ^-)$ is more negative than -200 mV, the reaction of SQ^- with dioxygen becomes diffusion-limited[246].

The mechanism of reduction of O_2 to O_2^- by the SQ^- radical is generally viewed as electron transfer process that follows the Marcus theory of electron transfer[252]. An alternative mechanism

proposes a chemical reaction of addition of oxygen to the SQ^- ring followed by release of the superoxide anion, which after protonation changes to the neutral, peroxyl radical[253].

$$SQ^- + O_2 \rightarrow SQ\text{-}OO^- + H^+ \rightarrow Q + HOO^* \qquad \text{(eq. 6)}$$

Valgimigli et al. showed evidence that reaction 6 is significantly slower in solutions in which a semiquinone can form H bonds with molecules of the solvent[253]. Therefore, it can be supposed that formation of a hydrogen bond to the SQ^- may be protective against superoxide formation in catalytic sites of enzymes (see section 7.5).

4.1.2 Stability constant of SQ^-.

Under equilibrium conditions Q, QH_2 and SQ are linked by a reaction of comproportionation (or in reverse direction by disproportionation)[246] :

$$Q + QH_2 = 2\ SQ^- + 2H^+ \qquad \text{(eq. 7)}$$

The equilibrium constant of this reaction defines the stability constant (K_s) of SQ^- which depends on the difference in E_m values of Q/SQ^- (E_1) and SQ^-/QH_2 (E_2) couples[258–260]:

$$K_s = \frac{[SQ^-]^2[H^+]^2}{[Q][QH_2]} = 10^{(E_m(Q/SQ) - E_m(SQ/QH_2))/59.1} = 10^{(E_1 - E_2)/59.1} \qquad \text{(eq. 8)}$$

The stability constant for SQ defines the equilibrium between concentrations of $Q/SQ^-/QH_2$ in this triad. It means that in equimolar mixtures of Q and QH_2 some SQ^- is also present but its relative amount depends on the equilibrium constant K_s. For some chlorine substituted quinones K_s can be higher than 1[247]. However, for biologically important quinone derivatives, the E_m of the Q/SQ^- couple is more negative than SQ^-/QH_2, thus the exponent in the equation 8 is always less than zero (and therefore $K_s < 1$). Any further increase in the split between the E_m values of these two couples (E_1 - E_2) leads to a decrease in the equilibrium concentration of SQ^- in solutions containing a mixture of Q and QH_2 forms. This, on one hand, increases the rate of reaction of SQ^- with O_2 but on the other hand, decreases the probability of superoxide generation as the concentration of SQ^- decreases.

Despite the fact that K_s for SQ^- is used in chemistry of quinones under equilibrium conditions, it is also widely used to describe the properties of semiquinones that are generated at catalytic sites of enzymes such as the Q_o/Q_p and Q_i/Q_n site of Cyt*bc* during catalysis[261–264].

The concentration of quinones within the membrane is usually expressed as the number of molecules (Q and QH_2) *vs* the number of C*c*O molecules. In mammal and plant mitochondria the number of quinones per C*c*O is around 6-8, while it is much larger in yeast mitochondria (~ 38 per C*c*O). In purple bacteria the estimated number of quinone molecules per reaction center (RC) is also quite large - in the order of 15 – 30. The number of quinones in humans depends significantly on the tissue and the age. The content of Q in mitochondria increases during the first 20 years and after that time gradually decreases to the level even lower than after birth (see discussion in ref.[13]).

A significant content of the quinone molecules in the membrane may suggest that the comproportionation reactions should be very efficient leading to generation of a significant amount of SQ, which after dismutation would lead to the process of electron self exchange:

$$Q^{(A)} + Q^{(B)}H_2 = Q^{(A)}H_2 + Q^{(A)} \text{ (eq. 9)}$$

However, such a reaction is very unlikely in membranes as it requires at least two steps that involve reactions of protonation and deprotonation[243,265], which is difficult in the lipid environment.

4.1.3 Chloroplast photoactive *vs* non photoactive plastoquinone pools.

The concepts discussed above apply to quinol or quinone ($Q(H_2)$) in bioenergetic membranes in ideal conditions. However, due to crowding of both the photosynthetic and respiratory membranes, differences exist between $Q(H_2)$ located in different lipid environments. In the case of photosynthetic membranes (the thylakoids) the proportion of $Q(H_2)$ that participates in electron transport (i.e. that feeds the Cytb_6f complex) does not correspond to the entire population of $PQ(H_2)$. This fraction (the photoactive $PQ(H_2)$ pool) makes up a relatively small percentage of the entire $PQ(H_2)$ pool, because 60-70% of the total $PQ(H_2)$ is non-photoactive, being stored inside thylakoid-associated lipid droplets known as plastoglobules[266–268]. There is increasing evidence that the size of this photoactive $PQ(H_2)$ pool is tightly regulated in response to environmental cues, for example changes in light intensity [269,270]. This homeostasis is necessary because the $PQ(H_2)$ pool fulfills multiple functions *in vivo*. Firstly, it shuttles electrons within the crowded thylakoid membranes, [271] probably via percolation through the lipid environment between other membrane complexes[272,273]. Moreover, its redox state controls physiological processes in response to environmental changes, such as changes in the PSII and PSI antenna size via state transitions [274]), as well as gene expression and pigment biosynthesis [275].

Recent results suggest that the amount of $PQ(H_2)$ active in electron transport is mainly regulated through exchanges between the photoactive pool (in the thylakoids) and the non-photoactive pool (in the plastoglobules). Homeostasis of photoactive $PQ(H_2)$ abundance seems to be under the control of ABC1 (Activity of Cytbc_1) atypical kinases [276]. Knocking out a member of this family (*pgr6*, [277], where the ABC1K1 kinase is inactivated (*abc1k1*) prevents changes in the size of the photoactive $PQ(H_2)$ pool, that would otherwise occur in response to high light, facilitating increased electron flow and replacing photo oxidized plastoquinones. Thereby, *abck1* mutants display decreased electron flow and photoacclimation responses in high light [278]. ABC1K1 acts in tandem with ABC1K3, another member of the ABC1 family, and the push pull relationship between these two kinases provides a fine tuning mechanism to control the size of the $PQ(H_2)$ pool in response to high light [279].

This tight control of the size of the photoactive $PQ(H_2)$ pool *in vivo* likely explains the phenotype of the *menD1* mutant of *Chlamydomoans reinhardtii.* This mutant is deficient in MenD, the enzyme catalyzing the first step of phylloquinone biosynthesis [280]. Therefore, the phylloquinones playing the role of electron acceptors within PSI are replaced by PQ in this mutant, making PSI less active. However, the *menD1* mutant has another phenotype - its photoactive $PQ(H_2)$ pool is decreased by 20–30%. This can be explained by assuming that the size of the photoactive $PQ(H_2)$ pool is constant between the WT and the mutant. Therefore, the overall number of diffusing $PQ(H_2)$ molecules would decrease from around 6 per Cytb_6f in the WT to around 4 per Cytb_6f complex in *menD1*[280]. Based on this result, it is tempting to propose that the mechanism by which ABC1K1/ABC1K3 maintains a constant photoactive $PQ(H_2)$ pool size depends on "quantification" of the total number of $PQ(H_2)$ molecules available per electron flow chain. If this were the case, the size of the pool would be unresponsive in *menD1*, as the ABC1K1/ABC1K3 machinery will not deliver two additional $PQ(H_2)$ per chain to the thylakoid membrane from the plastoglobuli to replace the PSI bound PQ.

4.2 Cytochrome *c* and plastocyanin as electron acceptors

Electron donation from both Cytbc_1 and Cytb_6f to soluble proteins at the *p* side has been extensively studied. These molecular events have often served as pioneering models for electron transfer between different proteins, and reflect the development of techniques and theories of how such processes occur. In both cases, a single electron passes from a cytochrome in the complex (Cytc_1 in Cytbc_1 or Cyt*f* in Cytb_6f) to a small, soluble redox protein that is specifically, but transiently bound.

Once reduced, the electron carrier protein must rapidly dissociate (so as not to block the catalytic cycle), and diffuse through the *p* side space to another large membrane bound protein complex. In mitochondrial respiration this is cytochrome *c* oxidase (CcO, complex IV) [281], while in plant photosynthesis this is photosystem I [282]. Protein acceptors vary between Cytc_1 and Cyt*f*. In the case of the respiratory complex the acceptor is a c-type heme containing protein, cytochrome *c* (Cyt*c*) [283], perhaps one of the most studied of all redox proteins. Cytbc_1 in purple bacteria uses a homologue of Cyt*c*, soluble Cytc_2, and/or membrane-anchored Cytc_y [284,285] as an electron acceptor, although this organism is photosynthetic and the final electron acceptor for the soluble electron carrier is a photosynthetic reaction center [286]. In the case of Cytb_6f, the dominant electron acceptor is a copper-containing protein called plastocyanin (PC) [287,288]. It is generally accepted that PC has evolved to replace a Cyt*c* homologue - Cytc_6, the primordial acceptor for electrons coming from the Cyt*f* subunit of Cytb_6f (see De la Rosa et al., and references therein [289]). Following oxygenation of the atmosphere, oxidation of Fe^{2+} to Fe^{3+} in the ocean would have made it considerably less bioavailable, whilst oxidation of Cu to Cu^{1+} would correspondingly have made it more soluble and therefore bioavailable. Interestingly, some prokaryotic photosynthetic organisms retain a cytochrome, Cytc_6 as their Cyt*f* electron acceptor, and in primitive oxygen evolving cyanobacteria this can be the only electron acceptor from Cyt*f*. Where both genes are present, Cytc_6 replaces PC under conditions of limiting copper [290]. Cytc_6 also occurs in some algae where it is also upregulated to act as an electron acceptor of the Cytb_6f under copper limiting growth conditions [291]. A Cytc_6 homologue gene is present in plant genomes [292]. However, despite initial reports, the surface charge distribution on higher plant Cyt*c* precludes its function as an effective *in vivo* electron acceptor from Cyt*f* [293].

The basic pattern of interaction is thought to be the same for electron transfer processes between Cytbc_1: Cyt*c* and Cytb_6f:PC. The redox centers are oriented for optimal electron transfer by long distance charge effects in an encounter complex, before formation of a transiently stabilized productive complex, dominated by hydrophobic interactions. Mismatched surfaces between the partners, along with the retention of some water molecules at the interface, prevents interaction being so strong that it inhibits dissociation following the electron transfer event. The following sub-sections will describe the soluble electron carrier proteins in more detail, and outline the mechanisms by which soluble electron carriers interact with, and oxidize the Cytbc_1 and Cytb_6f complexes.

4.2.1 Redox properties and Interaction of Cytochromes *c* with Cytochrome bc_1

Cytochrome *c* is a small globular heme protein (90-120 amino acids, 10-13 kDa) which in bioenergetic systems serves as a water-soluble electron carrier. This definition encompasses the representatives found in eukaryotic (mitochondrial Cyt*c*, yeast iso-Cyt*c*) and prokaryotic (Cytc_2 present in several bacteria species) respiratory chains. A more distinct relative — Cytc_6 — is also a member of this category. However, due to its occurrence in plant-related systems, Cytc_6 is discussed in the chapter devoted to plastocyanin. For the scope of this review we will briefly go through the most important properties of Cyt*c* with respect to its function and research in bioenergetic systems. More detailed information about the c-type family of cytochromes can be found in excellent reviews on cytochromes [294,295]. In the Cyt*c* molecule the heme is bound via two thioether linkages to the peptide. The covalent attachment of heme is a distinctive property of all c-type family cytochromes [296]. The bond is formed between a cysteine residue (C) and the penultimate carbon of a vinyl side-group of the heme moiety. Comparison analyses revealed a specific heme binding motif – CXXCH (present also in Cytc_1 and Cyt*f*, see sections3.5.2 and 3.6.2, respectively). The cysteine residues (C) involved in thioether bonds are separated by any two residues (XX). This four amino acid subsequence is immediately followed by a histidine residue, which is an axial ligand to the heme iron. The second axial ligand is the sulphur atom of a methionine residue which together with four pyrrole nitrogen atoms of porphyrin completes the octahedral ligand geometry of the heme iron.

Redox properties of Cyt*c* are related to the ability of heme iron to undergo reversible oxidation and reduction of ferrous (Fe^{2+}) and ferric (Fe^{3+}) states, respectively. The presence of a methionine ligand significantly elevates the redox potential of Cyt*c* compared to bis-His coordination [297]. Thus among biological compounds the redox midpoint potential of Cyt*c*, and its counterparts, is considered high — in the range of +260 mV for horse heart Cyt*c* [298] and bacterial Cytc_2 +360 mV [299]. This is consistent with a location of Cyt*c* in electron transport chains as an acceptor of electrons from quinol oxidising membrane complexes (i.e. Cyt*c* – Cytbc_1; Cytc_2 – Cytbc_1; Cytc_6 – Cytb_6f) [2,13,211].

Upon reduction Cyt*c* donates electrons to a terminal oxidase of the mitochondrial electron transport chain – C*c*O. In related systems cytochrome c-type electron carriers are oxidised by photosynthetic complexes of high oxidising power i.e. the bacterial photosynthetic reaction centre in case of Cytc_2 [300] or PSI for Cytc_6 in the case of cyanobacteria and some algae [301]. Beyond its primary role as a carrier shuttling electrons between membrane complexes, mitochondrial Cyt*c*, is also involved in the process of cellular apoptosis in higher organisms [302].

The amino acid sequence of Cyt*c* varies between different organism. The degree of identity spans quite high values (70%) among vertebrates [303] to low values (20%) when mitochondrial and

prokaryotic Cyt*c* are compared [304]. Nevertheless general structural features are evolutionarily conserved – the number of helices (5) and their general spatial arrangement [305]. The heme is buried in a hydrophobic pocket within the apoprotein with only one edge being exposed to the surface of the protein. Such an asymmetric cover insulates most of the heme moiety from the water environment and only exposes the heme to the area where the binding occurs with physiological partners.

Cyt*c*, as for other hemeproteins, absorbs strongly in the visible spectrum of electromagnetic radiation – in the range of 500-600 nm and the Soret band (around 400 nm). Reduced Cyt*c* (Fe^{2+}) shows a sharp peak at 550-556 nm (α band) and a slightly broader peak around 520 nm (β band). A unique feature of ferriheme c (Fe^{3+}) is the presence of a weak absorbance band around 700 nm due to interaction with the sulfur of the methionine ligand. The peak in the Soret band (γ band) of Cyt*c* shifts slightly when the redox state of heme *c* changes. The Soret peak is often used as a mark of the protein condition because when the protein denatures, significant changes in the γ band peak are observed. This was exploited in studies of Cyt*c* folding stages and its stability [306,307]. The heme *c* also possesses peaks in the UV region around 320 nm and 280 nm (δ and ε band, respectively) [308], which are, however of little use due to overlapping signals from aromatic amino acids residues.

Octahedral heme iron in Cyt*c* is in a low-spin configuration, hence, the reduced Cyt*c* (Fe^{2+}) is diamagnetic (S = 0) while oxidized (Fe^{3+}) is paramagnetic (S = 1/2). Oxidized Cyt*c* molecules from different organisms are the source of the EPR spectrum with significant g-factor anisotropy that usually exhibit rhombic symmetry with well resolved g-tensor principal values[309]. In some cases the EPR spectrum of Cyt*c* is a HALS type[310]. These differences originate from structural changes in the mutual orientation of the His and Met ligands. However, no simple rules have been found so far which allow prediction of the type of EPR spectrum [148]. Such peculiarities are assigned to rather weak interaction with Met that under some circumstances can be disrupted. It was shown that pH changes, denaturation stress, or interaction with lipids (cardiolipin) can even lead to the breakage of the coordination bond changing heme *c* from hexa- to pentacoordinated high-spin geometry [311–313].

Several studies involving measurement of the Cyt*c* reduction rate by Cytbc_1 and kinetics of electron transfer showed sensitivity to ionic strength [314–319]. This led to the notion that electrostatics is a key player in a “find-and-bind” game between the two protein contenders.

Chemical modification and site directed mutagenetic studies allowed identification of the crucial amino acid residues responsible for Cyt*c* – Cytbc_1 interaction. Indeed, it was established that the interaction is possible due to electrically charged surfaces. The surface of the Cyt*c* molecule around the heme pocket has a net positive charge due to the presence of basic amino acid residues (mostly lysine residues), while the binding domain on the Cytc_1 surface includes complementary (negative) charges of acidic residues [320–325]. These long range interactions are thought to orient the

Cyt*c* molecule in an encounter complex which enables maintenance of an electron-transfer-productive orientation at the early stages of interaction. Additionally the Cyt*c* molecule itself possesses negatively charged residues on the side opposite to the interaction domain. This spatial separation of charges makes the Cyt*c* molecule an electric dipole. It was shown that the presence of a dipole moment further facilitates the orientation of Cyt*c* in the Cyt*c* – Cyt*bc*$_1$ complex that is proper for physiologically efficient electron transfer [326].

Following initial orientation, the proteins form a productive complex, knowledge of which is based on the structure of co-crystalized yeast proteins, either both in the oxidised, or both in the reduced state [72,327]. Only subtle differences in structure are observed between the different redox states. In these complexes, the oppositely charged side-chain pairs on Cytc_1 and Cyt*c* do not directly interact, being 4 to 9.6 Å apart and therefore beyond the Debye length in physiological salt concentrations. Rather, the interface is dominated by non-polar interactions. The core surface area of interaction is 880 Å^2 around the heme clefts, and contains a core of 4 pairs of amino acids in non-polar interactions, including a cation-π interaction between a Cytc_1 Phe residue and a Cyt*c* Arg residue. The interface contains 30 water molecules, only 2 of which coordinate H bonds between the proteins. This highly solvated surface aids rapid dissociation of the complex. The two heme cofactors have an inter-planar angle of 55° and are very close – only 4.1 Å between the closest thioester bonded carbons of the tetrapyrrole rings, and 17.4 Å between the Fe centers. This short distance means that, in principal, electron transfer could already occur when Cyt*c* is approaching the Cyt*bc*$_1$. It is possible that many other, less stable, productive complexes are also possible aside from those in the crystallized structure. A molecular dynamics approach has attempted to rationalize the apparent importance of charged side chains in mutational studies with the dominance of non-polar interactions in the crystal structures [328]. This analysis indicates that many of the lysine side chains on Cyt*c*, which surround the hydrophobic interface, are highly dynamic, and capable of forming H-bonds or even salt bridges with Cytc_1. Based on this, the authors suggest a more dynamic mixture of interaction modes between Cyt*c* and Cytc_1.

No significant structural changes seem to occur between non-complexed and complexed proteins in the crystal structures, although one loop region that is poorly resolved in the crystal structure does change orientation in the molecular dynamics experiments [328]. This in combination with the small surface area of interaction and short distance between the cofactors probably contributes to the rapid rate of electron transfer by the complex. Interestingly, only one Cytc_1 site in the dimer is occupied by Cyt*c* in the crystal structures (Fig. 14 A), and this coincides with an increase in Q_i site occupancy in the same monomer, indicating binding of the substrates could be coordinated. Indeed, a change in the conformation of ISP-HD head group is observed on Cyt*c* binding to the

Cyt*bc*$_1$. The molecular dynamics studies on Cytc_1 — Cyt*c* interaction show that Cyt*c* binding to one monomer induces structural changes at the Cyt*c* binding site of Cytc_1 in the other monomer [328], perhaps explaining this. Co-crystalisation of yeast Cytc_1 with a second yeast isoform of Cyt*c* (Cyt*c* isoform 2), showed a nearly identical structural arrangement, although some of the charged pairs vary slightly [72].

Interestingly, an inspection of the electrostatic surface potential of crystal structures with different ISP-HD positions indicates that a negatively-charged area accessible to Cyt*c* is significantly larger when ISP-HD is in the b-position compared to the case when it is in the c-position (Fig. 14 B). This could potentially influence the molecular organization of Cyt*c* near the binding domain.

The idea of one Cyt*c* per dimer stoichiometry attracted some attention and brought some productive scientific effort. On one hand this idea suggested that binding of Cyt*c* to the one monomer disables the binding site in the other monomer as explored in context of *half-of-the-site* activity model of Cyt*bc*$_1$ regulation. This proposed that during enzyme turnover only one monomer of Cyt*bc*$_1$ is active at a time [329]. On the other hand it provoked other authors to investigate the stoichiometry issue by other experimental approaches. Titration data obtained by plasmon resonance spectroscopy suggested that Cytc_2 interacts with the Cyt*bc*$_1$ dimer in a biphasic manner which was interpreted as a modulating effect of ISP-HD on the binding [330]. The data obtained by NMR and ITC for Cyt*c* interaction with the soluble Cytc_1 head domain in low ionic strength (both in plant and bovine system) proteins revealed two binding sites of different affinity on Cytc_1 [331]. The authors proposed that Cytc_1 exposes a *proximal* site at which electron transfer takes place, and the *distal* site, which is too far for electron transfer, but maintains another molecule prior to electron transfer. In this way a subpool of Cyt*c* is trapped close to the surface of the Cyt*bc*$_1$ – C*c*O supercomplex. This restricts diffusion of Cyt*c* in the vicinity of the Cyt*bc*$_1$ – C*c*O complex leading to the enhancement of electron flow rate between the two complexes. The Cyt*c* then does not need to return to the intermembrane bulk phase. A somewhat similar finding was revealed by experiments in which titration of Cyt*bc*$_1$ binding sites was done by means of spin-labelling and pulse EPR [332]. Titration curves obtained at low ionic strength (no NaCl in buffer) were explained by a multiple-site-binding model. When electrostatic interactions are strong, Cytc_1 attracts many Cyt*c* molecules which organize in a molecular cloud near the Cytc_1 binding surface (Fig. 14 C).

The putative presence and a role of such supramolecular structures in the Cyt*c* pool are intriguing. However as the authors state in both cases (NMR, ITC) and (pulse EPR) the titration curves at higher ionic strength (25-50 mM NaCl) could be readily explained with one binding site per Cytc_1 [332,333]. This means that binding of Cyt*c* to the proposed additional sites under physiological conditions is much weaker than binding to the primary (electron transfer relevant) site on Cytc_1.

Hence in order for these additional collective interactions in the Cyt*c* subpool to be physiologically relevant, other factors including macromolecular crowding, may be involved. This matter remains to be determined.

All available titration data report dissociation constants in the range of several to tens of μM, indicating that Cyt*c* — Cytbc_1 affinity is not very strong [330–332]. What is even more striking is that EPR data indicates that when the ionic strength is increased to the physiological levels (100-150 mM NaCl) binding of Cyt*c* to the primary interaction site is not even detectable [334]. Even though the stationary concentration of stable long-lived Cyt*c* – Cytbc_1 complex is low, the proteins do interact because the electron transfer between them is not stopped [314]. Therefore this interaction is transient and the life-time of the complex is much shorter than the timescale of electron transfer. This would also explain the discrepancy between the measured rate of Cyt*c* — Cytc_1 electron transfer that turned out to be several orders of magnitude lower[314] than the calculated electron transfer rate based on crystallographic data [327]. This supports a diffusion-coupled (in contrast to diffusion limited) mechanism of electron transfer between Cyt*c* and Cytbc_1, in which the proteins constantly collide and several collisions are needed before one ET event occurs (Fig. 14 C) [332,334]. Therefore, the dynamic aspect of the Cyt*c* — Cytbc_1 interaction has tremendous impact on the flow of electrons from Cytbc_1 to Cyt*c* pool and it cannot be neglected.

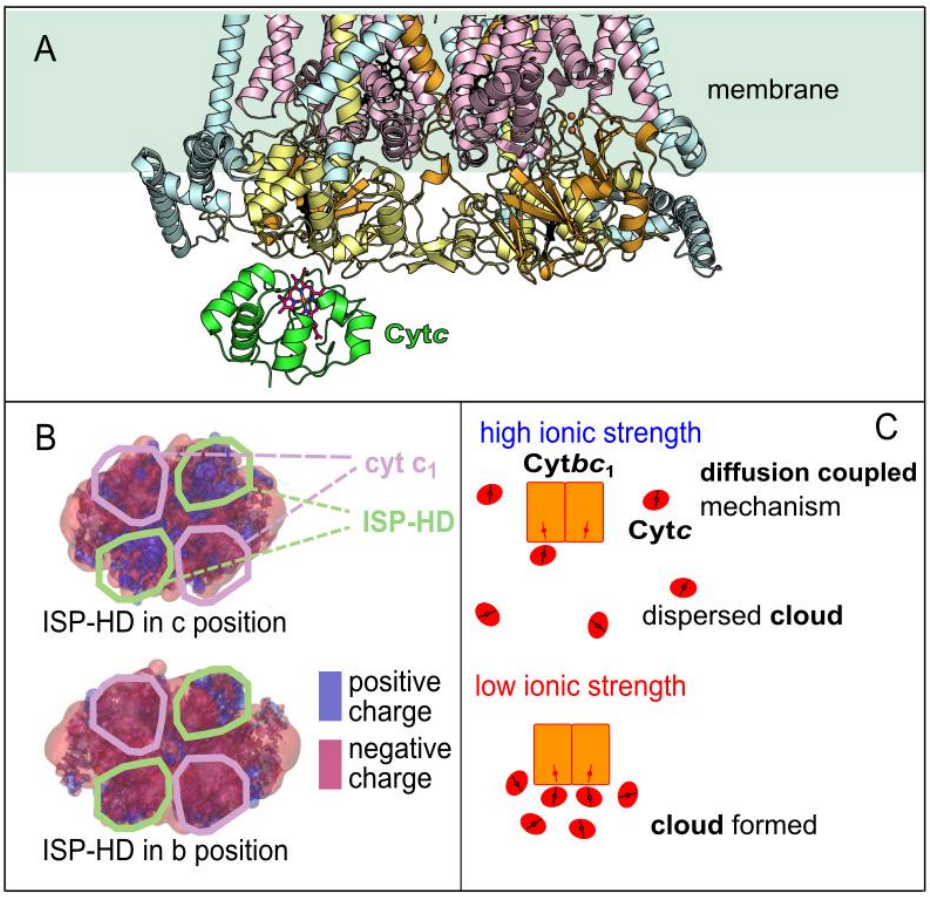

Figure 14. Binding of Cyt*c* to Cytbc_1. A) Fragment of the structure of Cytbc_1 co-crystallized with Cyt*c* (PDB: 1KYO). B) Comparison of electrostatic potential of the surface of Cytbc_1 accessible to Cyt*c* in two different positions of ISP-HD. C) Schematic representation showing different molecular organization of Cyt*c* near the binding domain of Cytbc_1 at low and high ionic strength.

4.2.2 Redox properties and Interaction of Plastocyanin with Cytochrome *b*$_6$*f*

A structure of co-crystalized Cyt*f* and PC is lacking, and so our understanding of their interaction is based on a combination of mutagenesis studies, nuclear magnetic resonance (NMR) and molecular dynamics. These have recently been augmented with atomic force microscopy (AFM) and 2D infra-red spectroscopy (2D-IR) experiments, meaning that although we lack a perfect snap-shot of any one interaction mode, we do have an excellent understanding of the dynamic events that occur during oxidation of Cytb_6f.

While the C-teminal domain of Cyt*f* forms a membrane spanning domain, the soluble, N-terminal portion contains the heme group. The heme lies below the surface for interaction with PC or Cytc_6 [171]. This is composed of a hydrophobic surface with a ridge of associated charged residues. The

hydrophobic surface is highly conserved between Cyt*f* proteins from different species, while there is great variation in the ridge residues, and even their charge, between different groups of photosynthetic organism [335–337]. In higher plants and algae, the ridge is functionalized by basic residues, and mutation of these disrupts interaction with PC [171,338–340]. The charged residues on the Cyt*f* ridge in cyanobacteria are by contrast usually acidic [341,342].

The secondary structure of PC is fundamentally different from Cyt*c*. It is an 11 kDa protein composed of eight β strands and a small α-helix [343–346]. It contains a single copper center, coordinated by one cysteine, one methionine and two histidine residues. There are two areas on the surface of PC involved in association with Cyt*f* [171,342,347–350]. The first (site 1) is a hydrophobic patch over the copper-His ligand, while the second (site 2) is functionalized by charged residues complementary to those on the Cyt*f*. These therefore vary between photosynthetic organisms, being predominantly acidic in plants and algae, but basic in cyanobacteria. Long distance attraction between the charged residues on the surface of Cyt*f* and PC are proposed to orient the molecules for optimal electron transfer, prior to formation of the catalytic complex. This is supported by the observation that low ionic strength results in a strongly bound complex incapable of turnover, while high ionic strength disrupts complex formation [351]. In addition, AFM experiments, with the Cytb_6f complex tethered to the surface and PC attached to the tip, indicate that ionic strength strongly impacts both frequency of initial interactions and unbinding forces [352]. Despite this evidence supporting the importance of electrostatics for Cyt*f*: PC interaction *in vitro*, the only *in vivo* analysis to date, on the alga *Chlamydomonas reinhardtii*, indicates that mutation of the basic ridge residues on Cyt*f* has little impact on its oxidation rate [339,340].

While a recent molecular dynamics study supported a role for the charged amino acid side chains at site 2 in the initial complex formed between higher plant Cyt*f* and PC [353], it also found no evidence for electrostatic pre-orientation in the cyanobacterium *Nostoc*. Moreover, there is little impact of electrostatics on formation of the Cyt*f*:PC complex from the thermophilic cyanobacterium *Phormidium laminosum*, where non-polar interactions appear to both orient the complex and stabilise it [342]. Recent 2D-IR experiments on cyanobacterial (*Nostoc*) PC:Cyt*f* interaction used site specific labelling of PC with cyanophenylalanine probes to measure very fast changes in conformation and orientation [354]. This indicated that a wide variety of initial encounter complexes are formed, with rapid (1-2 ps) changes in orientation. It should be noted that this experiment was performed with the proteins in redox states opposite to that expected in electron flow (oxidized Cyt*f* and reduced PC).

Following correct orientation of the electron transfer partners, interaction occurs mainly through non-polar interactions, with exclusion of some water from the interface. Chemical shift perturbation experiments indicate that in plants and cyanobacteria, the surface area of interaction is

around 600-850 Å^2, with the Cu-His ligand close to the Fe coordinating Tyr reside in Cyt*f* [349,350,355,356]. Different plants appear to have the PC rotated slightly relative to Cyt*f*, although the distance between the two redox centers remains around 11-14 Å. Although the surface charge distributions are reversed in cyanobacterial complexes, the orientation of PC relative to Cyt*f* is conserved between higher plants and the cyanobacterium *Nostoc* [347]. However, NMR studies [347] and modelling approaches [353,357] indicate that other cyanobacteria show different patterns of interaction: in *Phormidium laminosum*, where Cyt*f* lacks the charged ridge, computer modeling indicates that PC is highly mobile, with only the site 1 hydrophobic patch interacting. This also seems to be the case for *Prochlorothrix hollandica*, where NMR studies show that although electrostatics make a modest contribution, site 1 dominates the interaction, although PC is oriented slightly differently [358]. On binding to Cyt*f*, X-ray absorption spectroscopy indicates that the geometry of the co-ordination sphere around the Cu ligand changes dramatically [359]. This may be responsible for the -30 mV negative shift in PC redox potential of PC on Cyt*f* binding [360], which counterintuitively makes electron transfer to PC less energetically favourable. Nevertheless, electron transfer is rapid, on the order of 104 k_{et} s^{-1} [361,362]. It appears that the relative charge of the interaction partners also plays a large role in interaction, presumably in terms of the electrostatics of initial interaction. AFM experiments show a 5 fold increase in interaction frequency between the two proteins when redox states are opposite (irrespective of whether Cyt*f* or PC is reduced or oxidized) [352]. This suggests that the rate of PC dissociation might be enhanced by rapid re-reduction of Cyt*f*.

Cytb_6f also uses the Cyt*c* homologue, Cytc_6 as an electron acceptor in cyanobacteria and algae grown under copper deficiency condition [290]. It is reported to show a faster rate of electron transport between Cyt*f* and terminal oxygenases than does PC [363]. Intriguingly, Cytc_6 is also the principle electron acceptor in the heterocysts of the cyanobacterium *Anabaena*, even when Cu is replete [363]. These cells are specialised for N-fixation, a process dependent on an O_2 sensitive enzyme (nitrogenase), and so PSII activity is very low, and the environment anaerobic [364]. In heterocysts, the majority of electron transport is therefore thought to result in oxygen reduction or in cycling between PSI and Cytb_6f via PQH_2 and Cytc_6. *Anabaena* could no longer grow under diazotrophic conditions (obligatory N-fixing), when the gene for Cytc_6 was knocked out [363].

Cytc_6 is a 10 kDa single c-heme type cytochrome bound by a typical CXXCH motif, where the His and a Met act as axial coordinators [365]. The protein has a midpoint potential of +335 mV [366], close to that of PC. In cyanobacteria, Cytc_6 has a hydrophobic surface area around the heme, and a positively charged surface patch of amino acid side chains analogous to sites 1 and 2 in PC [367]. Although modelling of the *Chlamydomonas* Cyt*f*:Cytc_6 complex indicates that a charged patch on the Cytc_6 is important, many orientations are possible for the encounter complex [368]. A combination of NMR and

molecular dynamics [367,369] has shown that the heme edge region (where the cofactor breaks the surface of the protein) is critical for interaction with Cyt*f*, and long distance charge interactions approximately orient the two proteins in an encounter complex, as for PC. Many orientations of Cytc_6 result in cofactor-cofactor distances that are close enough for electron transfer, and thus no specific interaction complex is expected [369].

Our knowledge of the interactions between Cytbc_1 and Cytb_6f carriers and their *p* side electron carrier is not equivalent – in the case of the respiratory complex, co-crystalization has given a wealth of molecular detail about one particular productive complex. The absence of such a structure for the photosynthetic complex has lead to the innovative use of NMR and molecular dynamics, along with other recent techniques to provide abundant information on dynamic events. It is to be hoped that we will reach an equivalence of knowledge between these two fascinating systems soon, so that more detailed comparisons can be made.

4.3 FNR/Fd interactions with cytochrome b_6f

4.3.1 Potential *n* side donors

In the initial model of the Q cycle proposed by Mitchell, one of the electrons reducing the heme b_H site (heme b_n) in the Cytbc_1 complex came from a soluble *n* side electron donor [33]. He revised this idea not long after proposing the classical model of the Q cycle [32], and more recent studies have given us a much firmer grasp on the classical Q cycle mechanism (see [216,259] for detailed reviews). However, solution of the crystal structure of Cytb_6f complexes [41,42] prompted reassessment of whether an *n* side soluble electron donor might contribute to a modified Q cycle. The discovery of an additional heme group, named heme c_i, or heme c_n, 6 Å closer than heme b_n to the *n* side solute interface and in contact with the Q_n site has re-ignited the debate as to whether the Cytb_6f might indeed receive electrons from a soluble, *n* side source. By contrast, the Cytbc_1 lacks heme c_n, and it is reasonable to assume that such a mechanism is precluded. This may be a reflection of the different bioenergetic environments of the two complexes, where the Cytbc_1 can rely on consistent availability of quinols, while the Cytb_6f is maintaining a proton gradient in the face of variable quinone reduction by PSII, due to fluctuations in light intensity.

So, where could such *n* side soluble reductant come from? In photosynthetic systems, the final steps in electron transport involve the donation of electrons from photoexcited PSI to the soluble, single electron carrier protein ferredoxin (Fd), and subsequent oxidation of Fd by the Fd:NADP(H) reductase (FNR) [370]. In turn FNR transfers these electrons over a flavin moiety (flavin adenine dinucleotide, FAD) to the 2 electron carrier $NADP^+$, making NADPH (see [371,372] for a detailed

description of the reaction mechanism). Both Fd and NADPH are used as electron donors by multiple enzymes, supplying the cytosol (bacteria) or stroma (chloroplasts) with reducing equivalents. Crucially, the FAD in FNR enables the relatively safe storage of a single electron from Fd, before a second reduced Fd can donate the second electron necessary for $NADP^+$ reduction. The injection of these electrons back into the quinone pool from soluble, *n* side carriers in CET therefore depends upon events involving Fd and FNR.

The two dominant mechanisms of CET have been historically separated on the basis of their sensitivity to the inhibitor antimycin A. Curiously, despite the sensitivity of the Cytbc_1 to this inhibitor, the Cytb_6f was until recently thought to be insensitive [373], and linear electron transport to NADPH was not found to be impeded by antimycin A. For many years it proved extremely difficult to identify the proteins involved in quinone reduction by the antimycin A sensitive CET pathway. Three independent mechanisms have been proposed: 1) direct electron donation from Fd to the Cytb_6f [19,374,375] ; 2) electron donation from FNR to the Cytb_6f [180,376]; 3) electron donation from Fd via Cytb_6f associated Pgr5 and PgrL1 pathways [199]. It remains a possibility that all three of these pathways occur, depending on the bioenergetic situation. Although robustly debated [234,377–380], it has been the consensus among many researchers that a pathway involving Pgr5/PgrL1 catalyses the bulk of CET in most algae and higher plants [197,381–385]. However, results in *Arabidopsis* [386] and the green algae *Chlammydomonas reinhardtii* [387] lead the authors to propose that the role of these proteins is regulatory, rather than mechanistic [374,377,386,387]. Moreover, the PgrL1 protein appears to be significantly sub-stoichiometric to the Cytb_6f, and would therefore only be able to drive electron flux into a small proportion of Cytb_6f complexes present in the membrane[201]. Finally, it has recently been reported that Antimycin A can indeed act as an inhibitor of the Qi site on Cyt b6f in conditions of highly reduced PQ, dependent on the presence of the STT7 kinase and pgr5.[388] Given the controversy, it is timely to discuss how the relationship between these different candidates and the Cytb_6f might help to resolve this question.

4.3.2 Direct electron donation from Fd to cytochrome b_6f

As mentioned previously, the original Q-cycle proposed by Mitchell involved a single electron from the soluble *n* side [32], and if this were to be the case for the Cytb_6f, Fd would be an obvious candidate for such a donor. The advantages of such a system in amplifying the proton motive force (pmf) are evident, with additional electrons from the *n* side enabling immediate quinone reduction at the Q_n site on oxidation of a single quinone at the Q_p site, and also providing the means to close "incomplete" catalytic cycles in the Cytb_6f that would otherwise leave Cytb_6 in a reduced state [19]. It

is possible that this could be automatically poised by the redox state of the quinone and stromal electron carriers, but seems more likely that some regulation would be required, particularly in the dark, when reduced Fd is required for multiple other metabolic reactions [389] and continuous input of *n* side electrons to the Cytb_6f undesirable.

Nearly all photosynthetic organisms possess a suite of Fd proteins that are presumed, and in some cases proven, to have variable affinity for different electron acceptors [390–395]. Such a system means that, depending on the relative abundance of these Fd iso-proteins, electron flux into different pathways could either be increased or decreased. There is abundant evidence that Fd iso-proteins specific for CET exist (see [396] for a full discussion). For example, maize plants perform an adapted photosynthetic pathway known as C4, in which one cell type has a greatly increased ATP demand and low PSII activity – a situation that demands high CET. A specific Fd iso-protein (FdII) is exclusively present in this ATP demanding cell type [397] and when this is used to replace the native Fd in cyanobacteria it prompts massive CET [398]. Pea plants also possess an Fd iso-protein that is expressed only in times of high ATP demand [399–401] and when this is over-expressed in tobacco it also results in elevated CET [402]. At this point it is not clear whether these CET specific Fds operate in the antimycin A sensitive or insensitive pathways.

After the characterisation of Fd-dependent CET by Arnon and colleagues [403], the possibility of direct electron donation from Fd to the Cytb_6f was investigated in isolated spinach thylakoids [404]. The authors showed that although Cyt*b*-563 (heme b_n) is only slowly reduced by dithionite, addition of hydrophobic quinone mediators accelerated this reduction, while Fd had no effect. Moreover, the addition of NADPH and Fd in the dark had little effect on the redox state of the cytochrome. In these experiments, rapid re-reduction of the oxidized P700 center of PSI was measured in the presence of Fd and NADPH, indicating that Fd-CET was operating very efficiently. This result indicates that, in this system at least, Fd is a poor direct electron donor to the Cytb_6f. It remains possible, that direct electron donation from Fd to heme c_n is downregulated in the dark adapted membranes used in this experiment, or that it might not result in reduction of the heme b_n. Interestingly, the broken chloroplast assay, used extensively to characterize the *pgr5* and *pgrL1* mutant *Arabidopsis* plants [235,236] does not work if attempted on washed thylakoid membranes (personal observation, GH). The possibility therefore also remains that components only weakly associated with the Cytb_6f complex are required to regulate direct Fd: Cytb_6f interaction, and the obvious candidates for such proteins are *pgr5* and *pgrL1*, although documentation of the role of these proteins in competent electron transport reactions is minimal and their presence sub-stoichiometric. [201] If this is not the case then further experiments are necessary to identify 1) the interaction partners and 2) their mechanism of function.

As part of a possible model involving direct electron donation from Fd to the Cytb_6f [374], one can propose a docking model of Fd binding to the *n* side of the Cytb_6f. Although binding sites are notoriously difficult to predict, interactions between Fd and Fd-dependent enzymes are characterized by charge interactions between the proteins, whose purpose is to optimally orient the redox centers for electron transfer [405–407]. For example, Figure 15 shows the Fd-binding sites (highlighted in black) on two classical Fd-dependent enzymes (C, nitrite reductase; D, FNR). There is an obvious ring of basic charges around the active center to which Fd can dock. When the *n*-facing surface of the Cytb_6f is examined, such a patch does appear to exist on the *C. reinhardtii* complex, used in the model proposed by Nawrocki et al. [374], highlighted with a hashed circle (Figure 15 B). However, such a mechanism would be expected to be universal throughout CET performing organisms, and when the same surface of the cyanobacterial *M. Laminosus* complex is examined (Figure 15 A) the location of such a binding site is much less clear, although co-evolution of Fd iso-proteins with the Cytb_6f complex and auxiliary subunits could result in differences in Fd- Cytb_6f interactions.

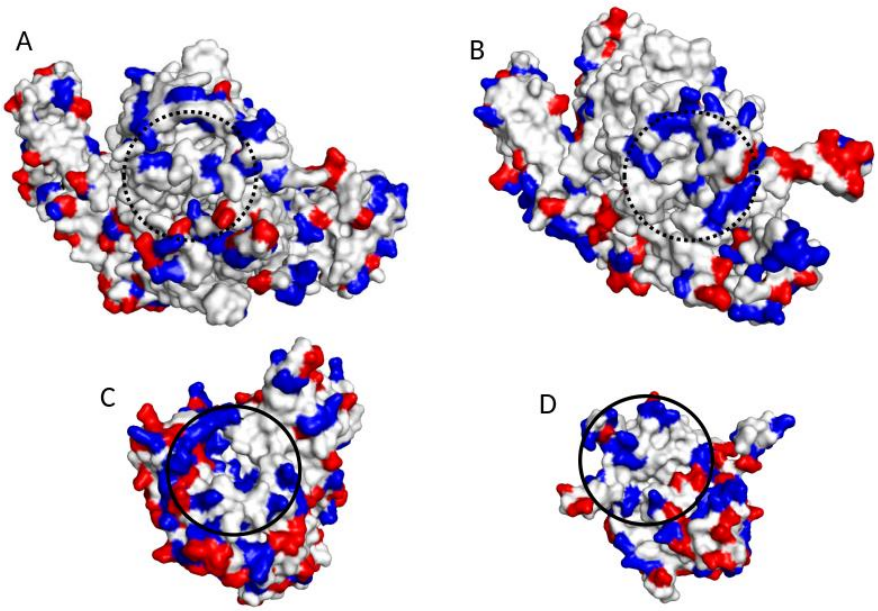

Figure 15. Comparison of charge distribution on the n side surface of the Cytb_6f with known Fd-binding sites. A) Cytb_6f monomer from *M. laminosa* (taken from 2D2C), seen as looking down from the n side B) Cytb_6f monomer from C. reinhardtii (taken from 1Q90), seen as looking down from the n side . C) Fd-dependent nitrite reductase (2AKJ), looking down on the Fd binding site, as defined by site directed mutagenesis studies. D) Fe:NADP(H) oxidoreductase (FNR, 1GAW), looking down on the Fd binding site, as defined by site directed mutagenesis studies and co-crystalization. Known Fd binding sites are highlighted with a black circle. The putative Fd binding site on Cytb_6f suggested by Nawrocki et al (2019)[374] is indicated by a hashed line. Positively charged groups in blue, negatively charged groups in red.

4.3.3 Direct electron donation from FNR to the cytochrome *b*$_6$*f*

Involvement of the FNR enzyme in re-injection of electrons into the quinone pool from the *n* side of the membrane has long been debated, and there is plenty of circumstantial evidence to suggest that this is the case. For example, CET appears inhibited in cyanobacteria when FNR is no longer tethered to the membrane [408], FNR is more strongly membrane bound in higher plant cells performing enhanced CET [409] and plants with diminished FNR content also show perturbed CET [410]. Moreover, FNR has been consistently co-localised with PgrL1[197,236], and FNR is no longer recruited efficiently to the membrane in the classic *pgr5* mutant of the alga *C. reinhardtii* [411]. Inhibitors of FNR indicate that the enzyme is essential to some CET pathways [233,375,412–416], although FNR does not bind antimycin A in solution [233], and is relatively insensitive to this CET inhibitor [417]. Immuno-inhibition studies show that blocking Fd to NADP(H) electron transfer by FNR does not affect CET activity [414,418], indicating that any CET role for FNR does not involve the $NADP^+$ binding site. On the other hand, It has been reported that Cyt*b*$_6$*f* complexes purified from spinach and incorporated into liposomes are only capable of NADPH mediated quinone reduction if the purification method is mild enough to preserve FNR binding [419]. It should be noted that the severe washes employed to remove FNR in this paper may also have removed other proteins important for this function, such as Fd and/or PgrL1. Importantly, addition of NADPH to the purified FNR:Cyt*b*$_6$*f* complex only results in reduction of Cyt*b*$_6$ in the presence of Fd [180].

Mutant studies on FNR would provide a definitive answer, but are lacking due to the difficulty in fully knocking out the gene for a protein that is essential for photo-autotrophic growth. Plants with minimal FNR downregulate the entire electron transport chain to compensate, leaving an extremely severe phenotype [420], making interpretation of CET measurements problematic.

The discovery that FNR is co-purified with the Cyt*b*$_6$*f* complex [180,421,422] prompted the suggestion that FNR could act as a conduit of electrons from Fd into the Cyt*b*$_6$*f*, potentially via the heme c_n [180,376]. As with Fd, the absence of information about where and how FNR docks to the Cyt*b*$_6$*f* is currently the major impediment to our understanding of a functional mechanism of electron transfer from FNR to the complex. It seems clear that the PgrL1 and Pgr5 proteins are involved in FNR recruitment to the membrane (and therefore probably the Cyt*b*$_6$*f*), at least in algae [411], but in higher plants FNR is recruited to the membrane by two tether proteins, Tic62 [423] and TROL [424]. Based on blue native PAGE analysis, it has been suggested that these are the only sites of FNR interaction[424,425]. However, this is likely a function of detergent disruption of interactions between FNR in complex with its tether proteins, and other thylakoid membrane components such as the Cyt*b*$_6$*f*. Indeed, in a blue native PAGE experiment using different solubilisation conditions, FNR co-migrated with several

complexes, including the Cytb_6f [426]. It remains unknown whether the tethering proteins Tic62 and TROL also play a role in FNR association with the Cytb_6f, or whether release of FNR from these tethers (which happens in response to the generation of ΔpH across the membrane) might prompt association with the Cytb_6f. Interestingly, only FNR iso-proteins capable of binding to the TROL tether were found co-purified with the Cytb_6f from maize [422].

If FNR acts as a conduit of electrons from Fd into the heme c_n, it prompts some energetic questions. The FAD moiety of FNR can be reduced by one electron from Fd to the flavin radical state (FNR_{ox} to FNR_{sq}), and a second electron can then fully reduce the FAD (FNR_{sq} to FNR_{red}), with redox midpoint potentials of -338 mV and -312 mV respectively measured at pH 8 [427], or NADPH can directly donate two electrons to fully reduce the FAD (FNR_{ox} to FNR_{red}), with a redox midpoint potential around -380 mV [428,429]. Any of these reduced centers would be adequate to reduce heme c_n, irrespective of whether the quinone site was occupied or not [430]. So, is the mechanism of FNR to Cytb_6f reduction a single or double electron transfer to the Q_n site from FNR? The dependence on Fd of NADPH mediated reduction of Cyt$b$ [180], and the seeming independence of CET on the NADPH binding site of FNR [414,418] implies that single electron reduction and oxidation of the FNR FAD moiety is sufficient for CET. It has also been suggested that rather than having an electron transfer function, FNR could simply act as an Fd recruiting module – providing a site for Fd to bind on the Cytb_6f complex before transfer of electrons directly to heme c_n or via PgrL1 [199]. A number of experiments are required to clarify the role of FNR recruitment to Cytb_6f in CET, principally: 1) more information is needed regarding the binding site of FNR on Cytb_6f, and its orientation; 2) the capacity for CET has to be correctly measured in membranes or cells where the FNR protein has no capacity to interact with the Cytb_6f or is missing. Finally, if electron donation from Fd or FNR directly to Cytb_6f is the major route of antimycin A sensitive CET, rates of electron transfer for this complex close to those estimated for the CET pathway – in the range of 10 e^{-1} s^{-1} PSI^{-1} to 130 e^{-1} s^{-1} PSI^{-1} [431] – would be the final proof.

5 Inhibitors

5.1 Cytochrome bc_1 specific inhibitors

Microorganisms often produce and secrete chemical substances in order to restrain or kill other species or strains. As Cytbc_1 is a crucial component of the respiratory chain in many bioenergetic systems, its quinone binding catalytic sites have become a critical target in this chemical warfare. Indeed, many compounds that bind to the catalytic sites and act as Cytbc_1 inhibitors can be

found in bacteria and fungi. Over the past few decades, these naturally-occurring toxins became popular templates for man-made chemicals, with many proposed functions, from medicinal drugs and treatments for parasitic infections, to fungicides in agriculture.

Depending on the site of action, the Cytbc_1 inhibitors are often divided into two groups. The first group is considered to be small, and consist of compounds with the ability to inhibit the Q_i site. The second group consists of the Q_o site inhibitors and is considered to be much larger, with numerous synthetic compounds developed over the years of research. Moreover, with recent developments, dual-mode inhibitors, capable of binding to both active sites, have been found or synthetized. It is important to note that this classification also excludes the inhibitors that do not act on the quinone-binding sites, such as cyanide, which has been shown to inhibit bacterial cytochrome *bc*1[136] or 2,3-dimercaptopropanol (also known as BAL or British anti-Lewisite) which is known as a respiratory inhibitor since the early studies on mitochondrial material[432] and later has been shown to destroy the Rieske cluster [433].

Inhibitors of the Q_i site. The best known compound that inhibits the Q_i site is antimycin A. However, this group consists also of naturally occurring ilicicolin H, funiculosin, funiculosin-related compounds, and various synthetic inhibitors (Fig. 16 and 17).

Antimycin A (Fig. 16 A) is a depsipeptide with an acyl- (R_1) and alkyl-substituted (R_2) dilactone ring with an amide linkage to a 3-formamidosalicylate moiety. In fact, antimycin A is a whole family of compounds (about 29)[434], produced by actinobacteria from the *Streptomyces* genus, with the first members isolated and identified in 1948.[435,436] Antimycin A1 has a high binding affinity to the Q_i site, with a dissociation constant (K_d) of 32 pM in bovine Cytbc_1.[437] It has been shown that antimycin is able to displace quinones and even other inhibitors from the active site.[438–440] Based on the crystal structures [63,79,123] it is known that the 3-formamidosalicylate group acts as the toxophore and forms hydrogen bonds with highly conserved residues of Q_i (Fig. 16 B), including the His, Asp and Lys, that serve as proton donors in Q reduction[163], and a conserved Ser. The dilactone ring of antimycin appears to control its solubility and hydrophobicity.[441] There have been attempts to create synthetic analogues (example in Fig. 16 C top) with the dilactone replaced by various other moieties[442–444], with promising *in vitro* results for biphenyl and biphenyl ether groups.[444] Some of synthetic inhibitors where the 3-formamidosalicylate moiety is replaced with benzazoles and the dilactone rings are replaced with a trifluoromethyl-substituted biphenyl ether moiety (Fig. 16 C, middle and bottom), were shown to be almost as potent as the natural antimycin A in *in vitro* inhibitor assays. However, they exhibited a negligible *in vivo* activity because of low uptake into the living cell.[442] Recently **UK-2A** (Fig. 16 D), which belongs to a group of dilactone compounds isolated from *Streptomyces* sp. 517-02[445,446], has been revisited and shown to bind to the Q_i site in a similar mode

to antimycin A.[447] In contrast to antimycin, UK-2A comprises a 4-methoxypyridin-3-ol moiety as its toxophore. Its inhibitory potency was estimated to be about 3-fold lower than that of antimycin.[448]

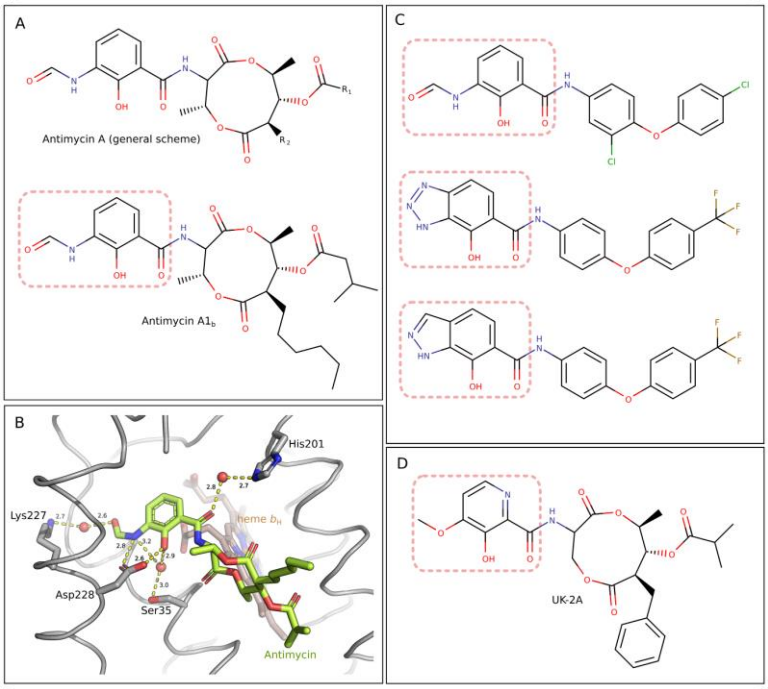

Figure 16. Structural features of antimycin and related compounds. **A**) Structural formulae of compounds belonging to the antimycin A family. The upper formula represents the general structural elements of antimycins A, the lower is a formula of antimycin $A1_b$. **B**) Stick/ribbon representation of binding of antimycin A in the Q_i site, as revealed by X-ray crystallography. Antimycin A (*pale green sticks*) forms a direct hydrogen bond to ^{Bt}Asp228 and additional, water-bridged bonds to ^{Bt}Lys227, ^{Bt}His201 and ^{Bt}Ser35 (*gray sticks*). Oxygen and nitrogen atoms are colored *red* and *blue*, respectively. Heme b_H shown in *brown*. The model is based on PDB entry 1PPJ. **C**) Structural formulae of synthetic antimycin analogues. **D**) Structural formula of UK-2A. In **A**, **C** and **D**, *pale-red, dotted* frames indicate the toxophore moiety of each compound.

Funiculosin (Fig. 17 A top) is an N-methyl-4-hydroxy-2-pyridone derivative, substituted with a cyclopentanetetrol moiety. It is a natural compound with antifungal properties, isolated from *Penicillium funiculosum*.[449,450] Funiculosin was shown to inhibit Cytbc_1 by a similar mechanism to antimycin A.[164,451,452] However, there is no structural data on funiculosin binding mode to the Q_i site. It is speculated that it binds in close proximity to heme b_H, as a rise in E_m of this heme by about 100 mV was observed in the inhibited enzyme.[164] Moreover, studies on yeast mutants of ^{Sc}Asp208 revealed that this residue can possibly be involved in funiculosin binding, which distinguishes it from antimycin.[452] Recently, funiculosin analogues were shown to be produced by other microorganisms, for example the compound **AS2077715** (Fig. 17 A, upper middle), isolated from fungal strain *Capnodium* sp. 33985. The AS2077715 has been shown to exhibit selective and highly inhibitory properties towards *Trichophyton mentagrophytes* Cytbc_1, while being a weak inhibitor of the

mammalian counterpart. Therefore, it has been proposed as a potential drug for *Trichophyton* infections.[453]

Another 2-pyridone deriviative, **Ilicicolin H** (Fig. 17 A, lower middle), was isolated from *Cylindrocladium ilicicola*[454] and *Gliocladium roseum*.[455] Despite some structural differences to funiculosins, ilicicolin was shown to act in similar way, being a potent and broad-spectrum antifungal agent[456], inhibiting yeast and fungal Cytbc_1 with high selectivity.[439,456] Thus, a 2-pyridone moiety is the suggested toxophore in both funiculosins and ilicicolins.[439] However, a closer examination of the influence of antimycin A, funiculosin and ilicicolin H on Cytbc_1 isolated from distinct organisms and yeast Q_i-site mutants, reveals some differences in sensitivity between the enzymes, which suggests that there is some variation in the binding mode of these inhibitors.[457]

The same 2-pyridone moiety as in funiculosin and ilicicolin H can be found in **sambutoxin** (Fig. 17 A, bottom) and related compounds isolated from *Fusarium sambucinum*[458,459] and other strains of *Fusarium*.[460,461] Sambutoxins have been also shown to be toxic to mitochondrial respiration and specific towards Cytbc_1.[459] Although their binding mode was not specified, they can be expected to bind to the Q_i site as well. More recently, several synthetic antimalarial compounds comprising a 4-pyridone ring with a biphenyl ether tail were also shown to inhibit the Q_i site, eg. **GSK932121**, **GW844520** (Fig. 17 B, top and middle)[462] or **MJM170** (Fig. 17 B, bottom)[463]. The co-crystal structures of bovine enzyme with these three novel inhibitors indicate that they all bind close to heme b_H, with the carbonyl group of the pyridone toxophore in a direct contact to the conserved ^{Bt}Ser35 [462,463].

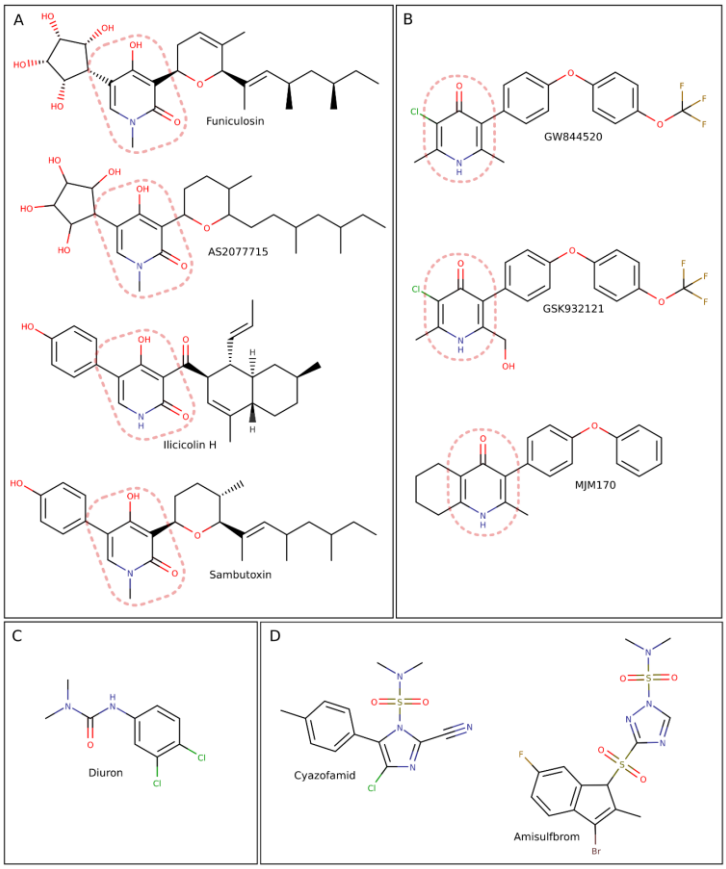

Figure 17. Structural formulae of Q_i site inhibitors: A) Naturally occurring 4-hydroxy-2-pyridone deriviatives. B) Synthetic 4-pyridone-based antimalarial drugs. C) Diuron. D) Sulfonamide-based commercial fungicides. *Pale-red, dotted* frames indicate the toxophore moiety of each compound.

Diuron (Fig. 17 C), 3-(3,4-dichlorophenyl)-1,1-dimethylurea, is a relatively simple synthetic compound which was shown to have strong inhibitory properties in photosynthesis and weak in mitochondrial respiration.[464] No structural data is available for its binding mode. The mechanism of action, through inhibition of the Q_i site, is known from genetic analysis of diurone- and antimycin-resistant mutations in the yeast model[465,466] and comparative kinetic studies.[467]

Cyazofamid (Fig. 17 D left) and **amisulbrom** (Fig. 17 D right) are commercial, synthetic compounds which are imidazole and triazole sulfonamides, respectively. Both are fungicides with high selectivity towards oomycetes.[468–470] Cyazofamid was shown to be almost inactive towards yeast, rat liver and potato tuber Cytbc_1[470] and a weak inhibitor of porcine Cytbc_1 Q_i site when compared to antimycin A.[437] Little is known about the binding mode of these inhibitors to the Q_i site.

However, based on computational docking studies, it has been suggested that cyazofamid forms a hydrogen bond to ^{Bt}Asp228.[437]

Inhibitors of the Q_o site. They are commonly divided into two subclasses. The compounds belonging to the first subclass, of which stigmatellin is the best known example, are capable of immobilizing the ISP-HD in a position near the Q_o site (in the *b*-position). The inhibitors belonging to the second subclass, such as myxothiazol or MOA-type compounds, bind deeper in the Q_o site cavity and do not fix the ISP-HD position. Therefore, these two subclasses are often refered to as P_f (with *f* originating from "fixed") and P_m (with *m* originating from "mobile") inhibitors, respectively. The influence of these inhibitors on movement of ISP-HD is explained in detail in section 3.4.

Stigmatellin A (Fig. 18 A, upper) is a natural compound isolated from the myxobacterium *Stigmatella aurantiaca*[471] and the inhibitor of Q_o site exhibiting the lowest K_d (<0.01 nM).[472] It consists of a chromone moiety, acting as its toxophore, substituted with a lipophylic alkenyl chain. Crystallographic studies have revealed that stigmatellin fixes the position of the ISP-HD near the Q_o site, by formation of hydrogen bond between carbonyl oxygen of chromone ring and one of the His residues acting as a ligand to the 2Fe2S (Fig. 18 B).[61,63,123,473] The second hydrogen bond is formed between the phenolic hydroxyl group of the compound and the carboxylate side chain of a conserved Glu residue (belonging to the PEWY motif) of the Cyt*b*.[63,474] The alkenyl tail of stigmatellin is not involved in any specific interactions, but studies on synthetic analogs indicate that modification of this tail can decrease the inhibitory potency of the compound.[472] However, such a modification was also made in the case of **tridecyl-stigmatellin** (Fig. 18 A, lower), which has the native tail replaced with tridecyl chain but retains its potency. It was developed as a stigmatellin replacement and a potential inhibitor of Cytb_6f.[475] Tridecyl-stigmatellin has been shown to bind to the Cytb_6f at both active sites[66] and also to inhibit the Q_o site of the bacterial Cytbc_1[151,263,472] in similar way to the natural compound.

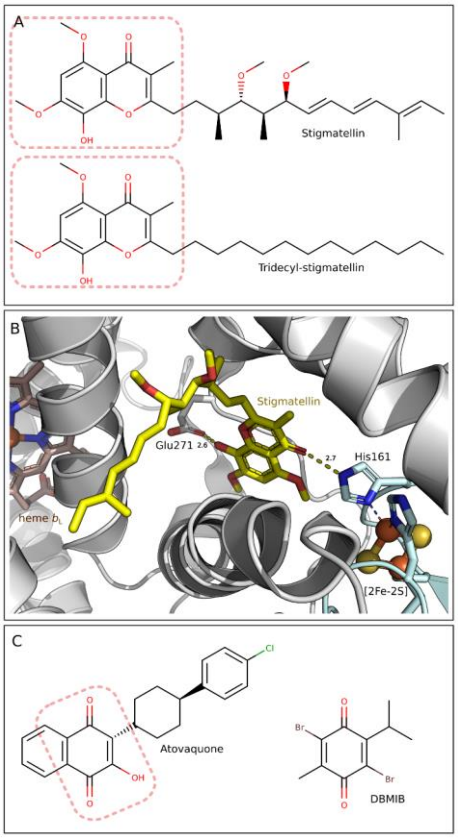

Figure 18. Q_o site inhibitors that fix ISP-HD at *b*-position. **A**) Structural formulae of natural stigmatellin A and synthetic tridecyl-stigmatellin. *Pale-red, dotted* frames indicate the toxophore moiety of each compound. **B**) Stick/cartoon representation of binding of stigmatellin A in the Q_o site, as revealed by X-ray crystallography. Stigmatellin A (*yellow sticks*) forms hydrogen bonds to ^{Bt}Glu271 of Cyt*b* (*gray sticks*) and to ^{Bt}His161 of ISP (*pale cyan sticks*). Oxygen and nitrogen atoms are colored *red* and *blue*, respectively. Heme b_L is shown in *brown*. Model is based on PDB entry 1PPJ. **C**) Structural formulae of atovaquone (left) and DBMIB (right). The toxophore of atovaquone is marked with a frame.

Atovaquone (Fig. 18 C left) is 2-hydroxynaphthoquinone substituted with a cyclohexyl-chlorophenyl moiety, which was developed as a drug for malaria in 1990s.[476] Among numerous other naphthoquinone derivatives created at the time, it was shown to be the most active against apicomplexan parasites, including several species of *Plasmodium*.[441,476–478] It is the only drug against Cytbc_1 currently in clinical use.[441] Atovaquone inhibits the enzyme of *P. falciparum* with nanomolar affinity,[476,479,480] and has much lower toxicity to the human counterpart.[480] The results of early studies, based on EPR and redox potentiometry, indicated that atovaquone has a similar binding mode to stigmatellin, and also arrests ISP-HD at *b*-position.[479] Moreover, based on the complementary molecular modeling studies, atovaquone was suggested to bind within the Q_o site, forming a hydrogen bond between its hydroxyl group and the 2Fe2S cluster-ligating His residue, and a water bridge between the carbonyl oxygen at position 1 of naphthoquinone ring and the conserved Glu of PEWY motif.[479] However, crystallographic studies on yeast showed that the only hydrogen bond is formed

between the ionized hydroxyl group of the inhibitor and the Nε atom of ^{Sc}His181. The ^{Sc}Glu272 residue side chain was shown to face the opposite direction with respect to the carbonyl oxygen, and does not appear to be involved in atovaquone binding.[71]

DBMIB (Fig. 18 C, right), 2,5-dibromothymoquinone, is a halogenated benzoquinone derivative. Although DBMIB is known more as a Cytb_6f inhibitor [110] (see section 5.2), it has been shown to exhibit similar potency against Cytbc_1.[481] DBMIB should not be considered as a regular inhibitor competing with QH_2, as has been commonly assumed. Rather, it binds to the Q_o site in the form of a semiquinone and there forms a spin-coupled state with 2Fe2S, which leads to locking of the ISP-HD at *b*-position.[482] (see section 7.6). The spin-coupled state can be detected in EPR experiments as the prominent g = 1.94 EPR signal in X-band at low temperatures.[84,108,110,483]

UHDBT and **HHDBT** (Fig. 19 A) are both 6-hydroxy-4,7-benzothiazolediones (HDBT) with undecyl and heptyl tails, respectively. HDBT compounds are synthetic inhibitors capable of binding to the Q_o site.[70,116,484,485] As they comprise the hydroxybenzoquinone moiety, they exist as a mixture of ortho- and para-quinone tautomers (Fig. 19 B). The 6-hydroxy group is ionizable, with a pK_a of 6.5, which is reflected in a distinctive color change from yellow to violet when pH changes from acidic to alkaline.[486] These compounds are also redox active and, as is typical for quinones, the E_m exhibits a pH dependence with a slope of about 60 mV/pH unit.[486] Thus, HDBTs may be regarded as substrate analogues. However, the E_m value of UHDBT was shown to be about -40 mV at pH 7[486], thus much lower than the ubiquinone pool (about 100 mV).[487,488] Cytochrome bc_1 inhibition by UHDBT was found to be pH dependent, with a 10-fold decrease in the binding rate constant at more alkaline pH.[485] This had been initially associated with ionization of the hydroxyl moiety. However, this effect was also noted for 6-bromo substituted UHDBT.[484] As indicated by the results of X-ray crystallography, HDBT compounds immobilize the ISP-HD in the *b*-position, via formation of a hydrogen bond with one of His ligands of the 2Fe2S cluster.[70,77,474] However, there is no agreement on the detailed mode of hydrogen bonding for HHDBT and UHDBT within the Q_o site. Based on the structure of yeast Cytbc_1 co-crystalized with HHDBT, hydrogen bonds are proposed to form between: 1) the oxygen from the ionized hydroxyl group of HHDBT and the protonated Nε of ^{Sc}His181 of the ISP, 2) the carbonyl O4 atom and the water molecule that is itself bonded to the backbone nitrogen of the Glu within the PEWY motif.[70] A slightly different model has been proposed in the case of bovine Cytbc_1 interaction with UHDBT. It was suggested that the protonated His of ISP interacts with the carbonyl O7, while its deprotonated form interacts with the hydroxyl group of the inhibitor. Moreover, the carbonyl O4 and N3 of UHDBT were suggested to form a hydrogen bond with the hydroxyl group of the conserved ^{Bt}Tyr131 of the Cyt*b* (^{Sc}Tyr132).[77].

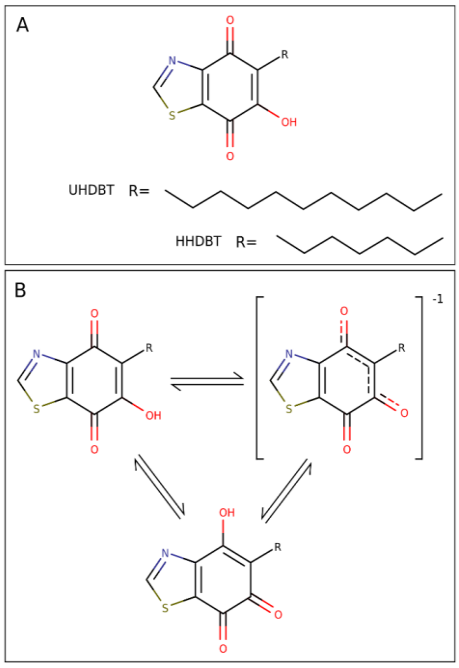

Figure 19. Structural features of 6-hydroxy-4,7-benzothiazolediones. **A**) General structural formulae of *n*HDBT compounds. **B**) Possible tautomeric states of nHDBT compounds.

Crocacin A and D (Fig. 20 A, upper and middle) are naturally occurring dipeptide deriviatives, comprising a Z-enamide moiety of glycine and either a aminohexadienoic or aminohexenoic acid (respectively), substituted with a polyketide acyl tail. They belong to a whole family of compounds isolated from the myxobacterium *Chondromyces crocatus*.[489–491] Some of the crocacins exhibit inhibitory properties against many strains of bacteria, yeasts and fungal plant pathogens, with (+)-crocacin D recognized as the most potent compound of the family.[75,491] In studies on bovine Cytbc_1 in SMP's it has been shown that the inhibitory mechanism of crocacins is based on binding to the Q_o site.[489] The model for binding of crocacin A and D was developed based on EPR studies and crystallographic analysis of the crocacin D analogue (Fig. 20 A, bottom) bound to the avian Cytbc_1, combined with molecular modeling and docking studies. Crocacins were shown to immobilize the ISP-HD in the *b*-position, with the Z-enamide carbonyl forming a hydrogen bond to Nε of the 2Fe2S-ligating His. Moreover, it was suggested that the glycine residue of crocacin can form hydrogen bonds to the backbone nitrogen with the PEWY motif Glu and to the carbonyl group of the conserved Met (^{Bt}Met138) of Cyt*b*. However, the existence of a hydrogen bond to the Met residue is not supported by the crystal structure. Interestingly, the Z-enamide seems to adopt a hairpin conformation, with an intramolecular hydrogen bond between the two amide groups.[75]

Because natural crocacins have been shown to exhibit a photostability of minutes under field conditions,[75] they are not suitable for use in agriculture, despite their inhibitory potency. However, in

recent years, several methods for synthesis of crocacins[491,492] and their simplified, more stable analogues have been developed.[493]

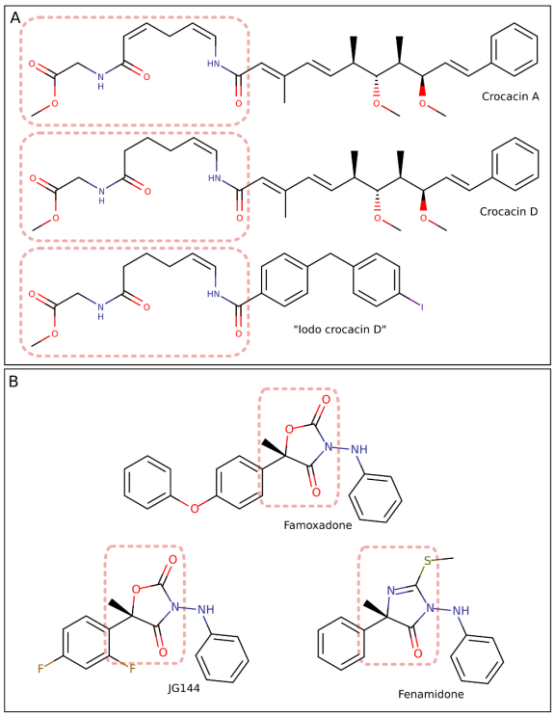

Figure 20. Crocacins and famoxadone-like compounds. **A**) Structural formulae of natural crocacins A and D (top and middle, respectively) and synthetic derivative of crocacin D (bottom). **B**) Structural formulae of famoxadone (upper), JG144 (lower, left) and fenamidone (lower, right). *Pale-red, dotted* frames indicate the toxophore moiety of each compound.

Famoxadone, **JG144** and **fenamidone** (Fig. 20 B) are synthetic fungicides. The toxophores of famoxadone and JG144 comprise 1,3-oxazolidine-2,4-dione, and that of fenamidone comprises imidazol-4-one [78,117,494,495]. The famoxadone molecule is chiral, and the S-(-)-enantiomer has been shown to be active against Cytbc_1.[496] The crystal structures of famoxadone [78,117,495] and its analogs[78,117,495] indicate that these inhibitors bind to the Q_o site in the same fashion, with carbonyl oxygen at ring position 4 forming a hydrogen bond to the backbone nitrogen of the PEWY motif Glu. This resembles the binding mode of MOA-like inhibitors, but in contrast to those, famoxadone-like inhibitors are capable of immobilizing the ISP-HD near the Q_o site, close to *b*-position (P_f inhibitors subclass).[474] However, famoxadone and its analogs do not form a hydrogen bond with the His of the ISP as in the case of other ISP-fixing compounds.[78,117] Rather, the inhibitor binding is thought to induce conformational changes, which result in formation of a hydrogen bond between the 2Fe2S His ligand and a highly conserved Tyr residue of the *ef* α-helix of Cyt*b*, thus immobilizing the ISP-HD in the near *b*-position.[117]

Myxothiazol A (Fig. 21 A, top) is a natural compound obtained from the predatory bacterium, *Myxococcus fulvus*.[497,498] It is the best known representative of the thiazole-based bacterial toxins that possess a β-methoxyacrylamide or β-methoxyacrylate (MOA) toxophores.[474,499,500] Myxothiazol is considered a classic P_m type Q_o inhibitor - its binding does not involve the immobilisation of the IPS-HD in the *b*-position. Based on the structure of the bovine Cytbc_1 co-crystallized with myxothiazol [77], it has been proposed that the inhibitor molecule is bound to the Q_o pocket, mostly through interactions of the dithiazole moiety with aromatic residues in the binding site and by a characteristic hydrogen bond formed between the amide oxygen atom of myxothiazol and the backbone amide of the conserved Glu in the PEWY motif. Moreover, the amide nitrogen of myxothiazol can form a hydrogen bond with the conserved Tyr of the PEWY motif. It was also suggested that the C18 methyl group of myxothiazol can serve as an unusual hydrogen bond donor to the sulfur atom of ^{Bt}Met124. It is worth mentioning, that myxothiazol-related compounds that demonstrate inhibitory properties towards the Q_o site are more abundant. In the case of *M. fulvus* toxins, myxothiazol Z, which comprises a β-methoxyacrylate moiety, has also been shown to exhibit antifungal properties *in vivo*.[501] This group also includes the **melithiazols** (Fig. 21 A, middle) isolated from *Melittangium lichenicola* and several other strains [502] and **cystothiazoles** (Fig. 21 A, bottom) from *Cystobacter fuscus* [503], which were shown to exhibit antifungal properties *in vivo*.[502,503] In the enzymatic assays with bovine SMP's, melithiazol A was shown to exert a similar spectroscopic effect on redox cofactors to that of myxothiazol.[502] Therefore, it can be expected that these inhibitors have a similar mode of binding to the Q_o site.

Another group of myxobacterial compounds, **cyrmenins** (Fig. 21 B), were obtained from *Cystobacter armeniaca* and *Archangium gephyra*. Cyrmenins are distinct from myxothiazol-related compunds, and comprise a MOA moiety substituted at the α-position.[504] **Cyrmenin B_1** has been shown to inhibit Cytbc_1, but the binding mode was not investigated in details.[505] The presence of the MOA toxophore suggests that cyrmenin targets the Q_o site as well.

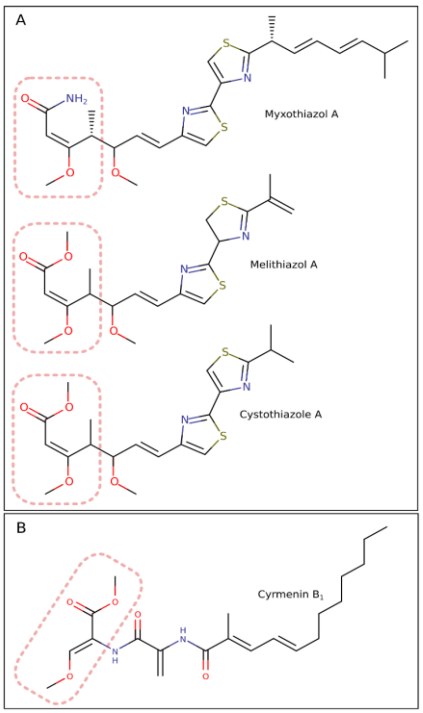

Figure 21. MOA-comprising myxobacterial toxins. **A)** Structural formulae of natural Q_o site inhibitors with dithiazole moieties: myxothiazol A (top) comprising β-methoxyacrylamide toxophore and two other, comprising the β-methoxyacrylate toxophore, melithiazol A (middle) and cystothiazole A (bottom). **B)** Structural formula of cyrmenin B_1. *Pale-red, dotted* frames indicate the toxophore moiety of each compound.

Strobilurins (Fig. 22) are currently recognized as a large group of synthetic P_m class Cytbc_1 inhibitors with various structures and toxophore moieties. However, such generalization can be confusing, and in fact they were all designed using natural fungal poliketydes as a template. These compounds were isolated from several species of large, wood-decaying Basidiomycetes, initially named strobilurins, eg. **strobilurin A** (also known as mucidin [506]), (Fig. 22 A left) from *Strobiluris tenacellus* [507] and **oudemansin A** (Fig. 22 A, right) from *Oudemansiella mucida* [508]. Later an Ascomycete*, Bolinea lutea* was also reported to produce strobilurins and their derivatives [509]. Natural strobilurins possess the β-methoxyacrylate (MOA) toxophore[499,510] (Fig. 22, **1** in *red frames*), which targets the heme b_L proximal part of the Q_o site[511,512]. In contrast to myxothiazol-like inhibitors, the β-methoxyacrylate moiety of strobilurins is substituted with a tail at the α-position, not the β-position. Due to this difference, their distinct origin, and their separate paths of biosynthesis[513], myxothiazol and other myxobacterial compounds should not be referred to as "strobilurins". The presence of MOA in both groups of compounds should be rather taken as a biochemical example of evolutionary convergence. Natural strobilurins exhibit a low photostability[510]. Therefore, various synthetic compounds (Fig. 22 B) with differently substituted MOA toxophores (Fig. 22, **1** in *red frames*) have been created, such as **MOA-stilbene** [57], **azoxystrobin**[77] or **picoxystrobin** [510,514]. Several deviations

from classic MOA toxophore were developed (Fig. 22 B, **2-8** in *red frames*), such as oximino-acetate (**2**) e.g. **kresoxim-methyl** [510,514] and **trifloxystrobin** [510,514], oximino-acetamide (**3**) e.g. **dimoxystrobin** [510], methyl N-methoxycarbamate (**4**) e.g. **pyraclostrobin**[514,515], triazolinone[516] (**5**) e.g. **JZZ**[117], tetrazolinone (**6**) eg. **metyltetraprole**[517], dihydro-dioxazine (**7**) eg. **fluoxastrobin**[510] and the methyl-carbamate (**8**) e.g**. pyribencarb**.[518] Such diversity of synthetic strobilurin analogues is mostly a result of "patent wars" between agrochemical companies, driven by a large demand from the global fungicidal market.[514] Despite apparent differences in structure, man-made strobilurins are expected to share the same binding mode to the Q_o site as the classic MOA inhibitors. This has been partially confirmed by the results of X-ray crystallographic studies on Cytbc_1 with bound MOA-stilbene[77,83], azoxystrobin[77], trifloxystrobin[474], iodinated derivative of kresoxim-methyl[474], and JZZ (PDB ID:3L73)[519], showing that the toxophores of these inhibitors superimpose within the binding site, with formation of a hydrogen bond to the backbone amide of the conserved PEWY motif Glu residue. Among the synthetic strobilurin-like inhibitors mentioned here, pyribencarb has been suggested as a novel, "benzylcarbamate" type of Q_o inhibitor.[518] Indeed, it has been shown to possess a higher selectivity than other MOA analogues. However, neither its methyl-carbamate toxophore nor binding mode are as unique as has been claimed because methyl-carbamate moiety is present in previously described natural crocacins, and also in macrolides isolated from sponges, such as **neopeltolide** (Fig. 23 A, upper) from unidentified *Daedalopelta* sp.[520,521] and **leucascandrolide A** (Fig. 23 A, lower) from *Leucascandra caveolata.*[522] Enzymatic assays confirmed that these compounds also exhibit inhibitory properties towards Cytbc_1.[523] Moreover, the recent molecular modeling docking studies revealed that pyribencarb, crocacin and neopeltolide all bind to the Q_o site through their methyl-carbamate moieties, in a way similar to the MOA moiety of azoxystrobin, forming a hydrogen bond to the backbone amide group of ^{Bt}Glu271.[524]

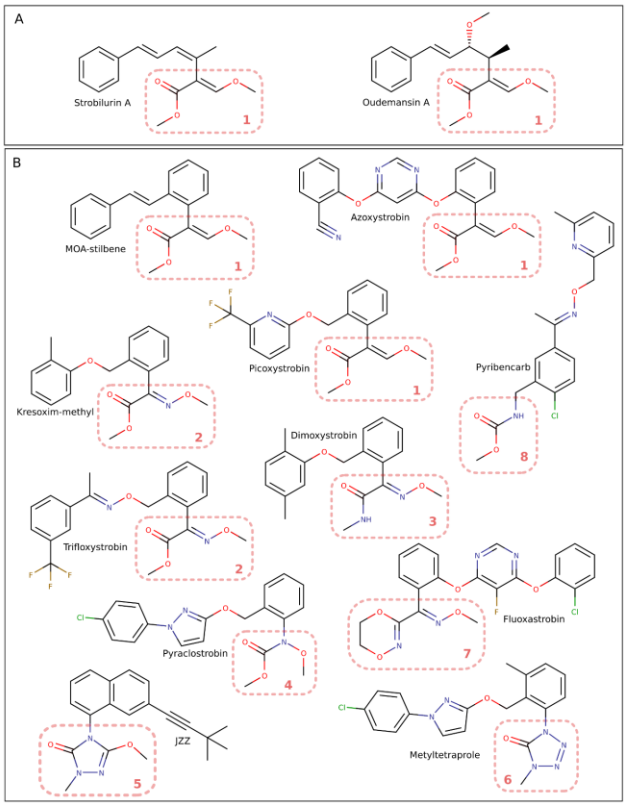

Figure 22. Structural formulae of selected natural (**A**) and synthetic (**B**) strobilurins**.** *Pale-red, dotted* frames indicate the toxophore moiety of each compound. Numbers within frames indicate the type of toxophore (explained in text).

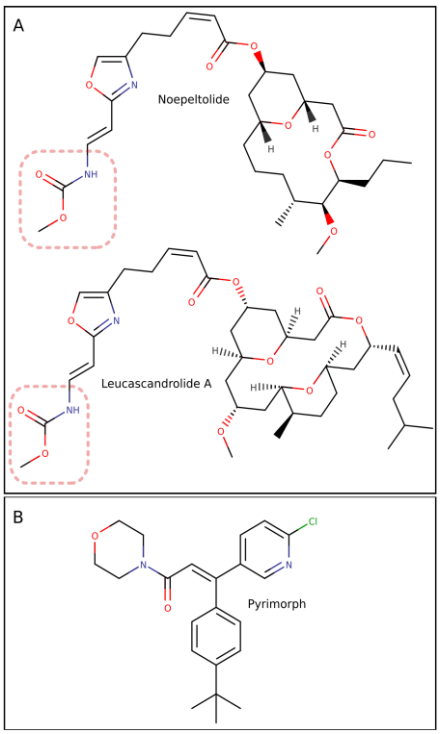

Figure 23. Structural formulae of (**A**) macrolides isolated from sea sponges, with their methyl-carbamate toxophores marked with frames, and (**B**) pyrimorph. *Pale-red, dotted* frames indicate the toxophore moiety of each compound.

Pyrimorph (Fig. 23 B) is a synthetic morpholine derivative, already in use as a fungicide against pathogens of plants.[525–527] It has been shown to exhibit inhibitory activity towards multiple targets, including cellulose synthase A [526] and Cyt*bc*$_1$.[527] Results of enzymatic assays indicate that pyrimorph acts as a non-competitive inhibitor of the Q_o site. Moreover, complementary molecular modeling studies showed that pyrimorph docks in the central cavity between Cyt*bc*$_1$ monomers, at the entrance of the Q_o site, and thus blocks access of the substrate. The binding mode of pyrimorph has no resemblance to any other Q_o site inhibitor. It was found that it does not form hydrogen bonds within the Q_o site, but instead it is held in place by hydrophobic and van der Waals interactions.[527] Thus, pyrimorph should be considered a unique inhibitor type, distinct from MOA-related compounds.

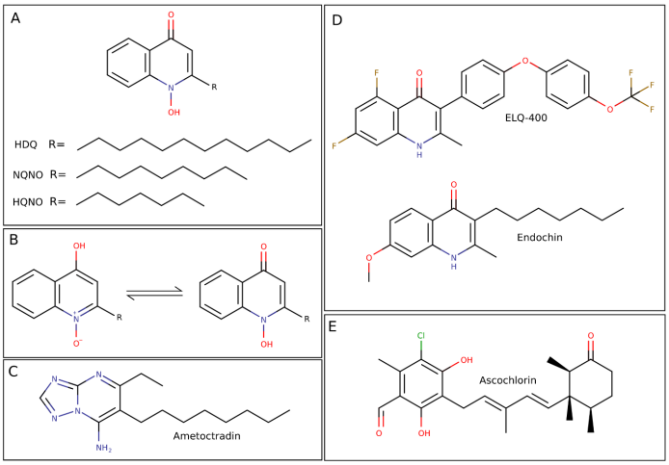

Figure 24. Structural formulae of dual-mode inhibitors of Cyt*bc*$_1$. A) 1-hydroxyquinolin-4-ones. B) Tautomeric states of 1-hydroxyquinolin-4-one. C) Ametoctradin. D) Quinolones. E) Ascochlorin.

Dual-mode inhibitors. Some inhibitors are capable of binding to both Q_i and Q_o catalytic sites, therefore they should be considered as a third, dual-mode class of Cyt*bc*$_1$ inhibitors. They are often quinone analogues or compounds semi-isosteric with quinones, and therefore able to mimic the natural substrate within both sites.

The 2-alkyl derivatives of 1-hydroxyquinoline-4-one, such as **HQNO**, **NQNO** or **HDQ** (Fig. 24 A) are usually considered Q_i site inhibitors, with a mechanism of action similar to that of antimycin A.[111,438,528] Some early reports suggested that HQNO and NQNO bound to Cyt*bc*$_1$ can be displaced by both antimycin A and UHDBT.[529,530] This effect was explained as a possible result of allosteric interactions between the two binding sites.[530] However, more recent crystallographic analysis has shown that NQNO is indeed capable of binding to both Q_i and Q_o sites. It has been proposed that in

solution, NQNO most likely exists as a mixture of two tautomers (Fig. 24 B), which is likely a determinant factor in this dual mode of binding. At the Q_i site, the NQNO tautomer with its hydroxyl group protonated (Fig. 24 B, left) can form a hydrogen bond to ^{Bt}Ser205, while the form with N-oxide protonated (Fig. 24 B, right) can hydrogen bond with ^{Bt}Asp228. In the structural model obtained in these studies, the ^{Bt}His201 imidazole ring was not in the correct orientation for hydrogen bonding. At the Q_o site, the N-oxide protonated form of NQNO can form two hydrogen bonds. The N-oxide oxygen forms a water-mediated hydrogen bond with ^{Bt}Glu271 of the PEWY motif, and the 4-carbonyl oxygen forms a hydrogen bond with the His (^{Bt}His161) ligand of 2Fe2S cluster, immobilizing the ISP-HD in *b*-position.[79] However, there is no data to confirm the dual-mode binding for other 1-hydroxyquinoline-4-ones. Recent studies suggest that HQNO induces changes in the environment of the Q_o site, but not due to binding in the site.[111]

ELQ-400 (Fig. 24 D, upper) is a 4(1H)-quinolone, one among a large number of derivatives of the antimalarial drug, **endochin** (Fig. 24 D, lower) [441,531]. Most of ELQ's (endochin-like quinolones) are expected to inhibit the Q_i site of apicomplexan Cytbc_1.[441,531,532] Thus, it was proposed that they be used in combination with the Q_o site-targeting atovaquone.[532] However, it has recently been suggested that the binding mode of ELQ-400 is more complex, with the inhibitor targeting both active sites [533]. This proposal was strongly supported by mutational analysis and molecular modeling studies. At the Q_i site, ELQ-400 was predicted to bind in a similar manner to the substrate or pyridone inhibitors (mentioned earlier). At the Q_o site, it was predicted to bind similarly to atovaquone or stigmatellin, with a hydrogen bond formed by the NH group of the quinolone to the His ligand of 2Fe2S cluster.[533]

Ametoctradin (Fig. 24 C) is a triazolopyrimidine derivative, acting as a highly selective inhibitor against the Cytbc_1 of oomycetes.[469,534,535] It has been shown to be active against mammalian (porcine)[468], but inactive towards yeast[535] Cytbc_1. Ametoctradin is commonly used in agriculture and available under trade name Initium®.[534] No cross-resistance of ametoctradin with MOA-like inhibitors has been observed, so it is speculated to bind in the Q_o site in a manner similar to stigmatellin.[535] However, the molecular modeling docking studies have shown that although ametoctradin binds in roughly the same part of Q_o pocket as stigmatellin, and forms a hydrogen bond to the carboxylate side chain of the conserved PEWY motif Glu residue, the distance to the 2Fe2S-ligating His residue is too far to expect formation of a strong hydrogen bond.[468] In addition there is no experimental indication that ISP-HD is immobilized by ametoctradin in the *b*-position, as in the presence of stigmatellin. More recent studies suggest that ametoctradin is a dual-mode inhibitor, targeting both the Q_i and Q_o site.[536] This model seems to be supported by the observation that ametoctradin is inactive towards the wild-type strain of *Saccharomyces cerevisiae* and active towards

a mutant with an altered Q_i site. Based on this finding it was suggested that, like NQNO, ametoctradin can bind to both active sites.

Ascochlorin (Fig. 24 E) is an isoprenoid compound, which was independently isolated from four distinct fungal strains (*Ascochyta viciae* [537,538], *Cylindrocladium ilicicola* [454], *Fusarium* sp. LL-Z 1272 [539] and *Acremonium luzulae* [540]) and described by four different research groups at about the same time. Because of this remarkable coincidence, it can be found in the literature and databases under three different names: ascochlorin, LL-Z 1272γ and ilicicolin D [541]. In the recent comprehensive biochemical, spectroscopic and crystallographic studies, ascochlorin has been shown to bind to both Q_i and Q_o sites of bacterial, yeast, mammalian and avian Cytbc_1 [542]. At the Q_i site the position of the aromatic ring of bound ascochlorin overlaps with the position of the bound ubiquinone aromatic ring. Moreover, at the Q_i site, it has been proposed that ascochlorin forms a halide bond between the Cl atom and the conserved His (the proton donor in Q reduction) and a hydrogen bond between its hydroxyl group in the para position to Cl and the conserved Asp (the second proton donor in Q reduction). At the Q_o site, ascochlorin occupies a position similar to stigmatellin. A hydrogen bond, is formed, possibly from both the hydroxyl group and the C=O group to the His ligand of 2Fe2S cluster, immobilizing ISP-HD at the *b*-position. On the other side of the aromatic ring, the Cl atom is suggested to form a halide bond with Glu in the conserved PEWY motif. However, as it has been pointed out that a mixture of conformations may exist, this remains uncertain. The dual mode of action can be explained in terms of ascochlorin and related compounds being in general, ubiquinone analogs, as they can mimic natural substrates also in other ubiquionol oxidoreductases.[543]

The inhibitors of Cytbc_1 already comprise numerous groups of compounds, both natural and synthetic, with new ones being discovered or developed almost every year.[524,544] Many were omitted in this section, as little is known about their mechanism of action, and any attempt to deduce or model it would go beyond the scope of this review. Some recent discoveries in the field are rather unexpected, for example the recent findings with **karrikinolide** (Fig. 25, upper), a naturally occurring byproduct from the combustion of plant material, which earlier had been shown to stimulate plant seed germination.[545] Karrikinolide itself exhibits almost negligible inhibitory properties towards Cytbc_1. However, some of its synthetic derivatives, such a 4-*n*-butylphenyl-substituted variant (Fig. 25, lower), have been shown to inhibit porcine Cytbc_1 with efficiency comparable to commercially available inhibitors [546].

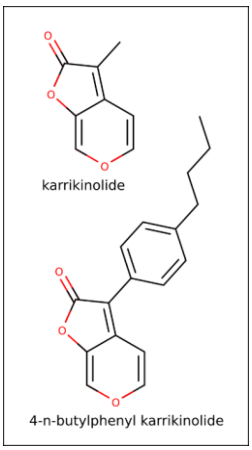

Figure 25. Structural formulae of karrikinolide (upper) and its 4-*n*-butylphenyl derivative (lower panel).

5.2 Cytochrome b_6f-specific inhibitors

Several inhibitors have been employed to characterize the functional and structural features of the Cytb_6f. These compounds act on both the Q_p and the Q_n sites similarly to the situation described above for the Cytbc_1.

Inhibitors of the Q_p site. Typical inhibitors of this site are: DNP-INT, stigmatellin and DBMIB.

DNP-INT (2,4- dinitrophenylether of 2-iodo-4-nitro-thymol) (Fig. 26) belongs to the family of dinitrophenyl ethers [547], i.e., compounds that compete with plastoquinol for its oxidising pocket without having redox properties. These compounds do not act as electron donors or redox mediators, unlike DBMIB (see below). DNP-INT inhibits photosynthetic electron flow *in vitro*, where its activity can be circumvented by addition of TMPD (N-tetramethyl-p-phenylenediamine), an artificial electron carrier able to mediate e- flow from PQH_2 to the Cyt*f* (Trebst 1980). DNP-INT is also active *in vivo* as demonstrated by the work of Delosme and colleagues in *Chlorella sorokiniana* [548]. In this organism, DNP-INT lowers the rate of Cytb_6 oxidation and of PC reduction under single turnover flash conditions. Furthermore, DNP-INT diminishes the amplitude of the slow phase of the Electrochromic Band Shift (ECS), a modification of the absorption spectrum of intra-membrane pigments in response to the transmembrane electrical field (ca. $3x10^5$ V/cm) an expression of the quantum-mechanical Stark Effect, following the establishement of the proton motive force across the thylakoids membrane, [549]. The ECS slow phase (phase B) has been proposed to be a consequence of the transfer of an electron across the low potential chain of the cytochrome complex[550]. A study by Fitzpatrick and colleagues challenged the efficiency of DNT-INT as an inhibitor of photosynthetic electron flow. A possible explanation for this finding is that DNP-INT would be a poor inhibitor in

continuous light, while efficiently blocking Cytb_6f under single turnover illumination, as previously reported[551].

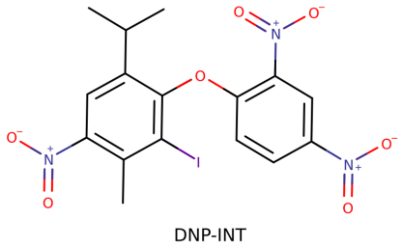

Figure 26. Chemical structure of DNP-INT inhibitor

Stigmatellin (Fig. 18A) is a potent antibiotic obtained from the myxobacterium *Stigmatella aurantiaca*, which inhibits both the Cytbc_1 and Cytb_6f. [552] This compound binds to the PQH_2 oxidising site, as shown by crystallographic studies in cyanobacteria and green algae [41,42], although not in the same position in the two organisms. Stigmatellin interacts with the 2Fe2S, raising its midpoint potential (in isolated Cytb_6f) from 320 to about 460 mV [553]. This increase in potential is accompanied by changes in the EPR spectrum of the 2Fe2S cluster. *In vivo*, its action mechanism is similar to that DNP-INT.[551] Under single turnover flash illumination, stigmatellin reduces, in parallel, the rate of Cyt*f* and of Cytb_6 reduction in a concentration-dependent manner.

In Cytbc_1, stigmatellin has been extensively used to probe conformational changes related to the moment of ISP-HD from a proximal site, i. e. close to the quinol, to a distal site, close to Cyt*c* (reviewed in Berry et al. [1]). This movement is required to facilitate electron flow in the high potential chain, and to promote electron bifurcation, as predicted by the Q cycle mechanism [1]. In Cytb_6f, the transition between these two positions has not been resolved by X-ray crystallographycally in the same clear cut manner as in Cytbc_1. Nonetheless, electron crystallography [554] has underlined movements of the ISP-HD in the Cytb_6f, via the comparison of projection maps of thin three-dimensional crystals of Cytb_6f prepared with or without stigmatellin. 2D crystallography has also suggested possible conformational changes in the transmembrane region of the complex, upon stigmatellin binding.

Unlike other inhibitors of Cytb_6f, stigmatellin binds not only to the luminal but also to the stromal side of the Cytb_6f [66,173]. The Q_n site has a lower affinity for stigmatellin than does the p-side lumenal site. In the Q_n site stigmatellin faces the quinone exchange cavity, being in interaction with Arg 207 of the Cytb_6 and the supplementary heme c_n. (see also section 3.6.2).

DBMIB (2,5-dibromothymoquinone) (Fig. 18 C) is probably the most representative of a class of inhibitors based on halogenated or hydroxylated lipophilic benzoquinones [547]. DBMIB has been extensively used as a specific inhibitor of PQH_2 oxidation. Early results by Haehnel indicate that it does not affect PQ reduction by PSII, while blocking its reoxidation by PSI [555]. The number of DBMIB molecules required for inhibition is one per 300 chlorophylls, i.e. one per electron-transport chain. This would argue in favour of a 1 to 1 binding stoichiometry with Cytb_6f. However, studies of the consequences of DBMIB on the EPR spectrum of the 2Fe2S by Roberts and Kramer led to the conclusion that two molecules of DBMIB bind to each monomer of the spinach Cytb_6f, both in the isolated form and in intact thylakoid membranes[556]. Binding likely occurs in two sites: a high affinity one, where DBMIB binding would cause small shifts in the EPR spectrum of the 2Fe2S similar to those induced by stigmatellin, and a low-affinity site, where binding was induced by super-stoichiometric amounts of the inhibitor. DBMIB binding is accompanied by the appearance of a new EPR signal (g = 1.94). The binding of two molecules of DBMIB to the Q_p/Q_o pocket would be consistent with the so-called "double-occupancy" models proposed in the case of Cytbc_1 (see paragraph **Erreur ! Source du renvoi introuvable.**). However, crystallographic data unambiguously showed that only one molecule of DBMIB can bind to the PQH_2 oxidation site.[67] To reconcile these findings, Roberts and coworkers, repeated the EPR spectra with oriented Cytb_6f [110], and found that DBMIB affects the orientation of the ISP-HD within Cytb_6f depending on the stoichiometry of the inhibitor at the Q_p/Q_o site. With a single DBMIB, the EPR signatures of the ISP-HD are consistent with this protein being in the proximal position (close to the Q_p/Q_o pocket), similar to the orientation observed in the X-ray crystal structure of the Cytb_6f in the presence of DBMIB [67]. With ≥ 2 equiv. of DBMIB bound, the ISP-HD would be in a position resembling the one observed in the *Chlamydomonas reinhardtii,* Cytb_6f in the presence of tridecylstigmatellin (TDS) [41], suggesting that the low-affinity DBMIB site is at the distal niche. This conclusion is consistent with earlier EPR measurements of isolated Cytb_6f poisoned with DBMIB [84], and can explain the peculiar mechanism of inhibition of PQH_2 oxidation by this compound observed *in vitro* and *in vivo*.

Early studies by Rich and colleagues [557] showed that reduced DBMIB ($DBMIBH_2$) does not block the Cytb_6f activity during its first turnover. Thus, DBMIB would bind the complex in its reduced form but only become inhibitory upon its oxidation. The inhibitory complex would thus involve a semiquinone or a quinone form of DBMIB. This hypothesis was subsequently confirmed in vivo [551]. The authors found that DNP-INT affects equally the low- and high-potential chain of Cytb_6f decreasing the rates of both Cyt$f$ reduction and Cytb_6 turnover. Conversely, DBMIB inhibits only the rate of Cyt$f$ reduction while reducing, at the same time, the amplitude of Cytb_6 redox signals. The

accessibility of DNP-INT to the Q_p site was unaffected by preillumination, while that of DBMIB was greatly enhanced, even after a single turnover. Overall, the authors propose that oxidation of $DBMIBH_2$ by a single turnover flash would trigger the same conformational changes of the ISP-HD that occurs during oxidation of PQH_2 in unpoisoned Cytb_6f. This would allow transferring one electron to the high-potential chain, and generating at the same time the inhibitory DBMIB species [551]. Slow reduction of DBMIB inside the Q_p pocket (see Rich et al. [557]) would regenerate $DBMIBH_2$, which would diffuse out of the quinol binding pocket, unlashing the inhibition. A relatively recent study by Sarewicz/Bujnowicz et. al. revealed that the EPR spectrum of 2Fe2S in DBMIB-supplemented spinach Cytb_6f is frequency-dependent which is a strong indication that DBMIB semiquinone at the Q_p site is spin-spin coupled to the reduced 2Fe2S [482].

Besides being extensively used to characterize electron flow in the photosynthetic chain, DBMIB has also been largely employed to study cell biological responses in photosynthetic organisms. Combining DBMIB with the PSII specific inhibitor DCMU allows the $PQ(H_2)$ pool to be either reduced (DBMIB) or oxidised (DCMU) in the light. Based on this approach, it was proposed that the redox state of the $PQ(H_2)$ pool regulates the transcription of a subset of chloroplast genes to adjust the relative stoichiometric amounts of the two reaction centres (PSII and PSI) (see, e.g. reviews by [558–560]). These findings have led to the concept of redox mediated plastid retrograde signalling that orchestrates the expression of genes by the plastid and nuclear genomes, a concept that is still discussed (review in Pfannschidt 2010 and Chan et al., 2016 [561,562]).

Ions. Divalent cations also inhibit the catalytic cycle of the Cytb_6f in concentration dependent manner. Inhibition was first reported for Cu^{2+} [112] and then for Zn^{2+} [108]. Both metals were proposed to hamper the movement of the ISP-HD. Based on EPR data, it was proposed that binding of the two ions in proximity of His143 in the ISP would induce the inhibition. Later crystallographic studies with Cd^{2+} poisoned Cytb_6f [173] provided a structural confirmation of this hypothesis, showing the existence of two Cd^{2+} binding sites, the strongest one being mediated by Cd-H143 interactions.

Inhibitors of the Q_n site. Typical inhibitors of this site are: N(H)QNO, MOA stilbene and, to a lower extent, stigmatellin.

NQNO (2-n-nonyl-4-hydroxy-quinoline N-oxide) was first investigated by Jones and Whitmarsh [563] *in vitro* and by Joliot and Joliot [564] in *Chlorella sorokiniana* cells. Jones and Whitmarsh [565] used single turnover and steady state absorption spectroscopy to show that NQNO binds to the stromal quinone site, thereby inhibiting the oxidation of the Cytb_6 heme, and slowing down electron

transfer between the two b-hemes. Based on the effect of NQNO on the ECS kinetics, the authors concluded that: *i)* the slow phase of the ECS under single turnover flash (phase b, see above) is due to electron transfer between the two *b* hemes, followed by a reaction associated with PQ reduction; *ii)* the two quinone binding sites would be separated by 70% of the dielectrically weighted distance across the membrane.

Joliot and Joliot further explored the relationship between this inhibitor, redox changes of Cytb_6 and changes in the kinetics and amplitude of phase b of the ECS. Based on the consequences of NQNO poisoning of phase b, the authors proposed that reduction of the quinone occurring at the stromal site (Q_n) would be coupled to protonation, implying that this site is connected to the outer face of the thylakoid by a proton channel. Recent crystallographic studies have provided a molecular interpretation for these findings, showing that at least two residues (Asp 20 and Arg 207) form a H^+ wire connecting the stroma to the quinone binding pocket [66] .

NQNO binds in close proximity to the heme c_n, acting as a direct axial ligand of the heme (Yamashita et al., 2007). This interaction explains why NQNO binding to the Cytb_6f leads to a strong modification of the properties of heme c_n [191]. This heme titrates as a one-electron Nernst curve with a E_m value of +100 mV in unpoisoned complexes. Its reduced minus oxidized spectrum displays a broad absorbance increase peaking at approximately 425 nm. Upon binding of NQNO two heme c_n titrations waves are visible: one with an E_m value similar to that observed in non-inhibited enzyme and the other with a midpoint shift by about -225 mV [191]. Moreover, the Soret spectrum of the heme is shifted by 1 nm to longer wavelengths upon NQNO binding [173]

MOA stilbene (Fig. 22, 1 in *red frames*) This inhibitor was first studied by Rich and colleagues [566], who showed that at variance with Cytbc_1, MOA-stibene does not affect quinol oxidation but instead quinone reduction. Its binding to Cytb_6f induces a red-shift of the Soret and visible absorbance bands of the *b* hemes, enhancing their 'oxidant-induced reduction' and slowing down their subsequent dark reoxidation at the same time. Its effect is therefore similar to that of NQNO.

Later, Kramer and Crofts [218] confirmed these results, showing that MOA-stilbene increases the reduction of the high potential form of Cytb_6 by 45% ca, and reduced the amplitude of the ECS signal by about 25%, again in agreement with results obtained with NQNO.

Stigmatellin (Fig. 18 A). As mentioned above, this inhibitor also binds to the Q_n site with very similar features as NQNO. However, due to its higher affinity for the Q_p site, this inhibitor cannot be used to test the mechanism of electron and proton transfer to PQ.

6 Thermodynamic background of cytochrome *bc* catalysis

This section covers the thermodynamic principles behind operation of Cyt-*bc*, using the reactions characteristic for Cytbc_1. If the Cytb_6f were to operate according to a "modified Q cycle", as described for Cytbc_1, then the equations below would be equally applicable to both complexes, simply by exchanging the parameters for PC/Cytc_6 and PQ(H_2) with those of Cyt*c* and UQ(H_2) respectively. However, as described in detail in section 3.6.5, significant doubts remain about the operation of a Q cycle at Cytb_6f, with the possibility that additional electrons may be added to the Q_n side from soluble components. In this case, the stoichiometry of the equations below will clearly be altered for the Cytb_6f

In aqueous solutions, the quinone-dependent enzymatic reaction of Cytbc_1 can be summarized as [1,567] :

$$2\ \mathrm{Cyt}c^{3+} + \mathrm{QH_2} = 2\ \mathrm{Cyt}c^{2+} + \mathrm{Q} + 2\ \mathrm{H^+} \qquad \text{(eq. 10)}$$

where $Cytc^{3+}$ and Cytc^{2+}stand for ferri- and ferro-Cyt*c,* respectively.

In this case, the change in ΔG associated with reaction of electron transfer from quinone molecules to Cyt*c* molecules after mixing UQH_2 derivatives with Cyt*c* can be estimated using the relationship [568] :

$$\Delta G = -\ nF\Delta E_h \qquad \text{(eq. 11)}$$

where ΔE_h is the difference in the actual redox potential between the couples of the donor ($E_{h(D)}$ of UQ/UQH_2) and acceptor ($E_{h(A)}$ of Cytc^{3+}/Cytc^{2+}) and n is the number of electrons in the reaction (here $n = 2$) and F is the Faraday constant.

$$\Delta E_h = E_{h(A)} - E_{h(D)} \qquad \text{(eq. 12)}$$

The corresponding $E_{h(A)}$ and $E_{h(D)}$ can be calculated using the Nernst equation which takes into account the redox midpoint potentials at pH 7 ($E_{m7}{}^{Q}$ and $E_{m7}{}^{Cyt}$) and actual concentrations of reduced and oxidized form of UQ/UQH_2 and Cytc^{3+}/Cytc^{2+}, the temperature (T) and the gas constant (R).[568].

$$E_{h7(A)} = E_{m7}{}^{Cyt} + RT/nF\ \ln([\mathrm{Cyt}c^{3+}]/[\mathrm{Cyt}c^{2+}]) \qquad \text{(eq. 13)}$$

$$E_{h7(D)} = E_{m7}{}^{Q} + RT/nF\ \ln([\mathrm{UQ}]/[\mathrm{UQH_2}]) \qquad \text{(eq. 14)}$$

During a typical measurement of Cytbc_1 turnover rate, the substrates are added to the solutions in total concentrations that should exceed Michaelis-Menten constants, while proportions of oxidized to reduced substrates are approximately 0.05 and 0.95 for [UQ]/[UQH_2] and [Cytc^{3+}]/[Cytc^{2+}], respectively [569].

Taking +260 mV as the E_m at the physiological pH of 7 (E_{m7}) of Cytc^{3+}/Cytc^{2+} [570], +70 mV as the E_{m7} of Q/QH_2 [488] and the number of electrons $n = 2$, one may calculate the energy released during the oxidation of 1 mol of QH_2 and reduction of 2 mols of Cyt*c*:

$$\Delta G = -\ nF\Delta E_h = -66\ \mathrm{kJ/mol}. \qquad \text{(eq. 15)}$$

For comparison, the ΔG of oxidation of 1 mol of NADH in complex I and reduction of O_2 in complex IV in the mitochondrial respiratory chain is approximately -224 kJ/mol [162].

However, for the enzyme operating in living cells, eq. 11 is too simple by far and ignores an important fact that Cyt*c* reduction by Cytbc_1 is associated with the coupling of two oppositely directed redox reactions taking place at the Q_o/Q_p and Q_i/Q_n catalytic sites. Moreover, these reactions are coupled to the release of protons to the *p* side, and uptake of protons from the *n* side of membrane. Therefore, the simple eq. 10 should be split into two equations in order to account for this spatial separation of the two different quinone redox reactions in Cytbc_1:

$$QH_2^{(p)} + Cyt c^{3+} + Q^{(n)} = Q^{(p)} + Cyt c^{2+} + SQ^{-(n)} + 2H^{+(p)} \quad \text{(eq. 16)}$$

$$QH_2^{(p)} + Cyt c^{3+} + SQ^{-(n)} + 2H^{+(n)} = Q^{(p)} + Cyt c^{2+} + QH_2^{-(n)} + 2H^{+(p)} \quad \text{(eq. 17)}$$

Superscripts (p) and (n) denotes that the respective reaction takes place at the Q_o/Q_p and Q_i/Q_n site, respectively.

These reactions lead to proton transfer across the membrane in which Cyt*bc* is embedded, i.e. 4 protons are released (from Q_o/Q_p site) to the positive side (*p* side), while 2 protons are taken (at the Q_i/Q_n site) from the *n* side of the membrane. In this way the proton transfer catalyzed by the enzyme contributes to an increase of the transmembrane electrochemical potential gradient (Δp) which is used to drive the energetically uphill reaction of ADP to ATP conversion in cells [162]. However, it is worth mentioning here that the protons are transferred across the membrane by coupling deprotonation of QH_2 at *p* side with protonation of Q at n side, according to Mitchelian redox loop mechanisms. This is different form other complexes such as C*c*O for example which catalyzes active pumping of protons through specific proton channels.

Proton motive force is a value expressed as the sum of two components: difference in proton concentration between two sides of membrane (ΔpH) and the electric potential difference ($\Delta\psi$) between the two sides of membrane. However, for simplicity Δp is commonly converted to equivalent differences in electric potential expressed in millivolts.

In mitochondria, ΔpH is usually small and thus Δp is largely dominated by $\Delta\psi$, which is on the order of 150 – 200 mV[162], depending on the actual state of mitochondria (ADP/ATP ratio, oxygen tension and the activity of decoupling proteins). The architecture of Cyt*bc* imposes an additional energetic barrier to electron transfer from the Q_o/Q_p site through heme b_L/b_p and b_H/b_n to the Q_i/Q_n

site as the electrons must be transferred against Δψ, when the enzyme is embedded in the coupled membrane[161,571–573]. Therefore equattion 15 must take into account this additional energetic barrier:

$$\Delta G = - nF(\Delta E_h - \Delta\psi) \qquad \text{(eq. 18)}$$

Under conditions in which the $Q(H_2)$ pool and Cyt*c/PC* pool are half reduced, the driving force is significantly lowered. As a result, increasing Δψ influences the ET process hence increasing the probability of reduction of heme b_L/b_p at the expense of heme b_H/b_n. Under extreme conditions, Δψ can be high enough to impair the QH_2 oxidation at the Q_o/Q_p site leading to an increase in superoxide generation during the catalysis [572].

7 Mechanistic insights into the catalytic Q_o / Q_p site

7.1 Overview of the structure of the Q_o site

Cyt*b* of Cyt*bc*$_1$ is built of 8 transmembrane helices arranged in two helical bundles with the first bundle (helices A to E) incorporating both hemes *b* (b_L and b_H). The second bundle (helices F to H) is located in the vicinity of heme b_L and together with the large helix-connecting loops at the intermembrane (periplasmic) side of the membrane, forms the Q_o site binding pocket [20,21,79,132]. This pocket is highly hydrophobic and contains many highly conserved residues. The major loop regions that participate in formation of the Q_o site include the two helices *cd1* and *cd2* of the CD loop and the *ef* helix of the EF loop. The helices *cd1* and *cd2* cap the pocket from the intermembrane (periplasmic) space where Cyt*b* interacts with the ISP-HD. Transient binding of the ISP-HD to Cyt*b* brings the 2Fe2S cluster into proximity with the substrate occupying the Q_o site pocket, which means that in this pocket the substrate can be flanked by two redox active cofactors: the 2Fe2S and heme b_L. This corresponds to the state when the two cofactors required for electron bifurcation are present close enough to the substrate bound at the Q_o site for fast electron transfer to occur (the exact distance is not known but approximated from the crystal position of the Q_o site inhibitors, see below). Due to the large-scale oscillatory movement of the ISP-HD between the Cyt*b* and Cytc_1, there are states of the Q_o site with 2Fe2S is not present at the site and therefore unable to interact with the bound substrate (precluding the bifurcation reaction). The movement itself is an inherent part of the catalytic cycle as it connects the Q_o site with heme *c* of Cytc_1: transient binding of the ISP-HD away from Cyt*b* to Cytc_1 brings the 2Fe2S and heme c_1 close enough for fast electron transfer between these two cofactors.

7.2 Quinone binding to the Q_o site

Binding of the QH_2 molecule to the Q_o site is an obvious requirement for initiating the catalytic QH_2 oxidation. Despite many years of study the way in which Q or QH_2 are bound to this site is still not fully understood. A major part of what is known about these interactions comes from measuring site-directed mutants of bacterial Cyt*bc*$_1$, usually of conserved residues at the Q_o site, in spectroscopic studies, mainly EPR spectroscopy and X-ray crystallography. The latter method has always been considered as the most promising tool for detection of specific chemical interactions between substrates and the protein. However, soon after solving the first structures of Cyt*bc*$_1$, it became clear that in the case of this protein (as in some other quinone-binding proteins) the crystallography failed to show natural substrate bound at the Q_o site and neither Q nor QH_2 has been resolved within this site[20]. It has been proposed that this failure is due to the Q molecules at the Q_o site being in a very dynamic state. However, a simple loss of the substrate during the isolation and crystallization of the protein also cannot be ruled out, in particular in the light of spectroscopic observations that samples of isolated Cyt*bc*$_1$ tend to have an empty Q_o site [59,127,260]

In the absence of structures containing natural substrate at the Q_o site, structures obtained with many different site-specific inhibitors have served as a starting point for the construction of models for Q binding to Q_o. Several of these proposals, including the most recent ones, considered specific interactions derived after substituting the chromane ring of stigmatellin with the natural quinone ring[91,95,96,574,575].

In studying the binding of QH_2 and Q to the Q_o site, EPR spectroscopy of the reduced 2Fe2S has been one of the most widely used methods. It has benefited from the observation that, for Cyt*bc*$_1$, the continuous wave EPR (CW-EPR) spectra of 2Fe2S is highly sensitive to variation in the type of molecule occupying the Q_o site and its redox state, providing a convenient means to monitor the status of the site in the native membranes. This approach seems to also be applicable for detection of PQ or PQH_2 bound to the Q_p site of Cyt*b*$_6$*f*.[576] From the very beginning it become apparent that CW-EPR spectra of 2Fe2S could not be simulated by modeling a single EPR component for the 2Fe2S [159] nor by using a statistical theory of *g* strain that has previously worked for other iron-sulfur clusters[577].

The sensitivity of the CW-EPR spectra of the reduced 2Fe2S to the occupant of the Q_o site is best documented for bacterial Cyt*bc*$_1$. It was observed that the shape of the spectrum differed depending whether Cyt*bc*$_1$ was embedded in native membranes or isolated and solubilized in detergent micelles[127]. It was also observed that the shape of the spectrum in the membranes was sensitive to the total quinone content in the membrane[109,260,578,579] as well as being a convenient tool for discriminating between Q or QH_2 occupancy of the Q_o site[580].

In bacterial chromatophores, the most characteristic spectral feature of 2Fe2S is the g_x transition which equals 1.800 when UQ bound at the Q_o site interacts with the cluster[579]. Among all the transitions of the 2Fe2S spectrum, the g_x component appears the most influenced by the occupant of the Q_o site. When the site contains UQH_2, g_x broadens significantly and shifts to approximately 1.777[109,578,579]. Other transitions (g_z, g_y) are also relatively narrow when UQ is bound to the Q_o site suggesting a relative small *g*-strain of the cluster[90,111,113,579,581]. These transitions also broaden, although less significantly comparing to g_x, when UQ exchanges with UQH_2.

Careful analysis of the g_x transition has established that measurements of relative proportions of g_x at 1.800 *vs* g_x at 1.777 signal can be used to monitor the redox state of the $Q(H_2)$ pool in the membrane. Most probably the g_x = 1.800 transition results from interaction of the 2Fe2S environment with the carbonyl group of UQ, while the g_x = 1777 results from interaction with the hydroxyl group of UQH_2[578]. However, this sensitivity of the 2Fe2S spectrum to UQ or UQH_2 is completely abolished when low-molecular-weight alcohols, such as methanol, ethanol, glycerol (a common cryoprotectant), are present[582]. This most likely results from interaction of the hydroxyl group with the ^{Rh}H156 ligand of 2Fe2S (^{Bt}H161). It follows that measurements of the redox state of the $Q(H_2)$ pool by CW-EPR spectra of 2Fe2S (which must be performed at low temperatures) must avoid cryoprotective agents as they usually contain hydroxyl groups[583]. On the other hand, the absolute necessity of using cryportectants in low-temperature pulse EPR measurements compromises sensitivity of the 2Fe2S spectra to UQ and UQH_2. Otherwise formation of ice may cause aggregation and denaturation and may significantly increase the efficiency of paramagnetic relaxation distorting the results, which are dependent on spin-lattice relaxation rates.

For the empty Q_o site, the g_x transition is very broad and its *g* value approaches 1.765[580]. A similar shape and *g* value for the g_x transition is detected when the Q_o site is occupied by the inhibitor myxothiazol or MOA-stilbene[578].

Interestingly, the experiments on partial extraction of UQ from purple bacterial membranes (chromatophores) revealed that when the ratio of the number of Q molecules per Q_o sites is between 2:1 and 1:1, the g_x value changes to approximately 1.78 and its linewidth lies in-between g_x = 1.800 (for UQ) and 1.777 (for UQH_2)[584]. Furthermore, this 1.78 transition could not be reproduced by a linear combination of "UQ g_x 1.800" and "empty-site g_x 1.765" lines. To explain these observations Ding et al, proposed that there are two niches, strong and weak quinone binding at Q_o: Q_{os} and Q_{ow}, with dissociation constants (K_d) of approximately ~0.05 and ~1 mM, respectively[260]. Taking these K_d values and assuming that, under normal conditions, the effective concentration of UQ in the membrane is ~30 mM[260], it was concluded that the Q_o site should be occupied by two molecules of UQ at the same time. This lead the authors to formulate a "double-occupancy" model, according to

which the Q_o site can accommodate 2 UQH_2 molecules simultaneously[260,578,580]. Further support for the double occupancy model has come from determination of the stoichiometry of UQH_2 binding to Cytbc_1 by NMR-based analysis of inhibitor displacements. With this approach, two molecules of $UQ(H_2)$ were shown to bind specifically to the Q_o site.[585] This observation was incorporated into a model that aimed to explain the mechanism of bifurcation. It was proposed that UQH_2 and UQ binds at the same time in the Q_o site and undergo a comproportionation reaction according to eq. 7, resulting in formation of two SQ molecules, each donating one electron to the c- or b- chain[585,586]. However, this concept has not been verified with other, more direct studies.

In the opinion of the authors of this review, the double-occupancy model remains problematic and it was previously the subject of debate[91]. When measuring the redox state of the $Q(H_2)$ pool in samples poised at ambient redox potentials (E_h) equal to or lower than the E_m of the UQ/UQH_2 couple, the Q_o site would be occupied by UQ at the Q_{os} niche with an increasing population of UQH_2 at the Q_{ow} niche as E_h shifts negatively. If this happened during redox titration of the membranous $UQ(H_2)$ pool, as monitored by EPR measurements of the 2Fe2S spectrum, the g_x would likely be different from the observed experimentally linear combination of $g_x = 1.800$ (corresponding to $UQ^{Qos}UQ^{Qow}$) and 1.777 (corresponding to $UQH_2{}^{Qos}UQH_2{}^{Qow}$) transitions. Such a titration should also reveal a separate component corresponding to the unique $UQ^{Qos}UQH_2{}^{Qow}$ state or respective molecules after comproportionation. Alternatively, the presence of two non-equivalent sites for $UQ(H_2)$ at the Q_o site would very likely lead to a non-Nernstian shape of the redox titration curve for the UQ/UQH_2 couple, detected in the g_x transition of 2Fe2S. However, none of these observations can be made, and the titration curve in such experiments closely follows the Nernst equation with n = 2[109,579]. In addition, the E_m values of UQ/UQH_2 obtained from EPR measurements of the 2Fe2S spectra remain consistent with spectrophotometric measurements of the redox midpoint potential of this couple[587]. This suggests that UQ and UQH_2 at the Q_o site are in dynamic equilibrium with UQ and UQH_2 of the membranous pool. Going further, one may conclude that if changes in EPR spectra follow the redox state of the $UQ(H_2)$ pool, UQ is not favorably bound to the site over UQH_2 and *vice versa.*

The first step of the QH_2 oxidation at the Q_o site involves binding of QH_2 and association of the ISP-HD with an oxidized 2Fe2S to the Q_o site. Thus, the initial step of the reaction is formation of the enzyme-substrate (ES) complex, which depends on equilibrium constants describing the ratio between the population of Q_o sites with QH_2 bound and those which are empty ($K_{QH2\text{-}Qo}$). Additionally, the association constant of ISP-HD containing oxidized 2Fe2S with the Q_o (K_{ISPox}) site is also a crucial parameter defining the probability of ES complex formation. While direct designation of $K_{QH2\text{-}Qo}$ and K_{ISPox} is not experimentally possible, the respective values for Cytbc_1 were approximated by Crofts et al.[23] who considered the following states:

$$K_{QH2\text{-}Qo} = [Q_o\text{-}QH_2] / [Q_o\text{-empty}] = \sim 10 \qquad \text{(eq. 19)}$$

$$K_{ISPox} = [Q_o\text{-}QH_2\text{-ISP-}HD_{Qo}] / [Q_o\text{-ISP-}HD_{remote}] = \sim 10 \qquad \text{(eq. 20)}$$

where: $[Q_o\text{-}QH_2]$ and $[Q_o\text{-empty}]$ are the concentrations of QH_2 at the Q_o site and empty Q_o site, respectively, at the time when ISP-HD containing oxidized 2Fe2S cluster is in position close to the Q_o site. $[Q_o\text{-}QH_2\text{-ISP-}HD_{Qo}]$ and $[Q_o\text{-ISP-}HD_{remote}]$ denote relative concentrations of ISP-HD containing oxidized 2Fe2S at position close to the Q_o site with bound QH_2 and remote from the site, respectively.

From eq. 19 it can be concluded that both QH_2 and oxidized 2Fe2S have a tendency to form the ES complex to initiate the first step of electronic bifurcation. Unfortunately, a direct observation of the interaction of QH_2 with oxidized 2Fe2S has not yet been made, as such a state can be generated only under non-equilibrium conditions, which would make the 2Fe2S diamagnetic and therefore not detectable by EPR spectroscopy. The EPR spectroscopy performed with cryoreduction of the 2Fe2S cluster in oriented membranes is also not informative. Although it can detect the position of ISP-HD with oxidized 2Fe2S, the Q_o site contains only UQ, not QH_2 [100].

7.3 Crucial amino acid residues involved in the binding and catalysis of QH_2 / PQH_2 oxidation at the Q_o/Q_p site

This paragraph focuses on some of the crucial amino acid residues of the Q_o site that are thought to be involved in $Q(H_2)$ binding, and of the Q_p site, involved in $PQ(H_2)$ binding. At a general level, understanding how individual structural elements contribute to $Q(H_2)$ or $PQ(H_2)$ binding is challenging because of the difficulty in defining specific and universal $Q(H_2)$ binding motifs in proteins[588] and the possibly related observation that many protein-$Q(H_2)$ interactions involve atoms of the main polypeptide chain.

Nevertheless, extensive mutational studies targeting residues of the Q_o site has identified those that affect catalysis, although some of these mutations were found to primarily affect the stability and/or assembly of the whole protein complex. It is of note that, despite a large number of mutations that have already been tested in the region of the Q_o site, relatively few were able to completely abolish enzymatic activity, implying significant robustness and tolerance for structural change of both $Q(H_2)$ binding and Q_o site catalysis.

Current models of Q and QH_2 binding to the Q_o site are derived from crystallographic structures of Cyt*bc*$_1$ with bound inhibitors replacing the natural substrate (structures with the substrate have not been solved yet). The models consider both P_m and P_f inhibitors, i.e. inhibitors exerting

different effects on the motion of ISP-HD as well as those occupying different niches of the Q_o pocket, (see section 5 for details). The latter difference is visualized by a comparison of the structures shown in Fig. 27, which compare binding of myxothiazol (representative of P_m group) at a position closer to heme b_L and further from ISP-HD with binding of stigmatellin (representative of P_f inhibitors) –at a position closer to ISP-HD and further from heme b_L.

7.3.1 ^{Rh}H156 (^{Bt}H161) in iron-sulfur protein and the ^{Rh}E295 (^{Bt}E271) in cytochrome *b*

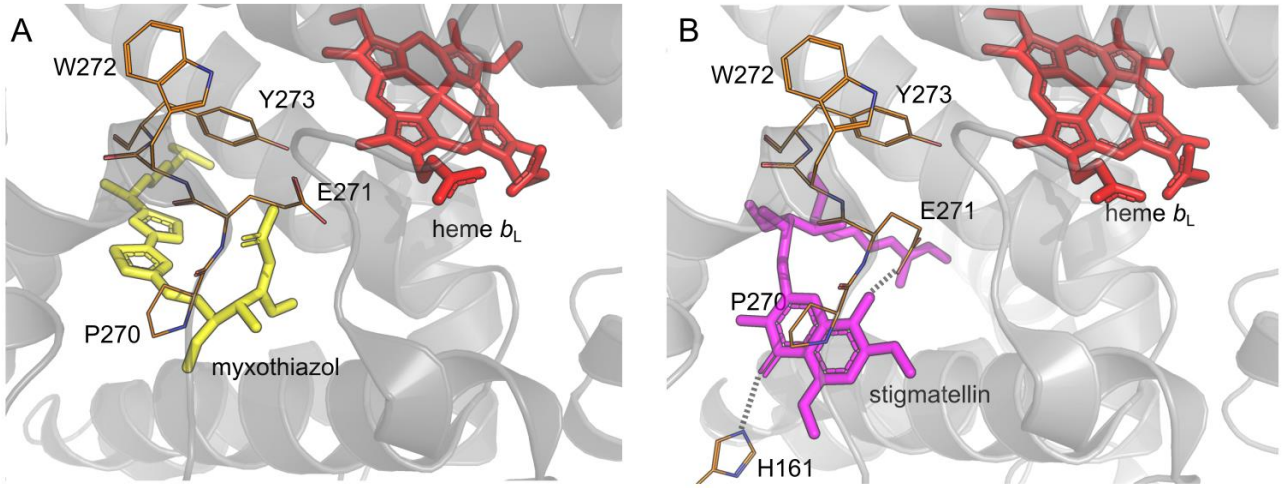

Figure 27. Comparison of structure of the Q_o site from *Bos taurus* with bound myxothiazol (A) or stigmatellin (B). Prepared on basis of 1SQP[77] and 1PP9[123], respectively. Amino acids of ISP are not shown in A, since myxothiazol induce c-position of ISP-HD. The imidazole ring of the 2Fe2S ligand – histidine 161, is shown in B as a structure forming an H bond to stigmatellin.

The two most prominent, and thus most frequently discussed, candidates for residues that directly participate in binding substrate are histidine ^{Bt}H161 (^{Rh}H156) - one of the ligands of the 2Fe2S and glutamate ^{Bt}271 (^{Rh}E295) from conserved PEWY motif of Cyt*b*. A binding mode for substrate involving these two residues is thought to be equivalent to the configuration of stigmatellin in the crystal structure. Stigmatellin forms two strong H bonds in the Q_o site (Fig. 27 B): one between the >C=O group of the inhibitor and N_τ atom of ^{Bt}H161 of ISP-HD and second between -OH group and carboxylic group of ^{Bt}E271 residue[123]. Interestingly, myxothiazol crystalised in the Q_o site does not form specific hydrogen bonds to either of these groups. A comparison of the two structures reveals variable positions for the ^{Bt}E271 side chain: it rotates further toward the chromane ring of stigmatellin in order to create a hydrogen bond with the -OH group at the C8 atom of the ring. It is highly unlikely that Q or QH_2 molecules at the Q_o site simultaneously form H bonds to ^{Bt}H161 and ^{Bt}E271 as

stigmatellin does. Therefore it was proposed that during the oxidation QH_2 undergoes a rapid movement between the two niches within the Q_o site filled by stigmatellin and myxothiazol[23,575,589,590]. According to this mechanism, QH_2 binds to the Q_o via ^{Bt}H161 (^{Rh}H156) and the first electron transfer to the oxidized 2Fe2S takes place. The first proton is released and then the neutral SQH moves to form a hydrogen bond to ^{Bt}E271. The Glu residue promotes deprotonation of SQH, which then donates an electron to heme b_L. After formation of Q, it shifts back to the position that allows interaction with ^{Bt}H161 and then it can be replaced with another QH_2. This mechanism has not been proven yet and it is a still a matter of debate[259]. While the SQ moving between the two niches should be trappable, the experiments generally fail to detect such an intermediate of reaction (see section 7.6). Importantly, it remains an open question as to whether stigmatellin is actually a good model for $Q(H_2)$ binding. The spatial separation of the two -OH groups differs between the QH_2 and the chromane ring of stigmatellin, with consequences for the capacity to form H bonds. Comparing structures crystallized with different inhibitors, it seems that binding of UHDBT[77] or atovaquone[71] at the Q_o site might more closely reflect binding of QH_2 as the structures of these inhibitors are more similar to natural quinones, (menaquinone and sulfolobus- or caldariellaquinone for example[591]), than the chromane ring of stigmatellin.

The idea that ^{Bt}H161 might participate in binding of Q and QH_2 to the Q_o was proposed after ENDOR measurements revealed that the 2Fe2S is coordinated by 2 Cys and 2 His side chains [592] which was later confirmed by crystallographic structures [593]. Electrochemical studies revealed that the E_m value of 2Fe2S is pH dependent, and therefore dependency requires two different pK values[594]. It was estimated that the pK_a for oxidized 2Fe2S is ~7.5 and increases to more than 10 upon reduction of the 2Fe2S. This suggests that the protonation of ^{Bt}H161 is tightly coupled to the redox state of the 2Fe2S. Such an increase in pK means that the energy of hydrogen bond formation between an occupant of the Q_o and ^{Bt}H161 is larger when 2Fe2S is reduced compared to when the 2Fe2S is oxidized. Stabilization of the ISP-HD by the reduced 2Fe2S through interaction with $Q(H_2)$ occupying the Q_o site is also inferred from EPR measurements. Typically, the EPR spectra of the reduced 2Fe2S in chromatophore membranes reflect close interactions with the $Q(H_2)$, revealing that the reduced state of 2Fe2S promotes ISP-HD occupancy of a position close to the Q_o site (see section 3.4) On the other hand, experiments in which Cytbc_1 containing oxidized 2Fe2S was frozen before the cluster was reduced for detection by EPR showed that the ISP-HD with oxidized cluster tends to occupy a position remote from the Q_o site.[100]

The 2Fe2S coordinating ^{Bt}His161 is well established as a crucial amino acid residue for the activity of all Cyt-*bc*. Its role in formation of initial ES complex is supported by many biochemical

and computational studies. However, all mutational studies aimed at replacing this residue result in loss of the whole ISP subunit[138], making definitive proof elusive.

The majority of the models describing formation of the initial ES complex assume that ^{B}His161 must be deprotonated before binding the QH_2, whereas Q can bind to the Q_o site when it is already protonated[595–597]. In some models, this His residue has therefore been proposed as the first proton acceptor during the oxidation of QH_2. However, MD simulations indicate that QH_2 can also form a stable H bond to the His, even when it has already been protonated.[95,96]

The role and significance of the conserved PEWY domain Glu residue in binding substrate and catalytic reaction are less understood[23,118,598]. In several models ^{Bt}E271 is considered to directly accept the second proton from QH_2 upon its oxidation. However, mutational studies of this residue in the bacterial enzyme revealed only a modest impact on turnover rate and no significant changes in the estimated binding affinity of QH_2 to the Q_o site[579]. On the other hand, mutation of the same residue in yeast (^{Sc}E272Q or ^{Sc}E272D) induced stigmatellin resistance[598]. These two observations suggest that ^{Bt}E271 may not be directly involved in either binding of Q or QH_2 to the Q_o site nor be critically required for proton uptake from QH_2 during the bifurcation reaction. Rather, it may be residue that increases stability of the water network at the Q_o site, which is necessary to create an appropriate environment for efficient and fast proton removal from the Q_o site. Clearly, further studies are needed to clarify the role of this residue in binding and/or proton events taking place at the site.

Interesting evolutionary aspects of the PEWY motif are beyond the scope of this review but interested readers will find a discussion on this subject in appropriate reference[118].

7.3.2 Cyt*b*:^{Rh}Y147 (^{Bt}Y131) and Cyt*b*:^{Rh}Y302 (^{Bt}Y278)

The Y147 residue is conserved among all Cytbc_1 complexes. Its importance in the activity of the Q_o site was postulated before crystallographic structures were available[599]. Mutations of this residue to Phe, Val, Ser or Ala have a dramatic effect on the activity of bacterial Cytbc_1[599]. This significant impairment of catalysis is not associated with a change in the redox potentials of heme b_L nor 2Fe2S. MD studies imply that Y147 can rotate to form a hydrogen bond between the -OH group at position 4 of UQH_2 and the -COO^- group of ^{Rh}E295[96], suggesting that this residue might play an important role in formation of the ES complex and the process of proton uptake during the bifurcation reaction. Quantum mechanics calculations performed on MD optimized structures, indicate that when UQH_2 interacts with protonated ISP:^{Rh}H156, proton transfer from the hydroxyl group of ^{Rh}Y147 to the carboxyl group of ^{Rh}E295 takes place, creating a negative ^{Rh}Y147 and neutral ^{Rh}E295. At the same time, the deprotonated hydroxyl of ^{Rh}Y147 forms a hydrogen bond to the O1 atom of the hydroxyl

group of UQH_2. When similar calculations were performed using the structure in which the hydroxyl O4 atom of UQH_2 forms a hydrogen bond to the already protonated ^{Rh}H156 of ISP-HD, and the H atom of the ubiquinol -OH group interacts with water molecules, this proton transfer from ^{Rh}Y147 to ^{Rh}E295 was not observed, despite the fact that ^{Rh}Y147 could still perform a relay function between UQH_2 and ^{Rh}E295[96]. Other MD simulations on the binding of UQH_2 to the Q_o site did not show involvement of ^{Rh}Y147 hydroxyl in interaction with UQH_2. Instead, a hydroxyl group at the C1 atom of UQH_2 formed a hydrogen bond with a network with water molecules[95].

Although a possible role of ^{Rh}Y147 and ^{Rh}E295 in binding and proton uptake from UQH_2 during the bifurcation reaction was proposed on the basis of biochemical and mutational studies[590,599], the concept of H bond network formation between UQH_2-^{Rh}Y147-^{Rh}E295 clearly needs further investigation.

An important role for Cyt*b*:^{Rh}Y302 (^{Sc}Y279) in the binding and oxidation of QH_2 by the Q_o site emerged from several studies on bacterial and mitochondrial Cytbc_1. Mutating this residue to Leu, Gly or Glu in *R. sphaeroides* Cytbc_1, was found to decrease catalytic rates by a factor between 3 – fold to 50 – fold[589,600] and to increase ROS generation[601]. These effects were also reported for ^{Sc}Y279C, a mutation associated with mitochondria-related diseases[602]. The g_x transition of the EPR spectra of 2Fe2S in this mutant suggested that the Q_o site was "partially empty"[600]. Furthermore, the spectrum of 2Fe2S with bound stigmatellin differed from the equivalent spectrum for typical wild-type enzymes, indicating much stronger binding of the chromane than the benzoquinone ring to the Q_o site of Cytbc_1. Analysis of the structure of yeast Cytbc_1 with the inhibitor HHDBT bound suggested that ^{Sc}Y279 might contribute to the binding of UQH_2 by creation of a H bond to the =O atom of the main chain of ^{Sc}C180 in ISP-HD[70]. Such a hydrogen bond is expected to stabilize UQH_2 binding with ^{Sc}H181 (^{Rh}H156 and ^{Bt}H161) of the ISP-HD.

In *Rhodobacter capsulatus,* the ^{Rh}Y302C mutation exerted a deleterious effect on stability of 2Fe2S due to disruption of a disulfide bridge in ISP-HD and resulting cross-linking between the Cyt*b* subunit and ISP-HD (^{Rh}Y302C-^{Rh}C155). This made the 2Fe2S more sensitive to oxidative damage[601,603].

In *Plasmodium falciparum* ^{Pf}Y268S (equivalent ^{Sc}Y279S and 7^{Rh}Y302S) was identified as a mutation responsible for resistance of the parasite to the anti-malarial drug, atovaquone[604]. This potent inhibitor of the Q_o site was found to completely block activity of the yeast Cytbc_1 (IC_{50} = 5 nM)[605]. Atovaquone arrests the ISP-HD at the Q_o site in a similar way to stigmatellin, despite the fact that unlike stigmatellin it does not form a direct H-bond with the conserved PEWY sequence Glu residue[71,606]. The crystal structure revealed that ^{Sc}Y279 forms hydrogen bonds to Cys180 in the ISP but it also interacts weakly with ionized hydroxyl group at C3. The loss of this Tyr residue in

Plasmodium is not lethal to the parasite, but significantly slows its Cytbc_1 activity, thus slowing the parasite growth rate[604].

7.3.3 Other residues involved in substrate binding to the Q_o site

Besides the amino acid side chains discussed above, it is expected that the binding of substrate to the Q_o site also engages other residues in the site, including atoms of the main polypeptide chain of Cyt*b* and ISP. Indeed, MD simulations investigating possible structures of bound UQH_2 and UQ at the Q_o site identified the =O atoms of ^{Rh}I292 (Cyt*b*) and ^{Rh}C155 (ISP) as potential residues participating in binding of UQH_2 and UQ through water molecules.

Another residue important for binding of the substrate to the Q_o site is conserved Gly ^{Rh}G158 (^{Sc}G143 and ^{Bt}G142) in the WGA sequence[260,569,607]. Mutagenesis studies have revealed that its replacement with residues that have bulkier side chains, particularly tryptophan, prevents binding of either UQ(H_2) or inhibitors such as stigmatellin. This effect is most probably due to a steric hindrance at the Q_o site, preventing catalytic activity of the enzyme.

It should be noted that the isoprenoid chain of UQ also constitutes an important part of the Q binding interface. Indeed, several hydrophobic residues of Cyt*b* interact with this tail. In *R. capsulatus* they are: F144, F166, F298, F337, I162, I169, V333, M336, L165, V161, F298, G141, M140, L201, L178[95].

7.3.4 Specific residues involved in PQ/PQH_2 binding to the Q_p site of Cytochrome b_6f

Studies to characterize residues of Cytb_6f involved in PQ(H_2) binding at the Q_p site are more limited than in the case of the Cytbc_1 counterpart. These studies have been mainly performed in *Chlamydomonas*, and have revealed strong similarities between the Q_p and Q_o sites of Cytb_6f and Cytbc_1, a concept that was later confirmed by crystallographic studies.

The first characterized mutant (FUD50) bears a 36 base pair duplication in the chloroplast petB gene, leading to a 12 amino acid duplication in the CD loop of Cytb_6. This modification decreases the affinity of the Q_p site for PQ(H_2)[608], likely by increasing the size of the Q_p site itself. Subsequent studies have also focused on this region of the Q_p site, revealing the essential role of the PEWY sequence in Q(H_2) binding and proton release. Later on, this concept that has been rationalized based on the structures of the Cytb_6f in this alga and cyanobacteria[41,42,66].

Additional mutants have been made in *Chlamydomonas* to study the role of the ISP flexible hinge in catalytic turnover of the complex. Six Gly residues in the flexible hinge critical for domain

movement in the Cytbc_1 (section 3.4) were replaced by alanine residues (6G6A). Moreover, substitutions were created near 2Fe2S (S128 and W163); and seven C-terminal residues were deleted (G171och). The 6G6A and G171och mutations affect highly conserved segments in the chloroplast ISP, but no phenotype was found in these lines. Although extensions of up to five residues or deletion of one residue in the flexible hinge had no significant effect on complex accumulation or electron transfer efficiency, deletion of just three residues (Δ3G) dramatically decreased reaction rates by a factor of ~10. Overall, these finding indicate that the chloroplast ISP hinge is also very flexible[609] and its movement is not limiting for catalysis, consistent with previous conclusions in the case of Cytbc_1 (see section 3.4).

Only one mutant has so far been reported to affect PQ(H_2) binding to the Q_p site in plants. This mutant (pgrl1)[610] was obtained by random mutagenesis and bears a point mutation in the ISP (P194L). Although the mutation does not affect photosynthetic electron transport at low light intensities, it drastically affects thermal dissipation of absorbed light energy in high light, suggesting that Pro194 may affect H^+/e^- coupling in the Cytb_6f. Single amino acid substitutions in Cytb_6 at the positions D148, A154, and S159 were generated in the cyanobacterium *Synechococcus* sp. PCC 7002. Mutant phenotyping revealed increased resistance to DBMIB in the mutants A154G and S159A, increased resistance to stigmatellin in A154G, and induction of myxothiazol sensitivity in the D148G mutant, confirming the role of these residues in PQ(H_2) binding and inhibitor sensitivity of the complex[611].

7.4 Catalytic and side reactions at the QH_2-oxidation site of Cytochromes *bc*

The oxidant-induced reduction of *b* hemes in sub-mitochondrial particles is an intriguing phenomenon first reported by Chance in 1952 during II International Congress of Biochemistry in Paris (see reference [612] and citations therein). This phenomenon was difficult to explain until a concept of a semiquinone-mediated electronic bifurcation was introduced by Wikstrom & Berden in 1972.[202]. The central role of a semiquinone in the mechanism of bifurcation was further developed by Peter Mitchell in the frames of his original idea of so-called proton-motive Q cycle mechanism. [32] This groundbreaking concept of electronic bifurcation, inherent to this mechanism, postulated that QH_2 at the Q_o/Q_p site undergoes two-electron oxidation reaction but routes for these two electrons are obligatorily different and very efficient. This entails the first electron being transferred to the oxidized

2Fe2S center (the first cofactor of the high-potential chain) while the second electron is transferred exclusively to heme b_L/b_p (the first cofactor of the low-potential chain) see section 3.2.

It is assumed that the mechanism of electron bifurcation is sequential, and involves formation of a transient semiquinone intermediate. While the time between the first electron transfer from QH_2 to 2Fe2S and the second electron transfer from SQ to heme b_L/b_p remains unknown, it seems reasonable to assume that it is not shorter than the time required for electron tunneling from the SQ to heme b_L/b_p.

According to Mitchell's principles QH_2 must donate its two electrons to two different chains of cofactors and the two redox couples involved in the first and the second electron transfer – SQ^-/QH_2 and Q/SQ^- couples, respectively, must therefore possess different redox midpoint potentials[32], as originally discussed by Wikstrom & Berden in 1972.[202] It has been proposed that the E_m of the SQ^-/QH_2 redox couple is very positive, and comparable to the high potential acceptor (2Fe2S and heme c_1/f), while the Q/SQ^- is expected to be a more reducing couple and therefore able to donate electrons to the low-potential chain (hemes b_L/b_p and b_H/b_n). This separation of E_m values (the split) of the two redox couples implies that the stability constant for the SQ^- intermediate at the Q_o/Q_p site must be very low and hence, detection of such an intermediate by spectroscopic methods might be difficult, especially under equilibrium conditions[487,488]. Indeed, until recently, the semiquinone intermediate state associated with the operation of the Q_o/Q_p site could not be experimentally detected (see section 7.6).

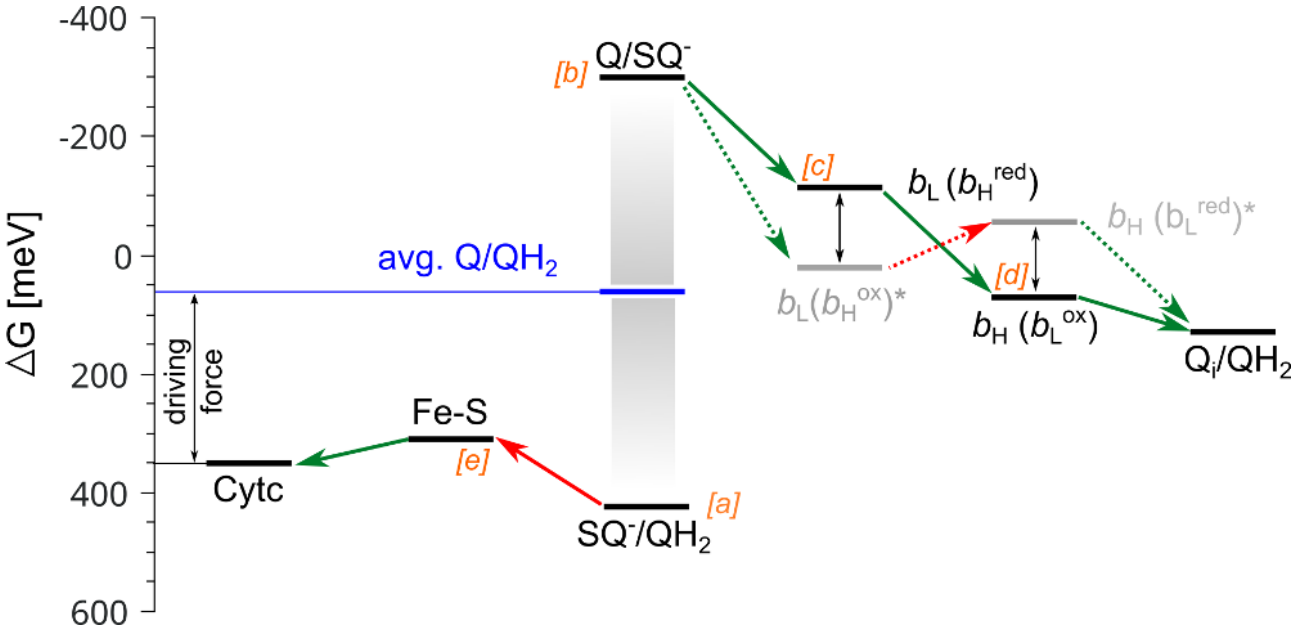

Figure 28. Energy diagram of electron transfer through cofactor chains in Cytbc_1. Horizontal black lines mark E_m values of the respective oxidized/reduced couple and are labeled with an orange letter in bracket. Gray gradient denotes a split in potentials between Q/SQ^- and SQ^-/QH_2 couples at the Q_o site. The average E_m value of membranous Q/QH_2 pool is

shown in blue. Red and green solid arrows show endothermic and exothermic reactions, respectively. Green dashed arrows show exothermic reaction to the heme states for which E_ms are not directly measurable by equilibrium redox titration. Gray horizontal lines shows a possible E_m values of hemes b_L and b_H modified by Coulombic interactions between the hemes (assuming the same energy of interactions ~ 80 mV for b_L and b_H[133,206]), that are not accessible for direct measurement. Vertical double arrows denotes the changes in E_m depending on the redox state of the coupled heme. Cyt*c* and Fe-S denote oxidized/reduced couples of Cytc_2 and 2Fe2S; $b_L(b_H^{ox})$ and $b_L(b_H^{red})$ denote oxidized /reduced couple of heme b_L, at a time when heme b_H is oxidized and reduced, respectively. $b_H(b_L^{red})$ and $b_H(b_L^{ox})$ redox couple of heme b_H at a time when heme b_L is reduced or oxidized respectively. Note that this scheme does not necessarily apply for Cytb_6f.

7.4.1 Forward, reverse and short-circuits reactions at the Q_o/Q_p site

A simple diagram of E_m values taken from *Rhodobacter capsulatus* Cytbc_1 with associated ΔG changes due to electron transfer through the cofactor chains is shown in Fig. 28 As originally proposed by Mitchell, there is a large, albeit unknown, split between E_m values (here ~800 mV) of the Q/SQ^- and SQ^-/QH_2 couples, and this split depends on the stability constant of the SQ^-. This makes the first electron transfer from QH_2 to 2Fe2S essentially endothermic and requires an energy debt for electron transfer to the acceptor of a more negative redox potential (2Fe2S) than the donor (QH_2). This energetic debt is repaid during the second electron transfer from SQ^- to heme b_L/b_p. The forward reactions, meaning the net electron transfer from QH_2 to Cyt*c*, is continued as long as there is a difference (driving force) between the E_h of membranous Q/QH_2, the *p* side acceptor pools (Cyt*c*, PC or Cytc_6) and all the cofactors of Cyt-*bc* complexes. Nevertheless, it has been shown by several experiments that under specific conditions Cytbc_1 has the capacity to catalyze a fast, reverse reaction of reduction of Q to QH_2 at the Q_o site. Such a process was observed in *in vitro* studies of Cytbc_1 reconstituted into liposomes[613] and also proposed to occur *in vivo* to support the growth of the chemolitotrophic bacteria *Thiobacillus ferrooxidans* using Fe^{2+} ions as a source of electrons[614]. This suggests that the reactions at the Q_o site are rapidly and efficiently reversible, where "efficient" means that these reactions do not lead to significant energy-wasting side reactions (short-circuits or leaks). Indeed, light-induced electron transfer measurements using cofactor knockouts of bacterial Cytbc_1 to dissect out individual electron transfer steps, demonstrated that the reactions of the Q_o site are reversible on a catalytically-relevant timescale (milliseconds)[615]. Fast reversibility of these reactions makes an understanding of the energetic efficiency of electronic bifurcation conceptually challenging. As long as one forgets about the reversibility, the diagram in Fig. 28 simply explains the energetic efficiency of electron transfer onto two different chains of cofactors. However, the fast reversibility of reactions at the Q_o/Q_p site means that the enzyme can potentially catalyze energy-wasting short circuit reactions[259,615]. Four possible short-cicuit reactions of the Q_o/Q_p site are shown in figure 29.

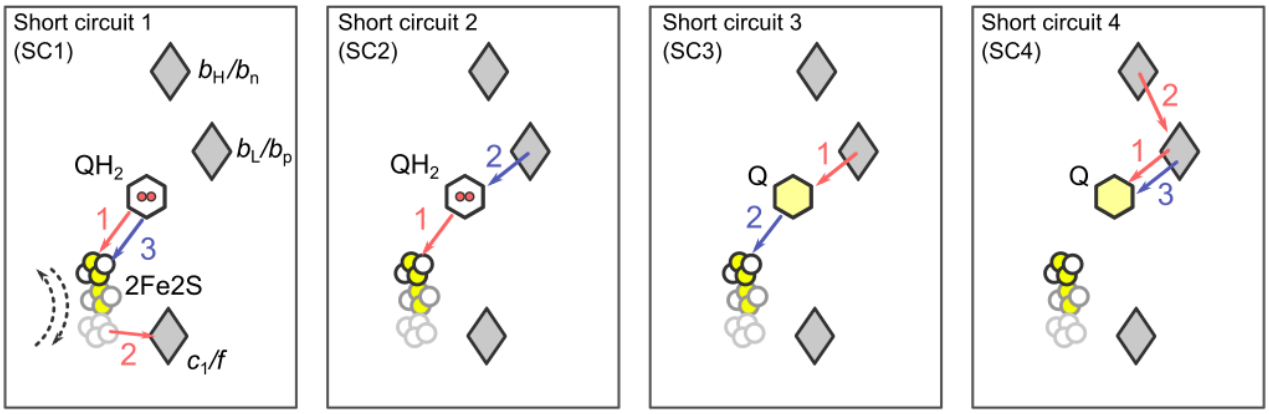

Figure 29. Scheme showing 4 types of short circuit reactions that are theoretically possible during the catalytic cycle of Cytbc_1 and Cytb_6f [259]. Red arrows show energy conserving ET while blue arrows shows energy-wasting short circuiting ET. Numbers denote the order of ET events. Short circuits start with QH_2 (SC1 and SC2) or Q (SC3 and SC4) present at the Q_o/Q_n site. Gray rhombuses denote hemes and white-yellow circles show 2Fe2S. Scheme does not consider redox states of cofactors. Dashed arrows and 3 positions of 2Fe2S denote movement of the ISP-HD (necessary to complete SC1). See text for details.

The first type of short circuit (SC1) is a reaction in which two electrons from QH_2 are transferred to the high potential chain according to the following reaction sequence:

$$QH_2 + 2Fe2S^{ox} = 2H^+ + 2Fe2S^{red} + SQ^-$$
$$2Fe2S^{red} + c_1{}^{ox}/f = 2Fe2S^{ox} + c_1{}^{red}/f$$
$$SQ^- + 2Fe2S^{ox} = 2Fe2S^{red} + Q$$

SC1 would be very exothermic since the electron transfer would be associated with a large potential energy change due to the transition from state *[b]* to *[e]* in figure 28. Despite the fact that SC1 is thermodynamically very favorable, it is avoided relatively easily, due to the requirement for the movement of ISP-HD (see section 3.4) during transfer of electrons from 2Fe2S to heme c_1 or *f*. Through this constrained diffusion of ISP-HD, the distance between SQ^- and the cluster increases significantly, slowing down any possible second electron transfer from the semiquinone to 2Fe2S. In the absence of ISP-HD in close proximity, the unstable SQ^- therefore pushes the second electron onto heme b_L/b_p. SC1 decreases the proton transfer efficiency across the membrane: it yields $+2H^+_p$ / $0H^+_n$ per oxidation of one QH_2, while an energy-conserving Q cycle yields $+4H^+_p$ / $-2H^+_n$ per 1 QH_2.

In contrast to SC1, the second type of short-circuit reaction (SC2) is extremely difficult to suppress without involvement of any additional mechanisms to lower the probability that it occurs. SC2 is a mixture of partial reactions of the forward and the reverse catalysis performed by the Q_o/Q_p

site and is a result of the following reactions (for simplicity in the following schemes b_L and b_H also represent hemes b_p and b_n, respectively):

$$QH_2 + 2Fe2S^{ox} = 2H^+ + 2Fe2S^{red} + SQ^-$$
$$b_L{}^{red} + SQ^- + 2H^+ = b_L{}^{ox} + QH_2$$

SC2 may take place when QH_2 undergoes oxidation by 2Fe2S as a part of the chemistry of the normal forward reaction, while heme b_L/b_p is reduced and unable to accept electron from SQ^-. In this situation, heme b_L/b_p can then donate an electron to SQ^-, reforming QH_2, as this reaction is also much more energetically favorable than any possible forward electron transfer from heme b_L/b_p to heme b_H/b_n (compare the difference in energy associated with *[b]* to *[a]* and *[b]* to *[c]* transition in fig. 28).

Energy conversion of this process is compromised as this short circuit gives the same stoichiometry as SC1 ($+2H^+_p$ / $0H^+_n$ per 1 oxidized QH_2), assuming that every SC2 is preceded by QH_2 oxidation.

Conditions in which SC2 could take place are created not only when an inhibitor such as antimycin, blocks electron transfer from heme b_H to Q at the Q_i/Q_n site, but also during reverse electron transfer from QH_2 bound at the Q_i/Q_n site, which is a natural consequence of the physiological reverse catalysis of Cyt-*bc*. It has been demonstrated (see section 8), that electrons from the Q_i site of one monomer can be transferred through the heme b_L to the other monomer, creating the possibility that heme b_L is already reduced when SQ^- is generated during oxidation of QH_2 by 2Fe2S at the Q_o site.

The third type of short circuit (SC3) is electron transfer from reduced heme b_L/b_p to Q that is bound concurrently with QH_2 to the Q_o/Q_p site, when the oxidized 2Fe2S is close to the Q_o/Q_p site. SC3 consists of two sequential reactions: first uphill (transition form states *[c]* to *[b]*), followed by downwhill ET (transition from *[b]* to *[e]* in fig. 28) which can be summarized as follows:

$$b_L{}^{red} + Q = b_L{}^{ox} + SQ^-$$
$$SQ^- + 2Fe2S^{ox} = Q + 2Fe2S^{red}$$

SC3 is quite similar to SC2 and the proton transfer efficiency is the same. The only difference is the fact that SC3 should be favored over SC2 when concentrations of Q in the $Q(H_2)$ pool are higher. However, in the absence of an inhibitor blocking the Q_i/Q_n site or mutation retarding electron transport from heme b_H/b_n to the Q_i/Q_n site, SC3 seems to be less probable than SC2.

The last type of short circuit (SC4) is the two-electron reduction of Q at the Q_o/Q_p site by the hemes b_L/b_p and b_H/b_n of the low-potential chain without involvement of the 2Fe2S. SC4 can be summarized as follows:

$$Q + b_L^{red} = SQ^- + b_L^{ox}$$
$$b_H^{red} + b_L^{ox} = SQ^- + b_H^{ox} + b_L^{red}$$
$$SQ^- + b_L^{red} = QH_2 + b_L^{ox}$$

According to the modified Q cycle[39], SC4 is obviously considered as the energy-wasting reaction since it diminishes the number of protons transferred across the membrane. However, calculations of the number of protons that are transferred per oxidized QH_2 under condition in which SC4 takes place is more complex than in the case of SC1, SC2 and SC3.

Let us first consider 4 cycles of QH_2 oxidation steps according to the energy-conserving Q cycle. If the modified Q cycle is operating, this will lead to $8H^+$ released to the *p* side, $4H^+$ taken from the *n* side and the net consumption of 2 QH_2 molecules from the $Q(H_2)$ pool. The overall stoichiometry of this modified Q cycle is $+8H^+_p/-4H^+_n$ and $-2QH_2/+2Q$ in the $Q(H_2)$ pool.

Now consider a similar sequence of 4 QH_2 oxidation reactions but with a single SC4 reaction occurring in the middle of the process: 2 QH_2 oxidations – SC4 reaction – another 2 QH_2 oxidations. For clarity let us divide the process into three parts. In the first part, 2 QH_2 oxidations yield $+4H^+_p/-2H^+_n$ and $-1QH_2/+1Q$. During the second part SC4 gives $-2H^+_p/+2H^+_n$ and $+1QH_2$. During the third part another 2 QH_2 oxidation take place yielding the same $+4H^+_p/-2H^+_n$ and $-1QH_2/+1Q$ as in the first part. Addition of all products from these three parts gives a net stoichiometry of $+6H^+_p/-2H^+_n$ and $-2QH_2/+2Q$ in the $Q(H_2)$ pool, which means that 1 occurrence of SC4 per 4 oxidized QH_2 decreases the number of protons released to the *p* side from 8 to 6. This would give an average $+3H^+_p/-1H^+_n$ per 1 QH_2 oxidized during this sequence *vs* $+4H^+_p/-2H^+_n$ per 1 QH_2 in the Q-cycle.

7.4.2 The possible physiological meaning of short-circuits

In general, short-circuit reactions decrease the efficiency of energy conversion by Cyt*bc* and the probability of their occurrence should be minimized or slowed down by two or three orders of magnitude in comparison to the productive forward and reverse reactions. It must be emphasized however, that it is still possible for some of the SC reactions to be catalyzed under specific conditions, such as severe mutation or presence of inhibitors which preclude normal catalysis. In fact it has been proposed that the reactions of SC2 could be a potential mechanism to support photosynthetic growth of green alga *Chlamydomonas reinhardtii* strains, in which normal function of Cytb_6f is disabled by mutation to replace the heme b_H ligand - histidine 202 with glutamine[616].

The reactions of SC4 could also be potentially considered as desirable for electron recirculation back to the PQ(H_2) pool in, for example, photosynthetic CET at the level of Cytb_6f (see section 4.3). Assuming alternating reactions of oxidation of PQH_2 and reduction of PQ at the Q_p site, using electrons delivered through the low-potential chain from the Fd/$NADPH^+$ pool, the overall proton pumping efficiency would be significantly increased yielding $+6H^+_p/-4H^+_n$, - $1PQH_2$ in the Q(H_2) pool and -2 Fd from the Fd/$NADPH^+$ pool. This would contribute to a much higher proton gradient per oxidized PQH_2 than $+4H^+_p/-2H^+_n$ per 1 PQH_2 resulting from the modified Q cycle mechanism. However, a possible involvement of SC4 in the mechanism of CET around Cytb_6f and PSI has not been proposed earlier and thus has never been tested experimentally.

Another potential physiological implication of short-circuits relates to the concept of kinetic competition between short-circuits and the leak of electrons (i.e. reactions that may lead to superoxide production). The completion of any type of short-circuit reaction retains electrons within the enzyme, therefore diminishing the probability of a leaks. Thus, this could be considered as a possible means of protection against unwanted release of superoxide, which might be of importance in the context of a postulated signaling role for superoxide release from the Q_o/Q_p site (see section 7.5).

7.4.3 Short-circuit suppression mechanisms

As indicated in section 7.4.1, understanding the fast reversibility of electron transfer in Cyt-*bc* and the efficient suppression of short circuit reactions is conceptually challenging[259,615,617,618]. Direct electron transfer between the low- and high-potential chains is significantly limited by the 2.3-nm distance between 2Fe2S and the ring of heme b_L/b_p[259]. Such a large spatial separation slows down electron transfer to a timescale of seconds, minimizing the probability of its occurrence on a catalytic time scale. However, the problem appears when a redox active molecule such as quinone (QH_2, Q or SQ^-) is bound at the Q_o/Q_p site and cuts the 2.3-nm distance into two much shorter distances, each being well below the 1.4 nm limit[56]. This means that any type of quinone molecule bound in the site (whether it is the substrate, product or intermediate of the QH_2 oxidation) can in principle act as mediator, to significantly enhance electron transfer between the low- and high potential chains.

To explain the general lack of experimentally detected short circuits several "gating" mechanisms were constructed. The problem is however, that in most cases the gating mechanisms are either very effective at suppressing short-circuits, therefore sacrificing reversibility, or if they allow reversibility they are prone to some short circuits[259,615]. It appears that to explain how the Cyt*bc* can accomplish full and rapid reversibility and short circuit suppression while limiting superoxide production, elaborate mechanisms involving more than a single gating factor are needed.

The necessity for elaborate gating is a consequence of the sequential mechanism that is considered to drive the reaction at the Q_o/Q_p site, which is obliged to form SQ^- as a true intermediate of the two-electron reactions of bifurcation. This mechanism assumes formation of SQ^- at the Q_o/Q_p site, albeit at low occupancy[224]. It is generally in line with many observations that the Q_o/Q_p site can, under specific conditions, generate superoxide and also with recent experiments reporting detection of a SQ^- intermediate at this site (see section 7.5 and 7.6 and references there). The sequential mechanism is also in agreement with the chemical properties of quinones and their ability to take part in single-electron redox reactions. However, the major problem with sequential electron transfer is its susceptibility to short-circuiting.

As an attractive alternative and seemingly the simplest solution to the short-circuit problem, a concerted reaction was also proposed for the Q_o/Q_p site. This reaction, based on a fundamentally different mechanism, assumes that the reaction takes place through a transition state devoid of semiquinone character. In the following sections we will first reflect on the concerted mechanism before discussing the various possible gating mechanisms related to the sequential mechanism of the bifurcation.

Short-circuit-proof and leak-proof concerted reaction

The "concerted" reaction initially proposed for the Q_o/Q_p site is 'thermodynamic' cooperativity of the bifurcation reaction, in which electron transfer is sequential, but with a transient semiquinone state that never accumulates enough to be observable (i.e. reduction and oxidation of reaction partners may appear concurrent)[155,619,620]. Together with the kinetic resolution of millisecond reversibility of all electron transfer steps within Cytbc_1, including the reactions at the Q_o/Q_p site, the "concerted" reaction was introduced as one of the possible mechanism allowing reversible operation of this site while preventing all short-circuits (the other mechanism introduced in parallel was a "double-gating", as described below)[259,615]. The term "concerted" was regarded as a "kinetic" definition of two events taking place without time for significant atomic rearrangement. This concept recognized that all short-circuits would be efficiently suppressed if QH_2 oxidation (forward catalysis) and Q reduction (reverse catalysis) took place as a virtually single step involving 2 electron and 2 proton transfers. Suppression would then simply be a consequence of forbidding one-electron transfer reactions, of which all short-circuits are composed (see Fig. 29)[155,259,615,619,620].

It follows that if the concerted reaction is the catalytic mechanism at the Q_o/Q_p site, the SQ^- intermediate would not be formed at all during either QH_2 oxidation or Q reduction as its lifetime is shorter than the time needed for nuclei reorganization of molecules taking part in the electron transfer reactions[259]. This mechanism elegantly explains the energetic efficiency of the reversible catalysis of

Cytbc_1, but it remains hypothetical. While theoretical and experimental descriptions of kinetically concerted two-electron transfer reactions do exist[621,622], the chemical and physical details of the any concerted reaction at the Q_o/Q_p site remain unknown, as is the mechanism that would explain how SQ^- formation is forbidden.

The concerted mechanism becomes difficult to reconcile with recent experiments reporting the detection of transient SQ^- intermediates in the Q_o/Q_p site (see section 7.6). As, the concerted reaction is by definition short-circuit-proof and leak-proof, it eliminates entirely the possibility of superoxide generation. It follows, that another mechanism of SQ^- formation by Cyt*bc* would therefore have to be envisaged to explain this activity of Cyt-*bc*, such as electron transfer from reduced heme b_L/b_p to O_2, for which there is no evidence.

Gating mechanisms of sequential reaction

i) Catalytic switch and QH_2/SQ/Q mobility-driven gating at the Q_o site

The "catalytic switch", proposed by Brandt et al. before the discovery of 2Fe2S motion can be considered the first gating model[57,58]. This model pointed to a key role of the redox state of the 2Fe2S on the bifurcation reaction. It was formulated based on the difference between the binding constants of two types of inhibitors, stigmatellin and MOA-stilbene to Cytbc_1, caused by changes in the reduction state of the 2Fe2S cluster and the discovery that ISP-HD can be found at two different positions. The model assumed that QH_2 and Q can interact with oxidized 2Fe2S while SQ^- interacts with oxidized heme b_L but not with the reduced 2Fe2S cluster. Thus, electron transfer to 2Fe2S or heme b_L strictly depends on the redox state of these two cofactors forcing the forward bifurcation reaction at the Q_o site[57].

A somewhat similar model was proposed recently to explain the forward electron transfer in bifurcation through the movement of SQ^- at the Q_o site, to drive electrons to the correct chain. This model was also based on structural studies of stigmatellin binding to the Q_o site[91]. It predicts that reduction of the 2Fe2S cluster and formation of semiquinone leads to disruption of the H bond between ^{Rh}H156 (^{Bt}H161) which favors the movement of ISP-HD to the c-position (see section 3.4 for details) and a rapid movement of the benzoquinone ring toward the ^{Rh}E295 (^{Bt}E271)[119,575]. The latter movement facilitates deprotonation of the semiquinone and therefore increases the rate of electron transfer from SQ^- to heme b_L by shortening the distance between the reagents[23,596]. After the second oxidation, Q returns to the niche that is close to the 2Fe2S cluster. In this way the redox state of Q and heme b_L determine the direction of electron transfer at the Q_o site. These two mechanisms: termed "catalytic switch" and "SQ motion" do not protect the enzyme from performing SC2 or SC4.

Furthermore, they do not describe the proton/electron sequence of the reverse direction and, as discussed in [259,615], they are not easily reversible.

ii) Surface-modulated motion switch of Cytbc1

Another gating mechanism proposes that the movement of ISP-HD after the 2Fe2S cluster is reduced is coupled to the oxidation of heme b_L by heme b_H[21,78,89,623]. The authors proposed that electron transfer from heme b_L to heme b_H triggers some conformational changes in the region of Cyt*b*[89] responsible for docking the ISP-HD, releasing this domain from the Q_o site and then releasing Q and binding QH_2.[78]. Although, this mechanism allows the reversible reactions at the Q_o site, some short-circuit reactions (SC2, SC3 and SC4) are still possible. Furthermore, this model predicts, that the presence of Q at the Q_o site would favour occupation of positions remote from the Q_o site by the ISP-HD. However, this seems at odds with the experimental observation that when Q is bound at the Q_o site it leads to EPR spectra typical of 2Fe2S interacting with Q for the whole population of the reduced 2Fe2S (see section 3.4 for details).

iii) Proton gated affinity change and proton gated charge-transfer mechanisms

The "proton gated affinity change" mechanism was formulated on the basis of the electrochemical properties of 2Fe2S, in particular the difference between the pK value of the ^{Rh}H156 (^{Bt}H161) for the reduced and oxidized 2Fe2S[574]. According to this mechanism, either QH_2 binds to the deprotonated histidine or QH^- binds to the protonated histidine. The first electron transfer to 2Fe2S then drastically increases affinity of SQ^- for the reduced 2Fe2S, leading to a positive shift in the redox potential of the 2Fe2S in the $2Fe2S^{red} – H^+ – SQH$ complex. Such a stabilization should lead to a relatively large occupancy of SQ^- at the Q_o site. However, when this proposal was framed, experiments had thus far failed to detect any SQ^- at the Q_o site. This discrepancy was explained on the ground of strong antiferromagnetic coupling between SQ^- and $2Fe2S^{red}$ leading to disappearance of the EPR signal.

Evoking antiferromagnetic coupling as a reason for the failure to detect an EPR signals implies that the energy of such interactions must be very high to depopulate the paramagnetic, excited state at temperatures > 10 K (typical experimental conditions). However, this kind of strong spin-spin exchange is very unlikely for most bonds through which SQ^- could interact with 2Fe2S, including a single H bond. Interestingly, experiments performed 16 years after the initial formulation of the "proton gated affinity change" mechanism established that a spin-spin exchange interaction between SQ^- and reduced 2Fe2S does occur, but that the energy of such coupling is very low in comparison to

the thermal energy of experimental EPR conditions; and that this state can be detected by EPR (this is described in detail in section 7.6).

As described in section 7.2, several experimental results have been interpreted as being indicative of binding two substrate molecules to the Q_o site at the same time. This concept was also used to formulate a "proton gated charge-transfer mechanism" in which a QH_2/Q pair must first undergo two deprotonation steps followed by electron transfer to 2Fe2S and heme b_L[586]. The two proton-gated mechanisms allow reversibility of the Q_o site but do not prevent SC2, SC3 nor SC4.

iv) Double-gating mechanism

More recent models of bifurcation take into account the fact that a single gating step is generally not sufficient to suppress all types of short-circuits for reversible sequential bifurcation.

The first model of this type was the "double gating" mechanism, introduced as an alternative to the concerted mechanism in providing a means for short-circuit-proof and efficient reversible operation of the Q_o site. It evoked the concept that changes in protonation/deprotonation of water molecules and/or amino acid side chains near the Q_o site occur upon changes to the redox state of immediate cofactors, 2Fe2S and heme b_L, in order to specifically modulate barriers in the sequential reaction [259,615]. Double gating allows QH_2 oxidation only when both 2Fe2S and heme b_L are oxidized and allows Q reduction only when both 2Fe2S and heme b_L are reduced. This would be accomplished by raising the barrier for SQ^- formation when QH_2 is bound at the Q_o site (involving a SQ^-/QH_2 couple) when heme b_L is reduced and the 2Fe2S cluster is oxidized, or by lowering that barrier when both cofactors are oxidized. This would prevent SC1 and SC2 (Fig. 29). On the other hand, the barrier for SQ formation when Q is bound at the Q_o site (involving Q/SQ^- couple), would be raised when heme b_L is reduced and the 2Fe2S cluster is oxidized, or the same barrier is lowered when both cofactors are reduced. This would prevent SC3 and SC4.

v) Logic-gating mechanism

A "logic-gating" mechanism is quite similar to the "double gating" mechanism. It also evokes a concept of changes in protonation/deprotonation of water molecules and/or amino acid side chains near the Q_o site upon changes in the redox state of the immediate cofactors 2Fe2S and heme b_L. The model proposes that crucial elements for energy-conserving redox reactions depend on specific H-bond formation in the Q_o site [597]. Binding of QH_2 requires ^{Rh}H156(^{Bt}H161) and ^{Rh}E295(^{Bt}E271) to be in deprotonated states, which is possible when 2Fe2S and heme b_L are oxidized. Otherwise, reduction of 2Fe2S and heme b_L induces protonation of the N_τ atom of the histidine and the carboxyl group of the glutamate, allowing binding of Q to the Q_o site. Such a mechanism imposes constraints on the

direction of reaction, as QH_2 binds predominantly when both 2Fe2S and heme b_L are oxidized and Q binds predominantly when both 2Fe2S and b_L are reduced. This mechanism, like the double-gating mechanism, protects against all short-circuits while still allowing reversibility [259]. It is also generally consistent with the fact that reduction of 2Fe2S is associated with a shift in the pK value of the 2Fe-2S protein from about 7.6 to more than 10 [594] and is in line with the observation that Q bound at the Q_o site strongly influences EPR spectra of the 2Fe2S (see section 7.2 for details). In this model a tentative coupling between hemes b_L and the Glu residue exists and thus the reduction of heme b_L would be associated with protonation of the Glu carboxylic group while oxidation of the heme would induce deprotonation of the same side chain. However, experimental results on a series of mutants that replace ^{Rh}E295(^{Bt}E271) with other amino acids revealed only minor effects on the redox midpoint potential of heme b_L [579,598]. Also, equilibrium redox titrations of the bacterial chromatophore $Q(H_2)$ pool, made by monitoring changes in the g_x EPR transition of the 2Fe2S, showed that the reduced cluster is still able to interact with QH_2 under conditions in which heme b_L remains oxidized. The experimental detection of Q bound to the Q_o site under conditions of reduced heme b_L is not feasible due to large difference in E_m values of the Q/QH_2 couple and heme b_L.

In this mechanism water dipoles are proposed to be the crucial elements that stabilize Q or QH_2 binding when 2Fe2S and heme b_L are either both reduced or both oxidized, respectively.

vi) Coulombic gating.

When the rapid reversibility of reactions at the Q_o site was established[136], it became clear that the "SQ^- movement" mechanism (see above) does not explain gating, nor does it prevent all types of short-circuit. In an attempt to modify this mechanism to accommodate reversibility and the prevention of all short-circuits *"Coulombic gating"* was proposed [596]. The crucial element of this model is an assumption that SQ^- is attracted by Coulombic interactions, and thus moves toward the oxidized heme b_L, so increasing the electron transfer rate. On the other hand, when SQ^- is formed while heme b_L is reduced, then it is repelled, moving toward the 2Fe2S and decreasing the probability of electron transfer from heme b_L to SQ^-. Although, this mechanism seems to explain the limited efficiency of short-circuit SC2, it is still not clear how it would allow rapid reversibility of the Q_o site.

Current status and emerging concepts of short-circuit suppression. Despite many proposals and the various models outlined above, the exact mechanism of gating and reversibility at the Q_o site that minimizes energy-wasting reactions is still not known. It appears that each of the mechanisms presented is able to explain the bifurcation reaction under certain specific conditions, but at the same time they may not be sufficient to explain observations under other conditions, or to provide a detailed

molecular basis, or be fully consistent with the ensemble of existing experimental data. Our intention in this review is not to favor any particular mechanism. Rather, in view of their diversity and general complexity, and also given that no obvious elements unifying them into one common mechanism can be proposed, we argue that the bifurcation at Q_o site is far from being satisfactorily understood and still deserves extensive experimental and theoretical exploration. This is particularly the case for the Cytb_6f, where the situation is further complicated by the possible injection of an additional electrons from the *n* side through the c-heme to heme b_n.

It is worth hypothesizing that the "true" mechanism of energy-conserving reversible bifurcation could be a process to which several of the many different gating mechanisms proposed by different authors could contribute, depending on the starting conditions. We also anticipate that the transition from forward to reverse electron transfer at the Q_o site may not be a simple reversal of the proton/electron transfer, and that dynamic events that start the reverse reaction may differ from the final step of forward reaction. It could very well be that the stability constant of the SQ^- formed during oxidation of QH_2 is different from the stability constant of SQ^- formed by reduction of Q. We believe that the key players are likely to be protons, as different proton configurations could favor different stabilities of the SQ^- formed during froward and reverse reactions. However, the proton events and paths for uptake and release have not been resolved yet.

7.5 Superoxide generation at the Q_o/Q_p site

The operation of any electron transfer chain (ETC) in the presence of oxygen is connected to the generation of superoxide radical. *In vivo*, superoxide is quickly converted into H_2O_2 in a reaction catalyzed by superoxide dismutase. This is presumably why first mentions of ETC-derived radicals were related to H_2O_2 and not superoxide. Indeed, the first information about reactive oxygen species (ROS) in mitochondria showed mitochondrial levels of H_2O_2 at 1-2% of total O_2 uptake in state 4 of respiration (the state not coupled to ATP synthesis)while the rate of H_2O_2 generation in state 3 of respiration (the state associated with ADP to ATP conversion) was negligible[624,625]. It was also noticed that antimycin enhances production of H_2O_2 in intact mitochondria [626,627].

Semiquinone at the Q_o/Q_p site as electron donor to molecular oxygen The first reports on superoxide production in antimycin-treated submitochondrial particles to suggest that ROS are Cytbc_1-derived appeared in Boveris and Cadenas work in 1975 [628–630]. Over the next few years, it was established that the origin of ROS in antimycin-inhibited Cytbc_1 of submitochondrial particles is the redox reaction in the UQH_2 oxidation site [254,631]. Using Cytbc_1 isolated from yeast, it was also shown that inhibition with antimycin A as well as with myxothiazol which binds to the proximal niche of the

Q_o site, leads to production of ROS at the Q_o site [632,633]. The link between superoxide production and the action of Q_o/Q_p site is consistent with the widely-accepted notion that a highly unstable SQ^- at the Q_o site (SQ_o) is a direct one-electron donor to oxygen [224].

In view of the reversibility of the catalytic reactions in the Q_o site, there are two possible reactions that can lead to the formation of semiquinone at this site: one electron oxidation of QH_2 by the oxidized 2Fe2S cluster (the "semiforward' reaction) [632,634] or one electron reduction of quinone by heme b_L (the "semireverse" reaction, [635,636]. It therefore follows that there are two possible reaction sequences leading to ROS production by the Q_o site. These sequences involve either semiforward or semireverse reaction followed by electron transfer from the formed SQ^- to molecular oxygen. Both sequences require the initial presence of reduced heme b_L which either blocks the heme b_L from accepting an electron from SQ^- formed via the semiforward reaction or donates an electron back to Q bound at the Q_o site, forming SQ^- via the semireverse reaction. This requirement is generally consistent with the observation that ROS are detected when electron transfer between heme b_L and heme b_H is impeded by blocking the Q_i site with antimycin A or by an increase in membrane potential [572,637].

In the currently discussed mechanisms of ROS production by the Q_o/Q_p site, both reaction sequences (i.e. involving semiforward or semireverse reaction for semiquinone formation) are taken into account. Some models propose that only one from these two sequences is responsible for ROS production, while other models consider a contribution from both. Indeed, it seems plausible that the detected ROS may be a combined product of both mechanisms, but that their relative contributions change depending on the experimental conditions and/or introduced electron transfer barriers within cofactor chains.

The specific rate of superoxide production in Cytb_6f, normalized to the rate of electron transport, is more than an order of magnitude greater than that measured in isolated yeast respiratory Cytbc_1 complex.[38] The higher rate of superoxide production in Cytb_6f could be a consequence of an increased residence time of plastosemiquinone/plastoquinol in its binding niche near ISP-HD, resulting from (i) occlusion of the quinone portal by the phytyl chain of the unique bound chlorophyll, (ii) an altered environment of the proton-accepting glutamate believed to be a proton acceptor from semiquinone, or (iii) a more negative redox potential of the heme b_p on the electrochemically positive side of the complex.[38]

"The semireverse-Rieske off" model of superoxide production

The mechanism involving the semireverse reaction (heme b_L to Q electron transfer) is a relatively new phenomenon that emerged from the observation that ROS production exhibits a bell-like shape dependence on the redox state of the Q(H_2) pool. This means that maximal production of ROS occurred when the pool was partially oxidized, which was taken as an indication that the semireverse reaction, for which the substrate is Q (not QH_2), is involved in superoxide generation [120,636].

A contribution of the semireverse reaction in ROS generation was also established in studies using mutated forms of the bacterial Cytbc_1, which introduced limitations in electron transfer at the level of different cofactors within the low and high potential chains [107,120,635]. Furthermore, these studies revealed an important constraint associated with the kinetic effects of the motion of ISP-HD. In the proposed model, production of radicals depends on the position of the ISP-HD with respect to the Q_o site. Mutants with the insertion of a single or two alanine residues (+1Ala, or +2Ala, respectively) at the neck region of ISP, which increases the probability of ISP-HD being located in close proximity to the Q_o site [90,107], were found to be less prone to ROS production in antimycin A inhibited Cytbc_1 [107,635] (Fig. 30). To explain this observation, it was proposed that molecular oxygen competes kinetically for electrons with cofactors of the Q_o/Q_p site. When ISP-HD is present at the Q_o/Q_p site during SQ^- formation, the probability of electron transfer between the 2Fe2S and SQ^- is high. The reduced 2Fe2S can then reduce the SQ^-, reforming QH_2 and completing the reverse reaction, while the oxidized cluster can accept an electron from SQ^- and completing short-circuit reaction (SC3 in Fig. 29). However, when ISP-HD occupies positions remote from the Q_o/Q_p site at the time of SQ^- formation, the rate of the electron transfer between SQ^- and the 2Fe2S decreases. Under these circumstances, the probability that molecular oxygen outcompetes 2Fe2S for electrons from the SQ^- increases, which leads to the release of detectable levels of superoxide from the Q_o/Q_p site.

Initial studies on the +2Ala mutant were not able to discriminate between the possible contributions of semiforward or semireverse reactions in ROS generation [635]. In addition to the suppression of ROS generation in the 2Ala mutant, this study described another mutant, ^{Rh}M183L, that changes one of the axial ligands of heme c_1, shifting the E_m of this heme by more than -300 mV. This introduced a large barrier to electron transfer between 2Fe2S cluster and heme c_1 without affecting the motion of ISP-HD, causing an increase in ROS production. Given that ROS production is also enhanced when electron transfer barrier is introduced at the level of the low potential chain (addition of antimycin A, a mutation disturbing the oxidation of QH_2 at the Q_o site, ^{Sc}E272Q (^{Rh}E295Q) [598] or mutations to change the axial ligands of hemes *b*, ^{Rh}H198N and ^{Rh}H111N [638]), it appears that in general any significant asymmetry in the overall rate of electron flow between the high- and low-potential chains might make the enzyme more prone to generate superoxide. One

exception to this is if it is caused by arresting the ISP-HD at the Q_o/Q_p site. Again, these studies could not discriminate between the relative contribution of semiforward or semireverse reactions to ROS generation by the Q_o/Q_p site.

Such discrimination became possible in subsequent studies with the use of the 1Ala mutant and in combination with ^{Rh}M183K (equivalent of ^{Rh}M183L described above). These studies clearly pointed toward the semireverse reaction as the dominant contributor in this process [107]. Mutational studies analyzing the molecular effects of mitochondrial disease-related mutations further substantiated the inclusion of both postulates (i.e the one related to involvement of the semireverse reaction in SQ^- formation and the other related to the probability of ISP-HD position-dependent interaction of SQ^- with oxygen) in what can be referred to as the *semireverse-Rieske off* model of ROS generation by the Q_o/Q_p site.

The ^{Rh}G167P mutation in *Rhodobacter capsulatus* is an equivalent of human mitochondrial S151P mutation in Cyt*b* which was found in patients with exercise intolerance [639]. This mutant exhibits enhanced production of ROS even without antimycin A [120]. In contrast to +nAla insertions, ^{Rh}G167P influences the motion of ISP-HD in such a way that it tends to occupy positions more remote from the Q_o site in comparison to WT (see section 3.4) This effect, in agreement with the *semireverse-Rieske off* model, increases the probability of SQ reaction with oxygen (Fig. 30). Furthermore, introduction of the +1Ala mutation to the ^{Rh}G167P mutant partially compensated the effect of ^{Rh}G167P, which resulted in diminished ROS production, again consistent with this model. The ^{Rh}G332D mutation, an equivalent of another mitochondrial disease-related mutation G290D (associated with exercise intolerance in humans [640]), was also found to influence motion of ISP-HD. However, this influence is less pronounced compared to ^{Rh}G167P, and accordingly the effects on ROS production are more subtle [121], (Fig. 30).

As introduced in section 7.4.1 the kinetic competition between the leaks of electrons and short-circuit reactions, inherent also to the *semireverse-Rieske off* model, might be of physiological importance. In general, both reactions lead to a drop in the efficiency of electron bifurcation at the Q_o site, but while short-circuits retain electrons within ETC, leaks generate ROS.

Assuming that high production of ROS is deleterious, in some cases short-circuit reactions may play a beneficial role in lowering of ROS generation. For various enzymes involved in bioenergetics it has been postulated that such energetic loss, which minimizes ROS-related damage, gives the organism a better chance of survival [641]. On the other hand, ROS are also postulated to play a redox signaling role [642], thus careful balancing of short-circuits and leaks must be considered as one of the possible elements of the redox signaling/control systems.

When disabled, the Q_i/Q_n site does not completely inhibit the function of the Q_o/Q_p site, and the enzyme can still sustain electron flux through the ETC. This residual flux is presumably possible via short-circuit reactions and electron leaks. In Cytbc_1 that flux is low enough to make the enzyme non-functional. Interestingly, in Cytb_6f, a residual flux can sustain the entire photosynthetic chain with the short-circuits that were proposed to act as an "emergency exit" pathway bypassing the Q-cycle and making it dispensable [616].

Other postulated reactions involving molecular oxygen. In addition to the reaction of molecular oxygen with SQ^- formed at the Q_o/Q_p site discussed above, it was also proposed that oxygen might act as a redox mediator between QH_2 and heme b_L [643]. According to this proposal, heme b_L would accept an electron from QH_2 via protonated superoxide (HOO) at the Q_o site, which would facilitate electron transfer within the low potential chain. This, so far purely hypothetical scenario was introduced to explain the observed enhanced enzymatic activity of Cytbc_1 in the presence of oxygen, compared to its activity under anaerobic conditions,

MD simulations showed that O_2 molecules spontaneously diffuse into the Q_o site of Cytbc_1 and can react with SQ^- while forming superoxide [644]. Molecular oxygen may also occasionally get within 5 Å of the central iron atom of the hemes b_L and b_H. Its presence near the heme b_L raises the question of whether this heme is also an immediate electron donor in the production of superoxide. Indeed, this hypothesis has never been definitively ruled out, and although much less popular compared to models based on SQ^-, can also be found in the literature [643]. It is based on the rationale that the redox potential of heme b_L is sufficiently low to make electron transfer to oxygen theoretically possible [645].

In this context an interesting concept concerning the evolutionary adaptation of Cyt-*bc* complexes to the presence of oxygen was proposed recently by Bergdoll et al [160]. By comparing redox properties of organisms that use different quinones and live in aerobic and anaerobic conditions, they concluded that the Great Oxidation Event occurred about 2.5 billion years ago when the rise of atmospheric oxygen resulted in an up-shift of the ambient redox potential of hemes *b* and the 2Fe2S cluster. The global response of organisms, which included up-shift of the redox potential of the $Q(H_2)$ pool by 150 mV (menaquinone versus ubi/plastoquinone) and a commensurable increase in the entire set of redox potentials of the cofactors of Cyt*bc* complexes, was aimed to avoid deleterious ROS generation.

A separate question that can be found in the literature is whether the Q_i/Q_n site is also able to produce ROS [646]. Under high concentrations of QH_2 and in the presence of an inhibitor of the Q_o site, it is possible to generate a stable SQ^- intermediate originating from the reverse reaction at the Q_i site

of Cytbc_1 (see section 8.3) [151,647,648]. If Q_i/Q_n-produced ROS have physiological significance, it should be exposed under such conditions. However, measurements conducted in the presence of stigmatellin – a Q_o/Q_p site inhibitor, did not show statistically significant production of radicals in such a system [633]. As discussed in section 8 Q_i-derived SQ^- can be stabilized *via* hydrogen bonding to prevent potential reaction of this SQ^- with molecular oxygen, as was shown for solution-generated SQ^-, which was found to be stabilized through hydrogen bonds with the acceptor solvent[253].

Physiological considerations. The currently available molecular mechanisms of superoxide generation by Cytbc_1 are derived mostly from analysis of conditions where electron flow through the cofactor chains was severely impeded by various experimentally imposed barriers (inhibitors, mutations). This raises the question whether the natively operating enzyme contributes to ROS generation in living cells, and if so how it does this. Despite some reports that uninhibited Cytbc_1 may produce trace amounts of radicals [38,572,649], there are no conclusive data to answer this question in a comprehensive manner. In our view further progress requires development of new spectroscopic approaches that not only allow experiments to be conducted in conditions closer to those encountered by the enzyme in the cells, but also provide high molecular and kinetic resolution of specific electron transfer steps. Nevertheless, several important physiological aspects of cytochrome Cytbc_1-related ROS production by ETC are worth discussing.

It is known that production of ROS is dependent on the respiration rate of mitochondria [37,650]. Factors enhancing ROS production in mitochondria include high pmf, a high NADH:NAD^+ ratio, high QH_2/Q ratio, low local O_2 concentration and nearly inactive ATPase[37,637,650–652]. As a rather general rule, the more reduced the cofactors of ETC are, the more prone ETC is to radical formation. Factors lowering production of ROS include high activity of uncoupling proteins which decrease pmf [653]. High respiration rate also lowers the probability of ROS production [37,650].

ROS generation is usually expressed in units of s^{-1} (as the amount of superoxide molecules produced by ETC complex in one second) or as a percentage of ROS production (as % of ETC-derived electrons that pass to oxygen forming superoxide). In state 3 of respiration (upon the addition of ADP) when the rate of oxygen consumption is maximal, the fractional ROS production is negligible. However, in state 4 of respiration (when the ADP levels are depleted) and where respiration chain is slowed down, production of ROS is at the level of 1-2 % [624]. Interestingly, expressing production in s^{-1} shows that the rate of ROS production in state 3 might be even higher than in state 4 [654].

The possible influence of physiological factors on ROS generation by Cytbc_1 is perhaps best exemplified by the effects of the membrane potential. In its absence, heme b_H is the preferred electron

acceptor within the pair of hemes $b_L - b_H$ [655]. In its presence, the apparent midpoint potentials of these two hemes become similar, leading to a more equal distribution of electrons between them [573]. Consequently, the reduction level of heme b_L increases which, as observed experimentally, is expected to lead to ROS production by the Q_o site [573].

However, a description of dynamic changes in electron distribution between the *b* hemes appears to be a more complex issue when possible communication between monomers in the dimer occurring at the level of the heme b_L-b_L bridge, is considered (see section 9). Any significant electron transfer between monomers is expected to decrease the reduction level of the *b* hemes (including heme b_L) which might decrease the levels of ROS released from the Q_o/Q_p site, in particular if the *semireverse-Rieske off* mechanism is considered.

The physiological role of superoxide released by the components of ETC remains an open issue, especially in view of the suggestions that it may be one of the components of cellular redox signaling [36]. Among four ETC complexes (Complex I – Complex IV) it is commonly acknowledged that only two of them generate the majority of ROS produced during the operation of the ETC: Complex I and Complex III (reviewed in [650,656]). These two complexes release superoxide into different compartments of mitochondrion: Complex I frees superoxide into the matrix, while Complex III- releases it into the intermembrane space (IMS). ROS in the IMS are more easily accessible to the cytosol compared to ROS in the matrix, as the former need to cross only the outer mitochondrial membrane while the latter have to cross both inner and outer mitochondrial membranes [657].

It should be emphasized that consideration of the role of ROS in cellular signaling should always account for the fact that the level of ROS released into the cytosol from mitochondria is the net result of ROS production and its scavenging inside the organelles.

Superoxide generated in the matrix is efficiently converted into H_2O_2 by the highly abundant MnSOD [627] and H_2O_2 is further consumed by catalase (CAT) and glutathione peroxidase (Gpx). Estimates indicate that H_2O_2 is kept at a low level in the matrix, around $5x10^{-9}$ M [658]. Supposedly, matrix-generated superoxide and H_2O_2 from its dismutation do not leave the matrix [657] and thus any putative signal derived from complex I is probably restricted to this compartment.

ROS signaling communication between the mitochondria and cytosol becomes more plausible for superoxide generated by complex III and released to IMS [642,659].

In the IMS superoxide can be transformed by CuZnSOD to H_2O_2 or, theoretically, scavenged by Cyt*c*. The latter reaction, in view of the ratio between superoxide and the high physiological concentration of Cyt*c* in the IMS (estimated to be in the range of 1 mM [660]), raises concern about whether the lifetime of superoxide released to IMS would be sufficient to carry out any meaningful

signaling purposes. However, the probability of superoxide oxidation by Cyt*c* may actually not be that high considering the rather low ratio of Cyt*c* to Cyt*bc*$_1$, (around 2:1 [204], as estimated based on the optical spectrum of reduced mitochondria [254,661]) and the fact that Cyt*c* pool is almost fully reduced in state 3 or 4 of respiration [662]. While superoxide cannot pass efficiently through the membrane, it can escape mitochondria via voltage-dependent anion channels [663]. After spontaneous or CuZnSOD-driven dismutation, superoxide is converted into H_2O_2, and in this form it can reach cytosol via diffusion much more readily. When overactivity of CuZnSOD in the IMS is observed, this leads to overproduction of H_2O_2, which in turn may lead to the formation of oxoferryl Cyt*c*. This may result in the oxidation of cardiolipin and turn on early pro-apoptotic processes [664].

Interestingly, until now no one has succeeded in detecting superoxide evolution from Cyt*bc*$_1$ by spin-trapping. This seems to stem from the methodological difficulty related to the large difference between rate constants for the superoxide reaction with Cyt*c* ($k = 2.5 \times 10^5$ $M^{-1}s^{-1}$, [665]) and the EPR spin trap DMPO ($k = 10$ $M^{-1}s^{-1}$, [666]). DMPO falls behind oxidized Cyt*c* when competing for superoxide. Cyt*c* is a substrate for Cyt*bc*$_1$ and achieving measurable level of radicals requires measurements to be done in the presence of high micromolar concentrations of Cyt*c*. In order for DMPO to be able to trap superoxide before it reacts with Cyt*c*, it would need to be in a high molar concentration range, which is unattainable due to its limited solubility.

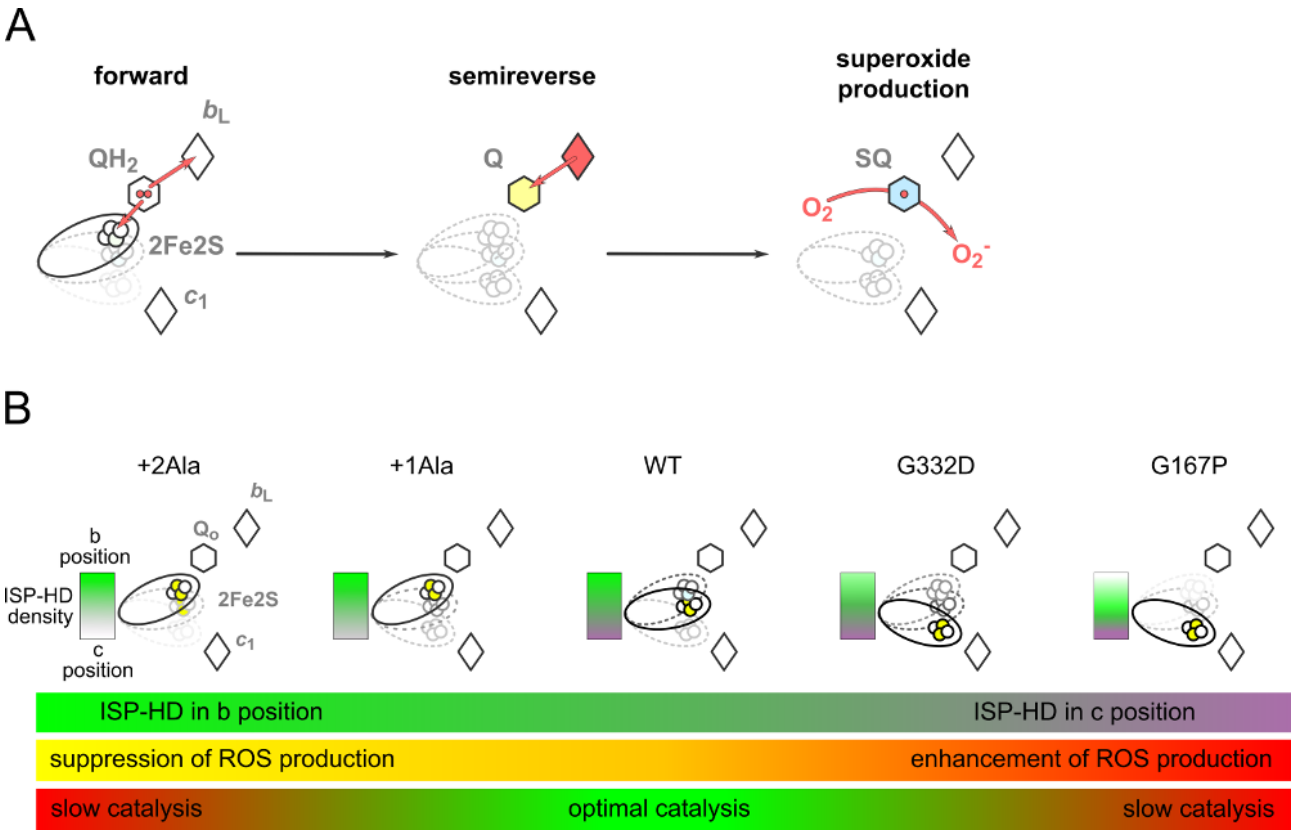

Figure 30. The „*semireverse-Rieske off"* model of ROS generation in the Q_o site. (A) A simplified static scheme showing one of the possible sequences of reactions leading to ROS formation at the Q_o site: oxidation of QH_2 ("forward" box), electron transfer from heme b_L to Q ("semireverse" box), electron transfer from SQ to molecular oxygen ("superoxide production" box). In "forward", and "semireverse" box, white and red rhombus correspond to the redox state of heme b_L before the reaction (oxidized and reduced, respectively). The reduced heme b_L necessary to start the semireverse reaction can also be a product of electron transfer from heme b_H (reaction 2 in SC4 in Fig. 29). Note that the semireverse reaction corresponds to reaction 1 in SC3 and SC4 or reaction 2 in SC2 in Fig. 29 (B) Scheme illustrating that a shift in the equilibrium distribution of the ISP-HD positions from the b-position toward the c-position (from left to right) induced by specific mutations correlates with an increase in the ability of the Q_o site to generate ROS.

7.6 Semiquinone intermediate at the Q_o / Q_p site

When discussing the mechanism of QH_2 oxidation at the Q_o/Q_p site, SQ is naturally considered as the transient state of the bifurcation reaction. Over the years the EPR signal related to this state was expected to be typical of a free radical single-line EPR spectrum at a g position close to 2. The very first report of detection of a g = 2 signal assigned to semiquinone at the Q_o site (SQ_o) in submitochondrial particles from 1981[667] was invalidated by studies from 1998 [668]. Since that time a notion about SQ_o being highly unstable and therefore undetectable by EPR has been popular in the literature until 2007, when two independent groups reported on detection of SQ_o [261,262] In 2013, three additional reports presenting g = 2 EPR signals assigned to SQ_o were published [263,264,590] All these relatively new reports reopened a discussion on the presence of SQ_o, its properties and its implications for the mechanism of bifurcation. In general, one would expect the signal to appear under conditions favoring electron transfer reactions at the Q_o/Q_p site and to be sensitive to all specific inhibitors of this site. It should also have paramagnetic properties related to its interactions with other metal cofactors of the site, the heme b_L/b_p and/or 2Fe2S (such as enhanced paramagnetic relaxation rates compared to a chemically generated SQ in solution). This, however, has not always appeared to be the case. For this reason, in our view, the issue remains debatable and requires further experimental exploration. A detailed discussion of different spectroscopic properties and controversies surrounding the g = 2 signals assigned as SQ_o is beyond the scope of this review. The reader is referred to a more detailed review by Pietras et al. [258].

In one of the reports on SQ_o from 2013, apart from the single-line signal at g ~2, measured at 200 K, a new, unexpected transition with the most prominent line at g = 1.94 in the region of the spectrum of 2Fe2S was recorded at 20 K [263] (see Fig. 31). The new signal was highly sensitive to the inhibitors of the Q_o site and was transient (i.e. was detected only under non-equilibrium conditions before the enzymatic reaction of Cytbc_1 with its substrates reached equilibrium). Furthermore it was observed that g=1.94 at the X band (~ 9.5 GHz) shifts to g=1.96 at the Q band (~ 33 GHz). These

findings, complemented by the simulation analysis of the EPR spectra led the authors to conclude that the g = 1.94 transition belongs to the spectrum originating from SQ_o coupled by spin-spin exchange interaction with the reduced 2Fe2S (SQ-2Fe2S). An isotropic exchange constant of the interaction was estimated at 3.5 GHz. This was all consistent with the theory of exchange interactions, which assume that in the case of spin-spin coupling with an exchange constant of several GHz, the position and shape of EPR transitions of a system of coupled paramagnetic centers will depend on the microwave band used to make the measurements [669,670]. It is of note that the spin-spin exchange interaction between SQ and the reduced 2Fe2S has already been put forward as an explanation for the failure to detect the g = 2 radical signal of SQ [574]. However, unlike the original proposal, the more recent data do not result from anti-ferromagnetic coupling of high energy.

Further research showed that a g = 1.94 signal of similar amplitude was observed when the samples were prepared under both aerobic and anaerobic conditions [482,671]. This dismissed concerns raised by others [672] that it might have resulted from oxidative damage to the 2Fe2S. This also pointed towards an interesting possibility that the SQ-2Fe2S state is not reactive toward molecular oxygen (see discussion below).

Upon optimization of reagent concentrations the SQ-2Fe2S signal was detected within the timescale of tens to hundreds of milliseconds, which was comparable to the time of a single turnover of enzyme under the applied conditions (inhibition of the Q_i site with antimycin).[671] On the other hand, the time scale of SQ-2Fe2S evolution was slower than the time scale of uninhibited enzyme turnover. Remarkably, so far the SQ-2Fe2S state has been found to coexist exclusively with oxidized heme b_L. All together, these results implicated that the semireverse reaction (heme b_L/b_p to Q electron transfer) at the Q_o/Q_p site is responsible for initiating formation of the SQ-2Fe2S state. This is partly because the semireverse reaction creates SQ_o which can undergo spin-spin exchange with reduced 2Fe2S provided that the ISP-HD is docked at the site [263].

Further studies revealed that the probability of formation of the SQ-2Fe2S state varies in mutants with decreased motion of ISP-HD [671]. It is highest in mutants which have ISP-HD shifted towards the Q_o site (+1Ala and +2Ala). In contrast, the SQ-2Fe2S state was not observed in the ^{Rh}G167P mutant, which has the oppositely effect to +1Ala or +2Ala and shows impaired docking of ISP-HD into the Q_o site [120] (^{Rh}G167P mutation).

The various combinations of these mutations have shown that direct interaction between the 2Fe2S and SQ_o is crucial for formation of SQ-2Fe2S state, and even minimal separation of the cluster from SQ_o induced by mutation breaks the spin-spin interaction.

The same family of mutants also revealed a clear negative correlation between superoxide production and the ability to form the SQ-2Fe2S state. Based on this observation and the non-

reactivity of SQ-2Fe2S center with molecular oxygen discussed earlier, it has been suggested that the SQ-2Fe2S state may be involved in protection against massive release of superoxide under conditions when electron flow through the Q_o site is impeded [671]. It should be noted that while the lack of the SQ-2Fe2S state is associated with an increase in the production of superoxide by Cytbc_1, a high superoxide production may not necessarily imply lack of the SQ-2Fe2S state. This seemingly paradoxical statement is easily explained assuming that the unstable SQ_o is a common substrate for production of superoxide and generation of the SQ-2Fe2S state. An increase in the probability of formation of SQ_o will result in both an increase in superoxide production as well as in more efficient generation of SQ-2Fe2S. Since the SQ-2Fe2S state is nonreactive with oxygen its formation can be regarded as an alternative route to leaks of electrons on oxygen thus it reduces the amount of superoxide production.

The SQ-2Fe2S signal was also detected in enzyme operating with native substrates in membranes of photosynthetic bacteria [607]. Remarkably, the signal was present only when light-activation of the membranes shifted the redox state of the substrate pools, ubiquione and Cytc_2 pools, to a more reduced and oxidized state, respectively.

Under these conditions, SQ-2Fe2S titrated at higher ambient redox potentials compared to the $Q(H_2)$ pool (see section 4.1), which suggests that the SQ-2Fe2S state is somewhat stabilized at the Q_o site. The redox potential at which the SQ-2Fe2S amplitude reaches its maximum increased with decreasing pH indicating that a proton is involved in stabilizing the SQ-2Fe2S state. The interaction of SQ_o through hydrogen bonding with the 2Fe2S coordinating residue ^{Rh}H156, and the role of this interaction in SQ_o stabilization have been postulated many times [258,574,596].

Interestingly the SQ-2Fe2S state is not restricted to Cytbc_1, but has as it was also observed in isolated spinach Cytb_6f exposed to its substrates, PQH_2 and PC [482]. In this case however, unlike in Cytbc_1, inhibition of the Q_n site was not required. This revealed that the probability of SQ-2Fe2S state formation when the enzyme operates without inhibition is higher in the Q_p site of Cytb_6f compared to the Q_o site Cytbc_1. The average redox potential of hemes b_n and b_p is probably more negative in Cytb_6f than respective *b* hemes in Cytbc_1, while the redox potential of PQ/PQH_2 couple is higher compared to the potential of the respective UQ/UQH_2 couple. These differences in the redox potentials of *b* hemes and quinones would foster the semireverse reactions at the Q_p site, and thus increase the probability of the SQ-2Fe2S state formation. In addition, electron transfer through heme c_n in Cytb_6f (not present in Cytbc_1) might slow electron flow through the low-potential chain, and this could lead to a more favorable semireverse reaction.

The importance of quinone redox potential to SQ-2Fe2S formation is well supported by the observation that the high-potential Q derivative (DBMIB) bound at the Q_p site also creates the SQ-

2Fe2S state with a g = 1.94 transition. However, in this case the state was already observed under equilibrium conditions, without PC present. In fact, its stability is so high that it inhibits the Q_p site. Indeed, the inhibition of Cytb_6f by DBMIB has long been known, as has its effect on the shape of the EPR spectrum in the region of 2Fe2S, [84,108,483] This has been interpreted over the years as a structural alteration of the cluster caused by inhibitor binding [110]. The frequency-dependent shift in the g value of the signal induced by DBMIB (similar to shifts discussed above) dismisses this interpretation, indicating that the signal must reflect a spin-spin exchange interaction between the SQ form of DBMIB and the reduced 2Fe2S [482] (see also section 5).

Considering all the details of the formation and properties of SQ-2Fe2S uncovered to date, an energy diagram was proposed for both Cytbc_1 and Cytb_6f, in which this state represents a local energetic minimum, placed below the state with the reduced heme b_L/b_p (given that SQ-2Fe2S is observed along with oxidized heme b_L/b_p), but above the state with reduced heme b_H/b_n (Fig. 32). It has been suggested that SQ-2Fe2S is a metastable state, which may play a role as a buffer for electrons, in particular under conditions when electrons cannot freely leave the low-potential chain through the Q_i/Q_n site. Although the physiological role of this state is not yet known, in view of the observed negative correlation between its presence and superoxide production, and the apparent non-reactivity of this state with molecular oxygen, it was proposed that SQ-2Fe2S may be associated with protection against side reactions at the Q_o/Q_p site. This concept further assumes that the probability of formation of SQ-2Fe2S might be adjusted to the oxygen tension in the cellular environment and varies between different species. This probability depends on the energy difference between SQ-2Fe2S and the states determined by the E_m values of Q/QH_2 couple and the E_m values of the oxidized/reduced couples of low-potential cofactors of Cyt-*bc* (Fig. 32). This notion was proposed in view of the observation that Cytb_6f, which experiences more than an order of magnitude higher levels of oxygen in chloroplasts than does Cytbc_1 in mitochondria, appears to have a greater tendency to reside in this buffered state.

An intriguing hypothesis was put forward for a possible role of the Cytb_6f SQ-2Fe2S in regulation of the electron transfer pathways in oxygenic photosynthesis. It was proposed that the SQ-2Fe2S state in Cytb_6f might serve as a factor that changes the efficiency of CET *vs* LET between photosystem I and II. This concept was based on the assumption that transient stabilization of the SQ-2Fe2S temporarily blocks the oxidation of further PQH_2 in the Q_p site, thus creating conditions in which the probability of delivering the second electron needed to complete the reduction of PQ in the Q_n site by Fd/FNR is significantly increased.[482]

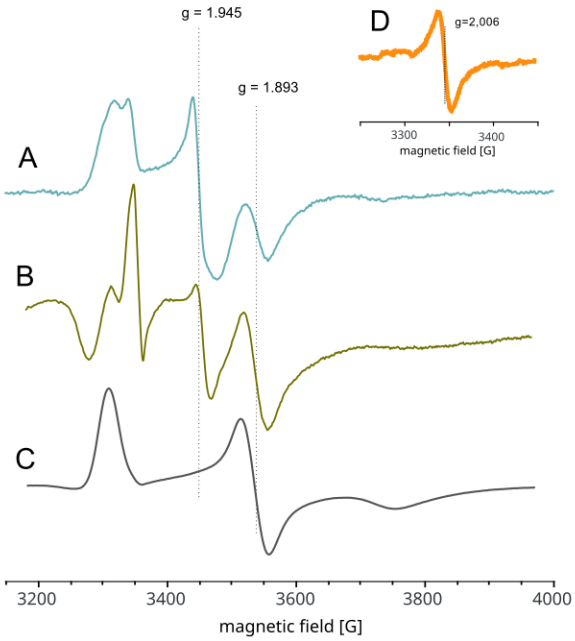

Figure 31. Two forms of SQ detected by EPR for the Q_o/Q_p site of Cyt*bc*: the spin coupled SQ-2Fe2S state (with prominent transition at g= 1.945) and the "free" SQ_o not coupled to 2Fe2S (with transition at g = 2.006). Experimental spectra of Cytbc_1 (A,C,D) and Cytb_6f (B) recorded at the X band. Spectra in A and B contain contributions from the spectrum of SQ-2Fe2S and the spectrum of 2Fe2S. C shows the spectrum of 2Fe2 alone, for comparison. The insert (D) presents the single-line spectrum of the SQ_o.

Figure 32. A simplified energy diagram of Cytbc_1 and b_6f. The diagram shows the states of the catalytic reaction at the Q_o/Q_p site. 1) Conditions before the start of the bifurcation reaction - Q_o/Q_p is occupied by QH_2,, 2Fe2S and heme b_L/b_p are oxidized. 2) Transition state - unstable semiquinone and the reduced 2Fe2S, oxidized heme b_L/b_p. 3) Conditions after full oxidation of QH_2 - Q_o/Q_p is occupied by Q, cluster 2Fe2S and heme b_L/b_p are reduced. 4) Stage after electron transfer from heme b_L/b_p to heme b_H/b_n. This state has different energy in the Cytbc_1 and Cytb_6f due to the different potential of heme b_H/b_n in both enzymes and the potential differences between PQ and UQ. 5) Spin-coupled SQ-2Fe2S state with

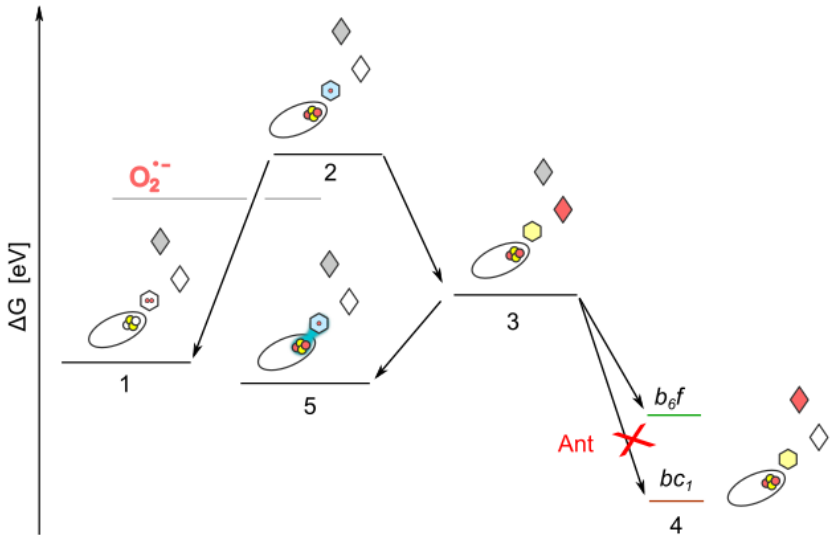

oxidized heme b_L/b_p. The redox state of heme b_H/b_n in all states (1-5) is not considered in the context of the system's energy. The level of the reaction of SQ with oxygen is also indicated as a gray line below state 2. [482]

8 Mechanistic insights into the catalytic Q_i/Q_n site

8.1 Overview of the structure of Q_i and the proton paths

The Q_i site binding pocket is located in the vicinity to heme b_H near the *n* side of the membrane and its entrance opens towards the membrane core allowing substrate and product molecule to enter and leave the site. The pocket is surrounded by residues from transmembrane helices A, D, E, the amphipatic surface helix a, the DE loop and the N-terminal peptide. The crystal structures identified not only the position of site-specific inhibitor (antimycin A) [79,123], but also the position of bound substrate (UQ) [61,63,79,123,673]. The binding sites of these compounds were found to significantly overlap with little rearrangements in the protein backbone and side-chains, as compared with the rearrangement of the protein around the Q_o site upon binding inhibitors. This indicates that the Q_i site is structurally more rigid than the Q_o site.

The quinone ring bound at the Q_i site is nearly perpendicular to the plane of heme b_H with the closest distance of 4.2 Å [79]. It appears to be stabilized by both hydrophobic and polar interactions. The former include interaction with ^{Bt}Phe220/^{Sc}Met221, the latter through formation of hydrogen bonds with three residues: ^{Bt}Ser205/^{Sc}Ser206, ^{Bt}Asp228/^{Sc}Asp229, and ^{Bt}His201 [79,673]. The His interacts directly with quinone in bovine [79] and also in bacterial enzyme (His217)[63], while in yeast (^{Sc}His202)– it interacts indirectly through a water molecule.[673]

As the Asp and His residues interact respectively with O1 and O4 of Q, they are considered to be involved in protonation of Q. In addition to these residues, the crystal structures identified other

structural elements that could potentially form proton paths from the protein surface towards the O1 and O4 of Q.

The path toward the O1 (referred to as the D/K path) involves a conserved Lys residue and a bound cardiolipin, which interacts further with a conserved Asp located next to the bound Q (Fig. 33). The cardiolipin has been suggested to act as a proton attracting antenna, which transfers protons to the nearby Lys[673]. The Lys further passes the protons to the conserved Asp through a string of interconnected water molecules [674], or alternatively undergoes a rotation towards the Q_i site and directly interacts with the Asp, as suggested by MD simulations [79,675].

The path toward the O4 involves a conserved Glu and a conserved Arg that may interact through the water molecules with a conserved His located next to the bound Q [673,674]. Site-directed mutations of this residue fully inactivated bacterial Cytbc_1 [676]. On the other hand the Asp/Lys path was found to be disabled only when both protonable groups were removed. With just one protonable residue from the Asp/Lys pair, the entrance of protons to the catalytic site was sustained, albeit at lower rates, indicating that protons in the Asp/Lys path can travel through parallel routes, possibly involving water molecules [677]. The Asp/Lys path thus appears to tolerate disruption, as long as all the elements available for functional cooperation secure efficient proton delivery to the catalytic site. In this context, the Q_i site is similar to other Q binding sites, such as the Q_B site of photosynthetic reaction center, for which a multiplicity for proton paths has also been considered [678]

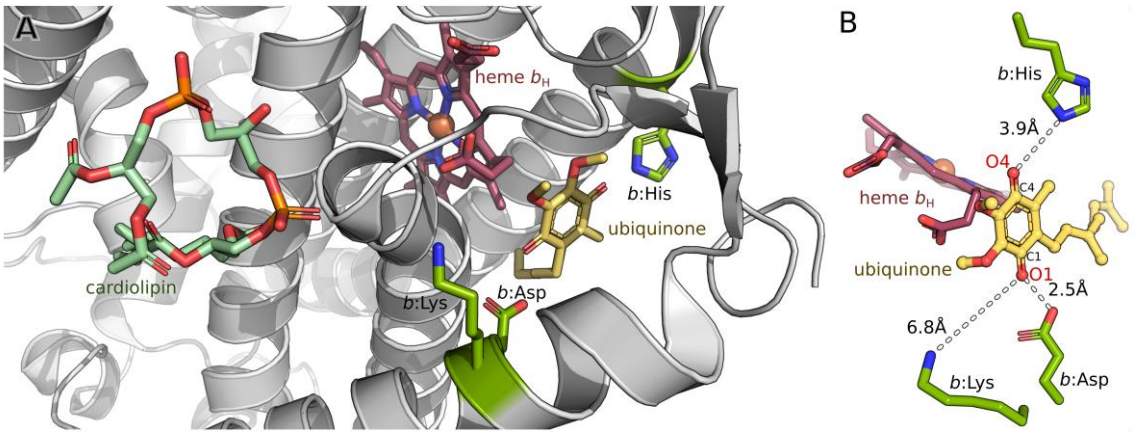

Figure 33. Structural details of the region around the Q_i site. A) Overall view of the Q binding environment and elements involved in proton transfer to Q. B) Geometry of the Q binding at the Q_i site. Labels indicate O1, O4, C1 and C4 atoms of the Q molecule and distances between Q and proton donors. Models based on PDB IDs: A206 and 1NTZ, A and B, respectively.

8.2 Catalytic electron and proton transfers at the Q_i site of Cyt*bc*$_1$

The reduction of Q to QH_2 at the Q_i site involves two sequential single electron transfer steps in which the electrons are delivered from the same cofactor chain [39]. Because the arrival of the electrons is separated in time, the reaction must involve the formation of an SQ intermediate (SQ_i) that is stabilized within the Q_i binding pocket before the final product (QH_2) is formed and leaves the site. Indeed, a stable radical signal originating from the Q_i site was recognized in early EPR studies on submitochondrial particles [440] and crude protein extracts [141,679] and has been explored since then as a key mechanistic element of models proposed for that site [151,163,245,647,648,677,680–684].

Considering electron transfer, reduced heme b_H acts as immediate electron donor to Q and then to SQ formed after the first electron transfer (SQ_i). These reactions are favored by the generally lower E_m of the heme compared to the average E_m of the Q(H_2) pool (under physiological pH, E_{m7} of heme b_H is around +50 mV, while that of the pool is around +100 mV) [149]. As these reactions leave heme b_H in an oxidized form, the SQ_i associated with the oxidized heme b_H (SQ_i-b_H^{3+}) is one of the key intermediate states of the catalytic forward reaction [2].

At alkaline pH, the E_m of heme b_H approaches that of the Q(H_2) pool and a partial reversal of the reaction can be observed. In this case QH_2 bound at the Q_i site reduces heme b_H, resulting in formation of SQ_i at this site [163]. As in this reaction, QH_2 instead of Q acts as a substrate for the Q_i site, and this is favored not only at alkaline pH but also at high QH_2 to Q ratios [647,685]. This reaction, unlike the forward reaction, leads to the formation of SQ that is present along with reduced heme b_H (SQ_i-b_H^{2+}). For many years, SQ_i-b_H^{2+} has been the dominant form of SQ_i detected and explored experimentally. However, more recent studies indicated that the analysis of both forms of SQ_i (i.e. SQ_i -b_H^{3+} and SQ_i -b_H^{2+}) is crucial to advance our understanding of the molecular mechanism of the operation of the Q_i site (see section 8.3).

In addition to the observation of a stable SQ_i radical by EPR, the stability of SQ_i is supported by data from light-induced electron transfer measurements. Under conditions of single-turnover at the Q_o site, the offset in the levels of light-induced heme b_H reduction observed in the absence and presence of antimycin corresponds to the amount of SQ_i that is formed in the forward reaction (electron transfer from heme b_H to Q). On the other hand, when the Q_o site is blocked by an inhibitor, the level of light-induced heme b_H reduction corresponds to the amount of SQ_i formed in the reverse reaction (electron transfer from QH_2 to heme b_H). The extent of the forward reaction reflects the difference between the E_m of heme b_H^{3+}/b_H^{2+} and the E_m of Q/SQ couples, while the extent of the reverse reaction indicates the difference between the E_m of heme b_H^{3+}/b_H^{2+} and the E_m of SQ/QH_2 couples. Further analysis of such extents might provide estimates of E_m for Q/SQ and E_m for SQ/QH_2, which in turn would provide information on the stability constant of SQ ($\log(K_s) = [E_m(Q/SQ) –$

$E_m(SQ/QH_2)]/60$. Using this approach with a specific mutant in which the $E_{m,7}$ of heme b_H was elevated to the level of the E_m of the QH_2 pool, the stability constant of SQ_i was estimated to be at the level of 3×10^{-1}.[149]

8.3 Fast- and slow-relaxing SQ_i as dominant intermediates of forward and reverse reactions at the Q_i site, respectively.

Until recently, EPR-based investigation of the SQ_i intermediate relied on the assumption that the SQ_i interacts antiferromagnetically with the oxidized heme b_H, forming an "EPR-silent exchange couple". Therefore only SQ_i present when heme b_H is also reduced (SQ_i -b_H^{2+}) was thought to be spectroscopically detectable [141,681]. This notion is no longer valid in light of the recent studies that identified two distinct populations of SQ_i differing in the rates of spin-lattice relaxation (Fig. 34 A) [151,163]. The first population, characterized by a slow relaxation (SQ_{iS}), corresponds to the well-known and extensively examined SQ_i -b_H^{2+} state, whereas the second population, characterized by a significantly faster relaxation time (SQ_{iF}), corresponds to the long-missing SQ_i -b_H^{3+} state. The dipolar interaction between SQ_{iF} and oxidized heme b_H manifests itself in the characteristic properties of SQ_{iF}, including fast spin-lattice relaxation leading to dominant homogeneous line broadening [686] and unusual behavior of the signal amplitude that does not follow Curie's law [687]. These findings established that, contrary to long-standing assumptions, the SQ_i-b_H^{3+} state is not antiferromagnetic and can be separated spectroscopically (as SQ_{iF}) if an appropriate combination of microwave power and temperature is applied during EPR measurements [151]

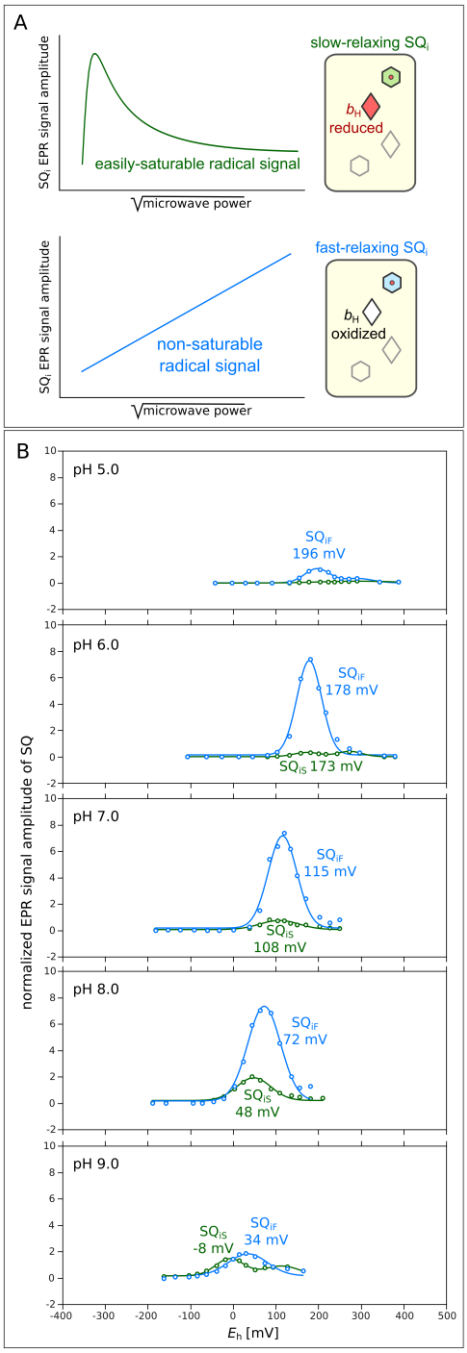

Figure 34. **A**) Two populations of SQ_i detected by EPR. Upper: slow-relaxing SQ_i (SQ_{iS}) associated with the presence of reduced (and diamagnetic) heme b_H near the Q_i site. Green line illustrates the expected MP saturation profile of SQ_{iS}. Lower: fast-relaxing SQ_i (SQ_{iF}) associated with the presence of oxidized (and paramagnetic) heme b_H near the Q_i site. Blue line illustrates the expected saturation profile of SQ_{iF}. **B**) EPR-monitored redox titrations of SQ_{iS} and SQ_{iF} in a range of pH from 5 to 9.[163]

Further studies revealed that SQ_{iS} and SQ_{iF} are separable in equilibrium redox titrations [163]. Remarkably, over a pH range from 6 to 8, SQ_{iF} represented a large, if not dominant, portion of the whole population of titrated SQ_i, indicating that early titrations [245] had indeed missed a significant

fraction of SQ in this pH range (Fig. 34 B). SQ_{iF} was also trapped as a stable intermediate at the Q_i site during steady-state turnover [163], which is consistent with the electron transfer reaction scheme predicting SQ_i -b_H^{3+} as the key intermediate state of the catalytic forward reaction (heme b_H to Q electron transfer) [2]. On the other hand, SQ_{iS} appeared as the dominant intermediate state observed under the conditions favoring the reverse reaction (QH_2 to heme b_H electron transfer).

Interestingly, when a single electron gets injected into heme b_H of one monomer through the reverse reaction at the Q_i site, there is a possibility of electron equilibration within all four hemes of the *b*-chain of the dimer (through the heme b_L-b_L bridge, see figure 5 and section 9). This way the electron can reach the second Q_i site (reducing Q to SQ_i) which overall will result in a formation of SQ_{iF} in both monomers (Fig. 35). The observation that both SQ_{iS} and SQ_{iF} are observed in the native enzyme with an inactivated Q_o site (when only the reverse reaction at Q_i is possible) indicates that electron equilibration within the *b*-chain of the dimer indeed traps some fraction of the molecules of Cytbc_1 with the SQ_i -b_H^{3+} state at both Q_i sites [151]. This conclusion was further supported by the observation that electron redistribution over *b* hemes /Q_i sites taking place within the dimer and monitored by analyzing the change in relative proportions of SQ_{iF} / SQ_{iS}, is effectively modulated in mutants that significantly raise the redox midpoint potential of either heme b_L or heme b_H. [149,151].

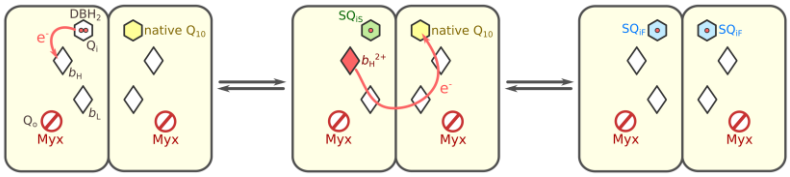

Figure 35. The cross-dimer electron equilibration leading to formation of SQ_{iF} (see details in the text)..

8.4 Charge polarization of SQ_i facilitates electron and proton reactions at the Q_i site.

The experimental exploration of both states of SQ_i (i.e. SQ_{iS} and SQ_{iF}) complemented by quantum mechanical calculations lead to the formulation of a hypothetical mechanism which places importance on the charge and spin polarization of SQ_i intermediates in the catalytic reactions at the Q_i site [163]. This polarization is imposed by the local electrostatic field induced by the specific distribution of residue charges within the Q-binding pocket. These are mainly His in the vicinity of the O4 atom and the Asp/Lys pair in the vicinity of the O1 atom.

This “charge polarization” mechanism is schematically presented in Fig. 35, right. The evolution of states A to G considers the direction of reduction of Q to QH_2. The reaction requires

initial entry of Q to the Q_i site (states A and B) and heme b_H in reduced state (state C). It starts when the O4 atom of the Q present at the site interacts with the protonated His. The electron is then transferred from this heme to Q resulting in the formation of the SQ_i anion (which is detected by EPR as SQ_{iF} when heme b_H is oxidized) (state D). The anionic SQ_i becomes more negative at the O4 atom than at the O1 atom, while the spin density is larger at the C1 side compared to the C4 side (Fig. 35, left). Such polarization and the resulting geometry favor a barrierless exchange of the proton originating from His between the His imidazole ring and the O4 atom of SQ_i. In this state, the SQ_i radical is stabilized, and equilibrates between the anionic and neutral forms. This equilibration also takes place after the reduction of heme b_H and is associated with the conversion of SQ_{iF} to SQ_{iS} (conversion of state E to F). This continues until the second electron reduces the neutral SQ_i to unstable QH^- (state F). When this equilibration takes place, the protonation of anionic SQ_i to the neutral form does not influence the spin density but causes an inversion of the direction of charge polarization: the C1 side becomes more negative than the C4 side. This increases the probability that the second proton will be transferred to the O1 atom. Consequently, the reduction of neutral SQ_i to QH^- is accompanied by the spontaneous transfer of a second proton from the Asp/Lys-path to the O1 atom, completing the reduction of Q to QH_2 followed by dissociation of the product (state G).

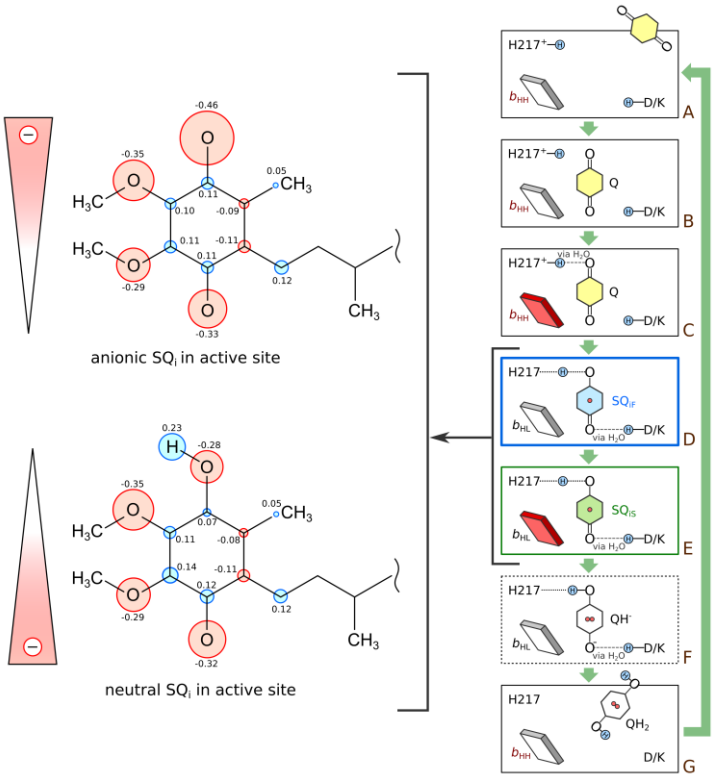

Figure.36. The charge polarization mechanisms of Q reduction at the Q_i site. Boxes on the right represent the reaction steps A to G (see text for details). SQ_i bound at the Q_i site (blue and green boxes refer to the Q_i site occupied by SQ_{iF} and SQ_{iS}, respectively) is stabilized by equilibration between neutral and anionic form of the radical (upper and lower scheme

in the left panel, respectively). Red and blue circles denote the negative and positive Mulliken charges, respectively. Radius of each circle is proportional to the charge of the respective atom (the values are shown as black numbers). Spikes on the left indicate the polarization of overall charge on the respective SQ form.[163]

The key feature of the proposed mechanism is an initial response of the radical anion to the local electrostatic field, as it triggers progression of the whole catalytic reaction. At the same time, polarized SQ_i exchanging a proton in the absence of barrier with His forms a stable intermediate which, during enzymatic turnover, safely "waits" for the second electron without the risk of generating other radicals (such as superoxide).

The charge polarization mechanism sheds new light on the protonation states of SQ_i described earlier by the pulse spin-echo-based EPR (ESEEM or HYSCORE) [647,648,683], which must have referred to just the SQ_{iS}, as the spin-lattice relaxation of SQ_{iF} is fast enough to lead to homogeneous line broadening that precludes the formation of a spin-echo signal. It was proposed that SQ_i (SQ_{iS} in view of the above assumption) is likely to be anionic [648,682] and ligated by a hydrogen bond from the imidazole-ring nitrogen of the His [647,648]. It was also suggested that the redox state of heme b_H might influence the protonation state of SQ_i and the His ligand, rendering SQ_i deprotonated at the time when heme is reduced [683]. This charge polarization mechanism implicates that SQ_i exists as neither an anion nor a neutral radical but should rather be treated as a resonant structure in which the proton undergoes exchange between His and SQ_i. If the frequency of this exchange is much higher than the hyperfine splitting of the radical spectrum caused by the interactions of the proton with unpaired electron spin, then EPR will be unable to detect the presence of protons due to large spectral diffusion effects.

The proposed catalytic role of charge and spin polarization of the SQ is likely to be relevant to other sites catalyzing the reduction/oxidation of Q/QH_2 via stable SQ intermediates. Such spin polarization has been noted before for the SQ bound at catalytic sites (including SQ_i [680], SQ_H of quinol bo_3 oxidase [688] and SQ_A of bacterial reaction center [689]), and could be associated with charge polarization induced by the electrostatic field provided by the catalytic site. Further support for this proposal comes from modeling of the effect of the electrostatic field on spin and charge polarization in diboryl monoradical anions [690].

8.5 Specific residues involved in PQ/PQH_2 binding to the Q_n site of Cytb_6f

Several attempts have been made in the past to study residues important for Q/QH_2 binding to the Q_n site of Cytb_6f via site directed mutagenesis approaches informed by previous results from work on the Cytbc_1 complex and by structural features of the Cytb_6f. They include residues bG37 and bF41, [691] because substitutions of the corresponding residues in *Rhodobacter*'s Cyt*b* (G48 and A52 respectively) led to impaired redox activity, loss of photosynthetic growth or failure to assemble a functional complex. The F41V mutant of *Chlamydomonas* displayed a 5-fold decrease in Q_n site activity and became sensitive to antimycin, an inhibitor of the Cytbc_1 Q_i site that is normally not effective against Cytb_6f. Conversely, the bF41G and bF44A mutants did not display any phenotype [692]. Substitutions of the Gly37 residue did not rescue phototrophic growth, suggesting that mutation of this residue is detrimental to photosynthesis. The same result was found in the case of a C35V mutant, which was unable to grow phototrophically because this substitution (affecting the residue that covalently bonds heme c_n to the Cytb_6) prevents the accumulation of the entire complex in thylakoids.[693]

Other mutants were generated affecting residues in the proximity of the heme: Leu36, Pro41 of SubIV. No clones were recovered after mutagenesis, indicating that these mutations were also detrimental for photosynthesis. On the other hand, a mutant was obtained after the P40T substitution. This mutant showed a significant slowing down of Cytb_6 reoxidation under single turnover flash illumination, consistent with impairment of interaction between the heme and its quinone substrate. The mutant also displayed a downshift of the c_n heme midpoint potential (from +100 mV to −200 mV at pH 7), but conserved WT Cytb_6f turnover rates under a continuous light regime. Based on the position of P40 in the Cytb_6f structure, it was proposed that this modified accessibility could originate from the ligation of the heme iron by the phenol(ate) side chain introduced by the mutation [430].

A similar approach has been used in cyanobacteria, where a mutant (R214H) was generated to substitute His for a conserved Arg in the Cytb_6 polypeptide of the cyanobacterium *Synechococcus* sp. SPCC 7002. At high light intensity, the R214H mutant grew ~2.5-fold more slowly than the WT, due to inhibition of the Cytb_6f complex turnover. Under single turnover flash illumination the R214H mutation partially blocked electron transfer to the Q_n site, mimicking the effect of the Q_n site inhibitor NQNO. Overall, these data define Pro 40 and Arg 214 as key residues for catalysis in the Q_n site of the Cytb_6f [694].

Other mutants were generated to modify the environment of the chlorophyll ring that is located close to the Q_n site [695]. Residues Val104, Gly136, Tyr124, and Arg125 did not dramatically affect electron transfer in the complex, but strongly affected state transitions (see section 10.3 below).

This indicates that besides catalysis, the reduction of the PQ at the stromal side Q_n site is also involved in sensing and signaling, two essential functions of the Cytb_6f (see sections 5.2 and 10.3) [696]

9 Inter-monomer electron transfer

Crystallographic structures of Cytbc_1 and Cytb_6f revealed a high degree of symmetry between monomers including structural arrangement of the redox active cofactors[20–22,48,173]. One of the most intriguing structural features of the dimer is the distance between hemes b_L/b_p of different monomers, which theoretically seems to be small enough to allow fast (i.e. ~μsec) electron transfer [56,195,697,698], in relation to catalytic rates [41,68,615,699]. For this reason, a discussion began about the possible implications of such an electronic connection between monomers for catalysis and opened the door to construction of models extensively utilizing the heme b_L-b_L bridge [86–88,125,329,700,701].

The fundamental question therefore arises as to whether electron transfer between the b_L/b_p hemes of the two monomers can be considered competitive to the intra-monomer path: from heme b_L/b_p, through heme b_H/b_n to the Q_i/Q_n site. Alternatively, is this simply a redundancy of the possible electron transfer paths that may be important only under specific and rare conditions[206,571,615].

The order of the rates for inter-monomer electron transfer can be approximated on the grounds of electron transfer theory [702] and the phenomenological approximation of the Moser-Dutton ruler [56,195,697,698]:

$$log(k_{ET}) = 13 - (1.2 - 0.8\rho)(R - 3.6) - 3.1\frac{(\Delta G+\lambda)^2}{\lambda},$$

where: ρ – is packing density (0 for vacuum, 1 – fully packed matrix), ΔG – Gibbs energy associated with electron transfer from donor to acceptor (in the case of electron transfer from heme b_L to b_L this is 0) and λ – reorganization energy, R – distance between donor and acceptor (between b_L heme-rings)

Using average values for electron transfer within a protein matrix – ρ and λ in the above equation can be simplified to account only for R [697]:

$$log(k_{ET}) = 12.8 - 0.6R$$

As distances between heme rings are ~13.2 – 15.2 Å, a crude estimation of the rates gives k_{ET} ~ 5×10^3 – 8×10^4 s^{-1}. A typical steady-state turnover rate obtained for Cytbc_1 or Cytb_6f does not exceed

10^3 s^{-1} [569,649] meaning that electron transfer between hemes b_L/b_p should not limit the catalytic turnover rate.

The experimental verification of whether intermonomer electron transfer is indeed as fast as theory predicts, required measuring the electron transfer rate between b_L/b_p hemes in the dimer, which in the native protein is generally difficult considering the structural symmetry of the complex, and the fact that electron transfer between the monomers leads to spectroscopically indistinguishable states. In fact, this has long been out of reach for direct experimental testing, due to the lack of a genetic tool to inactivate individual components of the dimer in an asymmetric manner. This is related to the fact that, in native systems, the genes coding for the subunits do not differentiate between monomers, thus any mutation is obligatorily introduced to both parts of the homodimer.

New strategies described in 2010 aimed at overcome these limitations.[47,329,703–707] In these studies two distinct genetic approaches were used: a fusion duplicating gene or a co-expression of two variants of the gene. Both targeted the Cyt*b* subunit of bacterial Cytbc_1.

The first approach was based on extending the native gene encoding Cyt*b* with a short linker followed by a second copy of the same gene [47,705–707]. As a result, each half of the fusion protein replaced one Cyt*b* subunit of the dimer, providing a template for construction of derivatives in which the two halves could be mutated independently. Using such a template, different mutations inactivating key steps of electron transfer were introduced in various combinations to eliminate selected paths and to force electron transfer through other available paths within the dimer (see all forms in Fig. 37). This was used to test all possible electron transfer routes for electrons from the Q_o to Q_i site.[47,707]

Because for a given combination of mutations, only one version of the complex with the fused Cyt*b* is expressed in the cells, it was possible to monitor the kinetics of light-induced electron transfer in the native membranes. Analysis of the cross-inactivated complex (a variant $_W$B-B^N in Fig. 37), for which electrons derived from the O_o site must have crossed the dimer to reach the Q_i site, revealed that electron transfer between hemes b_L occurs on a millisecond time scale, as theory had predicted. In addition, it was established that the complex remains enzymatically active even if the equivalent of only one monomer ($_W^N$B-B), or the equivalent of one monomer with a part of other monomer ($_W$B-B, ^{N}B-B) are available. This revealed that any path connecting either or both Q_o sites with either or both Q_i sites is competent in supporting enzymatic turnover at high rates [47,704,705]. Based on these findings it was proposed that cofactor chains in the native dimer assemble into an H-shaped electron

transfer system (two upper, two lower branches and a bridge) connecting the two Q_o sites with the two Q_i sites.

Interestingly, deactivation of only one branch (forms $_{W}$B-B, ^{N}B-B) or both branches of the same monomer ($_{W}^{N}$B-B) decreases V_{max} of the enzyme by approximately 50% when compared to the fusion protein without any disabling mutation (B-B) [569]. This suggests that the two monomers in the dimer contribute equally and independently of each other, thus any allosteric effect [19,87,88,708], if it exists, does not govern the catalytic turnover rate. Forcing electron transfer through the b_L heme "bridge" decreases V_{max} to ~70 s^{-1}, which is about 25 – 40% of the average activity obtained for $_{W}$B-B, $_{W}^{N}$B-B and ^{N}B-B forms, but is still enough to support multiple turnovers at high rates.

When using a fusion gene composed of two copies of the same gene, careful procedures must be employed in order to maintain high expression of the fusion protein during cell growth and prevent gene recombination.[706] Without rigorous growth and harvesting protocols there is a risk of losing the fusion or asymmetry of the mutations, which is especially critical if one wishes to test Cytbc_1-related support of photosynthetic growth of bacterial cells. Indeed, just such recombination was observed, but incorrectly interpreted by Hong et al. [709]

To overcome these limitations and gain the possibility to test functionality of the asymmetrically mutated complexes *in vivo*, the original system was modified by constructing a hybrid fusion system, in which the fusion protein was expressed from a gene linking two different genes encoding Cyt*b* from closely related bacteria *Rhodobacter sphaeroides* and *capsulatus* [704,705]. Careful analysis of photosynthetic competence of the various complexes containing asymmetrically mutated hybrid fusion proteins (analogous to the ones described above) demonstrated that in agreement with kinetic results, the cross-inactivated form relying exclusively on inter-monomer electron transfer is fully functional *in vivo*, as is the form with just one branch inactivated.

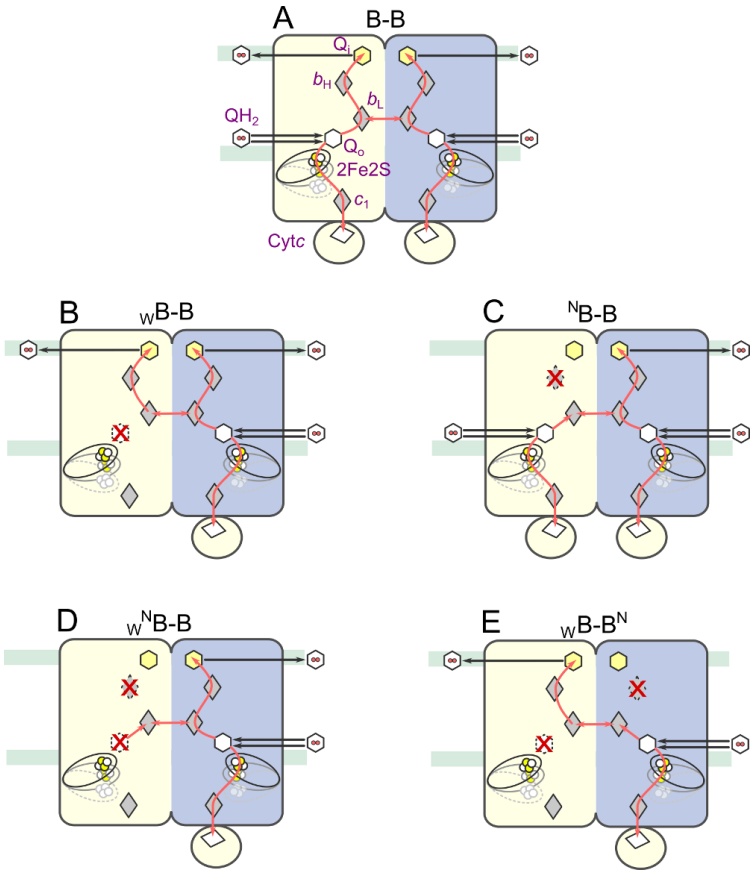

Figure 37. Schematic representation of various forms of Cyt*bc*$_1$-like complexes containing Cyt*b* fusion protein used to test possible combinations of electron transfer paths. A) Native-like system with all four branches active (B-B). B-E) Asymmetric forms containing one or more mutations inactivating either the Q_o site (Cyt*b*:^{Rh}G158W; designated as $_W$B) or heme b_H (Cyt*b*:^{Rh}H212N; designated as B^N): $_W$B-B – lower branch inactivated, ^{N}B-B – one upper branch inactivated; $_W^N$B-B – upper and lower branch on the same side inactivated; $_W$B-B^N – cross-inactivated enzyme.

A second approach for obtaining asymmetrically mutated variants of Cyt*bc*$_1$ was based on co-expression of two plasmids, each carrying one copy of the gene encoding for Cyt*b* with a sequence coding for a different tag attached (His-tag, Flag-tag or Strep-tag) [329,710,711]. The different mutations inactivating either the Q_o or the Q_i sites were placed on different plasmids and the two-step affinity chromatography was used to isolate the cross-inactivated form from the symmetric variants resulting from random assembly of the complexes in the cells [703,710]. These studies also demonstrated that inter-monomer electron transfer through b_L hemes occurs in milliseconds, thus in a catalytically-relevant timescale. In addition, some of the kinetic transients were interpreted as resulting from electron equilibration between the two Q_i sites and the four hemes *b* in the dimer [703]. The same type of equilibration (see Fig. 35) was considered as rationale for the existence of fast-relaxing semiquinone

(SQ_{iF}) in native Cytbc_1 exposed to conditions favoring one electron reduction of heme b_H by QH_2 bound at the Q_i site (described in section 8.3) [151].

Although the existence of inter-monomer transfer has been confirmed by several studies, its possible physiological meaning and role in the catalysis remain unclear.[13,699] Electron transfer between the b_L hemes could be just a simple coincidence of the conserved structure of the homodimer and as such does not play an important catalytic role, as all structural elements needed to perform catalytic cycle are present in each of the monomers[23,206,709].

On the other hand, it has been hypothesized that inter-monomer electron transfer to support efficient catalysis may offer some advantage for bioenergetic processes, in particular when unfavorable redox conditions and/or potential danger of superoxide generation exist. As pointed out by Sarewicz et al.[13,699] mitochondria usually posses several copies of genes coding for Cyt*b* and the appearance of a mutation in one or more genes is expected to lead to expression of a fraction of the dimers having damage in only one part of the monomer (and thus possibly having a "dead end" for electrons). If this monomer was isolated functionally from undamaged monomer, it would inevitably catalyze only energy-wasting short-circuits or free-radical generating reactions. However, if the damaged monomer is linked functionally with an undamaged one, the existence of the heme b_L-b_L bridge can provide an efficient way to remove electrons from the low-potential chain in the damaged monomer (Fig. 38). With such a mechanism, the amount of ROS generated during the QH_2 oxidation will be significantly lowered enabling electron flow through respiratory or photosynthetic chains.

Also, as shown by Pintscher et al.[151] electron exchange between monomers may increase the rate of SQ^-_i reduction to QH_2 by providing electron paths for dismutation of SQ^- from two Q_i sites of a dimer., which can be of advantage under shortage of QH_2.

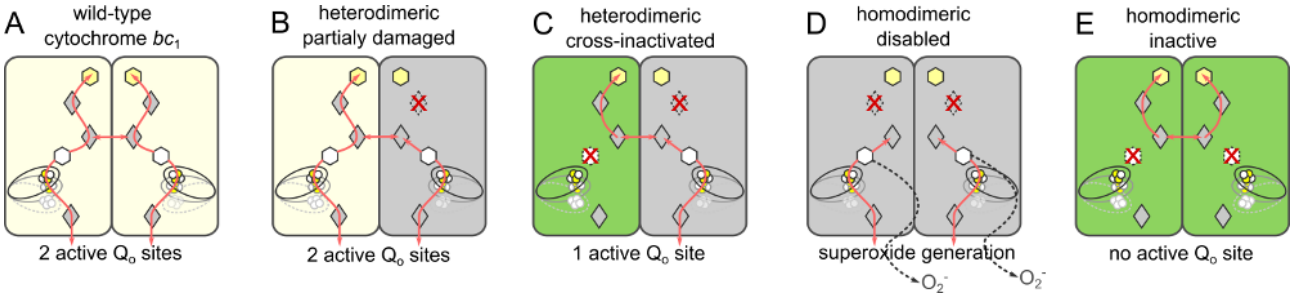

Figure 38. Putative advantage of dimers with possible ET through the hemes b_L. A) Homodimeric Cytbc_1 operates normally using two active monomers. B) A heterodimer in which one monomer has disabled heme b_H and or Q_i site (gray) is still still functional and able to oxidize QH_2 at two Q_o sites. C) A heterodimer containing two different mutations in each monomer, one with disabled Q_o site (green) and second with heme b_H or Q_i site, still catalyze QH_2 oxidation. D) and E) Homodimers containing mutations are inactive and/or contribute to elevated superoxide generation. Considering a sum of monomers from B to E, occurrence of intermonomer electron transfer gives: 3 active monomers, 3 inactive monomers

and 2 monomers generating O_2^-. If this electron transfer did not exist we would have 1 active monomer Q_o sites, 3 inactive monomers and 4 monomers generating O_2^-.

There are several models presenting more or less elaborate mechanisms of inter-monomer allosteric communication in which the role of heme b_L-b_L electron transfer is crucial for catalysis. Most of these were inferred from indirect kinetic measurements and/or effects of substoichiometric additions of inhibitors. The results of such experiments leave space open for discussion and future experimental exploration. While the existence and potential significance of allosteric effects have never been ruled out, the experiments that exploit the family of fusion proteins suggest the simplest mechanism, in which electrons travel ”blindly” using any available path through the H-shaped electron transfer system to complete redox reactions without generation of radicals.

10 Higher level of organization and regulation (supercomplexes, state transition, kinase activation)

10.1 A role for cytochrome *b*$_6$*f* in the regulation of linear *vs* cyclic electron flow?

Alternative to linear electron transfer (LET), which requires in series PSII and PSI activity, is the cyclic pathway (CET), which involves electron flow via PSI and the P700 reaction center complex via the plastoquinone pool through Cyt*b*$_6$*f* complex. It thus produces ATP without generating reducing power, and it is considered as a central element to readjust the ATP/NADPH balance for proper CO_2 assimilation in plants and green algae [230]. Actors involved in CET and CET regulation have been recapitulated in recent reviews [374,712–715]. Nonetheless, several aspects of this process remain enigmatic. While most of the CET electron carriers (the plastoquinone pool, Cyt*b*$_6$*f*, plastocyanin, PSI and ferredoxin and possibly NADPH) are shared with the LET pathway, electron transfer from Fd/NADPH to the quinone pool on the stromal side of the thylakoids may require an additional, CET specific, activity. This activity would be either by the NAD(P)H dehydrogenase (NDH) complex similar (but not identical) to Complex I of the mitochondrial respiratory chain [713,716], or the FQR (ferredoxin quinone reductase) complex. FQR would correspond either to a PGRL1 and PGR5 complex [199] or to the Cyt*b*$_6$*f* itself either Cyt*b*$_6$*f* complex interacting with Fd, most likely *via* FNR (as discussed paragraph **Erreur ! Source du renvoi introuvable.**) and/or possibly PGRL1 and PGR5, although as considered above involvement of the latter components is supported only by very qualitative electron transfer data and stoichiometries are small.

Mutants lacking the NDH complex lack a clear growth phenotype under a variety of environmental conditions[716,717], suggesting that the NDH activity, per se, is not essential for CET, since CET is an essential process for plant growth[235]. On the other hand, a mutant with enhanced CET activity, isolated in *Arabidopsis*, displays higher levels of the NDH complex[379]. Moreover, *Arabidopsis* photosynthetic embryos, which have a larger CET activity than mature leaves, also display an enhanced NDH activity[718]. While the FQR activity was initially identified with the Cytb_6f [719], this function has later been associated with a complex containing the PGR5, PGRL1 proteins[199], i.e. previously identified as CET actors[713]. Similarly to the NDH, mutants lacking the PGR5:PGRL1 complex show WT like CET rates in *Arabidopsis* [386] and *Chlamydomonas* [387], again pointing to a non-essential role of this complex in CET.

Overall, these results can be interpreted assuming that both the NDH and FQR pathways contribute to CET, each activity being compensated by the other when genetically disrupted. Consistent with this conclusion, previous genetic studies have highlighted that severe growth phenotype in *Arabidopsis* can only be observed upon concomitant disruption of the NDH and PGR5:PGRL1 complexes[720].

What is role for the Cytb_6f (if any) in a context where the role of the NDH and PGRL1:PGR5 pathways in CET is still controversial? Interactions of the Cytb_6f with PSI and/or FNR have been proposed as a mean to trigger CET [721,722]. This notion has received experimental support by the finding by Cramer and co-workers that Cytb_6f co-purified with FNR in plants [180]. However, recent ITC experiments show that there is no significant interaction between FNR and Cytb_6f. Moreover, interactions between subunit of PSI, Cytb_6, FNR and PGR5 were reported in a yeast two-hybrid assay using *Arabidopsis* genes[236]. In the green alga *Chlamydomonas reinhardtii*, Minagawa and colleagues[197] were able to isolate a PSI:Cytb_6f, which they considered as a specific component of CET. The existence/function of this complex is still debated. If real, why would a supercomplex be needed for CET? As mentioned above, most electron carriers are shared between the CET and LET pathways. Therefore, CET, which is a 'circular' process continually recycling electrons around PSI, would be easily overcompeted by LET every time that a cyclic electron is shunted towards the stromal sinks by LET. Two alternative models have been proposed to explain how LET does not overcompete CET [426,723,724].

The first one considers that CET and LET are, to some extent, segregated ('segregated CET'). It is well-known that the photosynthetic complexes are unevenly distributed in the thylakoids: PSII is mainly concentrated in the appressed grana, PSI is mainly found in the non appressed membranes (stroma lamellae, grana margins), while the Cytb_6f is roughly homogeneously distributed [725]. Moreover, the diffusion of PQ/PQH_2 in the thylakoid membrane is highly restricted, probably due to

the very high protein concentrations that characterize this membrane [272,726]. The 'segregated CET' model assumes that because the physical distance between the different domains is rather large and the PQ diffusion in the thylakoids is restricted, two electron carrier pools would exist with different functions. Photosynthetic complexes present in the grana and grana margins (PSII, Cytb_6f and PSI) would be involved in LET, while those in the stroma lamellae (Cytb_6f and PSI) would be the CET ones. Consistent with this hypothesis, recent affinity-mapping AFM studies has revealed nanodomains of co-localised PSII and Cytb_6f complexes [727]. The domains (previously hypothesized by Lavergne and Joliot [272]) would provide a structural rationale for the segregation of LET and CET and its regulation. Small changes in the distance between adjacent membranes in stacked grana regions might control the access of Cytb_6f to the grana because of steric hindrance [5]. Because the width of the stromal gap is variable and light regulated, this model predicts that changes in the lateral distribution of the Cytb_6f should affect CET and LET by modulating the amount of this complex present in the CET and LET compartments. Obviously, the presence of a supercomplex is an extreme case of the 'segregated CET' hypothesis, the CET domain becoming the PSI:Cytb_6f supercomplex itself.

Alternative to the 'segregated CET' model, a 'dynamic' hypothesis to explain CET cyclic flow has been proposed [410,426,723,728]. According to this model, CET and LET would not be segregated but actually directly compete for electrons. Under most physiological conditions, this competition would favour LET, because of electron leak toward stromal sinks. However, under particular conditions (high light, CO_2 limitation, low oxygen in microalgae) CET would become more efficient because the LET efficiency would be reduced by limitation at the PSI acceptor side. Competition would occur either at the PSI acceptor side (via competition for Fd, likely via the FNR- Cytb_6f complex [723] or at the level of the PQ(H_2) pool [374]. The model proposed by these authors is particularly interesting from a Cytb_6f perspective, as it postulates that a function interaction between the two Cytb_6f monomers at the PQ-reducing site would allow a 'direct' electron flow from the stromal to the luminal PQ, in a confined environment not in contact with the photoactive PQ(H_2) pool in the thylakoids, similar to the semiquinone version of the Q cycle proposed earlier [729]. This hypothesis is therefore somehow in between the 'segregated CET' and the redox competition hypotheses previously described.

10.2 The "elusive" Cytb_6f-PSI CET supercomplex.

As discussed above, the presence of a PSI- Cytb_6f complexes represent the most extreme case of the 'segregated CET' hypothesis. In the green alga *Chlamydomonas reinhardtii*, where CET can be a prominent process [728,730,731] Iwai and colleagues used a sucrose density gradient to isolate a supercomplex composed of the PSI-LHCI supercomplex with LHCIIs, Cytb_6f, FNR, and PGRL1 in

a fraction heavier than that of the single complexes (PSI-LHCI, Cytb_6f) alone. Its formation is enhanced by reducing conditions, which increases CET activity in this alga [221,732]. Spectroscopic analyses [732] indicate that PSI and Cytb_6f are able to exchange electrons within the supercomplex, PSI being able to reduce Cytb_6 in the presence of Fd and NADPH and to oxidise Cyt$f$ in the presence of plastocyanin [197]. Based on these results, the authors conclude that the PSI- Cytb_6f supercomplex corresponds to the CET supercomplex, the existence of which had been anticipated by theoretical predictions [733] and functional studies (e.g. Joliot and Joliot [734]).

Supercomplex formation in *Chlamydomonas reinhardtii* requires not only reducing conditions (anaerobiosis) but also Ca^{2+} signaling in *Chlamydomonas reinhardtii* [197,735]. Regulation by anaerobiosis would be mediated by a protein, Anaerobic Response 1 (ANR1). ANR1, as well as the plastid localized Ca^{2+} sensor (CAS) are found in the PSI- Cytb_6f supercomplex, together with PGRL1 [735]. The Cytb_6f associated subunit PETO co-fractionates with other thylakoid proteins involved in CET (ANR1, PGRL1, FNR). The absence of PETO impairs the formation of the supercomplex in anaerobic conditions.

Since its discovery and biochemical characterization, the existence/function of the *Chlamydomonas* CET supercomplex has been debated. The biochemical significance of the green band of high molecular weight in sucrose density gradient that was used to purify this complex has been recently questioned, because various PSI complexes can migrate in these sucrose density regions [376]. On the other hand, single-particle analysis of the PSI- Cytb_6f complex from *Chlamydomonas* [736] has provided a structural support for the existence of a true supercomplexes in this alga.

Until recently, no such supercomplex was found in plants [426], and it was argued that no such supercomplex is required for CET to occur in plants [410,714]. However, the isolation a PSI-Cytb_6f supercomplex has been reported starting from stroma lamellae of *Arabidopsis* [737]. However, even in this case the significance of this complex has been questioned [374], because in this preparation Cytb_6f complex bound to PSI was not only in its active (dimeric) conformation but also in the inactive (monomeric) one.

At variance with the respiratory chain, where several supercomplexes between different component of the electron flow chain have been characterized, no other photosynthetic supercomplex has been reported so far, besides the PSI-NDH supercomplex that was characterized in *Arabidopsis* [738]. Formation of the PSI-NDH supercomplex requires the presence of specific forms of the PSI Light Harvesting Complex (LHCI, [739]).

10.3 Role of cytochrome b_6f in state transitions

In oxygenic photosynthesis, the two photosystems have distinct pigment containing antenna complexes, and consequently different spectral absorption features. PSI has an enriched light absorption capacity in the far-red region, while PSII has a slightly higher absorption capacity in the spectral regions where chlorophyll *b* absorbs. Under natural light conditions, where both the quality and quantity fluctuate with time [740] light absorption by these two complexes may be unbalanced, with negative consequences on the quantum yield of photosynthesis, which requires a commensurate light utilization by PSI and PSII for optimum photosynthetic yield.

In plants and green algae, balanced light utilization is achieved via a regulatory mechanism called state transitions, which actively adjusts the absorption capacity of PSI and PSII, in response to chromatic changes in the light. Discovered by Murata and Sugahara (1969) and Bonaventura and Myers (1969) [741,742] state transitions rely on a redox triggered phosphorylation of the PSII antenna complexes (LHCII), which dissociates from PSII binding to PSI under conditions where absorption of the former is enhanced (e.g. when the light available for photosynthesis enhances light absorption by chlorophyll *b*). This state is called state 2. Conversely, over-excitation of PSI (e.g. by far red light) leads to the detachment of LHCII form PSI, and its re-association to PSII, leading to state 1, [230].

Pharmacological and genetic experiments have pinpointed the PSII electron acceptors (the plastoquinone, PQ) pool as the sensor triggering LHCII phosphorylation [743]. This occurs via the activation of a specific kinase [35], mediated by the Cytb_6f. The plastoquinone can act as the redox sensor because it is functionally 'located' between PSII and PSI. Thus, this redox active molecule 'senses' the relative imbalance in the light harvesting capacity of the two photosystems, becoming reduced when the PSII activity overcomes that of PSI, and oxidised when PSI is prevailing. The kinase responsible for LHCII phosphorylation has been first identified in *Chlamydomonas*, STT7 [744] and later in *Arabidopsis*, STN7 [745]. It is as a ser/thr kinase located in the thylakoids. A phosphatase (TAP38/PPH1) has also been found, which dephosphorylates LHCII [746,747] during the state 2 to state 1 transition.

Several pieces of evidence suggest that the PQ(H_2) pool activates the Stt7/STN7 kinase via Cytb_6f. Wollman and Lemaire [748] used *Chamydomonas* lines with mutations in the photosynthetic apparatus to demonstrate that state transitions were missing in mutants lacking the Cytb_6f. Later, independent spectroscopic [749] and genetic evidenced [576] suggested that the Cytb_6f mediates kinase activation upon PQH_2 binding to its lumenal binding pocket, via a still largely unknown mechanism.

Several models have been proposed so far to account for the Cytb_6f mediated activation of the sTT7/STN7 kinase [724,750–753]. They are summarized in a multistep model proposed in Fig. 39. There, PQH_2 binding to the cytochrome lumenal pocket would induce conformational changes (via

movements of the ISP-HD) making the Cytb_6f-*k*inase interaction possible. Formation of a Cytb_6f-kinase complex would activate this protein leading to the phosphorylation of the Cytb_6f-associated subunit PetO [743,754,755]. This step would precede LHCII phosphorylaytion, implying the existence of an additional step, where the active kinase would be released from Cytb_6f to interact with the PSII antenna. The existence of two separate steps for Cytb_6f and LHCII phosphorylation is suggested by the finding that PQ analogue stigmatellin, which blocks Cytb_6f activity likely by interfering with the movement of the ISP-HD [61,554,755] prevents LHCII phosphorylation but not the phosphorylation of PetO.

This model also accounts for additional information concerning the induction of state transitions. The first one is how the signal generated by PQH_2 binding in the lumenal part of the complex is transduced to the stromal site where the catalytic domain of STT7/STN7 is located. Several hypotheses have been conceived to address this point: Vener and colleagues [749] proposed that the putative transmembrane helix of the kinase could directly sense PQH_2 binding to the luminal site, leading to kinase activation. Consistent with this possibility, Shapiguzov and colleagues found that the N terminus moiety of the kinase (which is supposed to be on the lumenal side) interacts with the transmembrane part of the ISP, based on yeast two hybrid [751]. Alternatively, a chlorophyll-based hypothesis has been proposed by Zito and colleagues. These authors analyzed of a Cytb_6f mutant of *Chlamydomonas*, in which the small subunit PetL was fused to subunit IV to "transform" the Cytb_6f, which contains seven helices in its core complex subunits (Cytb_6- and sub IV), into a Cytbc_1-type of complex (which contains eight helices in its unique core complex subunit, Cyt*b*). They found that while this mutation was not affecting electron flow, it was able to completely abolish state transitions [756]. They conclude therefore that the mutation was sterically hindering kinase docking to Cytb_6f, i.e. that the kinase docking site was located in the proximity of the C terminus of subunit IV (where the subunit PetL was fused in the mutant). There, the tetrapyrrole ring of Cytb_6f bound chlorophyll is exposed to the lipid solvent. Conversely, the PQ phytol chain goes deeply into the complex structure ending up in the lumenal pocket (in *Chlamydomonas* [41]) or in proximity of the F helix, which sandwiches the chlorophyll ring in the cyanobacterium *Mastigocladus laminosus* [42]. There, it could sense PQH_2 binding to its luminal site via a conformational change [753] and transduce the signal via its chlorophyll ring. The possible involvement of the chlorophyll ring in kinase activation was later supported by the finding that mutants affecting the environment of the chlorophyll ring in the complex were altering the kinetics of state transitions in *Chlamydomonas* [695]. Hasan and colleagues further developed this concept, proposing that specific lipids located on the surface of Cytb_6f close to the chlorophyll could provide an adaptable surface for interaction with Stt7/STN7 [174]. More recently, this hypothesis has been refined by pinpointing several residues in the stromal loop linking helices F and

G of Cytb_6f subunit IV (where the chlorophyll ring is exposed) that are crucial for state transitions. This has led to the idea of an interaction between Cytb_6f and the Stt7 kinase mediated by the stromal side of the complex above the chlorophyll ring [696].

The second information concerns inhibition of state transitions in high-light treated *Chlamydomonas* cells [757] and plants [758,759]. It was proposed that this inhibition would stem from redox control by reduced stromal thioredoxins targeting a disulfide bond in the kinase [758]. Analysis of the Stt7/STN7 protein sequences revealed indeed the presence of two conserved Cys residues close to the N-terminal end of this kinase, which are highly conserved and essential for kinase activity [274,744]. However, mutagenesis of the Cys pair of the Stt7/STN7 kinase showed no change in the redox state of these Cys during state transitions and high-light treatment. Based on these results, a different role for Cys in kinase activation by the Cytb_6f was proposed [751] in which these residues would allow the formation of a dimer between two kinases bound to each monomer of the Cytb_6f dimer via formation of intermolecular disulfide bridges. Consistent with this idea, while no STN7 dimer was detectable *in vivo*, it could be clearly detected in the *Arabidopsis* STN7-Cys mutants in which C1 or C2 was stabilized [760]. Such dimer would be rather unstable and revert rapidly to an intramolecular disulfide bridge in each monomer when the luminal site is empty, explaining why the kinase rapidly inactivates upon oxidation of the PQ(H_2) pool.

The molecular description of the Stt7 kinase[753] and its interaction with Cytb_6f are unknown or unclear. The Stt7 kinase has been cloned, expressed, and purified in a heterologous host. The kinase is active *in vitro* in the presence of reductant and has been purified as a tetramer, determined by analytical ultracentrifugation, electron microscopy, and electrospray ionization mass spectrometry, with a molecular weight of 332 kDa, consisting of an 83.41-kDa monomer. Far-UV circular dichroism spectra have shown Stt7 to be mostly α-helical and document a physical interaction with Cytb_6f through increased thermal stability of Stt7 secondary structure. The activity of wild-type Stt7 and its Cys-Ser mutant at positions 68 and 73 in the presence of a reductant suggest that the enzyme does not require a disulfide bridge for its activity as suggested elsewhere. Kinase activation *in vivo* could result from direct interaction between Stt7 and Cytb_6f or long-range reduction of Stt7 by superoxide, known to be generated in Cytb_6f by quinol oxidation. Although kinase activation on the *n* side of the thylakoid membrane requires a transmembrane configuration of the kinase (Fig. 39), the only hydrophobic domain of the kinase, near the N-terminus, contains 3-4 prolines. There is no known precedent for such a transmembrane domain.

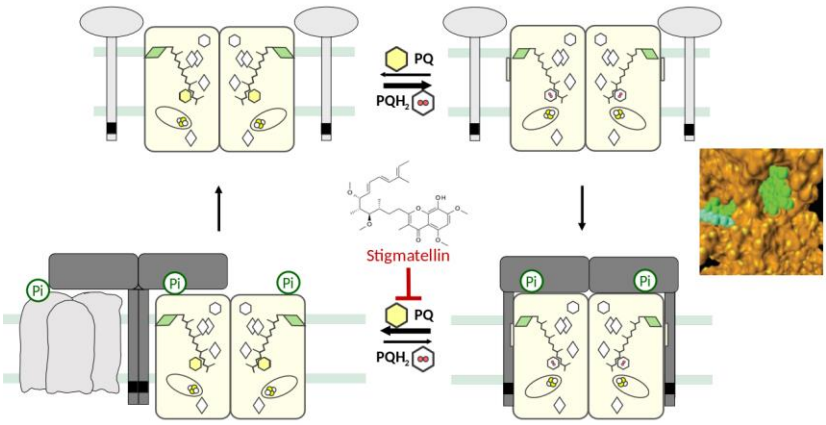

Figure 39. Multistep model for the activation of the state transitions kinase by Cytb_6f in photosynthetic eukaryotes. The model assumes that PQH_2 (red) interaction with the Q_n/Q_p site leads to conformational changes within the complex, likely mediated by the movement of the ISP-HD [554] (yellow). These changes would to promote the association between the cytochrome and the kinase responsible for state transitions (Stt7 in algae, STN7 in plants). Cytb_6f-kinase interaction would be mediated by residues surrounding the chlorophyll ring, as indicated by mutagenesis studies [756]. Upon binding, the kinase would become active and phosphorylate the Cytb_6f-associated subunit PetO. The active kinase would then be released from the cytochrome complex, in a step possibly involving PQH_2 oxidation, PQ release from the Q_n site and conformational changes of the ISP, as suggested by the inhibitory effect of the PQ analogue stigmatellin on this step [755]. The active kinase would be in a dimeric state, thanks to the interaction between conserved cysteines present on every monomer (black squares) [751]. It would interact with LHCII promoting its phosphorylation, and migration from PSII to PSI. Alternatively, a ternary binding complex might be formed between LHCII, Cytb_6f and the kinase. Finally, monomerization of the kinase would inactivate it, closing the activation cycle. See also Singh et al. [753], for a further discussion.

11 Comments on the nomenclature used for Cytbc_1 and Cytb_6f

In the literature there are number of differences in naming of similar structural and/or functional elements of Cytbc_1 and Cytb_6f. This section contains short comments on nomenclature to clarify the potentially confusing terms and, when needed, explains how they are used in this review.

Complexes: The term „Cyt-*bc*" refers to both Cytbc_1 and Cytb_6f as enzymes belonging to one group traditionally named cytochromes *bc*. This is how it is used in the review. Based on phylogenic analysis, it has been proposed to rename this group as "Rieske/*b* complexes", as it would better reflect the key and evolutionary unchanged subunits.[761] However this name, in spite of being scientifically justified, did not gain popularity in the literature.

In mitochondrial electron transport chain, Cytbc_1 is also named „mitochondrial complex III" or in short "complex III".

Quinone binding catalytic sites: The quinol oxidation site is named the "Q_o site" (in the case of Cytbc_1, in particular bacterial Cytbc_1) or "Q_p site" (in the case of Cytb_6f and sometimes eukariotic Cytbc_1/complex III). The same rule applies for the quinone reduction site which is named either the "Q_i site" (Cytbc_1) or the "Q_n site" (Cytb_6f and Cytbc_1/complex III). The subscripts "$_o$" and "$_i$" were originally used by Mitchell to indicate "out" and "in", respectively, as the direction of proton transfers catalyzed by the respective sites. The subscripts "$_p$" and "$_n$" refer to "positive" and "negative" side of the membrane. In brief : $Q_o = Q_p$ while $Q_i = Q_n$.

In this review we use "Q_o/Q_p "and "Q_i/Q_n" when referring to the sites in both Cytbc_1 and Cytb_6f ; "Q_o" and "Q_i" - when referring specifically to Cytbc_1; "Q_p" and "Q_n"– when referring specifically to Cytb_6f

Cofactor chains: In Cytbc_1 the "high-potential chain" is alternatively named the "c-chain" and the "low-potential chain" is the "b-chain".

Protein subunits: In Cytb_6f, the assembly of two subunits: Cytb_6 and Subunit IV corresponds to one larger subunit – Cyt$b$ of Cytbc_1.

Cofactors: The b hemes in Cytbc_1 and Cytb_6f are often named differently. Hemes b in Cytbc_1 are usually named b_H and b_L (to denote higher and lower E_m of the heme, respectively). Their counterparts in Cytb_6f are named b_n and b_p (to denote proximity of the heme to negative and positive side of the membrane, respectively). In brief: $b_H = b_n$ while $b_L = b_p$.

In this review we use heme b_H/b_n and b_L/b_p when referring to hemes in Cytbc_1 and Cytb_6f. Hemes b_H and b_L are used when referring specifically to hemes of Cytbc_1. Hemes b_n and b_p are used when referring specifically to hemes of Cytb_6f.

The atypical c-type heme present in Cytb_6f is designated using different symbols such as c_n and c_i and also c_x. All these symbols describe the same heme.

Other: When describing the motion of ISP-HD, the "Q_o-position" or "b-position" of ISP-HD refers to the same position of ISP-HD (when it is bound at the Q_o site/cytochrome b or the Q_p site/cytochrome b_6).

12 References

(1) Berry, E. A.; Guergova-Kuras, M.; Huang, L.; Crofts, A. R. Structure and Function of Cytochrome Bc Complexes. *Annu. Rev. Biochem.* **2000**, *69*, 1005–1075.

(2) Crofts, A. R. The Cytochrome Bc_1 Complex: Function in the Context of Structure. *Annu. Rev. Physiol.* **2004**, *66*, 689–733.

(3) Borek, A.; Ekiert, R.; Osyczka, A. Advances in Understanding Mechanism and Physiology of Cytochromes *Bc*. In *Mechanisms of primary energy transduction in biology*; Wikström, M., Ed.; Royal Society of Chemistry: London, **2018**; pp 192–214.

(4) Cramer, W. A. Structure–Function of the Cytochrome b_6f Lipoprotein Complex: A Scientific Odyssey and Personal Perspective. *Photosynth. Res.* **2019**, *139*, 53–65.

(5) Kirchhoff, H.; Li, M.; Puthiyaveetil, S. Sublocalization of Cytochrome b_6f Complexes in Photosynthetic Membranes. *Trends Plant Sci.* **2017**, *22*, 574–582.

(6) Schöttler, M. A.; Tóth, S. Z.; Boulouis, A.; Kahlau, S. Photosynthetic Complex Stoichiometry Dynamics in Higher Plants: Biogenesis, Function, and Turnover of ATP Synthase and the Cytochrome B6f Complex. *J. Exp. Bot.* **2015**, *66*, 2373–2400.

(7) Tikhonov, A. N. The Cytochrome B6f Complex at the Crossroad of Photosynthetic Electron Transport Pathways. *Plant Physiol. Biochem.* **2014**, *81*, 163–183.

(8) Tikkanen, M.; Grieco, M.; Nurmi, M.; Rantala, M.; Suorsa, M.; Aro, E. M. Regulation of the Photosynthetic Apparatus under Fluctuating Growth Light. *Philos. Trans. R. Soc. B Biol. Sci.* **2012**, *367*, 3486–3493.

(9) Cruz-Gallardo, I.; Díaz-Moreno, I.; Díaz-Quintana, A.; De La Rosa, M. A. The Cytochrome F-Plastocyanin Complex as a Model to Study Transient Interactions between Redox Proteins. *FEBS Lett.* **2012**, *586*, 646–652.

(10) Nelson, N. Photosystems and Global Effects of Oxygenic Photosynthesis. *Biochim. Biophys. Acta - Bioenerg.* **2011**, *1807*, 856–863.

(11) Nowaczyk, M. M.; Sander, J.; Grasse, N.; Cormann, K. U.; Rexroth, D.; Bernát, G.; Rögner, M. Dynamics of the Cyanobacterial Photosynthetic Network: Communication and Modification of Membrane Protein Complexes. *Eur. J. Cell Biol.* **2010**, *89*, 974–982.

(12) Trebst, A. Inhibitors in the Functional Dissection of the Photosynthetic Electron Transport System. *Photosynth. Res.* **2007**, *92*, 217–224.

(13) Sarewicz, M.; Osyczka, A. Electronic Connection between the Quinone and Cytochrome c Redox Pools and Its Role in Regulation of Mitochondrial Electron Transport and Redox Signaling. *Physiol. Rev.* **2015**, *95*, 219–243.

(14) Allen, J. F. Cytochrome B6f: Structure for Signalling and Vectorial Metabolism. *Trends Plant Sci.* **2004**, *9*, 130–137.

(15) Choquet, Y.; Wostrikoff, K.; Girard-Bascou, J.; Wollman, F.-A. Assembly-Controlled Regulation of Chloroplast Gene Translation. *Biochem. Soc. Trans.* **2001**, *29*, A51–A51.

(16) Nelson, N.; Ben-Shem, A. The Complex Architecture of Oxygenic Photosynthesis. *Nat. Rev. Mol. Cell Biol.* **2004**, *5*, 971–982.

(17) Cramer, W. A.; Hasan, S. S. Structure-Function of the Cytochrome b_6f Lipoprotein Complex. In *Cytochrome Complexes: Evolution, Structures, Energy Transduction, and Signaling*; Cramer, W. A., Kallas, T., Eds.; Springer: Dordrecht, **2016**; pp 177–207.

(18) Cramer, W. A.; Zhang, H.; Yan, J.; Kurisu, G.; Smith, J. L. Transmembrane Traffic in the Cytochrome b_6f Complex. *Annu. Rev. Biochem.* **2006**, *75*, 769–790.

(19) Mulkidjanian, A. Y. Activated Q-Cycle as a Common Mechanism for Cytochrome Bc_1 and Cytochrome b_6f Complexes. *Biochim. Biophys. Acta* **2010**, *1797*, 1858–1868.

(20) Berry, E. A.; De Bari, H.; Huang, L.-S. Unanswered Questions about the Structure of Cytochrome Bc_1 Complexes. *Biochim. Biophys. Acta* **2013**, *1827*, 1258–1277.

(21) Xia, D.; Esser, L.; Tang, W.-K.; Zhou, F.; Zhou, Y.; Yu, L.; Yu, C.-A. Structural Analysis of Cytochrome Bc_1 Complexes: Implications to the Mechanism of Function. *Biochim. Biophys. Acta* **2013**, *1827*, 1278–1294.

(22) Hasan, S. S.; Yamashita, E.; Cramer, W. A. Transmembrane Signaling and Assembly of the Cytochrome B6f-Lipidic Charge Transfer Complex. *Biochim. Biophys. Acta* **2013**, *1827*, 1295–1308.

(23) Crofts, A. R.; Hong, S.; Wilson, C.; Burton, R.; Victoria, D.; Harrison, C.; Schulten, K. The Mechanism of Ubihydroquinone Oxidation at the Q_o-Site of the Cytochrome Bc_1 Complex. *Biochim. Biophys. Acta* **2013**, *1827*, 1362–1377.

(24) Berry, E. A.; Lee, D.-W.; Huang, L.-S.; Daldal, F. Structural and Mutational Studies of the Cytochrome Bc_1 Complex. In *The Purple Phototrophic Bacteria*; Hunter, C. N., Daldal, F., Thurnauer, M. C., Beatty, J. T., Eds.; Springer Science, **2009**; pp 425–450.

(25) Kramer, D. M.; Nitschke, W.; Cooley, J. W. The Cytochrome Bc_1 and Related Bc Complexes: The Rieske/Cytochrome b Complex as the Functional Core of a Central Electron/Proton Transfer Complex. In *The Purple Phototrophic Bacteria*; **2009**; pp 451–473.

(26) Crofts, A. R.; Wilson, C. A.; Rose, S. W.; Dikanov, S. A.; Burton, R. L. The Bc1 Complex: A Physicochemical Retrospective and a Atomistic Perspective. In *Mechanisms of primary energy transduction in biology*; **2018**; pp 161–191.

(27) Mitchell, P. Possible Molecular Mechanisms of the Protonmotive Function of Cytochrome Systems. *J. Theor. Biol.* **1976**, *62*, 327–367.

(28) Mitchell, P. Coupling of Phosphorylation to Electron and Hydrogen Transfer by a Chemi-Osmotic Type of Mechanism. *Nature* **1961**, *191*, 144–148.

(29) Al-Attar, S.; de Vries, S. Energy Transduction by Respiratory Metallo-Enzymes: From Molecular Mechanism to Cell Physiology. *Coord. Chem. Rev.* **2013**, *257*, 64–80.

(30) Nicholls, D. G.; Ferguson, S. J. *Bioenergetics 4*, 4th ed.; Kim, C. H., Ozawa, T., Eds.; Academic Press: Amsterdam, **2013**.

(31) Cramer, W. A.; Kallas, T. *Cytochrome Complexes: Evolution, Structures, Energy Transduction, and Signaling*; Cramer, W. A., Kallas, T., Eds.; Springer Science: Dordrecht, **2016**.

(32) Mitchell, P. The Protonmotive Q Cycle: A General Formulation. *FEBS Lett.* **1975**, *59*, 137–139.

(33) Mitchell, P. Protonmotive Redox Mechanism of the Cytochrome B-C1 Complex in the Respiratory Chain: Protonmotive Ubiquinone Cycle. *FEBS Lett.* **1975**, *56*, 1–6.

(34) *The Purple Phototrophic Bacteria*; Hunter, C. N., Daldal, F., Thurnauer, M. C., Beatty, J. T., Eds.; Springer, **2009**.

(35) Rochaix, J. D.; Lemeille, S.; Shapiguzov, A.; Samol, I.; Fucile, G.; Willig, A.; Goldschmidt-Clermont, M. Protein Kinases and Phosphatases Involved in the Acclimation of the Photosynthetic Apparatus to a Changing Light Environment. *Philos. Trans. R. Soc. B Biol. Sci.* **2012**, *367*, 3466–3474.

(36) Sena, L. A.; Chandel, N. S. Physiological Roles of Mitochondrial Reactive Oxygen Species. *Mol. Cell* **2012**, *48*, 158–167.

(37) Adam-Vizi, V.; Chinopoulos, C. Bioenergetics and the Formation of Mitochondrial Reactive Oxygen Species. *Trends Pharmacol. Sci.* **2006**, *27*, 639–645.

(38) Baniulis, D.; Hasan, S. S.; Stofleth, J. T.; Cramer, W. A. Mechanism of Enhanced Superoxide Production in the Cytochrome b_6f Complex of Oxygenic Photosynthesis. *Biochemistry* **2013**, *52*, 8975–8983.

(39) Crofts, A. R.; Meinhardt, S. W.; Jones, K. R.; Snozzi, M. The Role of the Quinone Pool in the Cyclic Electron-Transfer Chain of *Rhodopseudomonas Sphaeroides*: A Modified Q-Cycle Mechanism. *Biochim. Biophys. Acta* **1983**, *723*, 202–218.

(40) Furbacher, P. N.; Girvin, M. E.; Cramer, W. A. On the Question of Interheme Electron Transfer in the Chloroplast Cytochrome B6f in Situ. *Biochemistry* **1989**, *28*, 8990–8998.

(41) Stroebel, D.; Choquet, Y.; Popot, J.-L.; Picot, D. An Atypical Haem in the Cytochrome B6f Complex. *Nature* **2003**, *426*, 413–418.

(42) Kurisu, G.; Zhang, H.; Smith, J. L.; Cramer, W. A. Structure of the Cytochrome b_6f Complex of Oxygenic Photosynthesis: Tuning the Cavity. *Science* **2003**, *302*, 1009–1014.

(43) Zatsman, A. I.; Zhang, H.; Gunderson, W. A.; Cramer, W. A.; Hendrich, M. P. Heme-Heme Interactions in the Cytochrome B6f Complex: EPR Spectroscopy and Correlation with Structure. *J. Am. Chem. Soc.* **2006**, *128*, 14246–14247.

(44) Buckel, W.; Thauer, R. K. Flavin-Based Electron Bifurcation, A New Mechanism of Biological Energy Coupling. *Chem. Rev.* **2018**, *118*, 3862–3886.

(45) Baniulis, D.; Hasan, S. S.; Miliute, I.; Cramer, W. A. Mechanisms of Superoxide Generation and Signaling in Cytochrome *Bc* Complexes. In *Cytochrome Complexes: Evolution, Structures, Energy Transduction, and Signaling*; Cramer, W., Kallas, T., Eds.; Springer: Dordrecht, **2016**; pp 397–417.

(46) Agarwal, R.; Hasan, S. S.; Jones, L. M.; Stofleth, J. T.; Ryan, C. M.; Whitelegge, J. P.; Kehoe, D. M.; Cramer, W. A. Role of Domain Swapping in the Hetero-Oligomeric Cytochrome B6 f Lipoprotein Complex. *Biochemistry* **2015**, *54*, 3151–3163.

(47) Świerczek, M.; Cieluch, E.; Sarewicz, M.; Borek, A.; Moser, C. C.; Dutton, P. L.; Osyczka, A. An Electronic Bus Bar Lies in the Core of Cytochrome Bc_1. *Science* **2010**, *329*, 451–454.

(48) Berry, E. A.; Huang, L.-S.; Saechao, L. K.; Pon, N. G.; Valkova-Valchanova, M.; Daldal, F. X-Ray Structure of *Rhodobacter Capsulatus* Cytochrome Bc_1: Comparison with Its Mitochondrial and Chloroplast Counterparts. *Photosynth. Res.* **2004**, *81*, 251–275.

(49) Tian, H.; White, S.; Yu, L.; Yu, C.-A. Evidence for the Head Domain Movement of the Rieske Iron-Sulfur Protein in Electron Transfer Reaction of the Cytochrome Bc_1 Complex. *J. Biol. Chem.* **1999**, *274*, 7146–7152.

(50) Darrouzet, E.; Valkova-Valchanova, M.; Daldal, F. Probing the Role of the Fe-S Subunit Hinge Region during Q_o Site Catalysis in *Rhodobacter Capsulatus* Bc_1 Complex. *Biochemistry* **2000**, *39*, 15475–15483.

(51) Darrouzet, E.; Valkova-Valchanova, M.; Moser, C. C.; Dutton, P. L.; Daldal, F. Uncovering the [2Fe2S] Domain Movement in Cytochrome Bc_1 and Its Implications for Energy Conversion. *Proc. Natl. Acad. Sci. U. S. A.* **2000**, *97*, 4567–4572.

(52) Darrouzet, E.; Moser, C. C.; Dutton, P. L.; Daldal, F. Large Scale Domain Movement in Cytochrome Bc_1: A New Device for Electron Transfer in Proteins. *Trends Biochem. Sci.* **2001**, *26*, 445–451.

(53) Darrouzet, E.; Daldal, F. Movement of the Iron-Sulfur Subunit beyond the *Ef* Loop of Cytochrome *b* Is Required for Multiple Turnovers of the Bc_1 Complex but Not for Single Turnover Q_o Site Catalysis. *J. Biol. Chem.* **2002**, *277*, 3471–3476.

(54) Sadoski, R. C.; Engstrom, G.; Tian, H.; Zhang, L.; Yu, C.-A.; Yu, L.; Durham, B.; Millett, F. Use of a Photoactivated Ruthenium Dimer Complex to Measure Electron Transfer between the Rieske Iron-Sulfur Protein and Cytochrome C1 in the Cytochrome Bc1 Complex. *Biochemistry* **2000**, *39*, 4231–4236.

(55) Rajagukguk, S.; Yang, S.; Yu, C.-A.; Yu, L.; Durham, B.; Millett, F. Effect of Mutations in the Cytochrome b Ef Loop on the Electron-Transfer Reactions of the Rieske Iron-Sulfur Protein in the Cytochrome Bc1 Complex. *Biochemistry* **2007**, *46*, 1791–1798.

(56) Page, C. C.; Moser, C. C.; Chen, X.; Dutton, P. L. Natural Engineering Principles of Electron Tunnelling in Biological Oxidation-Reduction. *Nature* **1999**, *402*, 47–52.

(57) Brandt, U.; von Jagow, G. Analysis of Inhibitor Binding to the Mitochondrial Cytochrome c Reductase by Fluorescence Quench Titration. Evidence for a “catalytic Switch” at the Qo Center. *Eur. J. Biochem.* **1991**, *195*, 163–170.

(58) Brandt, U.; Haase, U.; Schägger, H.; von Jagow, G. Significance of the “Rieske” Iron-Sulfur Protein for Formation and Function of the Ubiquinol-Oxidation Pocket of Mitochondrial Cytochrome c Reductase (Bc1 Complex). *J. Biol. Chem.* **1991**, *266*, 19958–19964.

(59) Xia, D.; Yu, C.-A.; Kim, H.; Xia, J.-Z.; Kachurin, A. M.; Zhang, L.; Yu, L.; Deisenhofer, J. Crystal Structure of the Cytochrome Bc1 Complex from Bovine Heart Mitochondria. *Science* **1997**, *277*, 60–66.

(60) Iwata, S.; Lee, J. W.; Okada, K.; Lee, J. K.; Iwata, M.; Rasmussen, B.; Link, T. A.; Ramaswamy, S.; Jap, B. K. Complete Structure of the 11-Subunit Bovine Mitochondrial Cytochrome Bc_1 Complex. *Science* **1998**, *281*, 64–71.

(61) Zhang, Z.; Huang, L.-S.; Shulmeister, V. M.; Chi, Y.-I.; Kim, K. K.; Hung, L.-W.; Crofts, A. R.; Berry, E. A.; Kim, S.-H. Electron Transfer by Domain Movement in Cytochrome Bc_1. *Nature* **1998**, *392*, 677–684.

(62) Kleinschroth, T.; Castellani, M.; Trinh, C. H.; Morgner, N.; Brutschy, B.; Ludwig, B.; Hunte, C. X-Ray Structure of the Dimeric Cytochrome Bc_1 Complex from the Soil Bacterium *Paracoccus Denitrificans* at 2.7-Å Resolution. *Biochim. Biophys. Acta* **2011**, *1807*, 1606–1615.

(63) Esser, L.; Elberry, M.; Zhou, F.; Yu, C.-A. A.; Yu, L.; Xia, D. Inhibitor-Complexed Structures of the Cytochrome Bc1 from the Photosynthetic Bacterium Rhodobacter Sphaeroides. *J. Biol. Chem.* **2008**, *283*, 2846–2857.

(64) Esser, L.; Zhou, F.; Yu, C. A.; Xia, D. Crystal Structure of Bacterial Cytochrome Bc1 in Complex with Azoxystrobin Reveals a Conformational Switch of the Rieske Iron–Sulfur Protein Subunit. *J. Biol. Chem.* **2019**, *294*, 12007–12019.

(65) Baniulis, D.; Yamashita, E.; Whitelegge, J. P.; Zatsman, A. I.; Hendrich, M. P.; Hasan, S. S.; Ryan, C. M.; Cramer, W. A. Structure-Function, Stability, and Chemical Modification of the Cyanobacterial Cytochrome B6f Complex from Nostoc Sp. PCC 7120. *J. Biol. Chem.* **2009**, *284*, 9861–9869.

(66) Hasan, S. S.; Yamashita, E.; Baniulis, D.; Cramer, W. A. Quinone-Dependent Proton Transfer Pathways in the Photosynthetic Cytochrome B6f Complex. *Proc. Natl. Acad. Sci. U. S. A.* **2013**, *110*, 4297–4302.

(67) Yan, J.; Kurisu, G.; Cramer, W. A. Intraprotein Transfer of the Quinone Analogue Inhibitor 2,5-Dibromo-3-Methyl-6-Isopropyl-p-Benzoquinone in the Cytochrome B6f Complex. *Proc. Natl. Acad. Sci. U. S. A.* **2006**, *103*, 69–74.

(68) Hunte, C.; Koepke, J.; Lange, C.; Roßmanith, T.; Michel, H. Structure at 2.3 Å Resolution of the Cytochrome Bc_1 Complex from the Yeast *Saccharomyces Cerevisiae* Co-Crystallized with an Antibody Fv Fragment. *Structure* **2000**, *8*, 669–684.

(69) Lange, C.; Hunte, C. Crystal Structure of the Yeast Cytochrome Bc_1 Complex with Its Bound Substrate Cytochrome *C*. *Proc. Natl. Acad. Sci.* **2002**, *99*, 2800–2805.

(70) Palsdottir, H.; Lojero, C. G.; Trumpower, B. L.; Hunte, C. Structure of the Yeast Cytochrome Bc_1 Complex with a Hydroxyquinone Anion Q_o Site Inhibitor Bound. *J. Biol. Chem.* **2003**, *278*, 31303–31311.

(71) Birth, D.; Kao, W.-C.; Hunte, C. Structural Analysis of Atovaquone-Inhibited Cytochrome Bc_1 Complex Reveals the Molecular Basis of Antimalarial Drug Action. *Nat. Commun.* **2014**, *5*, 1–11.

(72) Solmaz, S. R. N.; Hunte, C. Structure of Complex III with Bound Cytochrome C in Reduced State and Definition of a Minimal Core Interface for Electron Transfer. *J. Biol. Chem.* **2008**, *283*, 17542–17549.

(73) Malone, L. A.; Qian, P.; Mayneord, G. E.; Hitchcock, A.; Farmer, D. A.; Thompson, R. F.; Swainsbury, D. J. K.; Ranson, N. A.; Hunter, C. N.; Johnson, M. P. Cryo-EM Structure of the Spinach Cytochrome b_6f Complex at 3.6 Å Resolution. *Nature* **2019**, *575*, 535–539.

(74) Berry, E. A.; Huang, L. S.; Zhang, Z.; Kim, S. H. Structure of the Avian Mitochondrial Cytochrome Bc1 Complex. *J. Bioenerg. Biomembr.* **1999**, *31*, 177–190.

(75) Crowley, P. J.; Berry, E. A.; Cromartie, T.; Daldal, F.; Godfrey, C. R. A. A.; Lee, D.-W. W.; Phillips, J. E.; Taylor, A.; Viner, R. The Role of Molecular Modeling in the Design of Analogues of the Fungicidal Natural Products Crocacins A and D. *Bioorganic Med. Chem.* **2008**, *16*, 10345–10355.

(76) Berry, E. A.; Zhang, Z.; Bellamy, H. D.; Huang, L. Crystallographic Location of Two Zn^{2+}-Binding Sites in the Avian Cytochrome Bc_1 Complex. *Biochim. Biophys. Acta* **2000**, *1459*, 440–448.

(77) Esser, L.; Quinn, B.; Li, Y.-F.; Zhang, M.; Elberry, M.; Yu, L.; Yu, C.-A.; Xia, D. Crystallographic Studies of Quinol Oxidation Site Inhibitors: A Modified Classification of Inhibitors for the Cytochrome Bc1 Complex. *J. Mol. Biol.* **2004**, *341*, 281–302.

(78) Esser, L.; Gong, X.; Yang, S.; Yu, L.; Yu, C.-A.; Xia, D. Surface-Modulated Motion Switch: Capture and Release of Iron–Sulfur Protein in the Cytochrome Bc1 Complex. *Proc. Natl. Acad. Sci. U. S. A.* **2006**, *103*, 13045–13050.

(79) Gao, X.; Wen, X.; Esser, L.; Quinn, B.; Yu, L.; Yu, C.-A.; Xia, D. Structural Basis for the Quinone Reduction in the Bc_1 Complex: A Comparative Analysis of Crystal Structures of Mitochondrial Cytochrome Bc_1 with Bound Substrate and Inhibitors at the Q_i Site. *Biochemistry* **2003**, *42*, 9067–9080.

(80) Guo, R.; Zong, S.; Wu, M.; Gu, J.; Yang, M. Architecture of Human Mitochondrial Respiratory Megacomplex I2III2IV2. *Cell* **2017**, *170*, 1247-1257.e12.

(81) Gong, H.; Li, J.; Xu, A.; Tang, Y.; Ji, W.; Gao, R.; Wang, S.; Yu, L.; Tian, C.; Li, J.; Yen, H. Y.; Lam, S. M.; Shui, G.; Yang, X.; Sun, Y.; Li, X.; Jia, M.; Yang, C.; Jiang, B.; Lou, Z.; Robinson, C. V.; Wong, L. L.; Guddat, L. W.; Sun, F.; Wang, Q.; Rao, Z. An Electron Transfer Path Connects Subunits of a Mycobacterial Respiratory Supercomplex. *Science (80-.).* **2018**, *362*.

(82) Wiseman, B.; Nitharwal, R. G.; Fedotovskaya, O.; Schäfer, J.; Guo, H.; Kuang, Q.; Benlekbir, S.; Sjöstrand, D.; Ädelroth, P.; Rubinstein, J. L.; Brzezinski, P.; Högbom, M. Structure of a Functional Obligate Complex III2IV2 Respiratory Supercomplex from Mycobacterium Smegmatis. *Nat. Struct. Mol. Biol.* **2018**, *25*, 1128–1136.

(83) Kim, H.; Xia, D.; Yu, C.-A.; Xia, J.-Z.; Kachurin, A. M.; Zhang, L.; Yu, L.; Deisenhofer, J. Inhibitor Binding Changes Domain Mobility in the Iron-Sulfur Protein of the Mitochondrial Bc1 Complex from Bovine Heart. *Proc. Natl. Acad. Sci. U. S. A.* **1998**, *95*, 8026–8033.

(84) Schoepp, B.; Brugna, M.; Riedel, A.; Nitschke, W.; Kramer, D. M. The Q_o-Site Inhibitor DBMIB Favours the Proximal Position of the Chloroplast Rieske Protein and Induces a p*K*-Shift of the Redox-Linked Proton. *FEBS Lett.* **1999**, *450*, 245–250.

(85) Berry, E. A.; Huang, L. Observations Concerning the Quinol Oxidation Site of the Cytochrome Bc_1 Complex. *FEBS Lett.* **2003**, *555*, 13–20.

(86) Cooley, J. W. Protein Conformational Changes Involved in the Cytochrome Bc1 Complex Catalytic Cycle. *Biochim. Biophys. Acta* **2013**, *1827*, 1340–1345.

(87) Covian, R.; Trumpower, B. L. Regulatory Interactions in the Dimeric Cytochrome Bc1 Complex: The Advantages of Being a Twin. *Biochimica et Biophysica Acta - Bioenergetics*. Elsevier September 1, 2008, pp 1079–1091.

(88) Cooley, J. W.; Lee, D.-W.; Daldal, F. Across Membrane Communication between the Qo and Qi Active Sites of Cytochrome Bc1. *Biochemistry* **2009**, *48*, 1888–1899.

(89) Cen, X.; Yu, L.; Yu, C.-A. Domain Movement of Iron Sulfur Protein in Cytochrome Bc_1 Complex Is Facilitated by the Electron Transfer from Cytochrome b_L to b_H. *FEBS Lett.* **2008**, *582*, 523–526.

(90) Sarewicz, M.; Dutka, M.; Froncisz, W.; Osyczka, A. Magnetic Interactions Sense Changes in Distance between Heme b_L and the Iron-Sulfur Cluster in Cytochrome Bc_1. *Biochemistry* **2009**, *48*, 5708–5720.

(91) Crofts, A. R.; Barquera, B.; Gennis, R. B.; Kuras, R.; Guergova-Kuras, M.; Berry, E. A.; Huang, L.-S.; Kuras, R.; Zhang, Z.; Berry, E. A. Mechanism of Ubiquinol Oxidation by the Bc_1 Complex: Different Domains of the Quinol Binding Pocket and Their Role in the Mechanism and Binding of Inhibitors. *Biochemistry* **1999**, *38*, 15791–15806.

(92) Crofts, A. R.; Hong, S.; Zhang, Z.; Berry, E. A. Physicochemical Aspects of the Movement of the Rieske Iron Sulfur Protein during Quinol Oxidation by the Bc_1 Complex from Mitochondria and Photosynthetic Bacteria. *Biochemistry* **1999**, *38*, 15827–15839.

(93) Millett, F.; Durham, B. Kinetics of Electron Transfer within Cytochrome Bc_1 and between Cytochrome Bc_1 and Cytochrome *C*. *Photosynth. Res.* **2004**, *82*, 1–16.

(94) Crofts, A. R.; Shinkarev, V. P.; Kolling, D. R. J.; Hong, S. The Modified Q-Cycle Explains the Apparent Mismatch between the Kinetics of Reduction of Cytochromes c_1 and b_H in the Bc_1 Complex. *J. Biol. Chem.* **2003**, *278*, 36191–36201.

(95) Postila, P. A.; Kaszuba, K.; Sarewicz, M.; Osyczka, A.; Vattulainen, I.; Róg, T. Key Role of Water in Proton Transfer at the Q_o-Site of the Cytochrome Bc_1 Complex Predicted by Atomistic Molecular Dynamics Simulations. *Biochim. Biophys. Acta* **2013**, *1827*, 761–768.

(96) Barragan, A. M.; Crofts, A. R.; Schulten, K.; Solov'yov, I. A. Identification of Ubiquinol Binding Motifs at the Q_o-Site of the Cytochrome Bc_1 Complex. *J. Phys. Chem. B* **2014**, *119*, 433–447.

(97) Barragan, A. M.; Schulten, K.; Solov'yov, I. A. Mechanism of the Primary Charge Transfer Reaction in the Cytochrome Bc_1 Complex. *J. Phys. Chem. B* **2016**, *120*, 11369–11380.

(98) Darrouzet, E.; Valkova-Valchanova, M.; Ohnishi, T.; Daldal, F. Structure and Function of the Bacterial Bc_1 Complex: Domain Movement, Subunit Interactions, and Emerging Rationale Engineering Attempts. *J. Bioenerg. Biomembr.* **1999**, *31*, 275–288.

(99) Tian, H.; Yu, L.; Mather, M. W.; Yun, C.-A. Flexibility of the Neck Region of the Rieske Iron-Sulfur Protein Is Functionally Important in the Cytochrome Bc_1 Complex. *J. Biol. Chem.* **1998**, *273*, 27953–27959.

(100) Brugna, M.; Rodgers, S.; Schricker, A.; Montoya, G.; Kazmeier, M.; Nitschke, W.; Sinning, I. A Spectroscopic Method for Observing the Domain Movement of the Rieske Iron-Sulfur Protein. *Proc. Natl. Acad. Sci. U. S. A.* **2000**, *97*, 2069–2074.

(101) Liebl, U.; Sled, V.; Brasseur, G.; Ohnishi, T.; Daldal, F. Conserved Nonliganding Residues of the *Rhodobacter Capsulatus* Rieske Iron-Sulfur Protein of the Bc_1 Complex Are Essential for Protein Structure, Properties of the [2Fe-2S] Cluster, and Communication with the Quinone Pool. *Biochemistry* **1997**, *36*, 11675–11684.

(102) Brasseur, G.; Sled, V.; Liebl, U.; Ohnishi, T.; Daldal, F. The Amino-Terminal Portion of the Rieske Iron-Sulfur Protein Contributes to the Ubihydroquinone Oxidation Site Catalysis of the *Rhodobacter Capsulatus* Bc_1 Complex. *Biochemistry* **1997**, *36*, 11685–11696.

(103) Xiao, K.; Engstrom, G.; Rajagukguk, S.; Yu, C.-A.; Yu, L.; Durham, B.; Millett, F. Effect of Famoxadone on Photoinduced Electron Transfer between the Iron-Sulfur Center and Cytochrome c_1 in the Cytochrome Bc_1 Complex. *J. Biol. Chem.* **2003**, *278*, 11419–11426.

(104) Cieluch, E.; Pietryga, K.; Sarewicz, M.; Osyczka, A. Visualizing Changes in Electron Distribution in Coupled Chains of Cytochrome Bc1 by Modifying Barrier for Electron

Transfer between the FeS Cluster and Heme C1. *Biochim. Biophys. Acta* **2010**, *1797*, 296–303.

(105) Nett, J. H.; Hunte, C.; Trumpower, B. L. Changes to the Length of the Flexible Linker Region of the Rieske Protein Impair the Interaction of Ubiquinol with the Cytochrome Bc_1 Complex. *Eur. J. Biochem.* **2000**, *267*, 5777–5782.

(106) Darrouzet, E.; Valkova-Valchanova, M.; Daldal, F. The [2Fe-2S] Cluster E_m as an Indicator of the Iron-Sulfur Subunit Position in the Ubihydroquinone Oxidation Site of the Cytochrome Bc_1 Complex. *J. Biol. Chem.* **2002**, *277*, 3464–3470.

(107) Sarewicz, M.; Borek, A.; Cieluch, E.; Świerczek, M.; Osyczka, A. Discrimination between Two Possible Reaction Sequences That Create Potential Risk of Generation of Deleterious Radicals by Cytochrome Bc_1. Implications for the Mechanism of Superoxide Production. *Biochim. Biophys. Acta* **2010**, *1797*, 1820–1827.

(108) Roberts, A. G.; Bowman, M. K.; Kramer, D. M. Certain Metal Ions Are Inhibitors of Cytochrome b_6f Complex "Rieske" Iron-Sulfur Protein Domain Movements. *Biochemistry* **2002**, *41*, 4070–4079.

(109) Cooley, J. W.; Roberts, A. G.; Bowman, M. K.; Kramer, D. M.; Daldal, F. The Raised Midpoint Potential of the [2Fe2S] Cluster of Cytochrome Bc_1 Is Mediated by Both the Q_o Site Occupants and the Head Domain Position of the Fe-S Protein Subunit. *Biochemistry* **2004**, *43*, 2217–2227.

(110) Roberts, A. G.; Bowman, M. K.; Kramer, D. M. The Inhibitor DBMIB Provides Insight into the Functional Architecture of the Q_o Site in the Cytochrome b_6f Complex. *Biochemistry* **2004**, *43*, 7707–7716.

(111) Cooley, J. W.; Ohnishi, T.; Daldal, F. Binding Dynamics at the Quinone Reduction (Qi) Site Influence the Equilibrium Interactions of the Iron Sulfur Protein and Hydroquinone Oxidation (Qo) Site of the Cytochrome Bc1 Complex. *Biochemistry* **2005**, *44*, 10520–10532.

(112) Rao B. K., S.; Tyryshkin, A. M.; Roberts, A. G.; Bowman, M. K.; Kramer, D. M. Inhibitory Copper Binding Site on the Spinach Cytochrome B6f Complex: Implications for Qo Site Catalysis. *Biochemistry* **2000**, *39*, 3285–3296.

(113) Sarewicz, M.; Dutka, M.; Pietras, R.; Borek, A.; Osyczka, A. Effect of H Bond Removal and Changes in the Position of the Iron-Sulphur Head Domain on the Spin-Lattice Relaxation Properties of the [2Fe-2S]2+ Rieske Cluster in Cytochrome Bc1. *Phys. Chem. Chem. Phys.* **2015**, *17*, 25297–25308.

(114) von Jagow, G.; Ohnishi, T. The Chromone Inhibitor Stigmatellin-Binding to the Ubiquinol Oxidation Center at the C-Side of the Mitochondrial Membrane. *FEBS Lett.* **1985**, *185*, 311–315.

(115) Gurung, B.; Yu, L.; Yu, C. A. Stigmatellin Induces Reduction of Iron-Sulfur Protein in the Oxidized Cytochrome Bc1 Complex. *J. Biol. Chem.* **2008**, *283*, 28087–28094.

(116) Bowyer, J. R.; Edwards, C. A.; Ohnishi, T.; Trumpower, B. L. An Analogue of Ubiquinone Which Inhibits Respirationby Binding to the Iron-Sulfur Protein of the Cytochrome b-C1 Segment of the Mitochondrial Respiratory Chain. *J Biol Chem* **1982**, *257*, 3705–3713.

(117) Berry, E. A.; Huang, L.-S. Conformationally Linked Interaction in the Cytochrome Bc_1 Complex between Inhibitors of the Q_o Site and the Rieske Iron-Sulfur Protein. *Biochim. Biophys. Acta* **2011**, *1807*, 1349–1363.

(118) Kao, W.-C.; Hunte, C. The Molecular Evolution of the Q_o Motif. *Genome Biol. Evol.* **2014**, *6*, 1894–1910.

(119) Crofts, A. R.; Shinkarev, V. P.; Dikanov, S. A.; Samoilova, R. I.; Kolling, D. Interactions of Quinone with the Iron-Sulfur Protein of the Bc1 Complex: Is the Mechanism Spring-Loaded? *Biochim. Biophys. Acta - Bioenerg.* **2002**, *1555*, 48–53.

(120) Borek, A.; Kuleta, P.; Ekiert, R.; Pietras, R.; Sarewicz, M.; Osyczka, A. Mitochondrial Disease-Related Mutation G167P in Cytochrome *b* of *Rhodobacter Capsulatus* Cytochrome Bc_1 (S151P in Human) Affects the Equilibrium Distribution of [2Fe-2S] Cluster and Generation of Superoxide. *J. Biol. Chem.* **2015**, *290*, 23781–23792.

(121) Ekiert, R.; Borek, A.; Kuleta, P.; Czernek, J.; Osyczka, A. Mitochondrial Disease-Related Mutations at the Cytochrome *b*-Iron-Sulfur Protein (ISP) Interface: Molecular Effects on the Large-Scale Motion of ISP and Superoxide Generation Studied in *Rhodobacter Capsulatus* Cytochrome Bc_1. *Biochim. Biophys. Acta* **2016**, *1857*, 1102–1110.

(122) Darrouzet, E.; Daldal, F. Protein-Protein Interactions between Cytochrome *b* and the Fe-S Protein Subunits during QH_2 Oxidation and Large-Scale Domain Movement in the Bc_1 Complex. *Biochemistry* **2003**, *42*, 1499–1507.

(123) Huang, L.-S.; Cobessi, D.; Tung, E. Y.; Berry, E. A. Binding of the Respiratory Chain Inhibitor Antimycin to the Mitochondrial Bc_1 Complex: A New Crystal Structure Reveals an Altered Intramolecular Hydrogen-Bonding Pattern. *J. Mol. Biol.* **2005**, *351*, 573–597.

(124) Valkova-Valchanova, M.; Darrouzet, E.; Moomaw, C. R.; Slaughter, C. A.; Daldal, F. Proteolytic Cleavage of the Fe-S Subunit Hinge Region of *Rhodobacter Capsulatus* Bc_1 Complex: Effects of Inhibitors and Mutations. *Biochemistry* **2000**, *39*, 15484–15492.

(125) Covian, R.; Trumpower, B. L. Regulatory Interactions between Ubiquinol Oxidation and Ubiquinone Reduction Sites in the Dimeric Cytochrome Bc1 Complex. *J. Biol. Chem.* **2006**, *281*, 30925–30932.

(126) Covian, R.; Trumpower, B. L. The Dimeric Structure of the Cytochrome Bc1 Complex Prevents Center P Inhibition by Reverse Reactions at Center N. *Biochim. Biophys. Acta - Bioenerg.* **2008**, *1777*, 1044–1052.

(127) Robertson, D. E.; Ding, H.; Chelminski, P. R.; Slaughter, C.; Hsu, J.; Moomaw, C.; Tokito, M.; Daldal, F.; Dutton, P. L. Hydroubiquinone-Cytochrome C2 Oxidoreductase from

Rhodobacter Capsulatus: Definition of a Minimal, Functional Isolated Preparation. *Biochemistry* **1993**, *32*, 1310–1317.

(128) Shinkarev, V. P.; Kolling, D. R. J.; Miller, T. J.; Crofts, A. R. Modulation of the Midpoint Potential of the [2Fe-2S] Rieske Iron Sulfur Center by Q_o Occupants in the Bc_1 Complex. *Biochemistry* **2002**, *41*, 14372–14382.

(129) Tso, S.-C.; Shenoy, S. K.; Quinn, B. N.; Yu, L. Subunit IV of Cytochrome Bc 1 Complex from Rhodobacter Sphaeroides . *J. Biol. Chem.* **2000**, *275*, 15287–15294.

(130) Koch, H.-G.; Schneider, D. Folding, Assembly, and Stability of Transmembrane Cytochromes. *Curr. Chem. Biol.* **2007**, *1*, 59–74.

(131) Volkmer, T.; Becker, C.; Prodöhl, A.; Finger, C.; Schneider, D. Assembly of a Transmembrane B-Type Cytochrome Is Mainly Driven by Transmembrane Helix Interactions. *Biochim. Biophys. Acta* **2006**, *1758*, 1815–1822.

(132) Berry, E. A.; Walker, F. A. Bis-Histidine-Coordinated Hemes in Four-Helix Bundles: How the Geometry of the Bundle Controls the Axial Imidazole Plane Orientations in Transmembrane Cytochromes of Mitochondrial Complexes II and III and Related Proteins. *J. Biol. Inorg. Chem.* **2008**, *13*, 481–498.

(133) Yun, C.-H.; Crofts, A. R.; Gennis, R. B. Assignment of the Histidine Axial Ligands to the Cytochrome BH and Cytochrome BL Components of the Bc1 Complex from Rhodobacter Sphaeroides by Site-Directed Mutagenesis. *Biochemistry* **1991**, *30*, 6747–6754.

(134) Bertini, I.; Cavallaro, G.; Rosato, A. Cytochrome *c*: Occurrence and Functions. *Chem. Rev.* **2006**, *106*, 90–115.

(135) Osyczka, A.; Dutton, P. L.; Moser, C. C.; Darrouzet, E.; Daldal, F. Controlling the Functionality of Cytochrome c_1 Redox Potentials in the *Rhodobacter Capsulatus* Bc_1 Complex through Disulfide Anchoring of a Loop and a β-Branched Amino Acid near the Heme-Ligating Methionine. *Biochemistry* **2001**, *40*, 14547–14556.

(136) Osyczka, A.; Moser, C. C.; Dutton, P. L. Novel Cyanide Inhibition at Cytochrome c_1 of *Rhodobacter Capsulatus* Cytochrome Bc_1. *Biochim. Biophys. Acta* **2004**, *1655*, 71–76.

(137) Zhang, H.; Osyczka, A.; Moser, C. C.; Dutton, P. L. Resilience of Rhodobacter Sphaeroides Cytochrome Bc1 to Heme C1 Ligation Changes. *Biochemistry* **2006**, *45*, 14247–14255.

(138) Davidson, E.; Ohnishi, T.; Atta-Asafo-Adjei, E.; Daldal, F. Potential Ligands to the [2Fe-2S] Rieske Cluster of the Cytochrome Bc_1 of *Rhodobacter Capsulatus* Probed by Site-Directed Mutagenesis. *Biochemistry* **1992**, *31*, 3342–3351.

(139) Mason, J. R.; Cammack, R. The Electron-Transport Proteins of Hydroxylating Bacterial Dioxygenases. *Annu. Rev. Microbiol.* **1992**, *46*, 277–305.

(140) Gurbiel, R. J.; Doan, P. E.; Gassner, G. T.; Macke, T. J.; Case, D. A.; Ohnishi, T.; Fee, J. A.; Ballou, D. P.; Hoffman, B. M. Active Site Structure of Rieske-Type Proteins: Electron

Nuclear Double Resonance Studies of Isotopically Labeled Phthalate Dioxygenase from Pseudomonas Cepacia and Rieske Protein from Rhodobacter Capsulatus and Molecular Modeling Studies of a Rieske Cente. *Biochemistry* **1996**, *35*, 7834–7845.

(141) Siedow, J. N.; Power, S.; de la Rosa, F. F.; Palmer, G. The Preparation and Characterization of Highly Purified, Enzymically Active Complex III from Baker's Yeast. *J. Biol. Chem.* **1978**, *253*, 2392–2399.

(142) Kriauciunas, A.; Yu, L.; Yu, C. A.; Wynn, R. M.; Knaff, D. B. The Rhodospirillum Rubrum Cytochrome Bc1 Complex: Pep Tide Composition, Prosthetic Group Content and Quinone Binding. *BBA - Bioenerg.* **1989**, *976*, 70–76.

(143) Andrews, K. M.; Crofts, A. R.; Gennis, R. B. Large-Scale Purification and Characterization of a Highly Active Four-Subunit Cytochrome Bc1 Complex from Rhodobacter Sphaeroides. *Biochemistry* **1990**, *29*, 2645–2651.

(144) Ljungdahl, P. O.; Pennoyer, J. D.; Robertson, D. E.; Trumpower, B. L. Purification of Highly Active Cytochrome Bc1 Complexes from Phylogenetically Diverse Species by a Single Chromatographic Procedure. *BBA - Bioenerg.* **1987**, *891*, 227–241.

(145) Shinkarev, V. P.; Crofts, A. R.; Wraight, C. A. Spectral Analysis of the Bc1 Complex Components in Situ: Beyond the Traditional Difference Approach. *Biochim. Biophys. Acta - Bioenerg.* **2006**, *1757*, 67–77.

(146) Baymann, F.; Robertson, D. E.; Dutton, P. L.; Mäntele, W. Electrochemical and Spectroscopic Investigations of the Cytochrome Bc1 Complex from Rhodobacter Capsulatus. *Biochemistry* **1999**, *38*, 13188–13199.

(147) Palmer, G. The Electron Paramagnetic Resonance of Metalloproteins. *Biochem. Soc. Trans.* **1985**, *13*, 548–560.

(148) Zoppellaro, G.; Bren, K. L.; Ensign, A. A.; Harbitz, E.; Kaur, R.; Hersleth, H.-P. P.; Ryde, U.; Hederstedt, L.; Andersson, K. K. Studies of Ferric Heme Proteins with Highly Anisotropic/Highly Axial Low Spin (S = 1/2) Electron Paramagnetic Resonance Signals with Bis-Histidine and Histidine-Methionine Axial Iron Coordination. *Biopolym. - Pept. Sci. Sect.* **2009**, *91*, 1064–1082.

(149) Pintscher, S.; Kuleta, P.; Cieluch, E.; Borek, A.; Sarewicz, M.; Osyczka, A. Tuning of Hemes *b* Equilibrium Redox Potential Is Not Required for Cross-Membrane Electron Transfer. *J. Biol. Chem.* **2016**, *291*, 6872–6881.

(150) Valkova-Valchanova, M.; Saribaş, A. S.; Gibney, B. R.; Dutton, P. L.; Daldal, F. Isolation and Characterization of a Two-Subunit Cytochrome b-c_1 Subcomplex from *Rhodobacter Capsulatus* and Reconstitution of Its Ubihydroquinone Oxidation (Q_o) Site with Purified Fe-S Protein Subunit. *Biochemistry* **1998**, *37*, 16242–16251.

(151) Pintscher, S.; Pietras, R. R.; Sarewicz, M.; Osyczka, A. Electron Sweep across Four B-Hemes of Cytochrome Bc_1 Revealed by Unusual Paramagnetic Properties of the Qi Semiquinone Intermediate. *Biochim. Biophys. Acta - Bioenerg.* **2018**, *1859*, 459–469.

(152) Li, J.; Darrouzet, E.; Dhawan, I. K.; Johnson, M. K.; Osyczka, A.; Daldal, F.; Knaff, D. B. Spectroscopic and Oxidation–Reduction Properties of *Rhodobacter Capsulatus* Cytochrome c_1 and Its M183K and M183H Variants. *Biochim. Biophys. Acta* **2002**, *1556*, 175–186.

(153) Finnegan, M. G.; Knaff, D. B.; Qin, H.; Gray, K. A.; Daldal, F.; Yu, L.; Yu, C.-A.; Kleis-San Francisco, S.; Johnson, M. K. Axial Heme Ligation in the Cytochrome Bc_1 Complexes of Mitochondrial and Photosynthetic Membranes. A near-Infrared Magnetic Circular Dichroism and Electron Paramagnetic Resonance Study. *Biochim. Biophys. Acta* **1996**, *1274*, 9–20.

(154) Link, T. A.; Schägger, H.; von Jagow, G. Analysis of the Structures of the Subunits of the Cytochrome Bc1 Complex from Beef Heart Mitochondria. *FEBS Lett.* **1986**, *204*, 9–15.

(155) Zhu, J.; Egawa, T.; Yeh, S.-R.; Yu, L.; Yu, C.-A. Simultaneous Reduction of Iron-Sulfur Protein and Cytochrome b_L during Ubiquinol Oxidation in Cytochrome Bc_1 Complex. *Proc. Natl. Acad. Sci. U. S. A.* **2007**, *104*, 4864–4869.

(156) Schütz, M.; Schoepp-Cothenet, B.; Lojou, E.; Woodstra, M.; Lexa, D.; Tron, P.; Dolla, A.; Durand, M. C.; Stetter, K. O.; Baymann, F. The Naphthoquinol Oxidizing Cytochrome Bc1 Complex of the Hyperthermophilic Knallgasbacterium Aquifex Aeolicus: Properties and Phylogenetic Relationships. *Biochemistry* **2003**, *42*, 10800–10808.

(157) Link, T. A. The Structures of Rieske and Rieske-Type Proteins. *Adv. Inorg. Chem.* **1999**, *47*, 83–157.

(158) Hagen, W. R. EPR Spectroscopy of Iron-Sulfur Proteins. In *Advances in Inorganic Chemistry, Iron-Sulfur Proteins*; Academic Press, Inc.: San Diego, **1992**; pp 165–222.

(159) de Vries, S.; Albracht, S. P. J.; Leeuwerik, F. J. The Multiplicity and Stoichiometry of the Prosthetic Groups in QH2:Cytochrome c Oxidoreducatse as Studied by EPR. *Biochim. Biophys. Acta* **1979**, *546*, 316–333.

(160) Bergdoll, L.; ten Brink, F.; Nitschke, W.; Picot, D.; Baymann, F. From Low- to High-Potential Bioenergetic Chains: Thermodynamic Constraints of Q-Cycle Function. *Biochim. Biophys. Acta - Bioenerg.* **2016**, *1857*, 1569–1579.

(161) Shinkarev, V. P.; Crofts, A. R.; Wraight, C. A. The Electric Field Generated by Photosynthetic Reaction Center Induces Rapid Reversed Electron Transfer in the Bc_1 Complex. *Biochemistry* **2001**, *40*, 12584–12590.

(162) Nicholls, D. G.; Ferguson, S. *Bioenergetics*; Elsevier, **2013**.

(163) Pintscher, S.; Wójcik-Augustyn, A.; Sarewicz, M.; Osyczka, A. Charge Polarization Imposed by the Binding Site Facilitates Enzymatic Redox Reactions of Quinone. *Biochim. Biophys. Acta - Bioenerg.* **2020**, *1861*, 148216.

(164) Rich, P. R.; Jeal, A. E.; Madgwick, S. A.; Moody, A. J. Inhibitor Effects on Redox-Linked Protonations of the *b* Haems of the Mitochondrial Bc_1 Complex. *Biochim. Biophys. Acta* **1990**, *1018*, 29–40.

(165) Trumpower, B. L. Cytochrome Bc_1 Complexes of Microorganisms. *Microbiol. Rev.* **1990**, *54*, 101–129.

(166) Denke, E.; Merbitz-Zahradnik, T.; Hatzfeld, O. M.; Snyder, C. H.; Link, T. A.; Trumpower, B. L. Alteration of the Midpoint Potential and Catalytic Activity of the Rieske Iron-Sulfur Protein by Changes of Amino Acids Forming Hydrogen Bonds to the Iron-Sulfur Cluster. *J. Biol. Chem.* **1998**, *273*, 9085–9093.

(167) Rotsaert, F. A. J.; Covian, R.; Trumpower, B. L. Mutations in Cytochrome *b* That Affect Kinetics of the Electron Transfer Reactions at Center N in the Yeast Cytochrome Bc_1 Complex. *Biochim. Biophys. Acta* **2008**, *1777*, 239–249.

(168) T'Sai, A. L.; Palmer, G. Potentiometric Studies on Yeast Complex III. *BBA - Bioenerg.* **1983**, *722*, 349–363.

(169) Van Wielink, J. E.; Oltmann, L. F.; Leeuwerik, F. J.; De Hollander, J. A.; Stouthamer, A. H. A Method for in Situ Characterization of B- and c-Type Cytochromes in Escherichia Coli and in Complex III from Beef Heart Mitochondria by Combined Spectrum Deconvolution and Potentiometric Analysis. *BBA - Bioenerg.* **1982**, *681*, 177–190.

(170) Liu, X.; Yu, C. A.; Yu, L. The Role of Extra Fragment at the C-Terminal of Cytochrome b (Residues 421-445) in the Cytochrome Bc1 Complex from Rhodobacter Sphaeroides. *J. Biol. Chem.* **2004**, *279*, 47363–47371.

(171) Martinez, S. E.; Huang, D.; Szczepaniak, A.; Cramer, W. A.; Smith, J. L. Crystal Structure of Chloroplast Cytochrome Freveals a Novel Cytochrome Fold and Unexpected Heme Ligation. *Structure* **1994**, *2*, 95–105.

(172) Martinez, S. E.; Huang, D.; Ponomarev, M.; Cramer, W. A.; Smith, J. L. The Heme Redox Center of Chloroplast Cytochrome f Is Linked to a Buried Five-Water Chain. *Protein Sci.* **1996**, *5*, 1081–1092.

(173) Yamashita, E.; Zhang, H.; Cramer, W. A. Structure of the Cytochrome B6f Complex: Quinone Analogue Inhibitors as Ligands of Heme Cn. *J. Mol. Biol.* **2007**, *370*, 39–52.

(174) Hasan, S. S.; Cramer, W. A. Internal Lipid Architecture of the Hetero-Oligomeric Cytochrome b 6f Complex. *Structure* **2014**, *22*, 1008–1015.

(175) Widger, W. R.; Cramer, W. A.; Herrmann, R. G.; Trebst, A. Sequence Homology and Structural Similarity between Cytochrome b of Mitochondrial Complex III and the Chloroplast B6-f Complex: Position of the Cytochrome b Hemes in the Membrane. *Proc. Natl. Acad. Sci. U. S. A.* **1984**, *81*, 674–678.

(176) RIESKE, J. S.; HANSEN, R. E.; ZAUGG, W. S. Studies on the Electron Transfer System. 58. Properties of a New Oxidation-Reduction Component of the Respiratory Chain As

Studied By Electron Paramagnetic Resonance Spectroscopy. *J. Biol. Chem.* **1964**, *239*, 3017–3022.

(177) Schwenkert, S.; Legen, J.; Takami, T.; Shikanai, T.; Herrmann, R. G.; Meurer, J. Role of the Low-Molecular-Weight Subunits PetL, PetG, and PetN in Assembly, Stability, and Dimerization of the Cytochrome B6f Complex in Tobacco. *Plant Physiol.* **2007**, *144*, 1924–1935.

(178) Carrell, C. J.; Zhang, H.; Cramer, W. A.; Smith, J. L. Biological Identity and Diversity in Photosynthesis and Respiration: Structure of the Lumen-Side Domain of the Chloroplast Rieske Protein. *Structure* **1997**, *5*, 1613–1625.

(179) Pierre, Y.; Breyton, C.; Kramer, D.; Popot, J. L. Purification and Characterization of the Cytochrome B6 f Complex from Chlamydomonas Reinhardtii. *J. Biol. Chem.* **1995**, *270*, 29342–29349.

(180) Zhang, H.; Whitelegge, J. P.; Cramer, W. A. Ferredoxin:$NADP^+$ Oxidoreductase Is a Subunit of the Chloroplast Cytochrome b_6f Complex. *J. Biol. Chem.* **2001**, *276*, 38159–38165.

(181) Rexroth, S.; Rexroth, D.; Veit, S.; Plohnke, N.; Cormann, K. U.; Nowaczyk, M. M.; Rögner, M.; Rogner, M. Functional Characterization of the Small Regulatory Subunit PetP from the Cytochrome B6f Complex in Thermosynechococcus Elongatus. *Plant Cell* **2014**, *26*, 3435–3448.

(182) Huang, D.; Everly, R. M.; Cheng, R. H.; Heymann, J. B.; Baker, T. S.; Cramer, W. A.; Schägger, H.; Sled, V.; Ohnishi, T. Characterization of the Chloroplast Cytochrome B6f Complex as a Structural and Functional Dimer. *Biochemistry* **1994**, *33*, 4401–4409.

(183) Zhang, H.; Huang, D.; Cramer, W. A. Stochimetrically Bound β-Carotene in the Cytochrome b_6f Complex of Oxygenic Photosynthesis Protects against Oxygen Damage. *J. od Biol. Chem.* **1999**, *274*, 1581–1587.

(184) Hasan, S. S.; Zakharov, S. D.; Chauvet, A.; Stadnytskyi, V.; Savikhin, S.; Cramer, W. A. A Map of Dielectric Heterogeneity in a Membrane Protein: The Hetero-Oligomeric Cytochrome B6 f Complex. *J. Phys. Chem. B* **2014**, *118*, 6614–6625.

(185) Baymann, F.; Giusti, F.; Picot, D.; Nitschke, W. The c_i/b_H Moiety in the b_6f Complex Studied by EPR: A Pair of Strongly Interacting Hemes. *Proc. Natl. Acad. Sci. U. S. A.* **2007**, *104*, 519–524.

(186) Twigg, A. I.; Baniulis, D.; Cramer, W. A.; Hendrich, M. P. EPR Detection of an O_2 Surrogate to Heme c_n of the Cytochrome b_6f Complex. *J. Am. Chem. Soc.* **2009**, *131*, 12536–12537.

(187) Pierre, Y.; Breyton, C.; Lemoine, Y.; Robert, B.; Vernotte, C.; Popot, J. L. On the Presence and Role of a Molecule of Chlorophyll α in the Cytochrome B6f Complex. *J. Biol. Chem.* **1997**, *272*, 21901–21908.

(188) Dashdorj, N.; Zhang, H.; Kim, H.; Yan, J.; Cramer, W. A.; Savikhin, S. The Single Chlorophyll a Molecule in the Cytochrome B6 f Complex: Unusual Optical Properties Protect the Complex against Singlet Oxygen. *Biophys. J.* **2005**, *88*, 4178–4187.

(189) Kim, H.; Dashdorj, N.; Zhang, H.; Yan, J.; Cramer, W. A.; Savikhin, S. An Anomalous Distance Dependence of Intraprotein Chlorophyll-Carotenoid Triplet Energy Transfer. *Biophys. J.* **2005**, *89*, L28–L30.

(190) Zhang, H.; Primak, A.; Cape, J.; Bowman, M. K.; Kramer, D. M.; Cramer, W. A. Characterization of the High-Spin Heme *x* in the Cytochrome b_6f Complex of Oxygenic Photosynthesis. *Biochemistry* **2004**, *43*, 16329–16336.

(191) Alric, J.; Pierre, Y.; Picot, D.; Lavergne, J.; Rappaport, F. Spectral and Redox Characterization of the Heme Ci of the Cytochrome B6f Complex. *Proc. Natl. Acad. Sci. U. S. A.* **2005**, *102*, 15860–15865.

(192) Girvin, M. E.; Cramer, W. A. A Redox Study of the Electron Transport Pathway Responsible for Generation of the Slow Electrochromic Phase in Chloroplasts. *BBA - Bioenerg.* **1984**, *767*, 29–38.

(193) Palmer, G.; Esposti, M. D. Application of Exciton Coupling Theory to the Structure of Mitochondrial Cytochrome *B*. *Biochemistry* **1994**, *33*, 176–185.

(194) Schoepp, B.; Chabaud, E.; Breyton, C.; Verméglio, A.; Popot, J. L. On the Spatial Organization of Hemes and Chlorophyll in Cytochrome B6f. A Linear and Circular Dichroism Study. *J. Biol. Chem.* **2000**, *275*, 5275–5283.

(195) Moser, C. C.; Keske, J. M.; Warncke, K.; Farid, R. S.; Dutton, P. L. Nature of Biological Electron Transfer. *Nature* **1992**, *355*, 796–802.

(196) Gray, H. B.; Winkler, J. R. Electron Transfer in Proteins. *Annu. Rev. Biochem.* **1996**, *65*, 537–561.

(197) Iwai, M.; Takizawa, K.; Tokutsu, R.; Okamuro, A.; Takahashi, Y.; Mnagawa, J.; Minagawa, J. Isolation of the Elusive Supercomplex That Drives Cyclic Electron Flow in Photosynthesis. *Nature* **2010**, *464*, 1210–1213.

(198) Bhaduri, S.; Zhang, H.; Erramilli, S.; Cramer, W. A. Structural and Functional Contributions of Lipids to the Stability and Activity of the Photosynthetic Cytochrome B6f Lipoprotein Complex. *J. Biol. Chem.* **2019**, *294*, 17758–17767.

(199) Hertle, A. P.; Blunder, T.; Wunder, T.; Pesaresi, P.; Pribil, M.; Armbruster, U.; Leister, D. PGRL1 Is the Elusive Ferredoxin-Plastoquinone Reductase in Photosynthetic Cyclic Electron Flow. *Mol. Cell* **2013**, *49*, 511–523.

(200) Whitelegge, J. P.; Zhang, H.; Aguilera, R.; Taylor, R. M.; Cramer, W. A. Full Subunit Coverage Liquid Chromatography Electrospray Ionization Mass Spectrometry (LCMS+) of an Oligomeric Membrane Protein: Cytochrome b(6)f Complex from Spinach and the Cyanobacterium Mastigocladus Laminosus. *Mol. Cell. Proteomics* **2002**, *1*, 816–827.

(201) McKenzie, S. D.; Ibrahim, I. M.; Aryal, U. K.; Puthiyaveetil, S. Stoichiometry of Protein Complexes in Plant Photosynthetic Membranes. *Biochim. Biophys. Acta - Bioenerg.* **2020**, *1861*.

(202) Wikström, M. K. F.; Berden, J. A. Oxidoreduction of Cytochrome b in the Presence of Antimycin. *Biochim. Biophys. Acta* **1972**, *283*, 403–420.

(203) Trumpower, B. L. Function of the Iron-Sulfur Protein of the Cytochrome b-C1 Segment in Electron-Transfer and Energy-Conserving Reactions of the Mitochondrial Respiratory Chain. *BBA Rev. Bioenerg.* **1981**, *639*, 129–155.

(204) Wikstrom M. K.; Saraste, M. The Mitochondrial Respiratory Chain. In *New comprehensive biochemistry*; Elsevier, **1984**; pp 49–94.

(205) Rich, P. R. Mechanisms of Quinol Oxidation in Photosynthesis. *Photosynth. Res.* **1985**, *6*, 335–348.

(206) Crofts, A. R.; Holland, J. T.; Victoria, D.; Kolling, D. R. J.; Dikanov, S. A.; Gilbreth, R.; Lhee, S.; Kuras, R.; Guergova-Kuras, M. The Q-Cycle Reviewed: How Well Does a Monomeric Mechanism of the Bc_1 Complex Account for the Function of a Dimeric Complex? *Biochim. Biophys. Acta* **2008**, *1777*, 1001–1019.

(207) Crofts, A. R.; Berry, E. A. Structure and Function of the Cytochrome Bc_1 Complex of Mitochondria and Photosynthetic Bacteria. *Curr. Opin. Struct. Biol.* **1998**, *8*, 501–509.

(208) Iwaki, M.; Yakovlev, G.; Hirst, J.; Osyczka, A.; Dutton, P. L.; Marshall, D.; Rich, P. R. Direct Observation of Redox-Linked Histidine Protonation Changes in the Iron−sulfur Protein of the Cytochrome Bc_1 Complex by ATR-FTIR Spectroscopy. *Biochemistry* **2005**, *44*, 4230–4237.

(209) Cramer, W. A.; Savikhin, S.; Yan, J.; Yamashita, E. The Enigmatic Chlorophyll a Molecule in the Cytochrome B6f Complex. In *The Chloroplast*; Springer: Dordrecht, **2010**; pp 89–94.

(210) Cramer, W. A.; Baniulis, D.; Yamashita, E.; Zhang, H.; Zatsman, A. I.; Hendrich, M. P. Cytochrome B6f Complex, Colon Structure, Spectroscopy, and Function of Heme Cn n-Side Electron and Proton Transfer Reactions. *Photosynth. Protein Complexes A Struct. Approach* **2008**, 155–179.

(211) Baniulis, D.; Yamashita, E.; Zhang, H.; Hasan, S. S.; Cramer, W. A. Structure-Function of the Cytochrome B6f Complex. *Photochem. Photobiol.* **2008**, *84*, 1349–1358.

(212) Nitschke, W.; van Lis, R.; Schoepp-Cothenet, B.; Baymann, F. The “Green” Phylogenetic Clade of Rieske/Cytb Complexes. *Photosynth. Res.* **2010**, *104*, 347–355.

(213) Kallas, T. Cytochrome b 6 f Complex at the Heart of Energy Transduction and Redox Signaling. In *Photosynthesis*; Springer: Dordrecht, **2012**; pp 501–560.

(214) Dibrova, D. V.; Cherepanov, D. A.; Galperin, M. Y.; Skulachev, V. P.; Mulkidjanian, A. Y. Evolution of Cytochrome Bc Complexes: From Membrane-Anchored Dehydrogenases of

Ancient Bacteria to Triggers of Apoptosis in Vertebrates. *Biochim. Biophys. Acta - Bioenerg.* **2013**, *1827*, 1407–1427.

(215) Ten Brink, F.; Schoepp-Cothenet, B.; Van Lis, R.; Nitschke, W.; Baymann, F. Multiple Rieske/Cytb Complexes in a Single Organism. *Biochim. Biophys. Acta - Bioenerg.* **2013**, *1827*, 1392–1406.

(216) Cramer, W. A.; Hasan, S. S.; Yamashita, E. The Q Cycle of Cytochrome *Bc* Complexes: A Structure Perspective. *Biochim. Biophys. Acta* **2011**, *1807*, 788–802.

(217) Joliot, P.; Joliot, A. Mechanism of Electron Transfer in the Cytochrome b/f Complex of Algae: Evidence for a Semiquinone Cycle. *Proc. Natl. Acad. Sci. U. S. A.* **1994**, *91*, 1034–1038.

(218) Kramer, D. M.; Crofts, A. R. Re-Examination of the Properties and Function of the b Cytochromes of the Thylakoid Cytochrome Bf Complex. *Biochem. Biophys. Acta* **1994**, *1184*, 193–201.

(219) Deniau, C.; Rappaport, F. New Insights on the Proton Pump Associated with Cytochrome B6f Turnovers from the Study of H/D Substitution Effects on the Electrogenicity and Electron Transfer Reactions. *Biochemistry* **2000**, *39*, 3304–3310.

(220) Kramer, D. M.; Crofts, A. R. The Concerted Reduction of the High- and Low-Potential Chains of the Bf Complex by Plastoquinol. *BBA - Bioenerg.* **1993**, *1183*, 72–84.

(221) Finazzi, G.; Rappaport, F.; Furia, A.; Fleischmann, M.; Rochaix, J.-D.; Zito, F.; Forti, G. Involvement of State Transitions in the Switch between Linear and Cyclic Electron Flow in Chlamydomonas Reinhardtii. *EMBO Rep.* **2002**, *3*, 280–285.

(222) Böhme, H.; Cramer, W. A. Uncoupler-Dependent Decrease in Midpoint Potential of the Chloroplast Cytochrome B6. *BBA - Bioenerg.* **1973**, *325*, 275–283.

(223) Sacksteder, C. A.; Kanazawa, A.; Jacoby, M. E.; Kramer, D. M. The Proton to Electron Stoichiometry of Steady-State Photosynthesis in Living Plants: A Proton-Pumping Q Cycle Is Continuously Engaged. *Proc. Natl. Acad. Sci. U. S. A.* **2000**, *97*, 14283–14288.

(224) Cape, J. L.; Bowman, M. K.; Kramer, D. M. Understanding the Cytochrome Bc Complexes by What They Don't Do. The Q-Cycle at 30. *Trends Plant Sci.* **2006**, *11*, 46–55.

(225) Schobert, B.; Brown, L. S.; Lanyi, J. K. Crystallographic Structures of the M and N Intermediates of Bacteriorhodopsin: Assembly of a Hydrogen-Bonded Chain of Water Molecules between Asp-96 and the Retinal Schiff Base. *J. Mol. Biol.* **2003**, *330*, 553–570.

(226) Capitanio, G.; Martino, P. L.; Capitanio, N.; Papa, S. Redox Bohr Effects and the Role of Heme a in the Proton Pump of Bovine Heart Cytochrome c Oxidase. *Biochim. Biophys. Acta - Bioenerg.* **2011**, *1807*, 1287–1294.

(227) Arnon, D. I.; Allen, M. B.; Whatley, F. R. Photosynthesis by Isolated Chloroplasts. *Nature* **1954**, *174*, 394–396.

(228) Johnson, G. N. Cyclic Electron Transport in C3 Plants: Fact or Artefact? *J. Exp. Bot.* **2005**, *56*, 407–416.

(229) Steigmiller, S.; Turina, P.; Gräber, P. The Thermodynamic H+/ATP Ratios of the H+-ATPsynthases from Chloroplasts and Escherichia Coli. *Proc. Natl. Acad. Sci. U. S. A.* **2008**, *105*, 3745–3750.

(230) Allen, J. F. Photosynthesis of ATP-Electrons, Proton Pumps, Rotors, and Poise. *Cell* **2002**, *110*, 273–276.

(231) Peltier, G.; Aro, E.-M.; Shikanai, T. NDH-1 and NDH-2 Plastoquinone Reductases in Oxygenic Photosynthesis. *Annu. Rev. Plant Biol.* **2016**, *67*, 55–80.

(232) Desplats, C.; Mus, F.; Cuiné, S.; Billon, E.; Cournac, L.; Peltier, G. Characterization of Nda2, a Plastoquinone-Reducing Type II NAD (P) H Dehydrogenase in Chlamydomonas Chloroplasts. *J. Biol. Chem.* **2009**, *284*, 4148–4157.

(233) Bendall, D. S.; Manasse, R. S. Cyclic Photophosphorylation and Electron Transport. *Biochim. Biophys. Acta* **1995**, *1229*, 23–38.

(234) Sugimoto, K.; Okegawa, Y.; Tohri, A.; Long, T. A.; Covert, S. F.; Hisabori, T.; Shikanai, T. A Single Amino Acid Alteration in PGR5 Confers Resistance to Antimycin a in Cyclic Electron Transport around PSI. *Plant Cell Physiol.* **2013**, *54*, 1525–1534.

(235) Munekage, Y.; Hojo, M.; Meurer, J.; Endo, T.; Tasaka, M.; Shikanai, T. PGR5 Is Involved in Cyclic Electron Flow around Photosystem I and Is Essential for Photoprotection in Arabidopsis. *Cell* **2002**, *110*, 361–371.

(236) DalCorso, G.; Pesaresi, P.; Masiero, S.; Aseeva, E.; Schünemann, D.; Finazzi, G.; Joliot, P.; Barbato, R.; Leister, D. A Complex Containing PGRL1 and PGR5 Is Involved in the Switch between Linear and Cyclic Electron Flow in Arabidopsis. *Cell* **2008**, *132*, 273–285.

(237) Crane, F. L.; Hatefi, Y.; Lester, R. L.; Widmer, C. Isolation of a Quinone from Beef Heart Mitochondria. *Biochim. Biophys. Acta* **1957**, *25*, 220–221.

(238) Crane, F. L. Discovery of Ubiquinone (Coenzyme Q) and an Overview of Function. *Mitochondrion* **2007**, *7*, S2–S7.

(239) Ernster, L.; Lee, I.-Y.; Norling, B.; Persson, B. Studies with Ubiquinone-Depleted Submitochondrial Particles. Essentiality of Ubiquinone for the Interaction of Succinate Dehydrogenase, NADH Dehydrogenase, and Cytochrome B. *Eur. J. Biochem.* **1969**, *9*, 299–310.

(240) Schoepp-Cothenet, B.; Lieutaud, C.; Baymann, F.; Verméglio, A.; Friedrich, T.; Kramer, D. M.; Nitschke, W. Menaquinone as Pool Quinone in a Purple Bacterium. *Proc. Natl. Acad. Sci. U. S. A.* **2009**, *106*, 8549–8554.

(241) Nowicka, B.; Kruk, J. Occurrence, Biosynthesis and Function of Isoprenoid Quinones. *Biochim. Biophys. Acta* **2010**, *1797*, 1587–1605.

(242) Rich, P. R.; Harper, R. Partition Coefficients of Quinones and Hydroquinones and Their Relation to Biochemical Reactivity. *FEBS Lett.* **1990**, *269*, 139–144.

(243) Rich, P. R. Electron and Proton Transfers in Chemical and Biological Quinone Systems. *Faraday Discuss. Chem. Soc.* **1982**, *74*, 349–364.

(244) Zhu, Z.; Gunner, M. R. Energetics of Quinone-Dependent Electron and Proton Transfers in Rhodobacter Sphaeroides Photosynthetic Reaction Centers. *Biochemistry* **2005**, *44*, 82–96.

(245) Robertson, D. E.; Prince, R. C.; Bowyer, J. R.; Matsuura, K.; Dutton, P. L.; Ohnishi, T. Thermodynamic Properties of the Semiquinone and Its Binding Site in the Ubiquinol-Cytochrome c (C2) Oxidoreductase of Respiratory and Photosynthetic Systems. *J. Biol. Chem.* **1984**, *259*, 1758–1763.

(246) Song, Y.; Buettner, G. R. Thermodynamic and Kinetic Considerations for the Reaction of Semiquinone Radicals to Form Superoxide and Hydrogen Peroxide. *Free Radic. Biol. Med.* **2010**, *49*, 919–962.

(247) Song, Y.; Buettner, G. R.; Parkin, S.; Wagner, B. A.; Robertson, L. W.; Lehmler, H.-J. Chlorination Increases the Persistence of Semiquinone Free Radicals Derived from Polychlorinated Biphenyl Hydroquinones and Quinones. *J. Org. Chem.* **2008**, *73*, 8296–8304.

(248) Cape, J. L.; Aidasani, D.; Kramer, D. M.; Bowman, M. K. Substrate Redox Potential Controls Superoxide Production Kinetics in the Cytochrome *Bc* Complex. *Biochemistry* **2009**, *48*, 10716–10723.

(249) Gunner, M. R.; Madeo, J.; Zhu, Z. Modification of Quinone Electrochemistry by the Proteins in the Biological Electron Transfer Chains: Examples from Photosynthetic Reaction Centers. *J. Bioenerg. Biomembr.* **2008**, *40*, 509–519.

(250) Roginsky, V.; Barsukova, T. Kinetics of Oxidation of Hydroquinones by Molecular Oxygen. Effect of Superoxide Dismutase. *J. Chem. Soc. Perkin Trans. 2* **2000**, No. 7, 1575–1582.

(251) Butler, J.; Hoey, B. M.; Swallow, A. J. Reactions of the Semiquinone Free Radicals of Anti-Tumour Agents with Oxygen and Iron Complexes. *FEBS Lett.* **1985**, *182*, 95–98.

(252) Dohrmann, J. K.; Bergmann, B. Equilibria and Rates of Redox Reactions Involving the 2-Tert-Butyl-1,4-Benzosemiquinone Radical in Aqueous Solution: An Investigation by Potentiometry, ESR, and Pulse Radiolysis. *J. Phys. Chem.* **1995**, *99*, 1218–1227.

(253) Valgimigli, L.; Amorati, R.; Funo, M. G.; DiLabio, G. A.; Pedulli, G. F.; Ingold, K. U.; Pratt, D. A. The Unusual Reaction of Semiquinone Radicals with Molecular Oxygen. *J. Org. Chem.* **2008**, *73*, 1830–1841.

(254) Turrens, J. F.; Alexandre, A.; Lehninger, A. L. Ubisemiquinone Is the Electron Donor for Superoxide Formation by Complex III of Heart Mitochondria. *Arch. Biochem. Biophys.* **1985**, *237*, 408–414.

(255) Pereverzev, M. O.; Vygodina, T. V; Konstantinov, A. A.; Skulachev, V. P. Cytochrome *c*, an Ideal Antioxidant. *Biochem. Soc. Trans.* **2003**, *31*, 1312–1315.

(256) Takahashi, M. A.; Kono, Y.; Asada, K. Reduction of Plastocyanin with O_2^- and Superoxide Dismutase-Dependent Oxidation of Plastocyanin by H_2O_2. *Plant Cell Physiol.* **1980**, *21*, 1431–1438.

(257) Wikström, M.; Krab, K.; Sharma, V. Oxygen Activation and Energy Conservation by Cytochrome c Oxidase. *Chem. Rev.* **2018**, *118*, 2469–2490.

(258) Pietras, R.; Sarewicz, M.; Osyczka, A. Distinct Properties of Semiquinone Species Detected at the Ubiquinol Oxidation Qo Site of Cytochrome Bc1 and Their Mechanistic Implications. *J. R. Soc. Interface* **2016**, *13*, 1–11.

(259) Osyczka, A.; Moser, C. C.; Dutton, P. L. Fixing the Q Cycle. *Trends Biochem. Sci.* **2005**, *30*, 176–182.

(260) Ding, H.; Moser, C. C.; Robertson, D. E.; Tokito, M. K.; Daldal, F.; Dutton, P. L. Ubiquinone Pair in the Q_o Site Central to the Primary Energy Conversion Reactions of Cytochrome Bc_1 Complex. *Biochemistry* **1995**, *34*, 15979–15996.

(261) Cape, J. L.; Bowman, M. K.; Kramer, D. M. A Semiquinone Intermediate Generated at the Q_o Site of the Cytochrome Bc_1 Complex: Importance for the Q-Cycle and Superoxide Production. *Proc. Natl. Acad. Sci. U. S. A.* **2007**, *104*, 7887–7892.

(262) Zhang, H.; Osyczka, A.; Dutton, P. L.; Moser, C. C. Exposing the Complex III Q_o Semiquinone Radical. *Biochim. Biophys. Acta* **2007**, *1767*, 883–887.

(263) Sarewicz, M.; Dutka, M.; Pintscher, S.; Osyczka, A. Triplet State of the Semiquinone-Rieske Cluster as an Intermediate of Electronic Bifurcation Catalyzed by Cytochrome Bc_1. *Biochemistry* **2013**, *52*, 6388–6395.

(264) Vennam, P. R.; Fisher, N.; Krzyaniak, M. D.; Kramer, D. M.; Bowman, M. K. A Caged, Destabilized, Free Radical Intermediate in the Q-Cycle. *ChemBioChem* **2013**, *14*, 1745–1753.

(265) Rich, P. R. Electron Transfer Reactions between Quinols and Quinones in Aqueous and Aprotic Media. *Biochim. Biophys. Acta* **1981**, *637*, 28–33.

(266) Kruk, J.; Karpinski, S. An HPLC-Based Method of Estimation of the Total Redox State of Plastoquinone in Chloroplasts, the Size of the Photochemically Active Plastoquinone-Pool and Its Redox State in Thylakoids of Arabidopsis. *Biochim. Biophys. Acta - Bioenerg.* **2006**, *1757*, 1669–1675.

(267) Block, A.; Fristedt, R.; Rogers, S.; Kumar, J.; Barnes, B.; Barnes, J.; Elowsky, C. G.; Wamboldt, Y.; Mackenzie, S. A.; Redding, K.; Merchant, S. S.; Basset, G. J. Functional Modeling Identifies Paralogous Solanesyl-Diphosphate Synthases That Assemble the Side Chain of Plastoquinone-9 in Plastids. *J. Biol. Chem.* **2013**, *288*, 27594–27606.

(268) Ksas, B.; Légeret, B.; Ferretti, U.; Chevalier, A.; Pospíšil, P.; Alric, J.; Havaux, M. The Plastoquinone Pool Outside the Thylakoid Membrane Serves in Plant Photoprotection as a Reservoir of Singlet Oxygen Scavengers. *Plant Cell Environ.* **2018**, *41*, 2277–2287.

(269) Zbierzak, A. M.; Kanwischer, M.; Wille, C.; Vidi, P. A.; Giavalisco, P.; Lohmann, A.; Briesen, I.; Porfirova, S.; Bréhélin, C.; Kessler, F.; Dörmann, P. Intersection of the Tocopherol and Plastoquinol Metabolic Pathways at the Plastoglobule. *Biochem. J.* **2010**, *425*, 389–399.

(270) Ksas, B.; Becuwe, N.; Chevalier, A.; Havaux, M. Plant Tolerance to Excess Light Energy and Photooxidative Damage Relies on Plastoquinone Biosynthesis. *Sci. Rep.* **2015**, *5*, 10919.

(271) Blackwell, M.; Gibas, C.; Gygax, S.; Roman, D.; Wagner, B. The Plastoquinone Diffusion Coefficient in Chloroplasts and Its Mechanistic Implications. *Biochim. Biophys. Acta* **1994**, *1183*, 533–543.

(272) Lavergne, J.; Joliot, P. Restricted Diffusion in Photosynthetic Membranes. *Trends Biochem. Sci.* **1991**, *16*, 129–134.

(273) Kirchhoff, H. Diffusion of Molecules and Macromolecules in Thylakoid Membranes. *Biochim. Biophys. Acta - Bioenerg.* **2014**, *1837*, 495–502.

(274) Lemeille, S.; Rochaix, J. D. State Transitions at the Crossroad of Thylakoid Signalling Pathways. *Photosynth. Res.* **2010**, *106*, 33–46.

(275) Pfannschmidt, T. Chloroplast Redox Signals: How Photosynthesis Controls Its Own Genes. *Trends Plant Sci.* **2003**, *8*, 33–41.

(276) Lundquist, P. K.; Poliakov, A.; Bhuiyan, N. H.; Zybailov, B.; Sun, Q.; van Wijk, K. J. The Functional Network of the Arabidopsis Plastoglobule Proteome Based on Quantitative Proteomics and Genome-Wide Coexpression Analysis. *Plant Physiol.* **2012**, *158*, 1172–1192.

(277) Shikanai, T.; Munekage, Y.; Shimizu, K.; Endo, T.; Hashimoto, T. Identification and Characterization of Arabidopsis Mutants with Reduced Quenching of Chlorophyll Fluorescence. *Plant Cell Physiol.* **1999**, *40*, 1134–1142.

(278) Pralon, T.; Shanmugabalaji, V.; Longoni, P.; Glauser, G.; Ksas, B.; Collombat, J.; Desmeules, S.; Havaux, M.; Finazzi, G.; Kessler, F. Plastoquinone Homoeostasis by Arabidopsis Proton Gradient Regulation 6 Is Essential for Photosynthetic Efficiency. *Commun. Biol.* **2019**, *2*.

(279) Pralon, T.; Collombat, J.; Pipitone, R.; Ksas, B.; Shanmugabalaji, V.; Havaux, M.; Finazzi, G.; Longoni, P.; Kessler, F. Mutation of the Atypical Kinase ABC1K3 Partially Rescues the PROTON GRADIENT REGULATION 6 Phenotype in Arabidopsis Thaliana. *Front. Plant Sci.* **2020**, *11*, 337.

(280) Lefebvre-Legendre, L.; Rappaport, F.; Finazzi, G.; Ceol, M.; Grivet, C.; Hopfgartner, G.; Rochaix, J. D. Loss of Phylloquinone in Chlamydomonas Affects Plastoquinone Pool Size and Photosystem II Synthesis. *J. Biol. Chem.* **2007**, *282*, 13250–13263.

(281) Wikstrom M. K. Proton Pump Coupled to Cytochrome c Oxidase in Mitochondria. *Nature* **1977**, *266*, 673–678.

(282) Haehnel, W.; Pröpper, A.; Krause, H. Evidence for Complexed Plastocyanin as the Immediate Electron Donor of P-700. *Biochim. Biophys. Acta* **1980**, *593*, 384–399.

(283) Hatefi, Y.; Haavik, A. G.; Griffiths, D. E. Studies on the Electron Transfer System. XLI. Reduced Coenzyme Q (QH2)-Cytochrome c Reductase. *J. Biol. Chem.* **1962**, *237*, 1681–1685.

(284) Myllykallio, H.; Drepper, F.; Mathis, P.; Daldal, F. Membrane-Anchored Cytochrome c_y Mediated Microsecond Time Range Electron Transfer from the Cytochrome Bc_1 Complex to the Reaction Center in *Rhodobacter Capsulatus*. *Biochemistry* **1998**, *37*, 5501–5510.

(285) Myllykallio, H.; Zannoni, D.; Daldal, F. The Membrane-Attached Electron Carrier Cytochrome c_y from *Rhodobacter Sphaeroides* Is Functional in Respiratory but Not in Photosynthetic Electron Transfer. *Proc. Natl. Acad. Sci. U. S. A.* **1999**, *96*, 4348–4353.

(286) Cartron, M. L.; Olsen, J. D.; Sener, M.; Jackson, P. J.; Brindley, A. A.; Qian, P.; Dickman, M. J.; Leggett, G. J.; Schulten, K.; Hunter, C. N. Integration of Energy and Electron Transfer Processes in the Photosynthetic Membrane of *Rhodobacter Sphaeroides*. *Biochim. Biophys. Acta - Bioenerg.* **2014**, *1837*, e118.

(287) Ki Ho, K.; Krogmann, D. W. Cytochrome f from Spinach and Cyanobacteria. Purification and Characterization. *J. Biol. Chem.* **1980**, *255*, 3855–3861.

(288) Niwa, S.; Ishikawa, H.; Nikai, S.; Takabe, T. Electron Transfer Reactions between Cytochrome f and Plastocyanin from Brassica Komatsuna. *J. Biochem.* **1980**, *88*, 1177–1183.

(289) De La Rosa, M. A.; Navarro, J. A.; Díaz-Quintana, A.; De La Cerda, B.; Molina-Heredia, F. P.; Balme, A.; Murdoch, P. D. S.; Díaz-Moreno, I.; Durán, R. V.; Hervás, M. An Evolutionary Analysis of the Reaction Mechanisms of Photosystem I Reduction by Cytochrome C6 and Plastocyanin. *Bioelectrochemistry* **2002**, *55*, 41–45.

(290) Molina-Heredia, F. P.; Balme, A.; Hervás, M.; Navarro, J. A.; De la Rosa, M. A. A Comparative Structural and Functional Analysis of Cytochrome CM, Cytochrome C6 and Plastocyanin from the Cyanobacterium Synechocystis Sp. PCC 6803. *FEBS Lett.* **2002**, *517*, 50–54.

(291) Merchant, S.; Bogorad, L. Rapid Degradation of Apoplastocyanin in Cu(II)-Deficient Cells of Chlamydomonas Reinhardtii. *J. Biol. Chem.* **1986**, *261*, 15850–15853.

(292) Gupta, R.; He, Z.; Luan, S. Functional Relationship of Cytochrome C6 and Plastocyanin in Arabidopsis. *Nature* **2002**, *417*, 567–571.

(293) Díaz-Quintana, A.; Navarro, J. A.; Hervás, M.; Molina-Heredia, F. P.; De La Cerda, B.; De La Rosa, M. A. A Comparative Structural and Functional Analysis of Cyanobacterial Plastocyanin and Cytochrome C6 as Alternative Electron Donors to Photosystem I: Photosystem I Reduction in Cyanobacteria. *Photosynth. Res.* **2003**, *75*, 97–110.

(294) Liu, J.; Chakraborty, S.; Hosseinzadeh, P.; Yu, Y.; Tian, S.; Petrik, I.; Bhagi, A.; Lu, Y. Metalloproteins Containing Cytochrome, Iron-Sulfur, or Copper Redox Centers. *Chem. Rev.* **2014**, *114*, 4366–4369.

(295) Alvarez-Paggi, D.; Hannibal, L.; Castro, M. A.; Oviedo-Rouco, S.; Demicheli, V.; Tórtora, V.; Tomasina, F.; Radi, R.; Murgida, D. H. Multifunctional Cytochrome c: Learning New Tricks from an Old Dog. *Chem. Rev.* **2017**, *117*, 13382–13460.

(296) Barker, P. D.; Ferguson, S. J. Still a Puzzle: Why Is Haem Covalently Attached in c-Type Cytochromes? *Structure* **1999**, *7*.

(297) Dolla, A.; Blanchard, L.; Guerlesquin, F.; Bruschi, M. The Protein Moiety Modulates the Redox Potential in Cytochromes C. *Biochimie* **1994**, *76*, 471–479.

(298) Margalit, R.; Schejter, A. Cytochrome c: A Thermodynamic Study of the Relationships among Oxidation State, Ion-Binding and Structural Parameters: 1. The Effects of Temperature, PH and Electrostatic Media on the Standard Redox Potential of Cytochrome C. *Eur. J. Biochem.* **1973**, *32*, 492–499.

(299) Moore, G. R.; Harris, D. E.; Leitch, F. A.; Pettigrew, G. W. Characterisation of Ionisations That Influence the Redox Potential of Mitochondrial Cytochrome c and Photosynthetic Bacterial Cytochromes C2. *BBA - Bioenerg.* **1984**, *764*, 331–342.

(300) Daldal, F.; Mandaci, S.; Winterstein, C.; Myllykallio, H.; Duyck, K.; Zannoni, D. Mobile Cytochrome C2 and Membrane-Anchored Cytochrome Cy Are Both Efficient Electron Donors to the Cbb3- and Aa3-Type Cytochrome c Oxidases during Respiratory Growth of Rhodobacter Sphaeroides. *J. Bacteriol.* **2001**, *183*, 2013–2024.

(301) Howe, C. J.; Schlarb-Ridley, B. G.; Wastl, J.; Purton, S.; Bendall, D. S. The Novel Cytochrome C6 of Chloroplasts: A Case of Evolutionary Bricolage? *J. Exp. Bot.* **2006**, *57*, 13–22.

(302) S. D'Arcy, M. Cell Death: A Review of the Major Forms of Apoptosis, Necrosis and Autophagy. *Cell Biol. Int.* **2019**, *43*, 582–592.

(303) Margoliash, E. Primay Structure and Evolution of Cytochrome *C*. *Proc. Natl. Acad. Sci.* **1963**, *50*, 672–679.

(304) Ambler, R. P. Sequence Variability in Bacterial Cytochromes C. *BBA - Bioenerg.* **1991**, *1058*, 42–47.

(305) Dickerson, R. E.; Timkovich, R.; Almassy, R. J. The Cytochrome Fold and the Evolution of Bacterial Energy Metabolism. *J. Mol. Biol.* **1976**, *100*, 473–491.

(306) Latypov, R. F.; Maki, K.; Cheng, H.; Luck, S. D.; Roder, H. Folding Mechanism of Reduced Cytochrome c: Equilibrium and Kinetic Properties in the Presence of Carbon Monoxide. *J. Mol. Biol.* **2008**, *383*, 437–453.

(307) Droghetti, E.; Oellerich, S.; Hildebrandt, P.; Smulevich, G. Heme Coordination States of Unfolded Ferrous Cytochrome C. *Biophys. J.* **2006**, *91*, 3022–3031.

(308) Urry, D. W. The Heme Chromophore in the Ultraviolet. *J. Biol. Chem.* **1967**, *242*, 4441–4448.

(309) Brautigan, D. L.; Feinberg, B. A.; Hoffman, B. M.; Margoliash, E.; Peisach, J.; Blumberg, W. E.; Peisach, J.; Blumberg, W. E. Multiple Low Spin Forms of the Cytochrome c Ferrihemochrome. *J. od Biol. Chem.* **1977**, *252*, 574–582.

(310) Harbitz, E.; Andersson, K. K. Cytochrome C-554 from Methylosinus Trichosporium OB3b; a Protein That Belongs to the Cytochrome C2 Family and Exhibits a HALS-Type EPR Signal. *PLoS One* **2011**, *6*.

(311) Tomášková, N.; Varhač, R.; Lysáková, V.; Musatov, A.; Sedlák, E. Peroxidase Activity of Cytochrome c in Its Compact State Depends on Dynamics of the Heme Region. *Biochim. Biophys. Acta - Proteins Proteomics* **2018**, *1866*, 1073–1083.

(312) Ranieri, A.; Bernini, F.; Bortolotti, C. A.; Bonifacio, A.; Sergo, V.; Castellini, E. PH-Dependent Peroxidase Activity of Yeast Cytochrome c and Its Triple Mutant Adsorbed on Kaolinite. *Langmuir* **2011**, *27*, 10683–10690.

(313) Muenzner, J.; Pletneva, E. V. Structural Transformations of Cytochrome c upon Interaction with Cardiolipin. *Chem. Phys. Lipids* **2014**, *179*, 57–63.

(314) Engstrom, G.; Rajagukguk, R.; Saunders, A. J.; Patel, C. N.; Rajagukguk, S.; Merbitz-Zahradnik, T.; Xiao, K.; Pielak, G. J.; Trumpower, B.; Yu, C.-A.; Yu, L.; Durham, B.; Millett, F. Design of a Ruthenium-Labeled Cytochrome *c* Derivative to Study Electron Transfer with the Cytochrome Bc_1 Complex. *Biochemistry* **2003**, *42*, 2816–2824.

(315) Hall, J.; Kriaucionas, A.; Knaff, D. B.; Millett, F. The Reaction Domain on *Rhodospirillum Rubrum* Cytochrome c_2 and Horse Cytochrome *c* for the *Rhodospirillum Rubrum* Cytochrome Bc_1 Complex. *J. Biol. Chem.* **1987**, *262*, 14005–14009.

(316) Speck, S. H.; Dye, D.; Margoliash, E. Single Catalytic Site Model for the Oxidation of Ferrocytochrome c by Mitochondrial Cytochrome c Oxidase. *Proc. Natl. Acad. Sci. U. S. A.* **1984**, *81*, 347–351.

(317) Yu, C. A.; Yu, L.; King, T. E. Kinetics of Electron Transfer between Cardiac Cytochrome C1 and C. *J. Biol. Chem.* **1973**, *248*, 528–533.

(318) Güner, S.; Willie, A.; Millett, F.; Caffrey, M. S.; Cusanovich, M. A.; Robertson, D. E.; Knaff, D. B. The Interaction between Cytochrome C2 and the Cytochrome Bc1 Complex in the Photosynthetic Purple Bacteria Rhodobacter Capsulatus and Rhodopseudomonas Viridis. *Biochemistry* **1993**, *32*, 4793–4800.

(319) Janzon, J.; Eichhorn, A. C.; Ludwig, B.; Malatesta, F. Electron Transfer Kinetics between Soluble Modules of Paracoccus Denitrificans Cytochrome C1 and Its Physiological Redox Partners. *Biochim. Biophys. Acta - Bioenerg.* **2008**, *1777*, 250–259.

(320) Bosshard, H. R.; Wynn, R. M.; Knaff, D. B. Binding Site on *Rhodospirillum Rubrum* Cytochrome c_2 for the *Rhodospirillum Rubrum* Cytochrome Bc_1 Complex. *Biochemistry* **1987**, *26*, 7688–7693.

(321) Li, J.; Osyczka, A.; Conover, R. C.; Johnson, M. K.; Qin, H.; Daldal, F.; Knaff, D. B. Role of Acidic and Aromatic Amino Acids in *Rhodobacter Capsulatus* Cytochrome c_1. A Site-Directed Mutagenesis Study. *Biochemistry* **2003**, *42*, 8818–8830.

(322) Stonehuerner, J.; O'Brien, P.; Geren, L.; Millett, F.; Steidl, J.; Yu, L.; Yun, C.-A. Identification of the Binding Site on Cytochrome c_1 for Cytochrome *C*. *J. Biol. Chem.* **1985**, *260*, 5392–5398.

(323) Tian, H.; Sadoski, R.; Zhang, L.; Yu, C.-A.; Yu, L.; Durham, B.; Millett, F. Definition of the Interaction Domain for Cytochrome *c* on the Cytochrome Bc_1 Complex. *J. Biol. Chem.* **2000**, *275*, 9587–9595.

(324) Rieder, R.; Bosshard, H. R. Comparison of the Binding Sites on Cytochrome c for Cytochrome c Oxidase, Cytochrome Bc1, and Cytochrome C1. Differential Acetylation of Lysyl Residues in Free and Complexed Cytochrome C. *J. Biol. Chem.* **1980**, *255*, 4732–4739.

(325) Ahmed, A. J.; Smith, H. T.; Smith, M. B.; Millett, F. S. Effect of Specific Lysine Modification on the Reduction of Cytochrome c by Succinate-Cytochrome c Reductase. *Biochemistry* **1978**, *17*, 2479–2483.

(326) Sarewicz, M.; Pietras, R.; Froncisz, W.; Osyczka, A. Reorientation of Cytochrome c_2 upon Interaction with Oppositely Charged Macromolecules Probed by SR EPR: Implications for the Role of Dipole Moment to Facilitate Collisions in Proper Configuration for Electron Transfer. *Metallomics* **2011**, *3*, 404–409.

(327) Hunte, C.; Solmaz, S.; Lange, C. Electron Transfer between Yeast Cytochrome Bc_1 Complex and Cytochrome *c*: A Structural Analysis. *Biochim. Biophys. Acta* **2002**, *1555*, 21–28.

(328) Kokhan, O.; Wraight, C. A.; Tajkhorshid, E. The Binding Interface of Cytochrome c and Cytochrome C1 in the Bc1 Complex: Rationalizing the Role of Key Residues. *Biophys. J.* **2010**, *99*, 2647–2656.

(329) Castellani, M.; Covian, R.; Kleinschroth, T.; Anderka, O.; Ludwig, B.; Trumpower, B. L. Direct Demonstration of Half-of-the-Sites Reactivity in the Dimeric Cytochrome Bc_1 Complex. *J. Biol. Chem.* **2010**, *285*, 502–510.

(330) Devanathan, S.; Salamon, Z.; Tollin, G.; Fitch, J. C.; Meyer, T. E.; Berry, E. A.; Cusanovich, M. A. Plasmon Waveguide Resonance Spectroscopic Evidence for Differential Binding of Oxidized and Reduced Rhodobacter Capsulatus Cytochrome C2 to the Cytochrome Bc1 Complex Mediated by the Conformation of the Rieske Ir. *Biochemistry* **2007**, *46*, 7138–7145.

(331) Moreno-Beltrán, B.; Díaz-Quintana, A.; González-Arzola, K.; Velázquez-Campoy, A.; De La Rosa, M. A.; Díaz-Moreno, I. Cytochrome C1 Exhibits Two Binding Sites for Cytochrome c in Plants. *Biochim. Biophys. Acta - Bioenerg.* **2014**, *1837*, 1717–1729.

(332) Pietras, R.; Sarewicz, M.; Osyczka, A. Molecular Organization of Cytochrome c_2 near the Binding Domain of Cytochrome Bc_1 Studied by Electron Spin-Lattice Relaxation Enhancement. *J. Phys. Chem. B* **2014**, *118*, 6634–6643.

(333) Moreno-Beltrán, B.; Díaz-Moreno, I.; González-Arzola, K.; Guerra-Castellano, A.; Velázquez-Campoy, A.; De La Rosa, M. A.; Díaz-Quintana, A. Respiratory Complexes III and IV Can Each Bind Two Molecules of Cytochrome c at Low Ionic Strength. *FEBS Lett.* **2015**, *589*, 476–483.

(334) Sarewicz, M.; Borek, A.; Daldal, F.; Froncisz, W.; Osyczka, A. Demonstration of Short-Lived Complexes of Cytochrome *c* with Cytochrome Bc_1 by EPR Spectroscopy: Implications for the Mechanism of Interprotein Electron Transfer. *J. Biol. Chem.* **2008**, *283*, 24826–24836.

(335) Carrell, C. J.; Schlarb, B. G.; Bendall, D. S.; Howe, C. J.; Cramer, W. A.; Smith, J. L. Structure of the Soluble Domain of Cytochrome *f* from the Cyanobacterium *Phormidium Laminosum*. *Biochemistry* **1999**, *38*, 9590–9599.

(336) Chi, Y.-I.; Huang, L.-S.; Zhang, Z.; Fernández-Velasco, J. G.; Berry, E. A. X-Ray Structure of a Truncated Form of Cytochrome f from Chlamydomonas Reinhardtii † , ‡. *Biochemistry* **2000**, *39*, 7689–7701.

(337) Cramer, W. A.; Martinez, S. E.; Huang, D.; Tae, G. S.; Everly, R. M.; Heymann, J. B.; Cheng, R. H.; Baker, T. S.; Smith, J. L. Structural Aspects of the Cytochrome B6f Complex; Structure of the Lumen-Side Domain of Cytochrome F. *J. Bioenerg. Biomembr.* **1994**, *26*, 31–47.

(338) Gong, X. S.; Wen, J. Q.; Fisher, N. E.; Young, S.; Howe, C. J.; Bendall, D. S.; Gray, J. C. The Role of Individual Lysine Residues in the Basic Patch on Turnip Cytochrome f for Electrostatic Interactions with Plastocyanin in Vitro. *Eur. J. Biochem.* **2000**, *267*, 3461–3468.

(339) Soriano, G. M.; Ponamarev, M. V.; Piskorowski, R. A.; Cramer, W. A. Identification of the Basic Residues of Cytochrome f Responsible for Electrostatic Docking Interactions with Plastocyanin in Vitro: Relevance to the Electron Transfer Reaction in Vivo. *Biochemistry* **1998**, *37*, 15120–15128.

(340) Soriano, G. M.; Ponamarev, M. V.; Tae, G. S.; Cramer, W. A. Effect of the Interdomain Basic Region of Cytochrome f on Its Redox Reactions in Vivo. *Biochemistry* **1996**, *35*, 14590–14598.

(341) Albarrán, C.; Navarro, J. A.; De La Rosa, M. A.; Hervás, M. The Specificity in the Interaction between Cytochrome f and Plastocyanin from the Cyanobacterium Nostoc Sp. PCC 7119 Is Mainly Determined by the Copper Protein. *Biochemistry* **2007**, *46*, 997–1003.

(342) Schlarb-Ridley, B. G.; Bendall, D. S.; Howe, C. J. Role of Electrostatics in the Interaction between Cytochrome f and Plastocyanin of the Cyanobacterium Phormidium Laminosum. *Biochemistry* **2002**, *41*, 3279–3285.

(343) Bond, C. S.; Bendall, D. S.; Freeman, H. C.; Mitchell Guss, J.; Howe, C. J.; Wagner, M. J.; Wilce, M. C. J. The Structure of Plastocyanin from the Cyanobacterium Phormidium Laminosum. *Acta Crystallogr. Sect. D Biol. Crystallogr.* **1999**, *55*, 414–421.

(344) Collyer, C. A.; Guss, J. M.; Sugimura, Y.; Yoshizaki, F.; Freeman, H. C. Crystal Structure of Plastocyanin from a Green Alga, Enteromorpha Prolifera. *J. Mol. Biol.* **1990**, *211*, 617–632.

(345) Mitchell Guss, J.; Freeman, H. C. Structure of Oxidized Poplar Plastocyanin at 1·6 Å Resolution. *J. Mol. Biol.* **1983**, *169*, 521–563.

(346) Schmidt, L.; Christensen, H. E. M.; Harris, P. Structure of Plastocyanin from the Cyanobacterium Anabaena Variabilis. *Acta Crystallogr. Sect. D Biol. Crystallogr.* **2006**, *62*, 1022–1029.

(347) Díaz-Moreno, I.; Díaz-Quintana, A.; De La Rosa, M. A.; Crowley, P. B.; Ubbink, M. Different Modes of Interaction in Cyanobacterial Complexes of Plastocyanin and Cytochrome F. *Biochemistry* **2005**, *44*, 3176–3183.

(348) Crowley, P. B.; Otting, G.; Schlarb-Ridley, B. G.; Canters, G. W.; Ubbink, M. Hydrophobic Interactions in a Cyanobacterial Plastocyanin - Cytochrome f Complex. *J. Am. Chem. Soc.* **2001**, *123*, 10444–10453.

(349) Ubbink, M.; Ejdebäck, M.; Karlsson, B. G.; Bendall, D. S. The Structure of the Complex of Plastocyanin and Cytochrome f, Determined by Paramagnetic NMR and Restrained Rigid-Body Molecular Dynamics. *Structure* **1998**, *6*, 323–335.

(350) Ueda, T.; Nomoto, N.; Koga, M.; Ogasa, H.; Ogawa, Y.; Matsumoto, M.; Stampoulis, P.; Sode, K.; Terasawa, H.; Shimadaa, I. Structural Basis of Efficient Electron Transport between Photosynthetic Membrane Proteins and Plastocyanin in Spinach Revealed Using Nuclear Magnetic Resonance. *Plant Cell* **2012**, *24*, 4173–4186.

(351) Lange, C.; Cornvik, T.; Díaz-Moreno, I.; Ubbink, M. The Transient Complex of Poplar Plastocyanin with Cytochrome f: Effects of Ionic Strength and PH. *Biochim. Biophys. Acta - Bioenerg.* **2005**, *1707*, 179–188.

(352) Mayneord, G. E.; Vasilev, C.; Malone, L. A.; Swainsbury, D. J. K.; Hunter, C. N.; Johnson, M. P. Single-Molecule Study of Redox Control Involved in Establishing the Spinach Plastocyanin-Cytochrome B6f Electron Transfer Complex. *Biochim. Biophys. Acta - Bioenerg.* **2019**, *1860*, 591–599.

(353) Fedorov, V. A.; Kovalenko, I. B.; Khruschev, S. S.; Ustinin, D. M.; Antal, T. K.; Riznichenko, G. Y.; Rubin, A. B. Comparative Analysis of Plastocyanin–Cytochrome f Complex Formation in Higher Plants, Green Algae and Cyanobacteria. *Physiol. Plant.* **2019**, *166*, 320–335.

(354) Ramos, S.; Le Sueur, A. L.; Horness, R. E.; Specker, J. T.; Collins, J. A.; Thibodeau, K. E.; Thielges, M. C. Heterogeneous and Highly Dynamic Interface in Plastocyanin-Cytochrome f Complex Revealed by Site-Specific 2D-IR Spectroscopy. *J. Phys. Chem. B* **2019**, *123*, 2114–2122.

(355) Díaz-Moreno, I.; Díaz-Quintana, A.; De la Rosa, M. A.; Ubbink, M. Structure of the Complex between Plastocyanin and Cytochrome f from the Cyanobacterium Nostoc Sp. PCC 7119 as Determined by Paramagnetic NMR. The Balance between Electrostatic and Hydrophobic Interactions within the Transient Complex Determines the Relati. *J. Biol. Chem.* **2005**, *280*, 18908–18915.

(356) Crowley, P. B.; Hunter, D. M.; Sato, K.; McFarlane, W.; Dennison, C. The Parsley Plastocyanin-Turnip Cytochrome f Complex: A Structurally Distorted but Kinetically Functional Acidic Patch. *Biochem. J.* **2004**, *378*, 45–51.

(357) Gross, E. L.; Rosenberg, I. A Brownian Dynamics Study of the Interaction of Phormidium Cytochrome f with Various Cyanobacterial Plastocyanins. *Biophys. J.* **2006**, *90*, 366–380.

(358) Hulsker, R.; Baranova, M. V.; Bullerjahn, G. S.; Ubbink, M. Dynamics in the Transient Complex of Plastocyanin-Cytochrome f from Prochlorothrix Hollandica. *J. Am. Chem. Soc.* **2008**, *130*, 1985–1991.

(359) Díaz-Moreno, I.; Díaz-Quintana, A.; Díaz-Moreno, S.; Subías, G.; De la Rosa, M. A. Transient Binding of Plastocyanin to Its Physiological Redox Partners Modifies the Copper Site Geometry. *FEBS Lett.* **2006**, *580*, 6187–6194.

(360) Malkin, R.; Knaff, D. B.; Bearden, A. J. The Oxidation-Reduction Potential of Membrane-Bound Chloroplast Plastocyanin and Cytochrome F. *BBA - Bioenerg.* **1973**, *305*, 675–678.

(361) Albarrán, C.; Navarro, J. A.; Molina-Heredia, F. P.; Murdoch, P. D. S.; De La Rosa, M. A.; Hervás, M. Laser Flash-Induced Kinetic Analysis of Cytochrome f Oxidation by Wild-Type and Mutant Plastocyanin from the Cyanobacterium Nostoc Sp. PCC 7119. *Biochemistry* **2005**, *44*, 11601–11607.

(362) Hope, A. B. Electron Transfers amongst Cytochrome f, Plastocyanin and Photosystem I: Kinetics and Mechanisms. *Biochim. Biophys. Acta - Bioenerg.* **2000**, *1456*, 5–26.

(363) Torrado, A.; Ramírez-Moncayo, C.; Navarro, J. A.; Mariscal, V.; Molina-Heredia, F. P. Cytochrome C6 Is the Main Respiratory and Photosynthetic Soluble Electron Donor in Heterocysts of the Cyanobacterium Anabaena Sp. PCC 7120. *Biochim. Biophys. Acta - Bioenerg.* **2019**, *1860*, 60–68.

(364) Magnuson, A.; Cardona, T. Thylakoid Membrane Function in Heterocysts. *Biochim. Biophys. Acta - Bioenerg.* **2016**, *1857*, 309–319.

(365) Beißinger, M.; Sticht, H.; Sutter, M.; Ejchart, A.; Haehnel, W.; Rösch, P. Solution Structure of Cytochrome C6 from the Thermophilic Cyanobacterium Synechococcus Elongatus. *EMBO J.* **1998**, *17*, 27–36.

(366) Molina-Heredia, F. P.; Hervás, M.; Navarro, J. A.; De La Rosa, M. A. Cloning and Correct Expression in Escherichia Coli of the PetE and PetJ Genes Respectively Encoding Plastocyanin and Cytochrome C6 from the Cyanobacterium Anabaena Sp. PCC 7119. *Biochem. Biophys. Res. Commun.* **1998**, *243*, 302–306.

(367) Crowley, P. B.; Rabe, K. S.; Worrall, J. A. R.; Canters, G. W.; Ubbink, M. The Ternary Complex of Cytochrome f and Cytochrome c: Identification of a Second Binding Site and Competition for Plastocyanin Binding. *ChemBioChem* **2002**, *3*, 526–533.

(368) Gross, E. L.; Pearson, D. C. Brownian Dynamics Simulations of the Interaction of Chlamydomonas Cytochrome f with Plastocyanin and Cytochrome C6. *Biophys. J.* **2003**, *85*, 2055–2068.

(369) Díaz-Moreno, I.; Hulsker, R.; Skubak, P.; Foerster, J. M.; Cavazzini, D.; Finiguerra, M. G.; Díaz-Quintana, A.; Moreno-Beltrán, B.; Rossi, G. L.; Ullmann, G. M.; Pannu, N. S.; De La Rosa, M. A.; Ubbink, M. The Dynamic Complex of Cytochrome C6 and Cytochrome f Studied with Paramagnetic NMR Spectroscopy. *Biochim. Biophys. Acta - Bioenerg.* **2014**, *1837*, 1305–1315.

(370) Shin, M.; Tagawa, K.; Arnon, D. I. Crystallization of Ferredoxin-Tpn Reductase and Its Role in the Photosynthetic Apparatus of Chloroplasts. *Biochem. Z.* **1963**, *338*, 84–96.

(371) Carrillo, N.; Ceccarelli, E. A. Open Questions in Ferredoxin-NADP+ Reductase Catalytic Mechanism. *Eur. J. Biochem.* **2003**, *270*, 1900–1915.

(372) Cassan, N.; Lagoutte, B.; Sétif, P. Ferredoxin-NADP+ Reductase: Kinetics of Electron Transfer, Transient Intermediates, and Catalytic Activities Studied by Flash-Absorption Spectroscopy with Isolated Photosystem I and Ferredoxin. *J. Biol. Chem.* **2005**, *280*, 25960–25972.

(373) Moss, D. A.; Bendall, D. S. Cyclic Electron Transport in Chloroplasts. The Q-Cycle and the Site of Action of Antimycin. *BBA - Bioenerg.* **1984**, *767*, 389–395.

(374) Nawrocki, W. J.; Bailleul, B.; Picot, D.; Cardol, P.; Rappaport, F.; Wollman, F.-A.; Joliot, P. The Mechanism of Cyclic Electron Flow. *Biochim. Biophys. Acta - Bioenerg.* **2019**, *1860*, 433–438.

(375) Ravenel, J.; Peltier, G.; Havaux, M. The Cyclic Electron Pathways around Photosystem I in Chlamydomonas Reinhardtii as Determined in Vivo by Photoacoustic Measurements of Energy Storage. *Planta* **1994**, *193*, 251–259.

(376) Buchert, F.; Hamon, M.; Gäbelein, P.; Scholz, M.; Hippler, M.; Wollman, F. A. The Labile Interactions of Cyclic Electron Flow Effector Proteins. *J. Biol. Chem.* **2018**, *293*, 17559–17573.

(377) Avenson, T. J.; Cruz, J. A.; Kanazawa, A.; Kramer, D. M. Regulating the Proton Budget of Higher Plant Photosynthesis. *Proc. Natl. Acad. Sci. U. S. A.* **2005**, *102*, 9709–9713.

(378) Kanazawa, A.; Ostendorf, E.; Kohzuma, K.; Hoh, D.; Strand, D. D.; Sato-Cruz, M.; Savage, L.; Cruz, J. A.; Fisher, N.; Froehlich, J. E.; Kramer, D. M. Chloroplast ATP Synthase Modulation of the Thylakoid Proton Motive Force: Implications for Photosystem I and Photosystem II Photoprotection. *Front. Plant Sci.* **2017**, *8*, 1–12.

(379) Livingston, A. K.; Cruz, J. A.; Kohzuma, K.; Dhingra, A.; Kramer, D. M. An Arabidopsis Mutant with High Cyclic Electron Flow around Photosystem i (Hcef) Involving the Nadphdehydrogenase Complex. *Plant Cell* **2010**, *22*, 221–233.

(380) Wang, C.; Takahashi, H.; Shikanai, T. PROTON GRADIENT REGULATION 5 Contributes to Ferredoxin-Dependent Cyclic Phosphorylation in Ruptured Chloroplasts. *Biochim. Biophys. Acta - Bioenerg.* **2018**, *1859*, 1173–1179.

(381) Labs, M.; Rühle, T.; Leister, D. The Antimycin A-Sensitive Pathway of Cyclic Electron Flow: From 1963 to 2015. *Photosynth. Res.* **2016**, *129*, 231–238.

(382) Storti, M.; Alboresi, A.; Gerotto, C.; Aro, E. M.; Finazzi, G.; Morosinotto, T. Role of Cyclic and Pseudo-Cyclic Electron Transport in Response to Dynamic Light Changes in Physcomitrella Patens. *Plant Cell Environ.* **2019**, *42*, 1590–1602.

(383) Suorsa, M.; Järvi, S.; Grieco, M.; Nurmi, M.; Pietrzykowska, M.; Rantala, M.; Kangasjärvi, S.; Paakkarinen, V.; Tikkanen, M.; Jansson, S.; Aro, E. M. PROTON GRADIENT REGULATION5 Is Essential for Proper Acclimation of Arabidopsis Photosystem I to Naturally and Artificially Fluctuating Light Conditions. *Plant Cell* **2012**, *24*, 2934–2948.

(384) Suorsa, M.; Rossi, F.; Tadini, L.; Labs, M.; Colombo, M.; Jahns, P.; Kater, M. M. M.; Leister, D.; Finazzi, G.; Aro, E. M.; Barbato, R.; Pesaresi, P. PGR5-PGRL1-Dependent Cyclic Electron Transport Modulates Linear Electron Transport Rate in Arabidopsis Thaliana. *Mol. Plant* **2016**, *9*, 271–288.

(385) Yamamoto, H.; Shikanai, T. PGR5-Dependent Cyclic Electron Flow Protects Photosystem I under Fluctuating Light at Donor and Acceptor Sides. *Plant Physiol.* **2019**, *179*, 588–600.

(386) Nandha, B.; Finazzi, G.; Joliot, P.; Hald, S.; Johnson, G. N. The Role of PGR5 in the Redox Poising of Photosynthetic Electron Transport. *Biochim. Biophys. Acta - Bioenerg.* **2007**, *1767*, 1252–1259.

(387) Nawrocki, W. J.; Bailleul, B.; Cardol, P.; Rappaport, F.; Wollman, F. A.; Joliot, P. Maximal Cyclic Electron Flow Rate Is Independent of PGRL1 in Chlamydomonas. *Biochim. Biophys. Acta - Bioenerg.* **2019**, *1860*, 425–432.

(388) Buchert, F.; Hippler, M. Cytochrome B6f Complex Inhibition by Antimycin-A Requires Stt7 Kinase Activation but Not PGR5. *bioRxiv* **2020**, 2020.08.22.262592.

(389) Hanke, G.; Mulo, P. Plant Type Ferredoxins and Ferredoxin-Dependent Metabolism. *Plant, Cell Environ.* **2013**, *36*, 1071–1084.

(390) Cassier-Chauvat, C.; Chauvat, F. Function and Regulation of Ferredoxins in the Cyanobacterium, Synechocystis PCC6803: Recent Advances. *Life* **2014**, *4*, 666–680.

(391) Hanke, G. T.; Kimata-Ariga, Y.; Taniguchi, I.; Hase, T. A Post Genomic Characterization of Arabidopsis Ferredoxins. *Plant Physiol.* **2004**, *134*, 255–264.

(392) Hase, T.; Kimata, Y.; Yonekura, K.; Matsumura, T.; Sakakibara, H. Molecular Cloning and Differential Expression of the Maize Ferredoxin Gene Family. *Plant Physiol.* **1991**, *96*, 77–83.

(393) Matsumura, T.; Sakakibara, H.; Nakano, R.; Kimata, Y.; Sugiyama, T.; Hase, T. A Nitrate-Inducible Ferredoxin in Maize Roots: Genomic Organization and Differential Expression of Two Nonphotosynthetic Ferredoxin Isoproteins. *Plant Physiol.* **1997**, *114*, 653–660.

(394) Razquin, P.; Schmitz, S.; Peleato, M. L.; Fillat, M. F.; Gómez-Moreno, C.; Böhme, H. Differential Activities of Heterocyst Ferredoxin, Vegetative Cell Ferredoxin, and Flavodoxin as Electron Carriers in Nitrogen Fixation and Photosynthesis in Anabaena Sp. *Photosynth. Res.* **1995**, *43*, 35–40.

(395) Terauchi, A. M.; Lu, S. F.; Zaffagnini, M.; Tappa, S.; Hirasawa, M.; Tripathy, J. N.; Knaff, D. B.; Farmer, P. J.; Lemaire, S. D.; Hase, T.; Merchant, S. S. Pattern of Expression and Substrate Specificity of Chloroplast Ferredoxins from Chlamydomonas Reinhardtii. *J. Biol. Chem.* **2009**, *284*, 25867–25878.

(396) Goss, T.; Hanke, G. The End of the Line: Can Ferredoxin and Ferredoxin NADP(H) Oxidoreductase Determine the Fate of Photosynthetic Electrons? *Curr. Protein Pept. Sci.* **2014**, *15*, 385–393.

(397) Matsumura, T.; Kimata-Ariga, Y.; Sakakibara, H.; Sugiyama, T.; Murata, H.; Takao, T.; Shimonishi, Y.; Hase, T. Complementary DNA Cloning and Characterization of Ferredoxin Localized in Bundle-Sheath Cells of Maize Leaves. *Plant Physiol.* **1999**, *119*, 481–488.

(398) Kimata-Ariga, Y.; Matsumura, T.; Kada, S.; Fujimoto, H.; Fujita, Y.; Endo, T.; Mano, J.; Sato, F.; Hase, T. Differential Electron Flow around Photosystem I by Two C4-Photosynthetic-Cell-Specific Ferredoxins. *EMBO J.* **2000**, *19*, 5041–5050.

(399) Dutton, J. E.; Rogers, L. J.; Haslett, B. G.; Takruri, I. A. H.; Gleaves, J. T.; Boulter, D. Comparative Studies on the Properties of Two Ferredoxins from Pisum Sativum L. *J. Exp. Bot.* **1980**, *31*, 379–391.

(400) Khristin, M. S.; Akulova, E. A. Two Forms of Pea Leaf Ferredoxin. *Biokhimiia* **1976**, *41*, 500–505.

(401) Peltier, J.-B.; Friso, G.; Kalume, D. E.; Roepstorff, P.; Nilsson, F.; Adamska, I.; van Wijk, K. J. Proteomics of the Chloroplast: Systematic Identification and Targeting Analysis of Lumenal and Peripheral Thylakoid Proteins. *Plant Cell* **2000**, *12*, 319–341.

(402) Blanco, N. E.; Ceccoli, R. D.; Dalla Vía, M. V.; Voss, I.; Segretin, M. E.; Bravo-Almonacid, F. F.; Melzer, M.; Hajirezaei, M. R.; Scheibe, R.; Hanke, G. T. Expression of the Minor Isoform Pea Ferredoxin in Tobacco Alters Photosynthetic Electron Partitioning and Enhances Cyclic Electron Flow. *Plant Physiol.* **2013**, *161*, 866–879.

(403) Arnon, D. I.; Chain, R. K. Regulation of Ferredoxin-Catalyzed Photosynthetic Phosphorylations (Photophosphorylation/Photosynthesis/Energy Conversion). *Proc. Natl. Acad. Sci.* **1975**, *72*, 4961–4965.

(404) Cox, R. P. Chloroplast Cytochrome B-563, Hydrophobic Environment and Lack of Direct Reaction with Ferredoxin. *Biochem. J.* **1979**, *184*, 39–44.

(405) Hase, T.; Schürmann, P.; Knaff, D. B. The Interaction of Ferredoxin with Ferredoxin-Dependent Enzymes. In *Photosystem I*; Golbeck, J., Ed.; Springer Netherlands: Dordrecht, **2007**; pp 477–498.

(406) Hurley, J. K.; Hazzard, J. T.; Martínez-Júlvez, M.; Medina, M.; Gómez-Moreno, C.; Tollin, G. Electrostatic Forces Involved in Orienting Anabaena Ferredoxin during Binding to Anabaena Ferredoxin:NAdp + Reductase: Site-Specific Mutagenesis, Transient Kinetic Measurements, and Electrostatic Surface Potentials . *Protein Sci.* **1999**, *8*, 1614–1622.

(407) Schmitz, S.; Martínez-Júlvez, M.; Gómez-Moreno, C.; Böhme, H. Interaction of Positively Charged Amino Acid Residues of Recombinant, Cyanobacterial Ferredoxin:NADP+ Reductase with Ferredoxin Probed by Site Directed Mutagenesis. *Biochim. Biophys. Acta - Bioenerg.* **1998**, *1363*, 85–93.

(408) Van Thor, J. J.; Jeanjean, R.; Havaux, M.; Sjollema, K. A.; Joset, F.; Hellingwerf, K. J.; Matthijs, H. C. P. Salt Shock-Inducible Photosystem I Cyclic Electron Transfer in Synechocystis PCC6803 Relies on Binding of Ferredoxin:NADP+ Reductase to the Thylakoid Membranes via Its CpcD Phycobilisome-Linker Homologous N-Terminal Domain. *Biochim. Biophys. Acta - Bioenerg.* **2000**, *1457*, 129–144.

(409) Twachtmann, M.; Altmann, B.; Muraki, N.; Voss, I.; Okutani, S.; Kurisu, G.; Hase, T.; Hanke, G. T. N-Terminal Structure of Maize Ferredoxin:NADP+ Reductase Determines Recruitment into Different Thylakoid Membrane Complexes. *Plant Cell* **2012**, *24*, 2979–2991.

(410) Joliot, P.; Johnson, G. N. Regulation of Cyclic and Linear Electron Flow in Higher Plants. *Proc. Natl. Acad. Sci. U. S. A.* **2011**, *108*, 13317–13322.

(411) Mosebach, L.; Heilmann, C.; Mutoh, R.; Gäbelein, P.; Steinbeck, J.; Happe, T.; Ikegami, T.; Hanke, G.; Kurisu, G.; Hippler, M. Association of Ferredoxin:NADP+ Oxidoreductase with the Photosynthetic Apparatus Modulates Electron Transfer in Chlamydomonas Reinhardtii. *Photosynth. Res.* **2017**, *134*, 291–306.

(412) Cleland, R. E.; Bendall, D. S. Photosystem I Cyclic Electron Transport: Measurement of Ferredoxin-Plastoquinone Reductase Activity. *Photosynth. Res.* **1992**, *34*, 409–418.

(413) Mills, J. D.; Crowther, D.; Slovacek, R. E.; Hind, G.; McCarty, R. E. Electron Transport Pathways in Spinach Chloroplasts. Reduction of the Primary Acceptor of Photosystem II by Reduced Nicotinamide Adenine Dinucleotide Phosphate in the Dark. *BBA - Bioenerg.* **1979**, *547*, 127–137.

(414) Shahak, Y.; Crowther, D.; Hind, G. The Involvement of Ferredoxin-NADP+ Reductase in Cyclic Electron Transport in Chloroplasts. *Biochim. Biophys. Acta - Bioenerg.* **1981**, *636*, 234–243.

(415) Ye, J. Y.; Wang, Y. J. The Involvement of Ferredoxin-NADP Reductase in the Photosynthetic Cyclic Electron Transport. *Sheng Wu Hua Xue Yu Sheng Wu Wu Li Xue Bao* **1997**, *29*, 40–45.

(416) Hosler, J. P.; Yocum, C. F. Evidence for Two Cyclic Photophosphorylation Reactions Concurrent with Ferredoxin-Catalyzed Non-Cyclic Electron Transport. *Biochim. Biophys. Acta - Bioenerg.* **1985**, *808*, 21–31.

(417) Hosler, J. P.; Yocum, C. F. Heparin Inhibition of Ferredoxin-NADP Reductase in Chloroplast Thylakoid Membranes. *Arch. Biochem. Biophys.* **1985**, *236*, 473–478.

(418) Bohme, H. On the Role of Ferredoxin and Ferredoxin-NADP+ Reductase in Cyclic Electron Transport of Spinach Chloroplasts. *Eur. J. Biochem.* **1977**, *72*, 283–289.

(419) Szymańska, R.; Dłużewska, J.; Ślesak, I.; Kruk, J.; Dłuzewska, J.; Ślesak, I.; Kruk, J.; Dłużewska, J.; Ślesak, I.; Kruk, J. Ferredoxin:NADP + Oxidoreductase Bound to Cytochrome b 6f Complex Is Active in Plastoquinone Reduction: Implications for Cyclic Electron Transport. *Physiol. Plant.* **2011**, *141*, 289–298.

(420) Lintala, M.; Lehtimäki, N.; Benz, J. P.; Jungfer, A.; Soll, J.; Aro, E. M.; Bölter, B.; Mulo, P. Depletion of Leaf-Type Ferredoxin-NADP + Oxidoreductase Results in the Permanent Induction of Photoprotective Mechanisms in Arabidopsis Chloroplasts. *Plant J.* **2012**, *70*, 809–817.

(421) Clark, R. D.; Hawkesford, M. J.; Coughlan, S. J.; Bennett, J.; Hind, G. Association of Ferredoxin-NADP+ Oxidoreductase with the Chloroplast Cytochrome b-f Complex. *FEBS Lett.* **1984**, *174*, 137–142.

(422) Okutani, S.; Hanke, G. T.; Satomi, Y.; Takao, T.; Kurisu, G.; Suzuki, A.; Hase, T. Three Maize Leaf Ferredoxin:NADPH Oxidoreductases Vary in Subchloroplast Location, Expression, and Interaction with Ferredoxin. *Plant Physiol.* **2005**, *139*, 1451–1459.

(423) Benz, J. P.; Stengel, A.; Lintala, M.; Lee, Y. H.; Weber, A.; Philippar, K.; Gügel, I. L.; Kaieda, S.; Ikegami, T.; Mulo, P.; Soll, J.; Bölter, B. Arabidopsis Tic62 and Ferredoxin-NADP(H) Oxidoreductase Form Light-Regulated Complexes That Are Integrated into the Chloroplast Redox Poise. *Plant Cell* **2009**, *21*, 3965–3983.

(424) Jurić, S.; Hazler-Pilepić, K.; Tomašić, A.; Lepeduš, H.; Jeličić, B.; Puthiyaveetil, S.; Bionda, T.; Vojta, L.; Allen, J. F.; Schleiff, E.; Fulgosi, H. Tethering of Ferredoxin:NADP+ Oxidoreductase to Thylakoid Membranes Is Mediated by Novel Chloroplast Protein TROL. *Plant J.* **2009**, *60*, 783–794.

(425) Benz, J. P.; Lintala, M.; Soll, J.; Mulo, P.; Bölter, B. A New Concept for Ferredoxin-NADP(H) Oxidoreductase Binding to Plant Thylakoids. *Trends Plant Sci.* **2010**, *15*, 608–613.

(426) Breyton, C.; Nandha, B.; Johnson, G. N.; Joliot, P.; Finazzi, G. Redox Modulation of Cyclic Electron Flow around Photosystem I in C3 Plants. *Biochemistry* **2006**, *45*, 13465–13475.

(427) Faro, M.; Gomez-Moreno, C.; Stankovich, M.; Medina, M. Role of Critical Charged Residues in Reduction Potential Modulation of Ferredoxin-NADP+ Reductase. *Eur. J. Biochem.* **2002**, *269*, 2656–2661.

(428) Corrado, M. E.; Aliverti, A.; Zanetti, G.; Mayhew, S. G. Analysis of the Oxidation-Reduction Potentials of Recombinant Ferredoxin-NADP+ Reductase from Spinach Chloroplasts. *Eur. J. Biochem.* **1996**, *239*, 662–667.

(429) Pueyo, J. J.; Gomez-Moreno, C.; Mayhew, S. G. Oxidation-reduction Potentials of Ferredoxin-NADP+ Reductase and Flavodoxin from Anabaena PCC 7119 and Their Electrostatic and Covalent Complexes. *Eur. J. Biochem.* **1991**, *202*, 1065–1071.

(430) de Lavalette, A. de L.; Barucq, L.; Alric, J.; Rappaport, F.; Zito, F. Is the Redox State of the Ci Heme of the Cytochrome B6f Complex Dependent on the Occupation and Structure of the Qi Site and Vice Versa? *J. Biol. Chem.* **2009**, *284*, 20822–20829.

(431) Joliot, P.; Béal, D.; Joliot, A. Cyclic Electron Flow under Saturating Excitation of Dark-Adapted Arabidopsis Leaves. *Biochim. Biophys. Acta - Bioenerg.* **2004**, *1656*, 166–176.

(432) Deul, D. H.; Thorn, M. B. Effects of 2,3-Dimercaptopropanol and Antimycin on Absorption Spectra of Heart-Muscle Preparations. *BBA - Biochim. Biophys. Acta* **1962**, *59*, 426–436.

(433) Slater, E. C.; de Vries, S. Identification of the BAL-Labile Factor. *Nature* **1980**, *288*, 717–718.

(434) Liu, J.; Zhu, X.; Kim, S. J.; Zhang, W. Antimycin-Type Depsipeptides: Discovery, Biosynthesis, Chemical Synthesis, and Bioactivities. *Nat. Prod. Rep.* **2016**, *33*, 1146–1165.

(435) Leben, C.; Keitt, G. W. An Antibiotic Substance Active against Certain Phytopathogens. *Phytopathology* **1948**, *38*, 899–906.

(436) Dunshee, B. R.; Leben, C.; Keitt, G. W.; Strong, F. M. The Isolation and Properties of Antimycin A1. *J. Am. Chem. Soc.* **1949**, *71*, 2436–2437.

(437) Li, H.; Zhu, X. L.; Yang, W. C.; Yang, G. F. Comparative Kinetics of Qi Site Inhibitors of Cytochrome Bc 1 Complex: Picomolar Antimycin and Micromolar Cyazofamid. *Chem. Biol. Drug Des.* **2014**, *83*, 71–80.

(438) Van Ark, G.; Berden, J. A. Binding of HQNO to Beef-Heart Sub-Mitochondrial Particles. *BBA - Bioenerg.* **1977**, *459*, 119–137.

(439) Gutierrez-Cirlos, E. B.; Merbitz-Zahradnik, T.; Trumpower, B. L. Inhibition of the Yeast Cytochrome Bc1 Complex by Ilicicolin H, a Novel Inhibitor That Acts at the Qn Site of the Bc1 Complex. *J. Biol. Chem.* **2004**, *279*, 8708–8714.

(440) de Vries, S.; Berden, J. A.; Slater, E. C. Properties of a Semiquinone Anion Located in the QH2:Cytochrome c Oxidoreductase Segment of the Mitochondrial Respiratory Chain. *FEBS Lett.* **1980**, *122*, 143–148.

(441) Rodrigues, T.; Lopes, F.; Moreira, R. Inhibitors of the Mitochondrial Electron Transport Chain and de Novo Pyrimidine Biosynthesis as Antimalarials: The Present Status. *Curr. Med. Chem.* **2010**, *17*, 929–956.

(442) Bolgunas, S.; Clark, D. A.; Hanna, W. S.; Mauvais, P. A.; Pember, S. O. Potent Inhibitors of the Qi Site of the Mitochondrial Respiration Complex III. *J. Med. Chem.* **2006**, *49*, 4762–4766.

(443) Dickie, J. P.; Loomans, M. E.; Farley, T. M.; Strong, F. M. The Chemistry of Antimycin A. XI. N-Substituted 3-Formamidosalicylic Amides. *J. Med. Chem.* **1963**, *6*, 424–427.

(444) Tokutake, N.; Miyoshi, H.; Nakazato, H.; Iwamura, H. Inhibition of Electron Transport of Rat-Liver Mitochondria by Synthesized Antimycin A Analogs. *BBA - Bioenerg.* **1993**, *1142*, 262–268.

(445) Hanafi, M.; Shibata, K.; Ueki, M.; Taniguchi, M. UK-2A, B, C and D, Novel Antifungal Antibiotics From Streptomyces Sp. 517-02. II. Structural Elucidation. *J. Antibiot. (Tokyo).* **1996**, *49*, 1226–1231.

(446) Ueki, M.; Taniguchi, M. The Mode of Action of UK-2A and UK-3A, Novel Antifungal Antibiotics from Streptomyces Sp. 517-02. *J. Antibiot. (Tokyo).* **1997**, *50*, 1052–1057.

(447) Young, D. H.; Wang, N. X.; Meyer, S. T.; Avila-Adame, C. Characterization of the Mechanism of Action of the Fungicide Fenpicoxamid and Its Metabolite UK-2A. *Pest Manag. Sci.* **2018**, *74*, 489–498.

(448) Machida, K.; Takimoto, H.; Miyoshi, H.; Taniguchi, M. UK-2A, B, C and D, Novel Antifungal Antibiotics from Streptomyces Sp. 517-02 V. Inhibition Mechanism of Bovine Heart Mitochondrial Cytochrome Bc1, by the Novel Antibiotic UK-2A. *J. Antibiot. (Tokyo).* **1999**, *52*, 748–753.

(449) Ando, K.; Saeki, T.; Tamura, G.; Arima, K.; Suzuki, S. Funiculosin, a New Antibiotic. I Isolation, Biological and Chemical Properties. *J. Antibiot. (Tokyo).* **1969**, *22*, 189–194.

(450) Ando, K.; Matsuura, I.; Nawata, Y.; Endo, H.; Sasaki, H.; Okytomi, T.; Saehi, T.; Tamura, G. Funiculosin, a New Antibiotic. II: Structure Elucidation and Antifungal Activity. *J. Antibiot. (Tokyo).* **1978**, *31*, 533–538.

(451) Nelson, B. D.; Walter, P.; Ernster, L. Funiculosin: An Antibiotic with Antimycin-like Inhibitory Properties. *Biochem. Biophys. Acta- Bioenerg.* **1977**, *460*, 157–162.

(452) Brasseur, G.; Brivet-Chevillotte, P. Specificities of the Two Center N Inhibitors of Mitochondial Bc1 Complex, Antimycin and Funiculosin: Strong Involvement of Cytochrome b-Asparagine-208 in Funiculosin Binding. *FEBS Lett.* **1994**, *354*, 23–29.

(453) Ohsumi, K.; Watanabe, M.; Fujie, A. AS2077715 Is a Selective Inhibitor of Fungal Mitochondrial Cytochrome Bc1 Complex. *J. Antibiot. (Tokyo).* **2014**, *67*, 713–716.

(454) Hayakawa, S.; Minato, H.; Katagiri, K. The Ilicicolins, Antibiotics from Cylindrocladium Ilicicola. *J. Antibiot. (Tokyo).* **1971**, *24*, 653–654.

(455) Junker, B.; Zhang, J.; Mann, Z.; Reddy, J.; Greasham, R. Scale-up Studies on a Defined Medium Process for Pilot Plant Production of Illicicolin by *Gliocladium Roseum*. *Biotechnol. Prog.* **2001**, *17*, 278–286.

(456) Singh, S. B.; Liu, W.; Li, X.; Chen, T.; Shafiee, A.; Dreikorn, S.; Hornak, V.; Meinz, M.; Onishi, J. C. Structure-Activity Relationship of Cytochrome Bc1 Reductase Inhibitor Broad Spectrum Antifungal Ilicicolin H. *Bioorganic Med. Chem. Lett.* **2013**, *23*, 3018–3022.

(457) Rotsaert, F. A. J.; Ding, M. G.; Trumpower, B. L. Differential Efficacy of Inhibition of Mitochondrial and Bacterial Cytochrome Bc1 Complexes by Center N Inhibitors Antimycin, Ilicicolin H and Funiculosin. *Biochim. Biophys. Acta - Bioenerg.* **2008**, *1777*, 211–219.

(458) Kim, J. C.; Lee, Y. W.; Tamura, H.; Yoshizawa, T. Sambutoxin: A New Mycotoxin Isolated from Fusarium Sambucinum. *Tetrahedron Lett.* **1995**, *36*, 1047–1050.

(459) Kawai, K.; Suzuki, T.; Kitagawa, A.; Kim, J. C.; Lee, Y. W. A Novel Respiratory Chain Inhibitor, Sambutoxin from Fusarium Sambucinum. In *Cereal Research Communications*; **1997**; pp 325–326.

(460) Kim, J. C.; Lee, Y. W.; Yu, S. H. Sambutoxin-Producing Isolates of Fusarium Species and Occurrence of Sambutoxin in Rotten Potato Tubers. *Appl. Environ. Microbiol.* **1995**, *61*, 3750–3751.

(461) Sakai, K.; Unten, Y.; Iwatsuki, M.; Matsuo, H.; Fukasawa, W.; Hirose, T.; Chinen, T.; Nonaka, K.; Nakashima, T.; Sunazuka, T.; Usui, T.; Murai, M.; Miyoshi, H.; Asami, Y.; Ōmura, S.; Shiomi, K. Fusaramin, an Antimitochondrial Compound Produced by Fusarium Sp., Discovered Using Multidrug-Sensitive Saccharomyces Cerevisiae. *J. Antibiot. (Tokyo).* **2019**, *72*, 645–652.

(462) Capper, M. J.; O'Neill, P. M.; Fisher, N.; Strange, R. W.; Moss, D.; Ward, S. A.; Berry, N. G.; Lawrenson, A. S.; Hasnain, S. S.; Biagini, G. A.; Antonyuk, S. V. Antimalarial 4(1H)-Pyridones Bind to the Qi Site of Cytochrome Bc1. *Proc. Natl. Acad. Sci. U. S. A.* **2015**, *112*, 755–760.

(463) McPhillie, M.; Zhou, Y.; El Bissati, K.; Dubey, J.; Lorenzi, H.; Capper, M.; Lukens, A. K.; Hickman, M.; Muench, S.; Verma, S. K.; Weber, C. R.; Wheeler, K.; Gordon, J.; Sanders, J.; Moulton, H.; Wang, K.; Kim, T. K.; He, Y.; Santos, T.; Woods, S.; Lee, P.; Donkin, D.; Kim, E.; Fraczek, L.; Lykins, J.; Esaa, F.; Alibana-Clouser, F.; Dovgin, S.; Weiss, L.; Brasseur, G.; Wirth, D.; Kent, M.; Hood, L.; Meunieur, B.; Roberts, C. W.; Hasnain, S. S.; Antonyuk, S. V.; Fishwick, C.; McLeod, R. New Paradigms for Understanding and Step Changes in Treating Active and Chronic, Persistent Apicomplexan Infections. *Sci. Rep.* **2016**, *6*, 1–23.

(464) Inoue, Y.; Ishizuka, K.; Mitsui, S. Inhibition of Respiration of Yeast by Photosynthesis Inhibiting Herbicides. *Agric. Biol. Chem.* **1967**, *31*, 422–427.

(465) di Rago, J. P.; Colson, A.-M. Molecular Basis for Resistance to Antimycin and Diuron, Q-Cycle Inhibitors Acting at the Qi Site in the Mitochondrial Ubiquinol-Cytochrome c Reductase in *Saccharomyces Cerevisiae*. *J. Biol. Chem.* **1988**, *263*, 12564–12570.

(466) Weber, S.; Wolf, K. Two Changes of the Same Nucleotide Confer Resistance to Diuron and Antimycin in the Mitochondrial Cytochrome b Gene of Schizosaccharomyces Pombe. *FEBS Lett.* **1988**, *237*, 31–34.

(467) Convent, B.; Briquet, M. Properties of 3-(3,4-Dichlorophenyl)-1,1- Dimethylurea and Other Inhibitors of the Cytochrome Be, Segment of the Mitochondrial Respiratory Chain in *Saccharomyces Cerevisiae*. *Eur J Biochem* **1978**, *82*, 473–481.

(468) Zhu, X.; Zhang, M.; Liu, J.; Ge, J.; Yang, G. Ametoctradin Is a Potent Qo Site Inhibitor of the Mitochondrial Respiration Complex III. *J. Agric. Food Chem.* **2015**, *63*, 3377–3386.

(469) Fontaine, S.; Remuson, F.; Caddoux, L.; Barrès, B. Investigation of the Sensitivity of Plasmopara Viticola to Amisulbrom and Ametoctradin in French Vineyards Using Bioassays and Molecular Tools. *Pest Manag. Sci.* **2019**, *75*, 2115–2123.

(470) Mitani, S.; Araki, S.; Takii, Y.; Ohshima, T.; Matsuo, N.; Miyoshi, H. The Biochemical Mode of Action of the Novel Selective Fungicide Cyazofamid: Specific Inhibition of Mitochondrial Complex III in Phythium Spinosum. *Pestic. Biochem. Physiol.* **2001**, *71*, 107–115.

(471) Kunze, B.; Kemmer, T.; Höfle, G.; Reichenbach, H. Stigmatellin, a New Antibiotic from Stigmatella Aurantiaca (Myxobacterales): I. Production, Physico-Chemical and Biological Properties. *J. Antibiot. (Tokyo).* **1984**, *37*, 454–461.

(472) OHNISHI, T.; BRANDT, U.; von JAGOW, G. Studies on the Effect of Stigmatellin Derivative on Cytochrome Band the Rieske Iron-sulfur Cluster of Cytochrome c Reductase from Bovine Heart Mitochondria. *Eur. J. Biochem.* **1988**, *176*, 385–389.

(473) Lancaster, C. R. D.; Hunte, C.; Kelley III, J.; Trumpower, B. L.; Ditchfield, R. A Comparison of Stigmatellin Conformations, Free and Bound to the Photosynthetic Reaction Center and the Cytochrome Bc_1 Complex. *J. Mol. Biol.* **2007**, *368*, 197–208.

(474) Esser, L.; Yu, C.-A.; Xia, D. Structural Basis of Resistance to Anti-Cytochrome Bc_1 Complex Inhibitors: Implication for Drug Improvement. *Curr. Pharm. Des.* **2014**, *20*, 704–724.

(475) Hope, A. B.; Valente, P. Inhibitor Binding to Isolated Chloroplast Cytochrome *Bf* Complex. *Photosynth. Res.* **1996**, *49*, 37–48.

(476) Fry, M.; Pudney, M. Site of Action of the Antimalarial Hydroxynaphthoquinone, 2-[Trans-4-(4'-Chlorophenyl) Cyclohexyl]-3- Hydroxy-1,4-Naphthoquinone (566C80). *Biochem. Pharmacol.* **1992**, *43*, 1545–1553.

(477) Dike, S. Y.; Singh, D.; Thankachen, B. N.; Sharma, B.; Mathur, P. K.; Kore, S.; Kumar, A. A Single-Pot Synthesis of Atovaquone: An Antiparasitic Drug of Choice. *Org. Process Res. Dev.* **2014**, *18*, 618–625.

(478) Siregar, J. E.; Kurisu, G.; Kobayashi, T.; Matsuzaki, M.; Sakamoto, K.; Mi-ichi, F.; Watanabe, Y. ichi; Hirai, M.; Matsuoka, H.; Syafruddin, D.; Marzuki, S.; Kita, K. Direct Evidence for the Atovaquone Action on the Plasmodium Cytochrome Bc1 Complex. *Parasitol. Int.* **2015**, *64*, 295–300.

(479) Kessl, J. J.; Lange, B. B.; Merbitz-Zahradnik, T.; Zwicker, K.; Hill, P.; Meunier, B.; Pálsdóttir, H.; Hunte, C.; Meshnick, S.; Trumpower, B. L. Molecular Basis for Atovaquone Binding to the Cytochrome Bc_1 Complex. *J. Biol. Chem.* **2003**, *278*, 31312–31318.

(480) Nilsen, A.; LaCrue, A. N.; White, K. L.; Forquer, I. P.; Cross, R. M.; Marfurt, J.; Mather, M. W.; Delves, M. J.; Shackleford, D. M.; Saenz, F. E.; Morrisey, J. M.; Steuten, J.; Mutka, T.; Li, Y.; Wirjanata, G.; Ryan, E.; Duffy, S.; Kelly, J. X.; Sebayang, B. F.; Zeeman, A. M.; Noviyanti, R.; Sinden, R. E.; Kocken, C. H. M.; Price, R. N.; Avery, V. M.; Angulo-Barturen, I.; Jiménez-Díaz, M. B.; Ferrer, S.; Herreros, E.; Sanz, L. M.; Gamo, F. J.; Bathurst, I.; Burrows, J. N.; Siegl, P.; Guy, R. K.; Winter, R. W.; Vaidya, A. B.; Charman, S. A.; Kyle, D. E.; Manetsch, R.; Riscoe, M. K. Quinolone-3-Diarylethers: A New Class of Antimalarial Drug. *Sci. Transl. Med.* **2013**, *5*.

(481) Esposti, M. D.; Rotilio, G.; Lenaz, G. Effects of Dibromothymoquinone on the Structure and Function of the Mitochondrial Bc1 Complex. *BBA - Bioenerg.* **1984**, *767*, 10–20.

(482) Sarewicz, M.; Bujnowicz, Ł.; Bhaduri, S.; Singh, S. K.; Cramer, W. A.; Osyczka, A. Metastable Radical State, Nonreactive with Oxygen, Is Inherent to Catalysis by Respiratory and Photosynthetic Cytochromes Bc_1/b_6F. *Proc. Natl. Acad. Sci. U. S. A.* **2017**, *114*, 1323–1328.

(483) Malkin, R. Redox Properties of the DBMIB-Rieske Iron-Sulfur Complex in Spinach Chloroplast Membranes. *FEBS Lett.* **1981**, *131*, 169–172.

(484) Yang, F. D.; Yu, L.; Yu, C. A. The Nature of the Inhibition of 4,7-Dioxobenzothiazole Derivatives on Mitochondrial Ubiquinol-Cytochrome c Reductase. *J. Biol. Chem.* **1989**, *264*, 891–898.

(485) Zhang, L.; Snyder, C.; Trumpower, B. L.; Yu, L.; Yu, C. A. Determination of the Binding Rate Constants of Stigmatellin and UHDBT to Bovine Cytochrome Bc1 Complex by Cytochrome C1 Oxidation. *FEBS Lett.* **1999**, *460*, 349–352.

(486) Trumpower, B. L.; Haggerty, J. G. Inhibition of Electron Transfer in the Cytochrome B-C1 Segment of the Mitochondrial Respiratory Chain by a Synthetic Analogue of Ubiquinone. *J. Bioenerg. Biomembr.* **1980**, *12*, 151–164.

(487) Takamiya, K.-I.; Dutton, P. L. Ubiquinone in *Rhodopseudomonas Sphaeroides*. Some Thermodynamic Properties. *Biochim. Biophys. Acta* **1979**, *546*, 1–16.

(488) Zhang, H.; Chobot, S. E.; Osyczka, A.; Wraight, C. A.; Dutton, P. L.; Moser, C. C. Quinone and Non-Quinone Redox Couples in Complex III. *J. Bioenerg. Biomembr.* **2008**, *40*, 493–499.

(489) Kunze, B.; Jansen, R.; Höfle, G.; Reichenbach, H. Crocacin, a New Electron Transport Inhibitor from Chondromyces Crocatus (Myxobacteria). Production, Isolation, Physico-Chemical and Biological Properties. *J. Antibiot. (Tokyo).* **1994**, *47*, 881–886.

(490) Jansen, R.; Washausen, P.; Kunze, B.; Reichenbach, H.; Höfle, G. The Crocacins, Novel Antifungal and Cytotoxic Antibiotics from Chondromyces Crocatus and Chondromyces Pediculatus (Myxobacteria): Isolation and Structure Elucidation. *Eur. J. Org. Chem.* **1999**, *1999*, 10850–11089.

(491) Dias, L. C.; De Oliveira, L. G.; Vilcachagua, J. D.; Nigsch, F. Total Synthesis of (+)-Crocacin D. *J. Org. Chem.* **2005**, *70*, 2225–2234.

(492) Chakraborty, T. K.; Laxman, P. Total Synthesis of (+)-Crocacin A. *Tetrahedron Lett.* **2003**, *44*, 4989–4992.

(493) Pasqua, A. E.; Ferrari, F. D.; Crawford, J. J.; Whittingham, W. G.; Marquez, R. Synthesis of (+)-Crocacin D and Simplified Bioactive Analogues. *Bioorganic Med. Chem.* **2015**, *23*, 1062–1068.

(494) Sternberg, J. A.; Geffken, D.; Adams, J. B.; Pöstages, R.; Sternberg, C. G.; Campbell, C. L.; Moberg, W. K. Famoxadone: The Discovery and Optimisation of a New Agricultural Fungicide. *Pest Manag. Sci.* **2001**, *57*, 143–152.

(495) Esser, L.; Zhou, F.; Zhou, Y.; Xiao, Y.; Tang, W. K.; Yu, C. A.; Qin, Z.; Xia, D. Hydrogen Bonding to the Substrate Is Not Required for Rieske Iron-Sulfur Protein Docking to the Quinol Oxidation Site of Complex III. *J. Biol. Chem.* **2016**, *291*, 25019–25031.

(496) Zheng, Y. J.; Shapiro, R.; Marshall, W. J.; Jordan, D. B. Synthesis and Structural Analysis of the Active Enantiomer of Famoxadone, a Potent Inhibitor of Cytochrome Bc1. *Bioorganic Med. Chem. Lett.* **2000**, *10*, 1059–1062.

(497) Gerth, K.; Irschik, H.; Reichenbach, H.; Trowitzsch, W. Myxothiazol, an Antibiotic from *Myxococcus Fulvus* (Myxobacterales): I. Cultivation, Isolation, Physico-Chemical and Biological Properties. *J. Antibiot. (Tokyo).* **1980**, *33*, 1474–1479.

(498) Thierbach, G.; Reichenbach, H. Myxothiazol, a New Inhibitor of the Cytochrome b-C1 Segment of the Respiratory Chain. *BBA - Bioenerg.* **1981**, *638*, 282–289.

(499) Becker, W. F.; von Jagow, G.; Anke, T.; Steglich, W. Oudemansin, Strobilurin A, Strobilurin B, and Myxothiazol: New Inhibitors of the Bc1 Segment of the Respiratory Chain with an e-β-Methoxyacrylate System as Common Structural Element. *FEBS Lett.* **1981**, *132*, 329–333.

(500) von Jagow, G.; Ljungdahl, P. O.; Graf, P.; Ohnishi, T.; Trumpower, B. L. An Inhibitor of Mitochondrial Respiration Which Binds to Cytochrome-*b* and Displaces Quinone from the Iron-Sulfur Protein of the Cytochrome-Bc_1 Complex. *J. Biol. Chem.* **1984**, *259*, 6318–6326.

(501) Schieferdecker, S.; Exner, T. E.; Gross, H.; Roth, M.; Nett, M. New Myxothiazols from the Predatory Bacterium Myxococcus Fulvus. *J. Antibiot. (Tokyo).* **2014**, *67*, 519–525.

(502) Sasse, F.; Böhlendorf, B.; Hermann, M.; Kunze, B.; Forche, E.; Steinmetz, H.; Höfle, G.; Reichenbach, H. Melithiazols, New β-Methoxyacrylate Inhibitors of the Respiratory Chain Isolated from Myxobacteria. Production, Isolation, Physico-Chemical and Biological Properties. *J. Antibiot. (Tokyo).* **1999**, *52*, 721–729.

(503) Ojika, M.; Suzuki, Y.; Tsukamoto, A.; Sakagami, Y.; Fudou, R.; Yoshimura, T.; Yamanaka, S. Cystothiazoles A and B, New Bithiazole-Type Antibiotics from the Myxobacterium *Cystobacter Fuscus*. *J. Antibiot. (Tokyo).* **1998**, *51*, 275–281.

(504) Sasse, F.; Leibold, T.; Kunze, B.; Höfle, G.; Reichenbach, H. Cyrmenins, New β-Methoxyacrylate Inhibitors of the Electron Transport. Production, Isolation, Physico-Chemical and Biological Properties. *J. Antibiot. (Tokyo).* **2003**, *56*, 827–831.

(505) Chakor, N. S.; Dallavalle, S.; Musso, L.; Sardi, P. Synthesis and Evaluation of Structural Requirements for Antifungal Activity of Cyrmenin B_1 Analogues. *Tetrahedron Lett.* **2012**, *53*, 228–231.

(506) Von Jagow, G.; Gribble, G. W.; Trumpower, B. L. Mucidin and Strobilurin A Are Identical and Inhibit Electron Transfer in the Cytochrome Bc1 Complex of the Mitochondrial Respiratory Chain at the Same Site as Myxothiazol. *Biochemistry* **1986**, *25*, 775–780.

(507) Anke, T.; Oberwinkler, F.; Steglich, W.; Schramm, G. The Strobilurins - New Antifungal Antibiotics from the Basidiomycete Strobilurus Tenacellus (Pers. Ex Fr.) Sing. *J. Antibiot. (Tokyo).* **1977**, *30*, 806–810.

(508) Anke, T.; Hecht, H. J.; Schramm, G.; Steglich, W. Antibiotics from Basidiomycetes. IX Oudemansin, an Antifungal Antibiotic from *Oudemansiella Mucida* (Schrader Ex Fr.) Hoehnel (Agaricales). *J. Antibiot. (Tokyo).* **1979**, *32*, 1112–1117.

(509) Fredenhagen, A.; Kuhn, A.; Cuomo, V.; Giuliano, U. Strobilurins F, G and H, Three New Antifungal Metabolites from Bolinea Lutea: I. Fermentation, Isolation and Biological Activity. *J. Antibiot. (Tokyo).* **1990**, *43*, 655–660.

(510) Balba, H. Review of Strobilurin Fungicide Chemicals. *J. Environ. Sci. Heal. - Part B Pestic. Food Contam. Agric. Wastes* **2007**, *42*, 441–451.

(511) Brandt, U.; Schagger, H.; von Jagow, G. Characterisation of Binding of the Methoxyacrylate Inhibitors to Mitochondrial Cytochrome *c* Reductase. *Eur. J. Biochem.* **1988**, *173*, 499–506.

(512) Brandt, U.; Djafarzadeh-Andabili, R. Binding of MOA-Stilbene to the Mitochondrial Cytochrome Bc1 Complex Is Affected by the Protonation State of a Redox-Bohr Group of the “Rieske” Iron-Sulfur Protein. *Biochim. Biophys. Acta - Bioenerg.* **1997**, *1321*, 238–242.

(513) Nofiani, R.; de Mattos-Shipley, K.; Lebe, K. E.; Han, L. C.; Iqbal, Z.; Bailey, A. M.; Willis, C. L.; Simpson, T. J.; Cox, R. J. Strobilurin Biosynthesis in Basidiomycete Fungi. *Nat. Commun.* **2018**, *9*, 1–11.

(514) Bartlett, D. W.; Clough, J. M.; Godwin, J. R.; Hall, A. A.; Hamer, M.; Parr-Dobrzanski, B. Review: The Strobilurin Fungicides. *Pest Manag. Sci.* **2002**, *58*, 649–662.

(515) Arakawa, A.; Kasai, Y.; Yamazaki, K.; Iwahashi, F. Features of Interactions Responsible for Antifungal Activity against Resistant Type Cytochrome Bc1: A Data-Driven Analysis Based on the Binding Free Energy at the Atomic Level. *PLoS One* **2018**, *13*, 1–16.

(516) Brown, R. J.; Annis, G.; Casalnuovo, A.; Chan, D.; Shapiro, R.; Marshall, W. J. Synthesis and Properties of Axially-Chiral N-(2,6-Disubstituted)Phenyl Triazolones. *Tetrahedron* **2004**, *60*, 4361–4375.

(517) Matsuzaki, Y.; Yoshimoto, Y.; Arimori, S.; Kiguchi, S.; Harada, T.; Iwahashi, F. Discovery of Metyltetraprole: Identification of Tetrazolinone Pharmacophore to Overcome QoI Resistance. *Bioorganic Med. Chem.* **2020**, *28*, 115211.

(518) Takagaki, M.; Ozaki, M.; Fujimoto, S.; Fukumoto, S. Development of a Novel Fungicide, Pyribencarb. *J. Pestic. Sci.* **2014**, *39*, 177–178.

(519) Huang, L.; Berry, E. A. *Famoxadone and Related Inhibitors Bind like Methoxy Acrylate Inhibitors in the Qo Site of the BC1 Compl and Fix the Rieske Iron-Sulfur Protein in a Positio Close to but Distinct from That Seen with Stigmatellin and Other "DISTAL" Qo Inhibitors*.

(520) Gallon, J.; Reymond, S.; Cossy, J. Neopeltolide, a New Promising Antitumoral Agent. *Comptes Rendus Chim.* **2008**, *11*, 1463–1476.

(521) Wright, A. E.; Botelho, J. C.; Guzmán, E.; Harmody, D.; Linley, P.; McCarthy, P. J.; Pitts, T. P.; Pomponi, S. A.; Reed, J. K. Neopeltolide, a Macrolide from a Lithistid Sponge of the Family Neopeltidae. *J. Nat. Prod.* **2007**, *70*, 412–416.

(522) D'Ambrosio, M.; Guerriero, A.; Debitus, C.; Pietra, F. Leucascandrolide A, a New Type of Macrolide: The First Powerfully Bioactive Metabolite of Calcareous Sponges (Leucascandra Caveolata, a New Genus from the Coral Sea). *Helv. Chim. Acta* **1996**, *79*, 51–60.

(523) Ulanovskaya, O. A.; Janjic, J.; Suzuki, M.; Sabharwal, S. S.; Schumacker, P. T.; Kron, S. J.; Kozmin, S. A. Synthesis Enables Identification of the Cellular Target of Leucascandrolide A and Neopeltolide. *Nat. Chem. Biol.* **2008**, *4*, 418–424.

(524) Zhu, X. L.; Zhang, R.; Wu, Q. Y.; Song, Y. J.; Wang, Y. X.; Yang, J. F.; Yang, G. F. Natural Product Neopeltolide as a Cytochrome Bc1 Complex Inhibitor: Mechanism of Action and Structural Modification. *J. Agric. Food Chem.* **2019**, *67*, 2774–2781.

(525) Yan, X.; Qin, W.; Sun, L.; Qi, S.; Yang, D.; Qin, Z.; Yuan, H. Study of Inhibitory Effects and Action Mechanism of the Novel Fungicide Pyrimorph against Phytophthora Capsici. *J. Agric. Food Chem.* **2010**, *58*, 2720–2725.

(526) Pang, Z.; Shao, J.; Chen, L.; Lu, X.; Hu, J.; Qin, Z.; Liu, X. Resistance to the Novel Fungicide Pyrimorph in Phytophthora Capsici: Risk Assessment and Detection of Point Mutations in CesA3 That Confer Resistance. *PLoS One* **2013**, *8*.

(527) Xiao, Y. M.; Esser, L.; Zhou, F.; Li, C.; Zhou, Y. H.; Yu, C. A.; Qin, Z. H.; Xia, D. Studies on Inhibition of Respiratory Cytochrome Bc1 Complex by the Fungicide Pyrimorph Suggest a Novel Inhibitory Mechanism. *PLoS One* **2014**, *9*, 1–12.

(528) Vallières, C.; Fisher, N.; Antoine, T.; Al-Helal, M.; Stocks, P.; Berry, N. G.; Lawrenson, A. S.; Ward, S. A.; O'Neill, P. M.; Biagini, G. A.; Meunier, B. HDQ, a Potent Inhibitor of Plasmodium Falciparum Proliferation, Binds to the Quinone Reduction Site of the Cytochrome Bc1 Complex. *Antimicrob. Agents Chemother.* **2012**, *56*, 3739–3747.

(529) Papa, S.; Izzo, G.; Guerrieri, F. On the Inhibition of the Bc1 Segment on the Mitochondrial Respiratory Chain by Quinone Analogues and Hydroxyquinoline Derivatives. *FEBS Lett.* **1982**, *145*, 93–98.

(530) Riccio, P.; Bobba, A.; Quagliariello, E. Characterization of [3H]NoHOQnO Binding to Purified Complex III. *FEBS Lett.* **1982**, *137*, 222–226.

(531) Doggett, J. S.; Nilsen, A.; Forquer, I.; Wegmann, K. W.; Jones-Brando, L.; Yolken, R. H.; Bordón, C.; Charman, S. A.; Katneni, K.; Schultz, T.; Burrows, J. N.; Hinrichs, D. J.; Meunier, B.; Carruthers, V. B.; Riscoe, M. K. Endochin-like Quinolones Are Highly Efficacious against Acute and Latent Experimental Toxoplasmosis. *Proc. Natl. Acad. Sci. U. S. A.* **2012**, *109*, 15936–15941.

(532) Stickles, A. M.; Smilkstein, M. J.; Morrisey, J. M.; Li, Y.; Forquer, I. P.; Kelly, J. X.; Pou, S.; Winter, R. W.; Nilsen, A.; Vaidya, A. B.; Riscoe, M. K. Atovaquone and ELQ-300 Combination Therapy as a Novel Dual-Site Cytochrome Bc1 Inhibition Strategy for Malaria. *Antimicrob. Agents Chemother.* **2016**, *60*, 4853–4859.

(533) Song, Z.; Iorga, B. I.; Mounkoro, P.; Fisher, N.; Meunier, B. The Antimalarial Compound ELQ-400 Is an Unusual Inhibitor of the Bc1 Complex, Targeting Both Qo and Qi Sites. *FEBS Lett.* **2018**, *592*, 1346–1356.

(534) Merk, M.; Frechen, T.; Gold, R. E.; Schiffer, H.; Levy, T.; Saramago, J. INITIUM®: A New Innovative Fungicide of a New Chemical Class for the Control of Late Blight and Downy Mildew Diseases. *Acta Hortic.* **2011**, *917*, 143–148.

(535) Fehr, M.; Wolf, A.; Stammler, G. Binding of the Respiratory Chain Inhibitor Ametoctradin to the Mitochondrial Bc1 Complex. *Pest Manag. Sci.* **2016**, *72*, 591–602.

(536) Dreinert, A.; Wolf, A.; Mentzel, T.; Meunier, B.; Fehr, M. The Cytochrome Bc1 Complex Inhibitor Ametoctradin Has an Unusual Binding Mode. *Biochim. Biophys. Acta - Bioenerg.* **2018**, *1859*, 567–576.

(537) Tamura, G.; Takatsuki, A.; Ando, K.; Arima, K.; Suzuki, S. Ascochlorin, A New Antibiotic, Found by Paper-Disc Agar-Diffusion Method. I. *J. Antibiot. (Tokyo).* **1968**, *21*, 539–544.

(538) Sasaki, H.; Hosokawa, T.; Nawata, Y.; Ando, K. Isolation and Structure of Ascochlorin and Its Analogs. *Agric. Biol. Chem.* **1974**, *38*, 1463–1466.

(539) Ellestad, G. A.; Evans, R. H.; Kunstmann, M. P. Some New Terpenoid Metabolites from an Unidentified Fusarium Species. *Tetrahedron* **1969**, *25*, 1323–1334.

(540) Cagnoli-Bellavita, N.; Ceccherelli, P.; Fringuelli, R.; Ribaldi, M. Ascochlorin: A Terpenoid Metabolite from Acremonium Luzulae. *Phytochemistry* **1975**, *14*, 807.

(541) Minato, H.; Katayama, T.; Katagiri, K.; Hayakawa, S. Identification of Ilicicolins with Ascochlorin and LL-Z 1272. *J. Antibiot. (Tokyo).* **1972**, *25*, 315–316.

(542) Berry, E. A.; Huang, L. shar; Lee, D. W.; Daldal, F.; Nagai, K.; Minagawa, N. Ascochlorin Is a Novel, Specific Inhibitor of the Mitochondrial Cytochrome Bc1 Complex. *Biochim. Biophys. Acta - Bioenerg.* **2010**, *1797*, 360–370.

(543) Mogi, T.; Ui, H.; Shiomi, K.; Omura, S.; Miyoshi, H.; Kita, K. Antibiotics LL-Z1272 Identified as Novel Inhibitors Discriminating Bacterial and Mitochondrial Quinol Oxidases. *Biochim. Biophys. Acta - Bioenerg.* **2009**, *1787*, 129–133.

(544) Hao, G. F.; Wang, F.; Li, H.; Zhu, X. L.; Yang, W. C.; Huang, L. S.; Wu, J. W.; Berry, E. A.; Yang, G. F. Computational Discovery of Picomolar Q o Site Inhibitors of Cytochrome Bc 1 Complex. *J. Am. Chem. Soc.* **2012**, *134*, 11168–11176.

(545) Flematti, G. R.; Scaffidi, A.; Dixon, K. W.; Smith, S. M.; Ghisalberti, E. L. Production of the Seed Germination Stimulant Karrikinolide from Combustion of Simple Carbohydrates. *J. Agric. Food Chem.* **2011**, *59*, 1195–1198.

(546) Chen, C.; Wu, Q. Y.; Shan, L. Y.; Zhang, B.; Verpoort, F.; Yang, G. F. Discovery of Cytochrome Bc1 Complex Inhibitors Inspired by the Natural Product Karrikinolide. *RSC Adv.* **2016**, *6*, 97580–97586.

(547) Trebst, A. [65] Inhibitors in Electron Flow: Tools for the Functional and Structural Localization of Carriers and Energy Conservation Sites. *Methods Enzymol.* **1980**, *69*, 675–715.

(548) Delosme, R.; Joliot, P.; Trebst, A. Flash-Induced Oxidation of Cytochrome b-563 in Algae under Anaerobic Conditions: Effect of Dinitrophenylether of Iodonitrothymol. *Biochem. Biophys. Acta* **1987**, *893*, 1–6.

(549) Witt, H. T. Energy Conversion in the Functional Membrane of Photosynthesis. Analysis by Light Pulse and Electric Pulse Methods. The Central Role of the Electric Field. *BBA Rev. Bioenerg.* **1979**, *505*, 355–427.

(550) Bailleul, B.; Cardol, P.; Breyton, C.; Finazzi, G. Electrochromism: A Useful Probe to Study Algal Photosynthesis. *Photosynth. Res.* **2010**, *106*, 179–189.

(551) Barbagallo, R. P.; Finazzi, G.; Forti, G. Effects of Inhibitors on the Activity of the Cytochrome B6f Complex: Evidence for the Existence of Two Binding Pockets in the Lumenal Site. *Biochemistry* **1999**, *38*, 12814–12821.

(552) Oettmeier, W.; Godde, D.; Kunze, B.; Höfle, G. Stigmatellin. A Dual Type Inhibitor of Photosynthetic Electron Transport. *Biochim. Biophys. Acta* **1985**, *807*, 216–219.

(553) Nitschke, W.; Hauska, G.; Rutherford, A. W. The Inhibition of Quinol Oxidation by Stigmatellin Is Similar in Cytochrome Bc1 and B6f Complexes. *Biochim. Biophys. Acta* **1989**, *974*, 223–226.

(554) Breyton, C. Conformational Changes in the Cytochrome B6f Complex Induced by Inhibitor Binding. *J. Biol. Chem.* **2000**, *275*, 13195–13201.

(555) Haehnel, W. *In Bioenergetics of Membranes*; Elsevier: Amsterdam, **1977**.

(556) Roberts, A. G.; Kramer, D. M. Inhibitor "Double Occupancy" in the Q o Pocket of the Chloroplast Cytochrome b 6 f Complex. *Biochemistry* **2001**, *40*, 13407–13412.

(557) Rich, P. R.; Madgwick, S. A.; Moss, D. A. The Interactions of Duroquinol, DBMIB and NQNO with the Chloroplast Cytochrome Bf Complex. *Biochim. Biophys. Acta* **1991**, *1058*, 312–328.

(558) Surpin, M.; Larkin, R. M.; Chory, J. Signal Transduction between the Chloroplast and the Nucleus. *Plant Cell* **2002**, *14*.

(559) Nott, A.; Jung, H.-S.; Koussevitzky, S.; Chory, J. Plastid-To-Nucleus Retrograde Signaling. *Annu. Rev. Plant Biol.* **2006**, *57*, 739–759.

(560) Chi, W.; Sun, X.; Zhang, L. Intracellular Signaling from Plastid to Nucleus. *Annu. Rev. Plant Biol.* **2013**, *64*, 559–582.

(561) Pfannschmidt, T. Plastidial Retrograde Signalling - a True "Plastid Factor" or Just Metabolite Signatures? *Trends Plant Sci.* **2010**, *15*, 427–435.

(562) Chan, K. X.; Phua, S. Y.; Crisp, P.; McQuinn, R.; Pogson, B. J. Learning the Languages of the Chloroplast: Retrograde Signaling and Beyond. *Annu. Rev. Plant Biol.* **2016**, *67*, 25–53.

(563) Jones, R. W.; Whitmarsh, J. Origin of the Electrogenic Reaction in the Chloroplast Cytochrome b/f Complex. *Photobiochem.Photobiophys.* **1985**, *9*, 119–127.

(564) Joliot, P.; Joliot, A. Proton Pumping and Electron Transfer in the Cytochrome b f Complex of Algae. *Biochim. Biophys. Acta* **1986**, *849*, 211–222.

(565) Jones, R. W.; Whitmarsh, J. Inhibition of Electron Transfer and the Electrogenic Reaction in the Cytochrome b f Complex by 2-n-Nonyl-4-HydroxyquinolineN-Oxide (NQNO) and 2,5-Dibromo-3-Methyl-6-Isopropyl-p-Benzoquinone (DBMIB). *Biochim. Biophys. Acta* **1988**, *933*, 258–268.

(566) Rich, P. R.; Madgwick, S. A.; Brown, S.; von Jagow, G.; Brandt, U. MOA-Stilbene: A New Tool for Investigation of the Reactions of the Chloroplast Cytochrome Bf Complex. *Photosynth. Res.* **1992**, *34*, 465–477.

(567) Brandt, U.; Trumpower, B. The Protonmotive Q Cycle in Mitochondria and Bacteria. *Crit. Rev. Biochem. Mol. Biol.* **1994**, *29*, 165–197.

(568) Dutton, P. L. Redox Potentiometry: Determination of Midpoint Potentials of Oxidation-Reduction Components of Biological Electron-Transfer Sysyems. *Methods Enzymol.* **1978**, *54*, 411–435.

(569) Czapla, M.; Borek, A.; Sarewicz, M.; Osyczka, A. Enzymatic Activities of Isolated Cytochrome Bc_1-like Complexes Containing Fused Cytochrome *b* Subunits with Asymmetrically Inactivated Segments of Electron Transfer Chains. *Biochemistry* **2012**, *51*, 829–835.

(570) Eddowes, M. J.; Hill, H. A. O. Electrochemistry of Horse Heart Cytochrome C. *J. Am. Chem. Soc.* **1979**, *101*, 4461–4464.

(571) Shinkarev, V. P.; Wraight, C. A. Intermonomer Electron Transfer in the Bc_1 Complex Dimer Is Controlled by the Energized State and by Impaired Electron Transfer between Low and High Potential Hemes. *FEBS Lett.* **2007**, *581*, 1535–1541.

(572) Rottenberg, H.; Covian, R.; Trumpower, B. L. Membrane Potential Greatly Enhances Superoxide Generation by the Cytochrome Bc_1 Complex Reconstituted into Phospholipid Vesicles. *J. Biol. Chem.* **2009**, *284*, 19203–19210.

(573) Quinlan, C. L.; Gerencser, A. A.; Treberg, J. R.; Brand, M. D. The Mechanism of Superoxide Production by the Antimycin-Inhibited Mitochondrial Q-Cycle. *J. Biol. Chem.* **2011**, *286*, 31361–31372.

(574) Link, T. A. The Role of the "Rieske" Iron Sulfur Protein in the Hydroquinone Oxidation (QP) Site of the Cytochrome Bc1 Complex. *FEBS Lett.* **1997**, *412*, 257–264.

(575) Crofts, A. R.; Hong, S.; Ugulava, N.; Barquera, B.; Gennis, R.; Guergova-Kuras, M.; Berry, E. A. Pathways for Proton Release during Ubihydroquinone Oxidation by the Bc1 Complex. *Proc. Natl. Acad. Sci. U. S. A.* **1999**, *96*, 10021–10026.

(576) Zito, F.; Finazzi, G.; Delosme, R.; Nitschke, W.; Picot, D.; Wollman, F. A. The Qo Site of Cytochrome B6f Complexes Controls the Activation of the LHCII Kinase. *EMBO J.* **1999**, *18*, 2961–2969.

(577) Hagen, W. R.; Hearshen, D. O.; Harding, L. J.; Dunham, W. R. Quantitative Numerical Analysis of g Strain in the EPR of Distributed Systems and Its Importance for Multicenter Metalloproteins. *J. Magn. Reson.* **1985**, *61*, 233–244.

(578) Ding, H.; Robertson, D. E.; Daldal, F.; Dutton, P. L. Cytochrome Bc_1 Complex [2Fe-2S] Cluster and Its Interaction with Ubiquinone and Ubihydroquinone at the Q_o Site: A Double-Occupancy Q_o Site Model. *Biochemistry* **1992**, *31*, 3144–3158.

(579) Osyczka, A.; Zhang, H.; Mathe, C.; Rich, P. R.; Moser, C. C.; Dutton, P. L. Role of the PEWY Glutamate in Hydroquinone-Quinone Oxidation-Reduction Catalysis in the Q_o Site of Cytochrome Bc_1. *Biochemistry* **2006**, *45*, 10492–10503.

(580) Sharp, R. E.; Moser, C. C.; Gibney, B. R.; Dutton, P. L. Primary Steps in the Energy Conversion Reaction of the Cytochrome Bc_1 Complex Q_O Site. *J. Bioenerg. Biomembr.* **1999**, *31*, 225–234.

(581) Bowman, M. K.; Berry, E. A.; Roberts, A. G.; Kramer, D. M. Orientation of the G-Tensor Axes of the Rieske Subunit in the Cytochrome Bc_1 Complex. *Biochemistry* **2004**, *43*, 430–436.

(582) Sharp, R. E.; Palmitessa, A.; Gibney, B. R.; Moser, C. C.; Daldal, F.; Dutton, P. L. Non-Inhibiting Perturbation of the Primary Energy Conversion Site (Q_o Site) in *Rhodobacter Capsulatus* Ubihydroquinone:Cytochrome *c* Oxidoreductase (Cytochrome Bc_1 Complex). *FEBS Lett.* **1998**, *431*, 423–426.

(583) Bizzarri, A. R.; Cannistraro, S. Solvent Modulation of the Structural Heterogeneity in FeIII Myoglobin Samples: A Low Temperature EPR Investigation. *Eur. Bophysics J.* **1993**, *22*, 259–267.

(584) Sharp, R. E.; Gibney, B. R.; Palmitessa, A.; White, J. L.; Dixon, J. A.; Moser, C. C.; Daldal, F.; Dutton, P. L. Effect of Inhibitors on the Ubiquinone Binding Capacity of the Primary Energy Conversion Site in the *Rhodobacter Capsulatus* Cytochrome Bc_1 Complex. *Biochemistry* **1999**, *38*, 14973–14980.

(585) Bartoschek, S.; Johansson, M.; Geierstanger, B. H.; Okun, J. G.; Lancaster, C. R. D.; Humpfer, E.; Yu, L.; Yu, C.-A.; Griesinger, C.; Brandt, U. Three Molecules of Ubiquinone Bind Specifically to Mitochondrial Cytochrome Bc_1 Complex. *J. Bol. Chem.* **2001**, *276*, 35231–35234.

(586) Brandt, U. Bifurcated Ubihydroquinone Oxidation in the Cytochrome Bc_1 Complex by Proton-Gated Charge Transfer. *FEBS Lett.* **1996**, *387*, 1–6.

(587) Urban, P. F.; Klingenberg, M. On the Redox Potentials of Ubiquinone and Cytochrome b in the Respiratory Chain. *Eur. J. Biochem.* **1969**, *9*, 519–525.

(588) Fisher, N.; Rich, P. R. A Motif for Quinone Binding Sites in Respiratory and Photosynthetic Systems. *J. Mol. Biol.* **2000**, *296*, 1153–1162.

(589) Crofts, A. R.; Guergova-Kuras, M.; Kuras, R.; Ugulava, N.; Li, J.; Hong, S. Proton-Coupled Electron Transfer at the Q_o Site: What Type of Mechanism Can Account for the High Activation Barrier? *Biochim. Biophys. Acta* **2000**, *1459*, 456–466.

(590) Victoria, D.; Burton, R.; Crofts, A. R. Role of the -PEWY-Glutamate in Catalysis at the Qo-Site of the Cyt Bc1 Complex. *Biochim. Biophys. Acta - Bioenerg.* **2013**, *1827*, 365–386.

(591) Lübben, M. Cytochomes of Archaeal Electron Transfer Chains. *Biochim. Biophys. Acta* **1995**, *1229*, 1–22.

(592) Gurbiel, R. J.; Ohnishi, T.; Robertson, D. E.; Daldal, F.; Hoffman, B. M. Q-Band ENDOR Spectra of the Rieske Protein from Rhodobacter Capsulatus Ubiquinol-Cytochrome c

Oxidoreductase Show Two Histidines Coordinated to the [2Fe-2S] Cluster. *Biochemistry* **1991**, *30*, 11579–11584.

(593) Link, T. A.; Iwata, S. Functional Implications of the Structure of the "Rieske" Iron-Sulfur Protein of Bovine Heart Mitochondrial Cytochrome Bc1 Complex. *Biochim. Biophys. Acta* **1996**, *1275*, 54–60.

(594) Link, T. A.; Hagen, W. R.; Pierik, A. J.; Assmann, C.; von JAGOW, G. Determination of the Redox Properties of the Rieske [2Fe-2S] Cluster of Bovine Heart Bc_1 Complex by Direct Electrochemistry of a Water-soluble Fragment. *Eur. J. Biochem.* **1992**, *208*, 685–691.

(595) Hong, S.; Ugulava, N.; Guergova-Kuras, M.; Crofts, A. R. The Energy Landscape for Ubihydroquinone Oxidation at the Q_o Site of the Bc_1 Complex in *Rhodobacter Sphaeroides*. *J. od Biol. Chem.* **1999**, *274*, 33931–33944.

(596) Crofts, A. R.; Lhee, S.; Crofts, S. B.; Cheng, J.; Rose, S. Proton Pumping in the Bc_1 Complex: A New Gating Mechanism That Prevents Short Circuits. *Biochim. Biophys. Acta* **2006**, *1757*, 1019–1034.

(597) Rich, P. R. The Quinone Chemistry of *Bc* Complexes. *Biochim. Biophys. Acta* **2004**, *1658*, 165–171.

(598) Wenz, T.; Hellwig, P.; MacMillan, F.; Meunier, B.; Hunte, C. Probing the Role of E272 in Quinol Oxidation of Mitochondrial Complex III. *Biochemistry* **2006**, *45*, 9042–9052.

(599) Saribaş, A. S.; Ding, H.; Dutton, P. L.; Daldal, F. Tyrosine 147 of Cytochrome b Is Required for Efficient Electron Transfer at the Ubihydroquinone Oxidase Site (Qo) of the Cytochrome Bc1 Complex. *Biochemistry* **1995**, *34*, 16004–16012.

(600) Fisher, N.; Castleden, C. K.; Bourges, I.; Brasseur, G.; Dujardin, G.; Meunier, B. Human Disease-Related Mutations in Cytochrome *b* Studied in Yeast. *J. Biol. Chem.* **2004**, *279*, 12951–12958.

(601) Lee, D.-W.; Selamoglu, N.; Lanciano, P.; Cooley, J. W.; Forquer, I.; Kramer, D. M.; Daldal, F. Loss of a Conserved Tyrosine Residue of Cytochrome *b* Induces Reactive Oxygen Species Production by Cytochrome Bc_1. *J. Biol. Chem.* **2011**, *286*, 18139–18148.

(602) Ghelli, A.; Tropeano, C. V.; Calvaruso, M. A.; Marchesini, A.; Iommarini, L.; Porcelli, A. M.; Zanna, C.; De Nardo, V.; Martinuzzi, A.; Wibrand, F.; Vissing, J.; Kurelac, I.; Gasparre, G.; Selamoglu, N.; Daldal, F.; Rugolo, M. The Cytochrome b p.278Y>C Mutation Causative of a Multisystem Disorder Enhances Superoxide Production and Alters Supramolecular Interactions of Respiratory Chain Complexes. *Hum. Mol. Genet.* **2013**, *22*, 2141–2151.

(603) Lanciano, P.; Khalfaoui-Hassani, B.; Selamoglu, N.; Ghelli, A.; Rugolo, M.; Daldal, F. Molecular Mechanisms of Superoxide Production by Complex III: A Bacterial versus Human Mitochondrial Comparative Case Study. *Biochim. Biophys. Acta - Bioenerg.* **2013**, *1827*, 1332–1339.

(604) Hughes, L. M.; Lanteri, C. A.; O'Neil, M. T.; Johnson, J. D.; Gribble, G. W.; Trumpower, B. L. Design of Anti-Parasitic and Anti-Fungal Hydroxy-Naphthoquinones That Are Less Susceptible to Drug Resistance. *Mol. Biochem. Parasitol.* **2011**, *177*, 12–19.

(605) Barton, V.; Fisher, N.; Biagini, G. A.; Ward, S. A.; O'Neill, P. M. Inhibiting *Plasmodium* Cytochrome Bc_1: A Complex Issue. *Curr. Opin. Chem. Biol.* **2010**, *14*, 440–446.

(606) Nayak, S. K.; Mallik, S. B.; Kanaujia, S. P.; Sekar, K.; Ranganathan, K. R.; Ananthalakshmi, V.; Jeyaraman, G.; Saralaya, S. S.; Rao, K. S.; Shridhara, K.; Nagarajan, K.; Row, T. N. G. Crystal Structures and Binding Studies of Atovaquone and Its Derivatives with Cytochrome Bc_1: A Molecular Basis for Drug Design. *CrystEngComm* **2013**, *15*, 4871–4884.

(607) Sarewicz, M.; Bujnowicz, Ł.; Osyczka, A. Generation of Semiquinone-[2Fe-2S]+ Spin-Coupled Center at the Q_o Site of Cytochrome Bc_1 in Redox-Poised, Illuminated Photosynthetic Membranes from *Rhodobacter Capsulatus*. *Biochim. Biophys. Acta - Bioenerg.* **2018**, *1859*, 145–153.

(608) Finazzi, G.; Büschlen, S.; De Vitry, C.; Rappaport, F.; Joliot, P.; Wollman, F. A. Function-Directed Mutagenesis of the Cytochrome B6f Complex in Chlamydomonas Reinhardtii: Involvement of the Cd Loop of Cytochrome B6 in Quinol Binding to the Q0 Site. *Biochemistry* **1997**, *36*, 2867–2874.

(609) De Vitry, C.; Ouyang, Y.; Finazzi, G.; Wollman, F. A.; Kallas, T. The Chloroplast Rieske Iron-Sulfur Protein. At the Crossroad of Electron Transport and Signal Transduction. *J. Biol. Chem.* **2004**, *279*, 44621–44627.

(610) Munekage, Y.; Takeda, S.; Endo, T.; Jahns, P.; Hashimoto, T.; Shikanai, T. Cytochrome B6f Mutation Specifically Affects Thermal Dissipation of Absorbed Light Energy in Arabidopsis. *Plant J.* **2001**, *28*, 351–359.

(611) Lee, T. X.; Metzger, S. U.; Cho, Y. S.; Whitmarsh, J.; Kallas, T. Modification of Inhibitor Binding Sites in the Cytochrome Bf Complex by Directed Mutagenesis of Cytochrome B6 in Synechococcus Sp. PCC 7002. *Biochim. Biophys. Acta - Bioenerg.* **2001**, *1504*, 235–247.

(612) Erecinska, M.; Chance, B.; Wilson, D. F.; Dutton, P. L. Aerobic Reduction of Cytochrome B566 in Pigeon-Heart Mitochondria. *Proc. Natl. Acad. Sci.* **1972**, *69*, 50–54.

(613) Miki, T.; Miki, M.; Orii, Y. Membrane Potential-Linked Reversed Electron Transfer in the Beef Heart Cytochrome Bc_1 Complex Reconstituted into Potassium-Loaded Phospholipid Vesicles. *J. Biol. Chem.* **1994**, *269*, 1827–1833.

(614) Elbehti, A.; Brasseur, G.; Lemesle-Meunier, D. First Evidence for Existence of an Uphill Electron Transfer through the Bc1 and NADH-Q Oxidoreductase Complexes of the Acidophilic Obligate Chemolithotrophic Ferrous Ion-Oxidizing Bacterium Thiobacillus Ferrooxidans. *J. Bacteriol.* **2000**, *182*, 3602–3606.

(615) Osyczka, A.; Moser, C. C.; Daldal, F.; Dutton, P. L. Reversible Redox Energy Coupling in Electron Transfer Chains. *Nature* **2004**, *427*, 607–612.

(616) Malnoë, A.; Wollman, F.-A.; de Vitry, C.; Rappaport, F. Photosynthetic Growth despite a Broken Q-Cycle. *Nat. Commun.* **2011**, *2*, 1–6.

(617) Ransac, S.; Mazat, J.-P. How Does Antimycin Inhibit the Bc1 Complex? A Part-Time Twin. *Biochim. Biophys. Acta - Bioenerg.* **2010**, *1797*, 1849–1857.

(618) Ransac, S.; Parisey, N.; Mazat, J.-P. The Loneliness of the Electrons in the Bc1 Complex. *Biochim. Biophys. Acta* **2008**, *1777*, 1053–1059.

(619) Snyder, C. H.; Gutierrez-Cirlos, E. B.; Trumpower, B. L. Evidence for a Concerted Mechanism of Ubiquinol Oxidation by the Cytochrome Bc_1 Complex. *J. Biol. Chem.* **2000**, *275*, 13535–13541.

(620) Trumpower, B. L. A Concerted, Alternating Sites Mechanism of Ubiquinol Oxidation by the Dimeric Cytochrome Bc_1 Complex. *Biochim. Biophys. Acta* **2002**, *1555*, 166–173.

(621) Boman, P.; Eliasson, B.; Grimm, R. A.; Martin, G. S.; Strnad, J. T.; Staley, S. W. Kinetics of Bond Shift and Charge Transfer in Dialkynylphenylene- Bridged Dicyclooctatetraenes and Their Dianions. *J. Am. Chem. Soc.* **1999**, *121*, 1558–1564.

(622) Lambert, C. Concerted Two-Electron-Transfer Processes in Mixed-Valence Species with Square Topology. *ChemPhysChem* **2003**, *4*, 877–880.

(623) Yu, C.-A.; Wen, X.; Xiao, K.; Xia, D.; Yu, L. Inter- and Intra-Molecular Electron Transfer in the Cytochrome Bc1 Complex. *Biochim. Biophys. Acta - Bioenerg.* **2002**, *1555*, 65–70.

(624) Chance, B.; Williams, G. R. The Respiratory Chain and Oxidative Phosphorylation. In *Advances in Enzymology and Related Subjects of Biochemistry*; wiley, **1956**; Vol. 17, pp 65–134.

(625) Boveris, A.; Oshino, N.; Chance, B. The Cellular Production of Hydrogen Peroxide. *Biochem. J.* **1972**, *128*, 617–630.

(626) Loschen, G.; Azzi, A.; Richter, C.; Flohé, L. Superoxide Radicals as Precursors Mitochondrial Hydrogen Peroxide. *FEBS Lett.* **1974**, *42*, 68–72.

(627) Boveris, A.; Chance, B. The Mitochondrial Generation of Hydrogen Peroxide. General Properties and Effect of Hyperbaric Oxygen. *Biochem. J.* **1973**, *134*, 707–716.

(628) Boveris, A.; Cadenas, E. Mitochondrial Production of Superoxide Anions and Its Relationship to the Antimycin Insensitive Respiration. *FEBS Lett.* **1975**, *54*, 311–314.

(629) Boveris, A.; Cadenas, E.; Stoppani, A. O. M. Role of Ubiquinone in the Mitochondrial Generation of Hydrogen Peroxide. *Biochem. J.* **1976**, *156*, 435–444.

(630) Nohl, H.; Hegner, D. Do Mitochondria Produce Oxygen Radicals *in Vivo*? *Eur. J. Biochem.* **1978**, *82*, 563–567.

(631) Ksenzenko, M.; Konstantinov, A. A.; Khomutov, G. B.; Tikhonov, A. N.; Ruuge, E. K. Effect of Electron Transfer Inhibitors on Superoxide Generation in the Cytochrome Bc_1 Site of the Mitochondrial Respiratory Chain. *FEBS Lett.* **1983**, *155*, 19–24.

(632) Muller, F.; Crofts, A. R.; Kramer, D. M. Multiple Q-Cycle Bypass Reactions at the Q_o Site of the Cytochrome Bc_1 Complex. *Biochemistry* **2002**, *41*, 7866–7874.

(633) Muller, F. L.; Roberts, A. G.; Bowman, M. K.; Kramer, D. M. Architecture of the Q_o Site of the Cytochrome Bc_1 Complex Probed by Superoxide Production. *Biochemistry* **2003**, *42*, 6493–6499.

(634) Kramer, D. M.; Roberts, A. G.; Muller, F.; Cape, J. L.; Bowman, M. K. Q-Cycle Bypass Reactions at the Q_o Site of the Cytochrome Bc_1 (and Related) Complexes. *Methods Enzymol.* **2004**, *382*, 21–45.

(635) Borek, A.; Sarewicz, M.; Osyczka, A. Movement of the Iron-Sulfur Head Domain of Cytochrome Bc_1 Transiently Opens the Catalytic Q_o Site for Reaction with Oxygen. *Biochemistry* **2008**, *47*, 12365–12370.

(636) Dröse, S.; Brandt, U. The Mechanism of Mitochondrial Superoxide Production by the Cytochrome Bc1 Complex. *J. Biol. Chem.* **2008**, *283*, 21649–21654.

(637) Korshunov, S. S.; Skulachev, V. P.; Starkov, A. A. High Protonic Potential Actuates a Mechanism of Production of Reactive Oxygen Species in Mitochondria. *FEBS Lett.* **1997**, *416*, 15–18.

(638) Yang, S.; Ma, H.-W.; Yu, L.; Yu, C.-A. On the Mechanism of Quinol Oxidation at the Q P Site in the Cytochrome Bc 1 Complex. *J. Biol. Chem.* **2008**, *283*, 28767–28776.

(639) Legros, F.; Chatzoglou, E.; Frachon, P.; Ogier De Baulny, H.; Laforêt, P.; Jardel, C.; Godinot, C.; Lombès, A. Functional Characterization of Novel Mutations in the Human Cytochrome *b* Gene. *Eur. J. Hum. Genet.* **2001**, *9*, 510–518.

(640) Dumoulin, R.; Sagnol, I.; Ferlin, T.; Bozon, D.; Stepien, G.; Mousson, B. A Novel Gly290asp Mitochondrial Cytochrome b Mutation Linked to a Complex III Deficiency in Progressive Exercise Intolerance. *Mol. Cell. Probes* **1996**, *10*, 389–391.

(641) Rutherford, A. W.; Osyczka, A.; Rappaport, F. Back-Reactions, Short-Circuits, Leaks and Other Energy Wasteful Reactions in Biological Electron Transfer: Redox Tuning to Survive Life in O_2. *FEBS Lett.* **2012**, *586*, 603–616.

(642) Bleier, L.; Dröse, S. Superoxide Generation by Complex III: From Mechanistic Rationales to Functional Consequences. *Biochim. Biophys. Acta - Bioenerg.* **2013**, *1827*, 1320–1331.

(643) Zhou, F.; Yin, Y.; Su, T.; Yu, L.; Yu, C.-A. Oxygen Dependent Electron Transfer in the Cytochrome Bc_1 Complex. *Biochim. Biophys. Acta - Bioenerg.* **2012**, *1817*, 2103–2109.

(644) Husen, P.; Solov'yov, I. A. Spontaneous Binding of Molecular Oxygen at the Q_o-Site of the Bc_1 Complex Could Stimulate Superoxide Formation. *J. Am. Chem. Soc.* **2016**, *138*, 12150–12158.

(645) Nohl, H.; Jordan, W. The Mitochondrial Site of Superoxide Formation. *Biochem. Biophys. Res. Commun.* **1986**, *138*, 533–539.

(646) Raha, S.; McEachern, G. E.; Myint, A. T.; Robinson, B. H. Superoxides from Mitochondrial Complex III: The Role of Manganese Superoxide Dismutase. *Free Radic. Biol. Med.* **2000**, *29*, 170–180.

(647) Kolling, D. R. J.; Samoilova, R. I.; Holland, J. T.; Berry, E. A.; Dikanov, S. A.; Crofts, A. R. Exploration of Ligands to the Q_i Site Semiquinone in the Bc_1 Complex Using High-Resolution EPR. *J. Biol. Chem.* **2003**, *278*, 39747–39754.

(648) Dikanov, S. A.; Holland, J. T.; Endeward, B.; Kolling, D. R. J.; Samoilova, R. I.; Prisner, T. F.; Crofts, A. R. Hydrogen Bonds between Nitrogen Donors and the Semiquinone in the Q_i-Site of the Bc_1 Complex. *J. Biol. Chem.* **2007**, *282*, 25831–25841.

(649) Sun, J.; Trumpower, B. L. Superoxide Anion Generation by the Cytochrome Bc_1 Complex. *Arch. Biochem. Biophys.* **2003**, *419*, 198–206.

(650) Murphy, M. P. How Mitochondria Produce Reactive Oxygen Species. *Biochem. J.* **2009**, *417*, 1–13.

(651) Guzy, R. D.; Schumacker, P. T. Oxygen Sensing by Mitochondria at Complex III: The Paradox of Increased Reactive Oxygen Species during Hypoxia. *Exp. Physiol.* **2006**, *91*, 807–819.

(652) Solaini, G.; Baracca, A.; Lenaz, G.; Sgarbi, G. Hypoxia and Mitochondrial Oxidative Metabolism. *Biochim. Biophys. Acta* **2010**, *1797*, 1171–1177.

(653) Berry, B. J.; Trewin, A. J.; Amitrano, A. M.; Kim, M.; Wojtovich, A. P. Use the Protonmotive Force: Mitochondrial Uncoupling and Reactive Oxygen Species. *J. Mol. Biol.* **2018**, *430*, 3873–3891.

(654) Saborido, A.; Soblechero, L.; Megías, A. Isolated Respiring Heart Mitochondria Release Oxygen Species in States 4 and 3. *Free Radic. Res.* **2005**, *39*, 921–931.

(655) West, I. C.; Mitchell, P.; Rich, P. R. Electron Conduction between b Cytochromes of the Mitochondrial Respiratory Chain in the Presence of Antimycin plus Myxothiazol. *BBA - Bioenerg.* **1988**, *933*, 35–41.

(656) Zorov, D. B.; Juhaszova, M.; Sollott, S. J. Mitochondrial Reactive Oxygen Species (ROS) and ROS-Induced ROS Release. *Physiol. Rev.* **2014**, *94*, 909–950.

(657) Muller, F. L.; Liu, Y.; Van Remmen, H. Complex III Releases Superoxide to Both Sides of the Inner Mitochondrial Membrane. *J. Biol. Chem.* **2004**, *279*, 49064–49073.

(658) Boveris, A.; Cadenas, E. Mitochondrial Production of Hydrogen Peroxide Regulation by Nitric Oxide and the Role of Ubisemiquinone. *IUBMB Life* **2001**, *50*, 245–250.

(659) Dröse, S.; Hanley, P. J.; Brandt, U. Ambivalent Effects of Diazoxide on Mitochondrial ROS Production at Respiratory Chain Complexes I and III. *Biochim. Biophys. Acta* **2009**, *1790*, 558–565.

(660) Forman, H. J.; Azzi, A. On the Virtual Existence of Superoxide Anions in Mitochondria: Thoughts Regarding Its Role in Pathophysiology. *FASEB J.* **1997**, *11*, 374–375.

(661) Hollis, V. S.; Palacios-Callender, M.; Springett, R. J.; Delpy, D. T.; Moncada, S. Monitoring Cytochrome Redox Changes in the Mitochondria of Intact Cells Using Multi-Wavelength Visible Light Spectroscopy. *Biochim. Biophys. Acta - Bioenerg.* **2003**, *1607*, 191–202.

(662) Benard, G.; Faustin, B.; Galinier, A.; Rocher, C.; Bellance, N.; Smolkova, K.; Casteilla, L.; Rossignol, R.; Letellier, T. Functional Dynamic Compartmentalization of Respiratory Chain Intermediate Substrates: Implications for the Control of Energy Production and Mitochondrial Diseases. *Int. J. Biochem. Cell Biol.* **2008**, *40*, 1543–1554.

(663) Han, D.; Antunes, F.; Canali, R.; Rettori, D.; Cadenas, E. Voltage-Dependent Anion Channels Control the Release of the Superoxide Anion from Mitochondria to Cytosol. *J. Biol. Chem.* **2003**, *278*, 5557–5563.

(664) Goldsteins, G.; Keksa-Goldsteine, V.; Ahtoniemi, T.; Jaronen, M.; Arens, E.; Åkerman, K.; Chan, P. H.; Koistinaho, J. Deleterious Role of Superoxide Dismutase in the Mitochondrial Intermembrane Space. *J. Biol. Chem.* **2008**, *283*, 8446–8452.

(665) Butler, J.; Koppenol, W. H.; Margoliash, E. Kinetics and Mechanism of the Reduction of Ferricytochrome c by the Superoxide Anion. *J. Biol. Chem.* **1982**, *257*, 10747–10750.

(666) Finkelstein, E.; Rosen, G. M.; Rauckman, E. J. Spin Trapping. Kinetics of the Reaction of Superoxide and Hydroxyl Radicals with Nitrones. *J. Am. Chem. Soc.* **1980**, *102*, 4994–4999.

(667) de Vries, S.; Albracht, S. P.; Berden, J. A.; Slater, E. C. A New Species of Bound Ubisemiquinone Anion in QH_2: Cytochrome *c* Oxidoreductase. *J. Biol. Chem.* **1981**, *256*, 11996–11998.

(668) Jünemann, S.; Heathcote, P.; Rich, P. R. On the Mechanism of Quinol Oxidation in the $Bc<_1$ Complex. *J. Biol. Chem.* **1998**, *273*, 21603–21607.

(669) Fournel, A.; Gambarelli, S.; Guigliarelli, B.; More, C.; Asso, M.; Chouteau, G.; Hille, R.; Bertrand, P. Magnetic Interactions between a $[4Fe–4S]^{1+}$ Cluster and a Flavin Mononucleotide Radical in the Enzyme Trimethylamine Dehydrogenase: A High-Field Electron Paramagnetic Resonance Study. *J. Chem. Phys.* **1998**, *109*, 10905–10913.

(670) Calvo, R. EPR Measurements of Weak Exchange Interactions Coupling Unpaired Spins in Model Compounds. *Appl. Magn. Reson.* **2007**, *31*, 271–299.

(671) Bujnowicz, Ł.; Sarewicz, M.; Borek, A.; Kuleta, P.; Sarewicz, M.; Osyczka, A. Suppression of Superoxide Production by a Spin-Spin Coupling between Semiquinone and the Rieske Cluster in Cytochrome Bc_1. *FEBS Lett.* **2019**, *593*, 3–12.

(672) Fisher, N.; Bowman, M. K.; Kramer, D. M. Electron Transfer Reactions at the Qo Site of the Cytochrome Bc1 Complex : The Good , the Bad , and the Ugly. *Cytochrome Complexes Evol. Struct. Energy Transduction, Signal.* **2016**, No. JANUARY.

(673) Lange, C.; Nett, J. H.; Trumpower, B. L.; Hunte, C. Specific Roles of Protein-Phospholipid Interactions in the Yeast Cytochrome Bc1 Complex Structure. *EMBO J.* **2001**, *20*, 6591–6600.

(674) Hunte, C.; Palsdottir, H.; Trumpower, B. L. Protonmotive Pathways and Mechanisms in the Cytochrome Bc_1 Complex. *FEBS Lett.* **2003**, *545*, 39–46.

(675) Postila, P. A.; Kaszuba, K.; Kuleta, P.; Vattulainen, I.; Sarewicz, M.; Osyczka, A.; Róg, T. Atomistic Determinants of Co-Enzyme Q Reduction at the Qi-Site of the Cytochrome Bc1 Complex. *Sci. Rep.* **2016**, *6*, 33607.

(676) Gray, K. A.; Dutton, P. L.; Daldal, F. Requirement of Histidine 217 for Ubiquinone Reductase Activity (Q_i Site) in the Cytochrome Bc_1 Complex. *Biochemistry* **1994**, *33*, 723–733.

(677) Kuleta, P.; Sarewicz, M.; Postila, P. A.; Róg, T.; Osyczka, A. Identifying Involvement of Lys251/Asp252 Pair in Electron Transfer and Associated Proton Transfer at the Quinone Reduction Site of *Rhodobacter Capsulatus* Cytochrome Bc_1. *Biochim. Biophys. Acta - Bioenerg.* **2016**, *1857*, 1661–1668.

(678) Hanson, D. K.; Tiede, D. M.; Nance, S. L.; Chang, C. H.; Schiffer, M. Site-Specific and Compensatory Mutations Imply Unexpected Pathways for Proton Delivery to the QB Binding Site of the Photosynthetic Reaction Center. *Proc. Natl. Acad. Sci. U. S. A.* **1993**, *90*, 8929–8933.

(679) Ohnishi, T.; Trumpower, B. L. Differential Effects of Antimycin on Ubisemiquinone Bound in Different Environments in Isolated Succinate-Cytochrome c Reductase Complex. *J. Biol. Chem.* **1980**, *255*, 3278–3284.

(680) Hong, S.; de Almeida, W. B.; Taguchi, A. T.; Samoilova, R. I.; Gennis, R. B.; O'Malley, P. J.; Dikanov, S. A.; Crofts, A. R. The Semiquinone at the Qi Site of the Bc1 Complex Explored Using HYSCORE Spectroscopy and Specific Isotopic Labeling of Ubiquinone in Rhodobacter Sphaeroides via 13C Methionine and Construction of a Methionine Auxotroph. *Biochemistry* **2014**, *53*, 6022–6631.

(681) de la Rosa, F. F.; Palmer, G. Reductive Titration of CoQ-Depleted Complex III from Baker's Yeast: Evidence for an Exchange-Coupled Complex between QH· and Low-Spin Ferricytochrome *B*. *FEBS* **1983**, *163*, 140–143.

(682) Salerno, J. C.; Osgood, M.; Liu, Y.; Taylor, H.; Scholes, C. P. Electron Nuclear Double Resonance (ENDOR) of the $Q_c^{\cdot-}$ Ubisemiquinone Radical in the Mitochondrial Electron Transport Chain. *Biochemistry* **1990**, *29*, 6987–6993.

(683) Dikanov, S. A.; Samoilova, R. I.; Kolling, D. R. J.; Holland, J. T.; Crofts, A. R. Hydrogen Bonds Involved in Binding the Qi-Site Semiquinone in the Bc1 Complex, Identified through Deuterium Exchange Using Pulsed EPR. *J. Biol. Chem.* **2004**, *279*, 15814–15823.

(684) MacMillan, F.; Lange, C.; Bawn, M.; Hunte, C. Resolving the EPR Spectra in the Cytochrome Bc_1 Complex from *Saccharomyces Cerevisiae*. *Appl. Magn. Reson.* **2010**, *37*, 305–316.

(685) de Vries, S.; Albracht, S. P. J.; Berden, J. A.; Marres, C. A. M.; Slater, E. C. The Effect of PH, Ubiquinone Depletion and Myxothiazol on the Reduction Kinetics of the Prosthetic Groups of Ubiquinol:Cytochrome *c* Oxidoreductase. *Biochim. Biophys. Acta* **1983**, *723*, 91–103.

(686) Leigh, J. S. ESR Rigid-Lattice Line Shape in a System of Two Interacting Spins. *J. Chem. Phys.* **1970**, *52*, 2608–2612.

(687) Hagen, W. R. *Biomolecular EPR Spectroscopy*; CRC Press Taylor & Francis Group: Boca Raton, **2009**.

(688) Lin, M. T.; Baldansuren, A.; Hart, R.; Samoilova, R. I.; Narasimhulu, K. V; Yap, L. L.; Choi, S. K.; O'Malley, P. J.; Gennis, R. B.; Dikanov, S. A. Interactions of Intermediate Semiquinone with Surrounding Protein Residues at the QH Site of Wild-Type and D75H Mutant Cytochrome Bo3 from Escherichia Coli. *Biochemistry* **2012**, *51*, 3827–3838.

(689) Martin, E.; Samoilova, R. I.; Narasimhulu, K. V; Lin, T. J.; OMalley, P. J.; Wraight, C. A.; Dikanov, S. A. Hydrogen Bonding and Spin Density Distribution in the QB Semiquinone of Bacterial Reaction Centers and Comparison with the QA Site. *J. Am. Chem. Soc.* **2011**, *133*, 5525–5537.

(690) Wang, X.; Yu, L.; Inakollu, V. S. S.; Pan, X.; Ma, J.; Yu, H. Molecular Quantum Dot Cellular Automata Based on Diboryl Monoradical Anions. *J. Phys. Chem. C* **2018**, *122*, 2454–2460.

(691) de Lacroix de Lavalette, A.; Barbagallo, R. P.; Zito, F. Why Is It so Difficult to Construct Qi Site Mutants in Chlamydomonas Reinhardtii? *Comptes Rendus - Biol.* **2008**, *331*, 510–517.

(692) Ondarroa, M.; Zito, F.; Finazzi, G.; Joliot, P.; Wollman, F. A.; Rich, P. R. Characterization and Electron Transfer Kinetics of Wild Type and Mutant Strains of Chlamydomonas Reinhardtii. *Biochem. Soc. Trans.* **1996**, *24*, 398.

(693) Kuras, R.; De Vitry, C.; Choquet, Y.; Girard-Bascou, J.; Culler, D.; Büschlen, S.; Merchant, S.; Wollman, F. A. Molecular Genetic Identification of a Pathway for Heme Binding to Cytochrome B6. *J. Biol. Chem.* **1997**, *272*, 32427–32435.

(694) Nelson, M. E.; Finazzi, G.; Qing, J. W.; Middleton-Zarka, K. A.; Whitmarsh, J.; Kallas, T. Cytochrome b 6 Arginine 214 of Synechococcus Sp. PCC 7002, a Key Residue for Quinone-Reductase Site Function and Turnover of the Cytochrome Bf Complex. *J. Biol. Chem.* **2005**, *280*, 10395–10402.

(695) De Lavalette, A. D. L.; Finazzi, G.; Zito, F. B6f-Associated Chlorophyll: Structural and Dynamic Contribution to the Different Cytochrome Functions. *Biochemistry* **2008**, *47*, 5259–5265.

(696) Dumas, L.; Zito, F.; Blangy, S.; Auroy, P.; Johnson, X.; Peltier, G.; Alric, J. A Stromal Region of Cytochrome b_6f Subunit IV Is Involved in the Activation of the Stt7 Kinase in *Chlamydomonas*. *Proc. Natl. Acad. Sci.* **2017**, *114*, 12063 – 12068.

(697) Moser, C. C.; Farid, T. A.; Chobot, S. E.; Dutton, P. L. Electron Tunneling Chains of Mitochondria. *Biochem. Biophys. Acta* **2006**, *1757*, 1096–1109.

(698) Moser, C. C.; Chobot, S. E.; Page, C. C.; Dutton, P. L. Distance Metrics for Heme Protein Electron Tunneling. *Biochim. Biophys. Acta - Bioenerg.* **2008**, *1777*, 1032–1037.

(699) Sarewicz, M.; Ekiert, R.; Osyczka, A. Inter-Monomer Electron Transfer in Cytochrome *Bc* Complexes. In *Cytochrome complexes: Evolution, structures, energy transduction, and signaling*; Cramer, W. A., Kallas, T., Eds.; Dordrecht, **2016**; pp 281–294.

(700) Gopta, O. A.; Feniouk, B. A.; Junge, W.; Mulkidjanian, A. Y. The Cytochrome Bc_1 Complex of *Rhodobacter Capsulatus*: Ubiquinol Oxidation in a Dimeric Q-Cycle? *FEBS Lett.* **1998**, *431*, 291–296.

(701) Covian, R.; Trumpower, B. L. Rapid Electron Transfer between Monomers When the Cytochrome Bc1 Complex Dimer Is Reduced through Center N. *J. Biol. Chem.* **2005**, *280*, 22732–22740.

(702) Marcus, R. A.; Sutin, N. Electron Transfers in Chemistry and Biology. *Biochim. Biophys. Acta* **1985**, *811*, 265–322.

(703) Lanciano, P.; Khalfaoui-Hassani, B.; Selamoglu, N.; Daldal, F. Intermonomer Electron Transfer between the *b* Hemes of Heterodimeric Cytochrome Bc_1. *Biochemistry* **2013**, *52*, 7196–7206.

(704) Czapla, M.; Cieluch, E.; Borek, A.; Sarewicz, M.; Osyczka, A. Catalytically-Relevant Electron Transfer between Two Hemes b_L in the Hybrid Cytochrome Bc_1-like Complex Containing a Fusion of *Rhodobacter Sphaeroides* and *Capsulatus* Cytochromes *B*. *Biochim. Biophys. Acta* **2013**, *1827*, 751–760.

(705) Ekiert, R.; Czapla, M.; Sarewicz, M.; Osyczka, A. Hybrid Fusions Show That Inter-Monomer Electron Transfer Robustly Supports Cytochrome Bc_1 Function in Vivo. *Biochem. Biophys. Res. Commun.* **2014**, *451*, 270–275.

(706) Czapla, M.; Borek, A.; Sarewicz, M.; Osyczka, A. Fusing Two Cytochromes *b* of *Rhodobacter Capsulatus* Cytochrome Bc_1 Using Various Linkers Defines a Set of Protein Templates for Asymmetric Mutagenesis. *Protein Eng. Des. Sel.* **2012**, *25*, 15–25.

(707) Czapla, M.; Sarewicz, M.; Osyczka, A. Fusing Proteins as an Approach to Study Bioenergetic Enzymes and Processes. In *Biochimica et Biophysica Acta - Bioenergetics*; Elsevier, **2012**; Vol. 1817, pp 1847–1851.

(708) Mulkidjanian, A. Y. Proton Translocation by the Cytochrome Bc1 Complexes of Phototrophic Bacteria: Introducing the Activated Q-Cycle. *Photochem. Photobiol. Sci.* **2007**, *6*, 19–34.

(709) Hong, S.; Victoria, D.; Crofts, A. R. Inter-Monomer Electron Transfer Is Too Slow to Compete with Monomeric Turnover in Bc_1 Complex. *Biochim. Biophys. Acta* **2012**, *1817*, 1053–1062.

(710) Lanciano, P.; Lee, D.-W.; Yang, H.; Darrouzet, E.; Daldal, F. Intermonomer Electron Transfer between the Low-Potential *b* Hemes of Cytochrome Bc_1. *Biochemistry* **2011**, *50*, 1651–1663.

(711) Khalfaoui-Hassani, B.; Lanciano, P.; Daldal, F. A Robust Genetic System for Producing Heterodimeric Native and Mutant Cytochrome Bc_1. *Biochemistry* **2013**, *52*, 7184–7195.

(712) Kramer, D. M.; Avenson, T. J.; Edwards, G. E. Dynamic Flexibility in the Light Reactions of Photosynthesis Governed by Both Electron and Proton Transfer Reactions. *Trends Plant Sci.* **2004**, *9*, 349–357.

(713) Shikanai, T. Cyclic Electron Transport Around Photosystem I: Genetic Approaches. *Annu. Rev. Plant Biol.* **2007**, *58*, 199–217.

(714) Johnson, G. N. Physiology of PSI Cyclic Electron Transport in Higher Plants. *Biochim. Biophys. Acta - Bioenerg.* **2011**, *1807*, 384–389.

(715) Alric, J.; Johnson, X. Alternative Electron Transport Pathways in Photosynthesis: A Confluence of Regulation. *Curr. Opin. Plant Biol.* **2017**, *37*, 78–86.

(716) Rumeau, D.; Peltier, G.; Cournac, L. Chlororespiration and Cyclic Electron Flow around PSI during Photosynthesis and Plant Stress Response. *Plant, Cell Environ.* **2007**, *30*, 1041–1051.

(717) Lehtimäki, N.; Lintala, M.; Allahverdiyeva, Y.; Aro, E. M.; Mulo, P. Drought Stress-Induced Upregulation of Components Involved in Ferredoxin-Dependent Cyclic Electron Transfer. *J. Plant Physiol.* **2010**, *167*, 1018–1022.

(718) Allorent, G.; Osorio, S.; Ly Vu, J.; Falconet, D.; Jouhet, J.; Kuntz, M.; Fernie, A. R.; Lerbs-Mache, S.; Macherel, D.; Courtois, F.; Finazzi, G. Adjustments of Embryonic Photosynthetic Activity Modulate Seed Fitness in Arabidopsis Thaliana. *New Phytol.* **2015**, *205*, 707–719.

(719) Tagawa, K.; Tsujimoto, H. Y.; Arnon, D. I. Role of Chloroplast Ferredoxin in the Energy Conversion Process of Photosynthesis. *Proc. Natl. Acad. Sci. U. S. A.* **1963**, *49*, 567–572.

(720) Munekage, Y.; Hashimoto, M.; Miyake, C.; Tomizawa, K. I.; Endo, T.; Tasaka, M.; Shikanai, T. Cyclic Electron Flow around Photosystem I Is Essential for Photosynthesis. *Nature* **2004**, *429*, 579–582.

(721) Carrillo, N.; Vallejos, R. H. The Light-Dependent Modulation of Photosynthetic Electron Transport. *Trends Biochem. Sci.* **1983**, *8*, 52–56.

(722) Arnon, D. I. Divergent Pathways of Photosynthetic Electron Transfer: The Autonomous Oxygenic and Anoxygenic Photosystems. *Photosynth. Res.* **1995**, *46*, 47–71.

(723) Joliot, P.; Joliot, A. Cyclic Electron Flow in C3 Plants. *Biochim. Biophys. Acta - Bioenerg.* **2006**, *1757*, 362–368.

(724) Dumas, L.; Chazaux, M.; Peltier, G.; Johnson, X.; Alric, J. Cytochrome B6f Function and Localization, Phosphorylation State of Thylakoid Membrane Proteins and Consequences on Cyclic Electron Flow. *Photosynth. Res.* **2016**, *129*, 307–320.

(725) Dekker, J. P.; Boekema, E. J. Supramolecular Organization of Thylakoid Membrane Proteins in Green Plants. *Biochim. Biophys. Acta - Bioenerg.* **2005**, *1706*, 12–39.

(726) Tremmel, I. G.; Kirchhoff, H.; Weis, E.; Farquhar, G. D. Dependence of Plastoquinol Diffusion on the Shape, Size, and Density of Integral Thylakoid Proteins. *Biochim. Biophys. Acta - Bioenerg.* **2003**, *1607*, 97–109.

(727) Johnson, M. P.; Vasilev, C.; Olsen, J. D.; Hunter, C. N. Nanodomains of Cytochrome B6f and Photosystem II Complexes in Spinach Grana Thylakoid Membranes. *Plant Cell* **2014**, *26*, 3051–3061.

(728) Alric, J.; Lavergne, J.; Rappaport, F. Redox and ATP Control of Photosynthetic Cyclic Electron Flow in Chlamydomonas Reinhardtii (I) Aerobic Conditions. *Biochim. Biophys. Acta - Bioenerg.* **2010**, *1797*, 44–51.

(729) Wikström, M.; Krab, K. The Semiquinone Cycle. A Hypothesis of Electron Transfer and Proton Translocation in Cytochrome Bc-Type Complexes. *J. Bioenerg. Biomembr.* **1986**, *18*, 181–193.

(730) Finazzi, G.; Furia, A.; Barbagallo, R. P.; Forti, G. State Transitions, Cyclic and Linear Electron Transport and Photophosphorylation in *Chlamydomonas Reinhardtii*. *Biochim. Biophys. Acta - Bioenerg.* **1999**, *1413*, 117–129.

(731) Alric, J. Redox and ATP Control of Photosynthetic Cyclic Electron Flow in Chlamydomonas Reinhardtii: (II) Involvement of the PGR5-PGRL1 Pathway under Anaerobic Conditions. *Biochim. Biophys. Acta - Bioenerg.* **2014**, *1837*, 825–834.

(732) Takahashi, H.; Clowez, S.; Wollman, F. A.; Vallon, O.; Rappaport, F. Cyclic Electron Flow Is Redox-Controlled but Independent of State Transition. *Nat. Commun.* **2013**, *4*.

(733) Laisk, A. Mathematical Modelling of Free-Pool and Channelled Electron Transport in Photosynthesis: Evidence for a Functional Supercomplex around Photosystem 1. *Proc. R. Soc. B Biol. Sci.* **1993**, *251*, 243–251.

(734) Joliot, P.; Joliot, A. Cyclic Electron Transfer in Plant Leaf. *Proc. Natl. Acad. Sci. U. S. A.* **2002**, *99*, 10209–10214.

(735) Terashima, M.; Petroutsos, D.; Hüdig, M.; Tolstygina, I.; Trompelt, K.; Gäbelein, P.; Fufezan, C.; Kudla, J.; Weinl, S.; Finazzi, G.; Hippler, M. Calcium-Dependent Regulation of Cyclic Photosynthetic Electron Transfer by a CAS, ANR1, and PGRL1 Complex. *Proc. Natl. Acad. Sci. U. S. A.* **2012**, *109*, 17717–17722.

(736) Steinbeck, J.; Ross, I. L.; Rothnagel, R.; Gäbelein, P.; Schulze, S.; Giles, N.; Ali, R.; Drysdale, R.; Sierecki, E.; Gambin, Y.; Stahlberg, H.; Takahashi, Y.; Hippler, M.; Hankamer, B. Structure of a PSI-LHCI-Cyt B6f Supercomplex in Chlamydomonas Reinhardtii

Promoting Cyclic Electron Flow under Anaerobic Conditions. *Proc. Natl. Acad. Sci. U. S. A.* **2018**, *115*, 10517–10522.

(737) Yadav, K. N. S.; Semchonok, D. A.; Nosek, L.; Kouřil, R.; Fucile, G.; Boekema, E. J.; Eichacker, L. A. Supercomplexes of Plant Photosystem I with Cytochrome B6f, Light-Harvesting Complex II and NDH. *Biochim. Biophys. Acta - Bioenerg.* **2017**, *1858*, 12–20.

(738) Peng, L.; Shimizu, H.; Shikanai, T. The Chloroplast NAD(P)H Dehydrogenase Complex Interacts with Photosystem I in Arabidopsis. *J. Biol. Chem.* **2008**, *283*, 34873–34879.

(739) Otani, T.; Yamamoto, H.; Shikanai, T. Stromal Loop of Lhca6 Is Responsible for the Linker Function Required for the NDH-PSI Supercomplex Formation. *Plant Cell Physiol.* **2017**, *58*, 851–861.

(740) Allen, J. F. Protein-Phosphorylation in Regulation of Photosynthesis. *Biochim. Biophys. Acta - Bioenerg.* **1992**, *1098*, 275–335.

(741) Murata, N.; Sugahara, K. Control of Excitation Transfer in Photosynthesis. III. Light-Induced Decrease of Chlorophyll a Fluorescence Related to Photophosphorylation System in Spinach Chloroplasts. *Biochem. Biophys. Acta* **1969**, *189*, 182–192.

(742) Bonaventura, C.; Myers, J. Fluorescence and Oxygen Evolution from Chlorella Pyrenoidosa. *BBA - Bioenerg.* **1969**, *189*, 366–383.

(743) Wollman, F. A. State Transitions Reveal the Dynamics and Flexibility of the Photosynthetic Apparatus. *EMBO J.* **2001**, *20*, 3623–3630.

(744) Depège, N.; Bellafiore, S.; Rochaix, J. D. Role of Chloroplast Protein Kinase Stt7 in LHCII Phosphorylation and State Transition in Chlamydomonas. *Science (80-.).* **2003**, *299*, 1572–1575.

(745) Bellaflore, S.; Barneche, F.; Peltler, G.; Rochalx, J. D. State Transitions and Light Adaptation Require Chloroplast Thylakoid Protein Kinase STN7. *Nature* **2005**, *433*, 892–895.

(746) Pribil, M.; Pesaresi, P.; Hertle, A.; Barbato, R.; Leister, D. Role of Plastid Protein Phosphatase TAP38 in LHCII Dephosphorylation and Thylakoid Electron Flow. *PLoS Biol.* **2010**, *8*, e1000288.

(747) Shapiguzov, A.; Ingelsson, B.; Samol, I.; Andres, C.; Kessler, F.; Rochaix, J. D.; Vener, A. V.; Goldschmidt-Clermont, M. The PPH1 Phosphatase Is Specifically Involved in LHCII Dephosphorylation and State Transitions in Arabidopsis. *Proc. Natl. Acad. Sci. U. S. A.* **2010**, *107*, 4782–4787.

(748) Wollman, F. A.; Lemaire, C. Studies on Kinase-Controlled State Transitions in Photosystem II and B6f Mutants from Chlamydomonas Reinhardtii Which Lack Quinone-Binding Proteins. *BBA - Bioenerg.* **1988**, *933*, 85–94.

(749) Vener, A. V.; van Kan, P. J. M. M.; Rich, P. R.; Ohad, I.; Andersson, B. Plastoquinol at the Quinol Oxidation Site of Reduced Cytochrome Bf Mediates Signal Transduction between

Light and Protein Phosphorylation: Thylakoid Protein Kinase Deactivation by a Single-Turnover Flash. *Proc. Natl. Acad. Sci.* **1997**, *94*, 1585–1590.

(750) Finazzi, G. The Central Role of the Green Alga Chlamydomonas Reinhardtii in Revealing the Mechanism of State Transitions. *J. Exp. Bot.* **2005**, *56*, 383–388.

(751) Shapiguzov, A.; Chai, X.; Fucile, G.; Longoni, P.; Zhang, L.; Rochaix, J. D. Activation of the Stt7/STN7 Kinase through Dynamic Interactions with the Cytochrome B6 f Complex. *Plant Physiol.* **2016**, *171*, 82–92.

(752) Finazzi, G.; Minagawa, J.; Johnson, G. N. The Cytochrome b_6f Complex: A Regulatory Hub Controlling Electron Flow and the Dynamics of Photosynthesis? In *Cytochrome Complexes: Evolution, Structures, Energy Transduction, and Signaling*; **2016**; pp 437–452.

(753) Singh, S. K.; Hasan, S. S.; Zakharov, S. D.; Naurin, S.; Cohn, W.; Ma, J.; Whitelegge, J. P.; Cramer, W. A. Trans-Membrane Signaling in Photosynthetic State Transitions: Redox- and Structure-Dependent Interaction *in Vitro* between Stt7 Kinase and the Cytochrome b_6f Complex. *J. Biol. Chem.* **2016**, *291*, 21740–21750.

(754) Hamel, P.; Olive, J.; Pierre, Y.; Wollman, F. A.; De Vitry, C. A New Subunit of Cytochrome B6f Complex Undergoes Reversible Phosphorylation upon State Transition. *J. Biol. Chem.* **2000**, *275*, 17072–17079.

(755) Finazzi, G.; Zito, F.; Barbagallo, R. P.; Wollman, F. A. Contrasted Effects of Inhibitors of Cytochrome B6f Complex on State Transitions in Chlamydomonas Reinhardtii: The Role of Qo Site Occupancy in LHCII Kinase Activation. *J. Biol. Chem.* **2001**, *276*, 9770–9774.

(756) Zito, F.; Vinh, J.; Popot, J. L.; Finazzi, G. Chimeric Fusions of Subunit IV and PetL in the B6f Complex of Chlamydomonas Reinhardtii: Structural Implications and Consequences on State Transitions. *J. Biol. Chem.* **2002**, *277*, 12446–12455.

(757) Schuster, G.; Dewit, M.; Staehelin, L. A.; Ohad, I. Transient Inactivation of the Thylakoid Photosystem II Light-Harvesting Protein Kinase System and Concomitant Changes in Intramembrane Particle Size during Photoinhibition of Chlamydomonas Reinhardtii. *J. Cell Biol.* **1986**, *103*, 71–80.

(758) Rintamäki, E.; Martinsuo, P.; Pursiheimo, S.; Aro, E. M. Cooperative Regulation of Light-Harvesting Complex II Phosphorylation via the Plastoquinol and Ferredoxin-Thioredoxin System in Chloroplasts. *Proc. Natl. Acad. Sci. U. S. A.* **2000**, *97*, 11644–11649.

(759) Hou, C. X.; Pursiheimo, S.; Rintamäki, E.; Aro, E. M. Environmental and Metabolic Control of LHCII Protein Phosphorylation: Revealing the Mechanisms for Dual Regulation of the LHCII Kinase. *Plant, Cell Environ.* **2002**, *25*, 1515–1525.

(760) Wunder, T.; Xu, W.; Liu, Q.; Wanner, G.; Leister, D.; Pribil, M. The Major Thylakoid Protein Kinases STN7 and STN8 Revisited: Effects of Altered STN8 Levels and Regulatory Specificities of the STN Kinases. *Front. Plant Sci.* **2013**, *4*.

(761) Schütz, M.; Brugna, M.; Lebrun, E.; Baymann, F.; Huber, R.; Stetter, K. O.; Hauska, G.; Toci, R.; Lemesle-Meunier, D.; Tron, P.; Schmidt, C.; Nitschke, W. Early Evolution of Cytochrome Bc Complexes. *J. Mol. Biol.* **2000**, *300*, 663–675.

Acknowledgments

AO acknowledges financial support from National Science Centre, Poland, (grant 2015/18/A/NZ1/00046) and from Foundation for Polish Science (programme TEAM, POIR.04.04.00-00-5B54/17-00)

WAC acknowledges support for the research studies described in this Review, supported at different times by the U. S. National Institutes of Health/General Medical Sciences (GMS-038323) and the U. S. Dept. of Energy (DOE DE-SC0018238).

GF acknowledges support by the French national funding agency ANR ('Momix' Projet-ANR-17-CE05-0029); the excellence cluster LabEX GRAL (ANR-10-LABX-49-01 financed within the University Grenoble Alpes graduate school -Ecoles Universitaires de Recherche- CBH-EUR-GS ANR-17-EURE-0003) and the European Research Council (ERC AdG 'Chloro-mito', grant no. 833184)

Short biographical notes

Marcin Sarewicz was born in Poland in 1979. In the years 2003 - 2007 he was a Ph.D. student at the Faculty of Biochemistry, Biophysics and Biotechnology of the Jagiellonian University in Krakow and his dissertation was awarded by "Prime Minister Award for the PhD thesis". After postdoctoral studies, he was employed as a lecturer at the same department, where he began working on the study of the molecular mechanisms of cytochrome bc_1 catalysis. In 2013 he obtained "Scientific Scholarchop for an outstanding young scientist" awarded by the Ministry of Science and Higher Education. In 2019 he obtained the degree of habilitated doctor, and currently he is an assistant professor at the Department of Molecular Biophysics. His research program focuses on the use of electron paramagnetic resonance in conjunction with rapid freezing techniques to study the molecular mechanisms of electron transfer processes in enzymes involved in cellular bioenergetics.

Sebastian Pintscher received his Ph.D. from the Jagiellonian University in 2016 for his work on the semiquinone intermediates of the cytochrome bc1. Currently he is a postdoctoral fellow at the

Jagiellonian University, pursuing research on the cyclic electron transfer in plant chloroplasts. His research interests include the redox chemistry of quinone oxidoreductases, properties of free-radical intermediates and evolution of bioenergetic systems.

Rafał Pietras (Kielce, Poland, 1985) graduated from Jagiellonian University in Kraków (Poland) where he also received his Ph.D. in biophysics in 2015. His research activities are focused around interactions between components of bioenergetic systems. In his scientific endeavour he applies EPR spectroscopy to investigate spin-labelled proteins and metaloenzymes. Currently he is involved in a project on the regulation of cyclic electron transfer in photosynthesis as a post-doc fellow at Jagiellonian University.

Arkadiusz Borek received a Ph.D. degree in biophysics from Jagiellonian University (Poland) in 2015. His PhD research was focused on the understanding of the mechanism of superoxide production by cytochrome bc1. He is a member of Molecular Bioenergetics Group of the Jagiellonian University led by prof. A. Osyczka. His postdoctoral studies concern the search for a mechanism of regulation of the operation of complex III. He is a grantee of the National Science Center, Poland. The topic of his project is understanding of the molecular effects of human mitochondrial cytochrome b mutations.

Łukasz Bujnowicz is currently a postdoc in Department of Molecular Biophysics at the Faculty of Biochemistry, Biophysics and Biotechnology of Jagiellonian University in Kraków. He received MSc (2013) and PhD in biophysics at the same faculty. The PhD thesis written by Łukasz was awarded as the best polish thesis in biochemistry in 2018 by The Polish Biochemical Society. He is interested in molecular mechanisms of electron transfer, development of methods of kinetic measurements with usage of Electron Paramagnetic Resonance combined with optical spectroscopy and occasionally image analysis but his passion is fly fishing.

Guy Hanke received his PhD from the University of Manchester in 1999 after working in the research groups of Professor Mike Emes and Caroline Bowsher. He then worked until 2008 first as a Japan Society of the Promotion of Science Research Fellow and Royal Society Research Fellow, then an Assistant Professor in the group of Professor Toshiharu Hase at Osaka University, before moving to

become an assistant in the group of Professor Renate Scheibe at the University of Osnabrueck. In 2015 he was appointed as a Senior Lecturer in Plant Cell and Molecular Biology at Queen Mary University of London. His research interest throughout his career has been how the distribution of energy - in particular electrons - is controlled within photosynthetic cells. This is explored using plant and cyanobacterial genetics, 'omics approaches, physiology and protein biochemistry to examine the function of proteins at the interface between energy generation in thylakoid membranes, and energy consumption by soluble enzymes.

William A. Cramer received a B. S. and M. S. in Physics from the Massachusetts Institute of Technology and the University of Chicago, respectively, the M. I. T. thesis on “anisotropy in the arrival direction of high energy cosmic rays.” Initial studies were published on (a) “μ meson capture rates” and (b) “optical birefringence of muscle proteins.” The Chicago Doctorate in Biophysics focused on photodynamically-induced mutagenesis of T4 bacteriophage. As an NSF postdoctoral Fellow with W. L. Butler at the University of California/San Diego, biophysical studies on the photosynthetic electron transport chain provided some of the first quantitative information on in situ properties of the cytochrome transport proteins. The latter studies became part of a research program subsequently pursued at Purdue University, where Cramer became Distinguished Professor of Biological Sciences, on structure-function of membrane proteins including membrane-active bactericidal toxins (“colicins”). These studies were recognized by Fellowships from the EMBO, and the Alexander von Humboldt and Guggenheim Foundations, by recognition as a ‘Fellow’ by (i) the American Association for the Advancement of Science (AAAS) and (ii) by the Biophysical Society for which Cramer participated in the establishment of the Bioenergetics Sub-Group of the Society and served as Chair, and (iii) by selection as Chair of two international Gordon Conferences on (1) “Biochemical Aspects of Photosynthesis,” and (2) “Bioenergetics.”.

Giovanni Finazzi got his PhD in Cellular and Molecular Biology (specializing in biophysics) at the University of Milano (Italy), under the supervision of Giorgio Forti. After a post doc at the Institut de Biologie Physico Chimique (IBPC) in Paris on the biophysics of photosynthesis under the supervision of Pierre Joliot, he joined the Italian Research Council as a junior research scientist. He pursued his career in the French CNRS, first in Paris (IBPC) and then in the Laboratory of Plant and Cell Physiology of the CEA of Grenoble as a Research Director. His main interest is understanding how

photosynthetic organisms manage their energy resources to thrive in different environments. He has studies photosynthetic light harvesting, electron transport, ATP synthesis and stress acclimation responses using a multidisciplinary approach, including biophysics, photophysiology, cell and molecular biology and 3D imaging.

Artur Osyczka is a professor in the Department of Molecular Biophysics at the Jagiellonian University (JU) in Kraków. His interest in redox-active proteins dates back to his graduate studies. In 1999, he completed his doctoral degree in the group of professor Katsumi Matsuura at Tokyo Metropolitan University working on bacterial photosynthetic reaction center. His post-doctoral work (1999-2006), carried out at the University of Pennsylvania in the group of professor P. Leslie Dutton, focused on molecular mechanism of energy conservation in cytochrome bc_1. In 2006 he established the Laboratory of Molecular Bioenergetics which now constitutes the major part of the Department of Molecular Biophysics at JU. He was twice the recipient of Senior Research Fellowship from the Wellcome Trust (in 2006-2012 and in 2011-2016). His research aims at understanding operation of energy conserving systems from the physico-chemical point of view and also in relation to cellular physiology. The topics include enzymatic catalysis and regulation of respiratory and photosynthetic protein complexes, electron and proton transfers, reactive oxygen species, mitochondrial diseases, dynamics of macromolecular interactions in redox systems.

TOC Figure

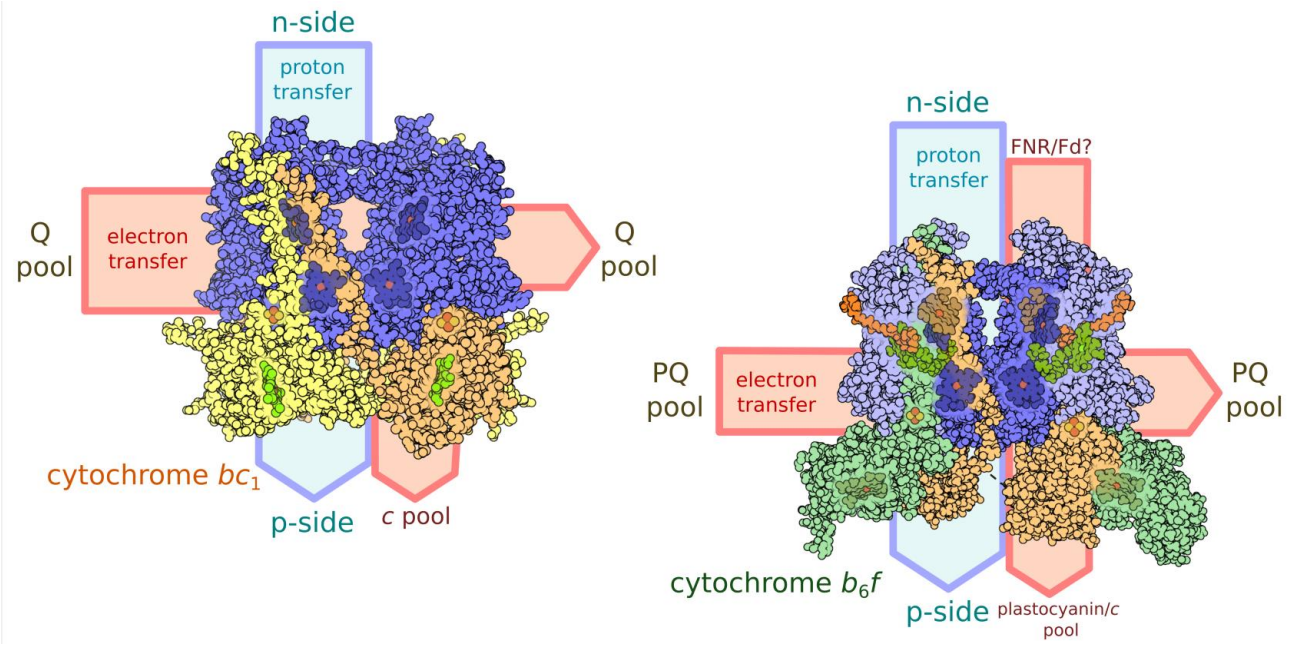
n-side
proton transfer
Q pool
electron transfer
Q pool
cytochrome bc_1
p-side
c pool
n-side
proton transfer
FNR/Fd?
PQ pool
electron transfer
PQ pool
cytochrome b_6f
p-side
plastocyanin/c pool